



**HAL**  
open science

# Pickering interfacial catalysis for oxidation: synergies at water/oil interface

Yaoyao Feng

► **To cite this version:**

Yaoyao Feng. Pickering interfacial catalysis for oxidation: synergies at water/oil interface. Catalysis. Université de Lille, 2022. English. NNT : 2022ULILR066 . tel-04357849

**HAL Id: tel-04357849**

**<https://theses.hal.science/tel-04357849v1>**

Submitted on 21 Dec 2023

**HAL** is a multi-disciplinary open access archive for the deposit and dissemination of scientific research documents, whether they are published or not. The documents may come from teaching and research institutions in France or abroad, or from public or private research centers.

L'archive ouverte pluridisciplinaire **HAL**, est destinée au dépôt et à la diffusion de documents scientifiques de niveau recherche, publiés ou non, émanant des établissements d'enseignement et de recherche français ou étrangers, des laboratoires publics ou privés.



**Université de Lille – Faculté des Sciences et Technologies**

**École Doctorale**

Sciences de la Matière, du Rayonnement et de l'Environnement

Thèse pour obtenir le titre de

**Docteur de l'Université de Lille**

Chimie organique, minérale, industrielle

**Yaoyao FENG**

---

**Pickering interfacial catalysis for oxidation: Synergies at water/oil interface**

**Catalyse interfaciale de Pickering pour l'oxydation : Synergies à l'interface  
eau/huile**

---

Soutenance le 14 Décembre 2022

Thèse dirigée par:

**Prof. Véronique NARDELLO-RATAJ, Directrice**  
**Dr. Jean-François DECHEZELLES, Co-Encadrant**

**Membres du Jury**

Dr. Bédèn ALBELA	Ecole Normale Supérieure de Lyon	Rapportrice
Prof. Karine DE OLIVEIRA VIGIER	Université de Poitiers	Rapportrice Présidente
Prof. Marc PERA-TITUS	Cardiff University	Examineur
Dr. Vincent DE WAELE	CNRS	Examineur
Prof. Véronique NARDELLO-RATAJ	Institut Centrale de Lille	Directrice
Dr. Jean-François DECHEZELLES	Institut Centrale de Lille	Co-encadrant



## Acknowledgements

---

This doctoral thesis was carried out in team C<sup>3</sup>SCO (Colloïdes, Catalyse et Oxydation) in University of Lille. The realization of this work would not be accomplished without the support and assistance from many people. As my adventures in France is coming to the end, I would like to express my deepest gratitude to all those people before starting the presentation of my dissertation.

First and foremost, I would like to express my sincere gratitude to my supervisor Prof. V éronique Nardello-Rataj, for giving me the opportunity to work abroad and providing me this promising project. Her precious guidance and critical mind had profoundly broadened my insight and strengthened the quality of the work. I would also like to express my appreciation to my co-supervisor Prof. Marc Pera-Titus for his guidance and kindness during these years. He offered me the opportunity to work on this interesting project and provided constant guidance and support throughout my research work. Their suggestions and passions in the research field not only improve my scientific knowledge, but also set an example I hope to follow in my future career development.

I would like to thank Dr. Jean-Fran çois Dechézelles who co-directed my thesis, who accompany me in my daily work. His patience and encouragement support me to finish this work.

I would also like to express my gratitude to Prof. Karine Vigier, from Université de Poitiers, and Dr. B én Albel, from Ecole Normale Sup érieure de Lyon, who kindly accepted to judge this thesis, for their acceptance to be members of the thesis committee.

My special thanks to Dr. Vincent De Waele for his kind help in light irradiation measurement in the laboratory of Lasire and discussion of light irradiation experiments. I would also love to express my gratitude to Dr. Emmanuel Courtade and Dr. Quentin Dacremont from the laboratory of PhLAM, for their invaluable assistance and suggestions for manipulation of laser irradiation test.

I would like to thank the lecturer and permanent members in our groups for their kind help and valuable discussions. First of all, I would like to express my gratitude to Dr. Raphaël Lebeuf for his assistance in NMR measurement. Special thanks to Dr. Christel Pierlot, Dr. Loïc Leclercq, Dr. Jesús Fermin Ontiveros and Prof. Jean-Marie Aubry for their generous help and valuable discussions. Also, special thanks to Mr. Mike Ortega-Vaz for his kind help in the lab.

I would like to thank Dr. Bingyu Yang for providing me the sincere help before I came to Lille and at the beginning of my PhD study. The video meeting between Prof. Véronique Nardello-Rataj, Dr. Bingyu Yang, and me five years ago really changed my life direction. I also would like to express my appreciation to Dr. Grégory Douyere for his countless help in the lab during these three years.

My special thanks to all the colleagues in the group: Agathe, Guillaume, Tristan, Lucie, Valentin, Adrien, Jordan. I really appreciate their sincere help in the lab and specific instruction in daily life in Lille. I would also like to thank my Chinese friend in Lille, Dr. Jianying DENG, for her support and the memory we had together in France.

I would like to express my sincere gratitude to the China Scholarship Council for providing financial support for my PhD study.

Last but not the least, I would like to express my great gratitude to my parents and family for their firm support and unconditional love. Their countless encouragement beyond the telephone line support me to finish my study abroad during this pandemic situation. I would like to especially thank my boyfriend Mr. Yuhao ZHANG for his support and encouragement during my PhD study.

For me, everything did not go smoothly, I have passed through adversity and struggle during the last twelve years. I really appreciated all the warm moments I've had in France, which is also a precious fortune in my life. Now, it's time to start a new chapter and I hope I can stay true to keep my original aspiration all along in the future.

## Abstract

---

Due to their localized surface plasmonic resonance properties, gold nanoparticles can efficiently convert light into heat for rapid energy transfer in their microenvironment. Taking advantage of this property, we have developed a new Pickering interfacial catalysis (PIC) platform for the catalytic oxidation of cyclooctene at room temperature. Hydrophobic silica and gold (Au/SiO<sub>2</sub>-C<sub>3</sub>) nanoparticles were combined with tri(dodecyltrimethylammonium) dodecatungstophosphate ([C<sub>12</sub>]<sub>3</sub>[PW<sub>12</sub>O<sub>40</sub>]) nanoparticles acting both as on-site heaters/plasmon activators and as in situ catalysts at the water/oil interface, under light radiation. The catalytic performance of these new systems was significantly improved due to the synergistic effect of the particles. In a second step, the grafting of ultra-small gold nanoparticles (< 3 nm) on the surface of modified silica particles allowed the oxidation of alcohols such as benzyl alcohol in Pickering emulsions. The systems obtained show better catalytic performances without addition of base. Finally, the grafting of temperature-sensitive polymers such as polyethylene glycol (PEG) onto silica nanoparticles (SiO<sub>2</sub>@PEG) has allowed the development of new thermos-sensitive emulsion systems that can be destabilized at 80 °C instead of centrifugation. The grafting of polyoxometalate onto these nanoparticles allowed the transposition of the PIC concept to the oxidation of cyclooctene. The advantages of these “smart” PIC systems hold great promise for the development of sustainable and green chemical conversion process.

**Keywords:** Pickering emulsion; Pickering Interfacial Catalysis (PIC); Oxidation; Nanoparticles; Silica; Gold; Polyoxometalate; Plasmonic; Synergy.

## Résumé

---

Grâce à leurs propriétés de résonance plasmonique de surface localisée, les nanoparticules d'or peuvent convertir efficacement la lumière en chaleur pour un transfert d'énergie rapide dans leur microenvironnement. En tirant profit de cette propriété nous avons développé une nouvelle plateforme de catalyse interfaciale de Pickering (PIC) pour l'oxydation catalytique du cyclooctène à température ambiante. Des nanoparticules de silice hydrophobée et d'or (Au/SiO<sub>2</sub>-C<sub>3</sub>) ont été combinées à des nanoparticules de tri(dodécyltriméthylammonium) dodécátungstophosphate ([C<sub>12</sub>]<sub>3</sub>[PW<sub>12</sub>O<sub>40</sub>]) agissant à la fois comme chauffages sur site/activateurs plasmoniques et comme des catalyseurs *in situ* à l'interface eau/huile, le tout sous rayonnement lumineux. Les performances catalytiques de ces nouveaux systèmes ont été significativement améliorées grâce à l'effet synergique des particules. Dans un second temps, le greffage de nanoparticules d'or ultra-fines (< 3 nm) à la surface de particules de silice modifiées a permis l'oxydation d'alcools tels que l'alcool benzylique en émulsions de Pickering. Les systèmes obtenus présentent de meilleures performances catalytiques sans ajout de base. Enfin, le greffage de polymères sensibles à la température tels que le polyéthylène glycol (PEG) sur des nanoparticules de silice (SiO<sub>2</sub>@PEG) a permis d'élaborer de nouveaux systèmes d'émulsions thermosensibles pouvant être déstabilisées à 80 °C au lieu d'utiliser la centrifugation. Le greffage de polyoxométallate sur ces nanoparticules a permis de transposer le concept PIC à l'oxydation du cyclooctène. Les avantages de ces systèmes PIC "intelligents" sont très prometteurs pour le développement de procédés de conversion chimique durables et écologiques.

**Mots-clés:** Emulsion de Pickering; Catalyse Interfaciale de Pickering (PIC); Oxydation; Nanoparticules; Silice; Or; Polyoxométallate; Plasmonique; Synergie.

# Table of contents

---

<b>General introduction</b> .....	<b>1</b>
<b>Chapter I. State of the art: Synergies at the water/oil interface in Pickering emulsions</b> .....	<b>9</b>
<b>1. Introduction</b> .....	<b>11</b>
<b>2. Interactions between stabilizers at the W/O interface in Pickering emulsions</b> .....	<b>13</b>
2.1. Particle/particle interactions .....	14
2.2. Particle/surfactant interactions .....	18
2.2.1. Conventional surfactants .....	18
2.2.2. Bio-based surfactants .....	22
2.3. Particle/polymer interactions.....	23
2.3.1. Synthetic polymer .....	23
2.3.2. Biopolymer.....	25
2.4. Particle/enzyme interaction .....	28
2.5. Interfacial interaction with different types of particles .....	30
<b>3. Physicochemical properties of Pickering emulsions</b> .....	<b>32</b>
3.1. Droplet size of Pickering emulsions.....	32
3.2. Stability of Pickering emulsions .....	33
3.3. Emulsion types and phase inversion of Pickering emulsion .....	35
3.4. Rheology properties of Pickering emulsions .....	38
<b>4. Mechanism of synergism at the Pickering emulsion</b> .....	<b>40</b>
4.1. Wettability alteration .....	40
4.2. Increment in viscoelasticity.....	43
4.3. <i>In situ</i> formation of Pickering interfacial catalyst.....	43
4.4. Film formation.....	45
<b>5. Applications of Pickering emulsions</b> .....	<b>46</b>
5.1. Catalysis .....	46
5.2. Photocatalysis.....	48
5.3. Enhanced oil recovery .....	49
5.4. Biomedical .....	51
5.5. Cosmetics and personal care product.....	52



<b>6. Conclusion.....</b>	<b>53</b>
<b>7. References .....</b>	<b>55</b>

**Chapter II . Light-driven Pickering interfacial catalysis for oxidation of cyclooctene at room temperature..... 67**

<b>1. Introduction .....</b>	<b>69</b>
<b>2. Experimental part .....</b>	<b>74</b>
<b>3. Results and discussion.....</b>	<b>81</b>
3.1 Synthesis and characterization of NPs .....	81
3.1.1. Dynamic light scattering measurements .....	81
3.1.2. Transmission electron microscopy characterization .....	84
3.1.3. X-ray photoelectron spectroscopy analysis .....	84
3.1.4. UV-vis spectroscopy.....	85
3.1.5. Thermostability .....	86
3.1.6. Fourier transform infrared spectroscopy .....	87
3.1.7. Water contact angle analysis .....	88
3.2. Physicochemical properties of the Pickering emulsions .....	89
3.2.1. Synergistic effect between Au/SiO <sub>2</sub> -C <sub>3</sub> and polyoxometalates (POMs) nanoparticles.....	89
3.2.2. Emulsion stability.....	91
3.3. Study of plasmon-induced photothermal effect .....	96
3.4. Catalytic performance .....	98
3.4.1. Plasmon-driven interfacial activation.....	98
3.4.2. Effect of power density .....	100
3.4.3. Effect of reaction time .....	101
3.4.4. Effect of the type of POM .....	102
3.4.5. Effect of [C <sub>12</sub> ] <sub>3</sub> [PW <sub>12</sub> O <sub>40</sub> ] concentration.....	104
3.3.6. Effect of stirring speed .....	104
3.4.7. Effect of solvent .....	105
3.4.8. Effect of water/oil ratio .....	106
3.4.9. Effect of pulsed laser.....	107
3.5. Scope of substrates .....	110
3.6. Reusability.....	111
3.7. Discussion .....	113
<b>4. Conclusions .....</b>	<b>116</b>
<b>5. References .....</b>	<b>117</b>

**Chapter III. Grafting of ultra-small Au nanoparticles on silica particles as catalysts for alcohol oxidation at the water/oil interface..... 125**

<b>1. Introduction .....</b>	<b>127</b>
<b>2. Experimental section.....</b>	<b>129</b>
<b>3. Results and discussion.....</b>	<b>134</b>
3.1. Synthesis and characterization of NPs .....	134
3.1.1. Preparation of nanoparticles .....	134
3.1.2. Transmission electron microscopy characterization .....	136
3.1.3. UV-vis spectroscopy.....	138
3.1.4. X-ray photoelectron spectroscopy analysis .....	138
3.1.5. Fourier transform infrared spectroscopy .....	139
3.1.6. Thermostability .....	140
3.1.7. Water contact angle analysis .....	141
3.2. Physicochemical properties of the Pickering emulsions .....	142
3.2.1. Influence of the organic solvents.....	142
3.2.2. Emulsion stability.....	143
3.3. Catalytic performance .....	145
3.4. Reusability.....	148
<b>4. Conclusions .....</b>	<b>150</b>
<b>5. References .....</b>	<b>151</b>

## **Chapter IV. Temperature-responsive Pickering emulsion stabilized by poly(ethylene glycol)-functionalized silica particles .....**

<b>1. Introduction .....</b>	<b>159</b>
<b>2. Experimental section.....</b>	<b>161</b>
<b>3. Results and Discussion .....</b>	<b>165</b>
3.1. Synthesis and characterizations.....	165
3.1.1. Transmission electron microscopy characterization .....	165
3.1.2. Dynamic light scattering measurements .....	166
3.1.3. Nuclear magnetic resonance spectroscopy.....	167
3.1.4. Thermostability .....	168
3.1.5. Surface tension measurement.....	169
3.2. Physicochemical properties of the Pickering emulsions .....	171
3.2.1. Influence of the nanoparticles .....	171
3.2.2. Temperature-responsive behavior of the Pickering emulsion .....	172
3.3. Elaboration of Pickering interfacial catalysis (PIC) system.....	175
3.3.1. Transmission electron microscopy characterization .....	176
3.3.2. Preparation of Pickering emulsion .....	176
3.3.3. Catalytic results .....	177
<b>4. Conclusion.....</b>	<b>179</b>
<b>5. References .....</b>	<b>180</b>

<b>Conclusion and outlooks .....</b>	<b>183</b>
<b>Appendix .....</b>	<b>191</b>
<b>Appendix 1 Detailed information of Pickering emulsion for chapter II .....</b>	<b>191</b>
<b>Appendix 2 Detailed information of Pickering emulsion for chapter III.....</b>	<b>198</b>
<b>Appendix 3 Detailed information of Pickering emulsion for chapter IV .....</b>	<b>200</b>
<b>Appendix 4 The UV spectral distribution of the lamp for chapter II.....</b>	<b>202</b>
<b>Appendix 5 Product identification for chapter II.....</b>	<b>204</b>
<b>Appendix 6 Product identification for chapter III .....</b>	<b>206</b>
<b>Appendix 7 Product identification for chapter IV .....</b>	<b>207</b>
<b>Appendix 8 Published article .....</b>	<b>209</b>

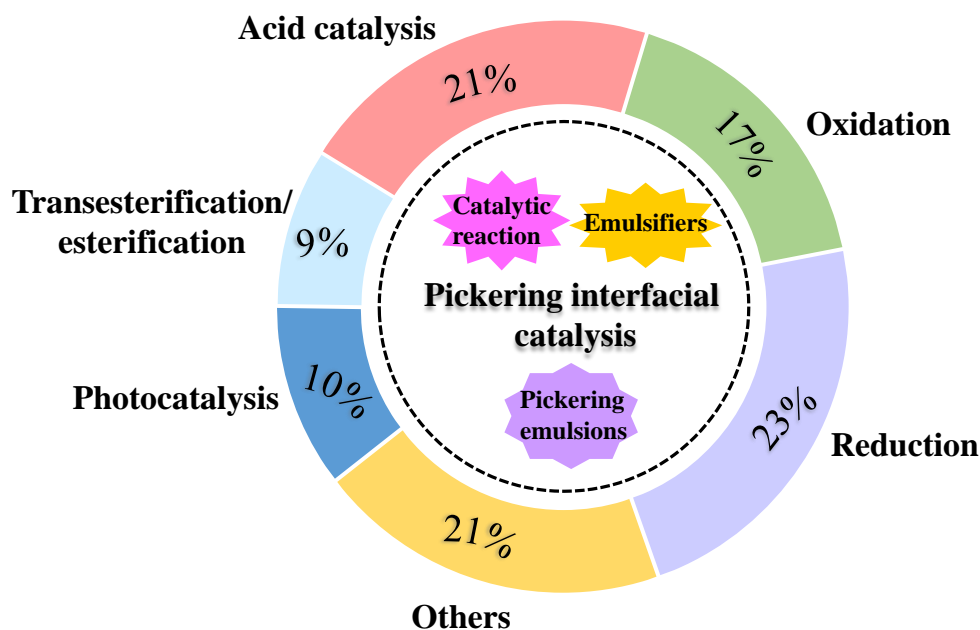
## General introduction

---

Catalytic oxidation plays an important role in the fine chemical industries [1-3]. The traditional methods for catalytic oxidation have generally employed homogeneous catalysts (*e.g.* metal salts or complexes) and stoichiometric oxidants (*e.g.* dichromate, permanganate, and manganese dioxide), but the unrecyclable and toxic nature restrict their wider application [4, 5]. Green and sustainable processes are now the long-standing target for the development of chemicals production. Researchers have investigated different alternatives for catalysts: metal-organic frameworks (MOF) [6] and supported noble metal catalysts [7], and also alternatives for conventional oxidants: H<sub>2</sub>O<sub>2</sub> [8], O<sub>2</sub> [9] and *tert*-butyl hydroperoxide [10]. However, we still face some challenges: how to increase activity and selectivity? how to develop green solvent reaction or solvent-free systems? and how to reduce waste during the catalytic processes? Moreover, a problem arises for the catalysts and the reactants located in different and non-miscible phases. Biphasic reaction systems often suffer from low reaction efficiency because of the high mass/heat transfer resistance, which is linked to the limited water/oil contact area [11]. To overcome this limitation, co-solvents [12] and phase-transfer reagents [13] are used. They allow the increase of the contact area and facilitate the transfer between phases. However, the introduction of new additives can make their separation from the reaction system difficult and harmful for the environment.

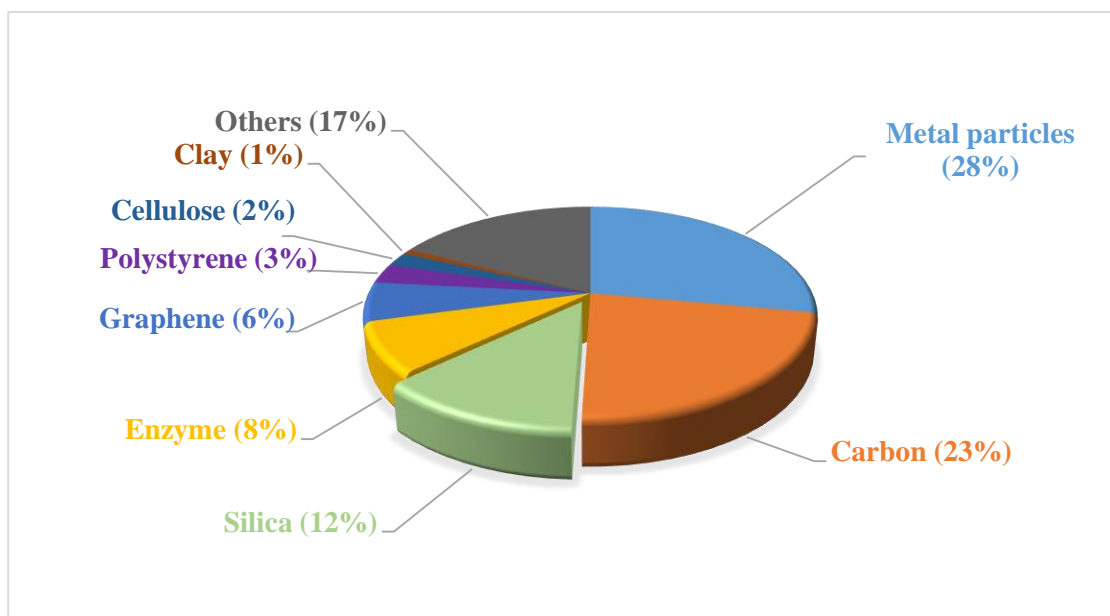
**Pickering emulsions**, composed of two immiscible phases stabilized by solid micro- or nanosized particles, which was firstly reported by Ramsden (1903) [14] and Pickering (1907) [15], have received increasing concerns in many different fields including pharmaceuticals, drug delivery, cosmetics, food industry, and more recently, catalysis [16, 17]. In the past decade, the use of Pickering emulsions for catalysis has emerged as an advanced biphasic reaction platform to overpass the limitations of the traditional technique [18, 19]. Conventional biphasic reaction system often suffers from a low interfacial area of the two immiscible phases. The use of **Pickering interfacial catalysis (PIC)** system (*i.e.* emulsion stabilized by catalytic amphiphilic NPs) is a promising strategy to improve the efficiency of biphasic reaction [20]. The location

of solid catalysts at the interface can provide large oil-water interface areas to facilitate the mass transfer of the reactants. Since the pioneering research conducted by Crossley *et al.* [21] in 2010, PIC systems have demonstrated a great potential for different reactions, particularly in reduction, acid catalysis, oxidation, photocatalysis, and transesterification/esterification (Figure 1).



**Figure 1.** Main catalytic reaction types in Pickering interfacial catalysis system according to the data extracted from SciFinder®.

So far, various nature of particles with tailored wettability have been used to stabilize PIC systems, including metal, carbon, silica and enzyme based materials (Figure 2). Subsequently, **stimuli-responsive PIC systems** have been developed by tuning the surface chemistry of the particles sensitive to pH, temperature, light, gas, light or magnetic field [22]. Continuous flow reactor and packed bed-like flow systems have been reported to take a step towards the industrial needs [23, 24]. Also, such a PIC system can be used as a vehicle to carry out multi-step cascade reactions to limit purification and isolation of intermediates [25].



**Figure 2.** Main particles used in Pickering interfacial catalysis system according to the data from SciFinder<sup>®</sup>.

The booming development in PIC let us promoting the design of “smart” PIC system for a sustainable and green chemical conversion. The goal of this thesis was to develop new Pickering emulsion systems for catalytic hydrogen peroxide-based oxidation applications. The manuscript has been divided into four chapters. **Chapter I** is a state of the art focusing on emulsion stabilized by hybrid nanoparticles with an emphasis on the synergistic effects at the water/oil interface. First, it is presented a list of different combination types of NPs and other compounds with synergistic interactions for stabilizing emulsions. Secondly, the physicochemical properties of the emulsion are discussed, such as their droplet size, long-term stability, emulsion types and phase inversion, and rheological properties. The corresponding mechanisms of synergism are then addressed. Finally, applications of such Pickering emulsions are presented with their benefits for catalysis, photocatalysis, enhanced oil recovery, biomedical and cosmetics and personal care product.

**Chapter II** reports the development of catalytic nanomaterials for the light-driven oxidation of cyclooctene in a PIC system. The system combines amphiphilic silica NPs decorated with gold nanoparticles, acting as on-site heaters/plasmon activators, and  $[C_{12}]_3[PW_{12}O_{40}]$  nanoparticles acting as catalysts. The preparation and characterization of the

amphiphilic Au/SiO<sub>2</sub>-C<sub>3</sub> NPs are detailed as well as the stability and plasmonic effects of the dual NPs-stabilized emulsions. Then, the catalytic performances have been evaluated for the plasmon-driven catalytic oxidation of cyclooctene using H<sub>2</sub>O<sub>2</sub> as an oxidant. The effect of different experimental parameters on the catalytic performance have been investigated such as the power density, the type of polyoxometalate (POM), the nature of solvent and the stirring rate. Reusability test of the catalyst has also been studied.

**Chapter III** deals with the synthesis and characterization of amphiphilic Au@SiO<sub>2</sub>-C<sub>3</sub> nanoparticles especially designed to be both catalysts and emulsifiers for improving the reaction activity of the oxidation of benzyl alcohol under base-free conditions. The Au@SiO<sub>2</sub>-C<sub>3</sub> NPs are composed of hydrophobic silica core, and highly dispersed ultra-small Au NPs *in situ* grafted onto the surface of the silica to be precisely localized ultra-small Au NPs at water/oil interface. The catalysts are characterized by combining different techniques, including transmission electron microscopy, infrared spectroscopy, thermal gravimetric analysis, X-ray photoelectron spectroscopy and inductively coupled plasma. The physicochemical properties of the emulsions stabilized by Au@SiO<sub>2</sub>-C<sub>3</sub> NPs are presented as well as the catalytic performance of Au@SiO<sub>2</sub>-C<sub>3</sub> for the oxidation of alcohol in the PIC system, in comparison with hydrophilic Au@SiO<sub>2</sub> in single phase catalysis system.

In **chapter IV**, the preparation of a series of polyethylene glycol (PEG) functionalized silica (SiO<sub>2</sub>@PEG) NPs with various molecular weights through a one-step synthesis are reported. The physicochemical properties of the NPs are determined by transmission electron microscopy, thermal gravimetric analysis, dynamic light scattering, tensiometry and zeta potential measurements, and the formed emulsions have been characterized by optical microscopy. The emulsions stabilized with SiO<sub>2</sub>@PEG NPs are used for the elaboration of temperature-responsive Pickering emulsions. The effect of different oils has been investigated for the temperature-triggered destabilization properties. Further, a PIC system based on the self-assembly of SiO<sub>2</sub>@PEG and POMs is presented. The oxidative cleavage of cyclooctene in Pickering emulsion is chosen as a reaction model in order to evaluate the efficiency of the SiO<sub>2</sub>@PEG-POMs composites.

Finally, a general conclusion highlights the results obtained and the main advantages of the PIC concept are underlined. Outlooks of this work are also discussed.



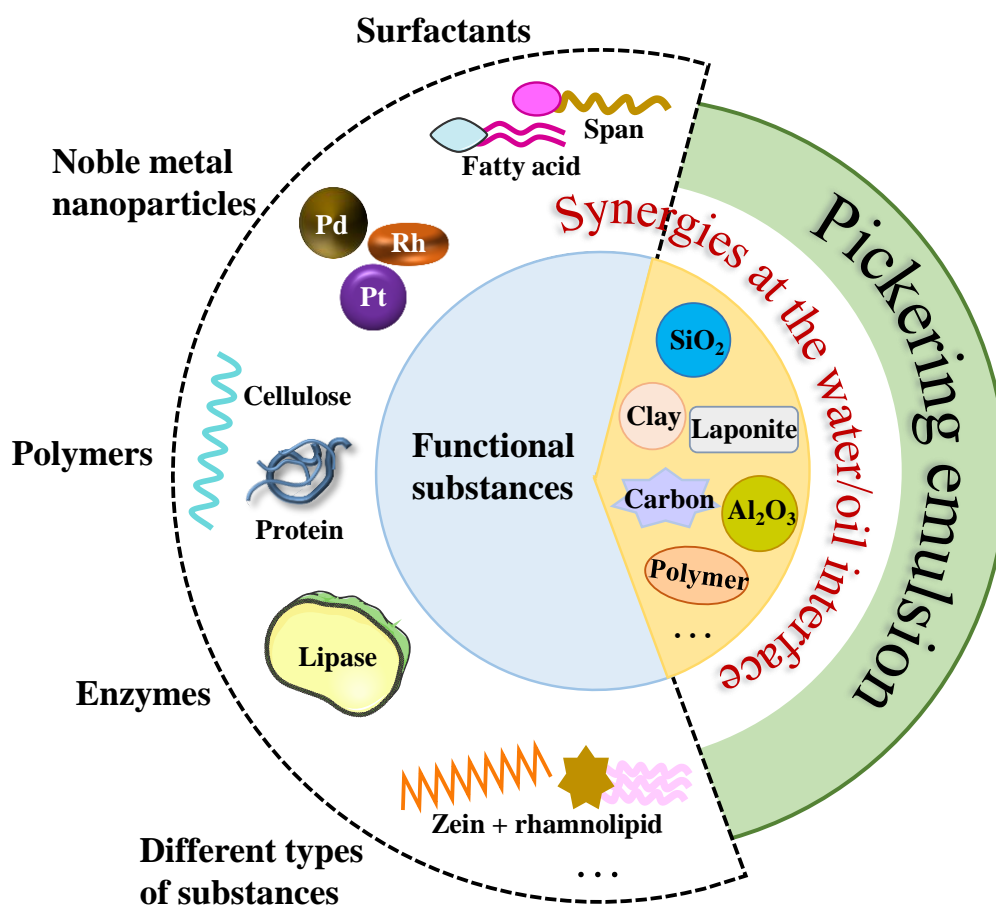
## References

- [1] F. Cavani, J.H. Teles, Sustainability in catalytic oxidation: an alternative approach or a structural evolution?, *ChemSusChem: Chemistry & Sustainability Energy & Materials*, 2 (2009) 508-534.
- [2] Z. Guo, B. Liu, Q. Zhang, W. Deng, Y. Wang, Y. Yang, Recent advances in heterogeneous selective oxidation catalysis for sustainable chemistry, *Chemical Society Reviews*, 43 (2014) 3480-3524.
- [3] F. Cavani, Catalytic selective oxidation: The forefront in the challenge for a more sustainable chemical industry, *Catalysis Today*, 157 (2010) 8-15.
- [4] R.A. Sheldon, Industrial Catalytic Oxidations: An Overview, *Studies in Surface Science and Catalysis*, 66 (1991) 573-594.
- [5] P.T. Anastas, M.M. Kirchhoff, Origins, current status, and future challenges of green chemistry, *Accounts of chemical research*, 35 (2002) 686-694.
- [6] M. Tonigold, Y. Lu, B. Breidenkötter, B. Rieger, S. Bahnmüller, J. Hitzbleck, G. Langstein, D. Volkmer, Heterogeneous Catalytic Oxidation by MFU-1: A Cobalt (II)-Containing Metal–Organic Framework, *Angewandte Chemie International Edition*, 48 (2009) 7546-7550.
- [7] Z. Jin, L. Wang, E. Zuidema, K. Mondal, M. Zhang, J. Zhang, C. Wang, X. Meng, H. Yang, C. Mesters, Hydrophobic zeolite modification for in situ peroxide formation in methane oxidation to methanol, *Science*, 367 (2020) 193-197.
- [8] R. Joseph, A. Sudalai, T. Ravindranathan, Selective catalytic oxidative cleavage of oximes to carbonyl compounds with H<sub>2</sub>O<sub>2</sub> over TS-1, *Tetrahedron letters*, 35 (1994) 5493-5496.
- [9] X.-H. Li, X. Wang, M. Antonietti, Solvent-free and metal-free oxidation of toluene using O<sub>2</sub> and g-C<sub>3</sub>N<sub>4</sub> with nanopores: nanostructure boosts the catalytic selectivity, *ACS Catalysis*, 2 (2012) 2082-2086.
- [10] K.R. Reddy, C.U. Maheswari, M. Venkateshwar, S. Prashanthi, M.L. Kantam, Catalytic oxidative conversion of alcohols, aldehydes and amines into nitriles using KI/I<sub>2</sub>–TBHP system, *Tetrahedron Letters*, 50 (2009) 2050-2053.
- [11] P. Tundo, A. Perosa, Multiphasic heterogeneous catalysis mediated by catalyst-philic liquid phases, *Chemical Society Reviews*, 36 (2007) 532-550.
- [12] C.M. Cai, T. Zhang, R. Kumar, C.E. Wyman, THF co-solvent enhances hydrocarbon fuel precursor yields from lignocellulosic biomass, *Green Chemistry*, 15 (2013) 3140-3145.
- [13] P. Gaudin, R. Jacquot, P. Marion, Y. Pouilloux, F. Jérôme, Acid-Catalyzed Etherification of Glycerol with Long-Alkyl-Chain Alcohols, *ChemSusChem*, 4 (2011) 719-722.
- [14] W. Ramsden, Separation of solids in the surface-layers of solutions and ‘suspensions’ (observations on surface-membranes, bubbles, emulsions, and mechanical coagulation).—Preliminary account, *Proceedings of the royal Society of London*, 72 (1904) 156-164.
- [15] S.U. Pickering, Cxcvi.—emulsions, *Journal of the Chemical Society, Transactions*, 91 (1907) 2001-2021.
- [16] D.G. Ortiz, C. Pochat-Bohatier, J. Cambedouzou, M. Bechelany, P. Miele, Current trends in Pickering emulsions: Particle morphology and applications, *Engineering*, 6 (2020) 468-482.
- [17] A.M.B. Rodriguez, B.P. Binks, Catalysis in Pickering emulsions, *Soft Matter*, 16 (2020) 10221-10243.
- [18] D.P. Fapojuwo, C.O. Oseghale, C.A. Akinnawo, R. Meijboom, Bimetallic PdM (M= Co, Ni) catalyzed hydrogenation of nitrobenzene at the water/oil interface in a Pickering emulsion, *Colloids*

- and Surfaces A: Physicochemical and Engineering Aspects, 619 (2021) 126513.
- [19] R. Röllig, C. Plikat, M.B. Ansorge-Schumacher, Efficient and Selective Carbonylation with Whole-Cell Biocatalysts in Pickering Emulsion, *Angewandte Chemie International Edition*, 58 (2019) 12960-12963.
- [20] F. Chang, C.M. Vis, W. Ciptonugroho, P.C. Bruijninx, Recent developments in catalysis with Pickering Emulsions, *Green Chemistry*, 23 (2021) 2575-2594.
- [21] S. Crossley, J. Faria, M. Shen, D.E. Resasco, Solid nanoparticles that catalyze biofuel upgrade reactions at the water/oil interface, *Science*, 327 (2010) 68-72.
- [22] J. Tang, P.J. Quinlan, K.C. Tam, Stimuli-responsive Pickering emulsions: recent advances and potential applications, *Soft Matter*, 11 (2015) 3512-3529.
- [23] M. Zhang, L. Wei, H. Chen, Z. Du, B.P. Binks, H. Yang, Compartmentalized droplets for continuous flow liquid-liquid interface catalysis, *Journal of the American Chemical Society*, 138 (2016) 10173-10183.
- [24] X. Zhang, Y. Hou, R. Ettelaie, R. Guan, M. Zhang, Y. Zhang, H. Yang, Pickering emulsion-derived liquid-solid hybrid catalyst for bridging homogeneous and heterogeneous catalysis, *Journal of the American Chemical Society*, 141 (2019) 5220-5230.
- [25] B. Yang, L. Leclercq, V. Schmitt, M. Pera-Titus, V. Nardello-Rataj, Colloidal tectonics for tandem synergistic Pickering interfacial catalysis: oxidative cleavage of cyclohexene oxide into adipic acid, *Chemical science*, 10 (2019) 501-507.



# Chapter I. State of the art: Synergies at the water/oil interface in Pickering emulsions





## 1. Introduction

Emulsions are widely used in various industrial processes and commercial products, such as cosmetic, drug delivery, food industry [1]. Usually, emulsions are stabilized by surfactant molecules which adsorb at the oil-water interface to decrease the interfacial tension between the phases. However, it is known that some adverse effects such as difficult recovery, environment contamination, or microorganisms damage may be associated with the surfactants [2, 3]. Moreover, there has been an increasing demand for “biocompatibility”, which limits their use in some fields, food industry in particular. Alternatively, emulsions stabilized with micro- or nano-sized particles - known as Pickering emulsions - are promising to address this issue [4, 5]. Solid particles play a pivotal part in the preparation of Pickering emulsions since they provide a robust physical barrier against droplet coalescence thanks to their partial wettability for each of the two immiscible phases. The nanoparticles (NPs) adsorb at the oil/water interface to form an effective steric and electrostatic protective shield for the droplets. The type of emulsion (oil-in-water (O/W) or water-in-oil (W/O)) is determined by the wettability of solid particles at oil-water interface. The hydrophilic particles which are more easily wetted by the water phase ( $\theta < 90^\circ$ ), form oil droplets [6]. The opposite phenomenon occurs for more lipophilic particles (*i.e.* water droplets). A wide variety of particles have been used in the past, including inorganic, organic and hybrid NPs as Pickering emulsifiers [7-9]. There are several advantages of using solid NPs compared to surfactants. Firstly, specific chemical functionalities can be grafted onto solid particles giving some advantageous features in different applications, like the existence of catalytic sites for catalytic reactions [10]. Secondly, the presence of amphiphilic solid particles allows the increase of the interface areas between hydrophilic and hydrophobic reagents at the nano- and microscales [11]. Thirdly, compared to molecular surfactants, solid particles can be easily extracted from the emulsion after the destabilization of the emulsion by different means such as centrifugation, salt addition, temperature increase [12, 13]. This character makes them as potential candidates in many significant processes, in particular oil extraction and heterogeneous catalysis. Moreover, stimuli-responsive Pickering

emulsion can be formed by the surface modification of NPs which can switch between emulsification/demulsification and phase inversion through appropriate external stimuli (*e.g.* pH [14], light [15], magnetic field [16], redox [17], temperature [18], *etc.*), and play an increasingly role in specific applications, including drug delivery, catalyst recovery and emulsion polymerization [19].

Since two decades, special attentions have been devoted to the development of Pickering emulsion, including their preparation and properties, the morphology and chemical nature of solid emulsifiers, and the different applications. For example, Yang *et al.* [20] described various practical solid NPs used for the formation of Pickering emulsions, including hydroxyapatite, silica, clay, magnetic NPs, chitosan, cyclodextrin, nanotube, and some food-grade stabilizers. Ortiz *et al.* [21] compared the effect of the NPs morphologies on the type and stability of the emulsion, and the current application of these emulsions. Wu *et al.* [22] introduced the effect of the characteristics of NPs on the preparation and properties of Pickering emulsions. Especially, they described the preparation methods of uniform-sized emulsions, including microfluidic devices and membrane emulsification. Finally, they also discussed many biomedical applications of Pickering emulsion, such as topical and oral drug delivery systems and related materials using Pickering emulsions as templates. Zhu evaluated the recent advances in starch modifications for the formation of emulsions, presenting a new sight for food application [23]. Xiao *et al.* focused on emulsions stabilized by food-grade particles, and their stabilization mechanisms based on interfacial microstructure observations as well as promising research trends in basic research and fields of applications [24].

Currently, Pickering emulsions have dramatically changed the research scope of traditional solid emulsifiers. This statement can be especially evidenced in terms of their interaction and compatibility with material actively studied in other fields, such as polymer materials, biomaterials and metal NPs. Synergistic interactions of NPs and additional substances allow to create "smart" functional-hybrid with improved properties compared to individual components. Hybrid NPs have attracted many attentions and opened the possibility to develop novel system of Pickering emulsions. Remarkable synergistic effects have been observed in materials that

combine NPs and different types of materials. Up to now, NPs have successfully formed many functional hybrids with metal NPs, enzymes, surfactants, biomaterials and more. Such hybrids are intensively explored for use in catalysis processes, food industry, enhanced oil recovery, and so on.

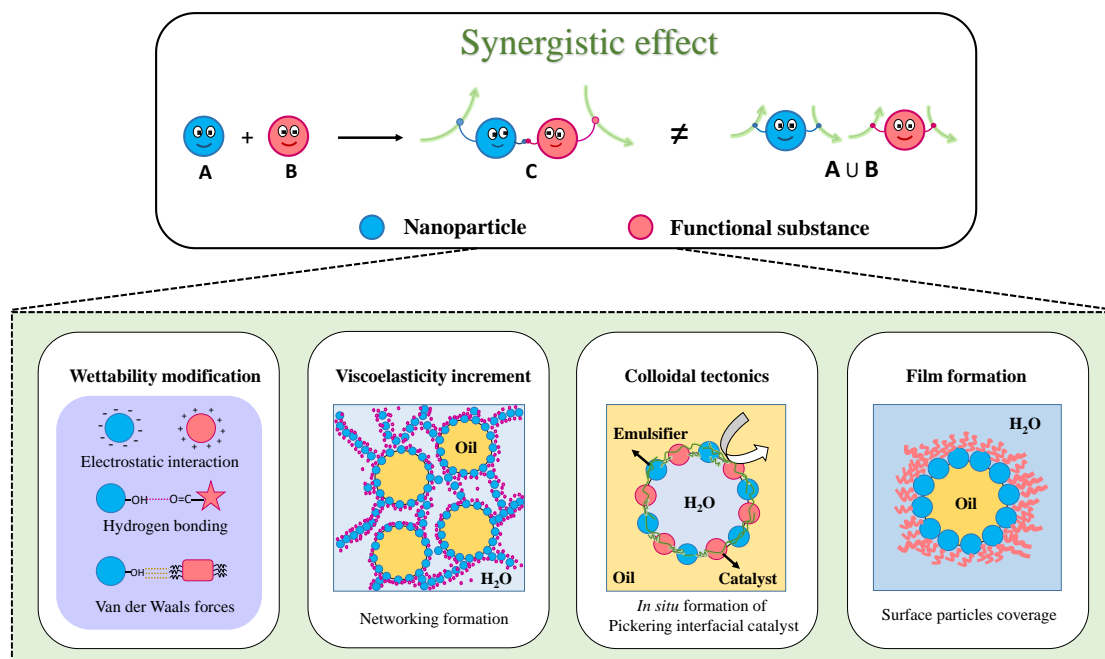
This review aimed at giving an overview on the advancement of hybrid NPs at the water/oil interface for the stabilization of emulsions. Different combinations of NPs with synergistic interactions for stabilizing emulsions are listed below. The physicochemical properties of these emulsions are discussed. Moreover, different mechanisms of wettability modification or film formation are analyzed. Different applications of those Pickering emulsions are presented.

## **2. Interactions between stabilizers at the W/O interface in Pickering emulsions**

The long-term stability *versus* the coalescence of Pickering emulsions ensures the form of multitudinous micrometer-sized or even millimeter-sized emulsions, the stability, type (O/W or W/O), morphology, characters of Pickering emulsions can be controlled by the properties of solid particles. Encouraged by such unique merits, various solid particles, such as TiO<sub>2</sub> [25], CuO [26], silica [27], clay [28], polymer [29] and carbon material [30], with the advantages of rigidity, dimensional stability, and thermal stability, have been widely researched for further improving the properties or applications of Pickering emulsions. With the increased requirements of highly efficient Pickering emulsions, a single particle is insufficient for complex functions. In addition to single particle-laden interfaces, there has been growing interest in stabilizing emulsions by particle-based composites. The synergistic effects between different components cannot only keep the original properties of each components, but also achieve further improvements by integrating the advantage of the different entities. Further development of those promising nanomaterials requires a better understanding of particle interactions, as well as of the nature of the assemblies. The connected particles and substances



at the liquid-liquid interfaces provides new insights into the design and fabrication of a new generation of Pickering emulsions (**Figure 1**). In this respect, the combination of different types of substance with the Pickering particles, is presented and discussed in detail.



**Figure 1.** Schematic illustration of the combination of particles with functional substances for the formation of Pickering emulsion.

## 2.1. Particle/particle interactions

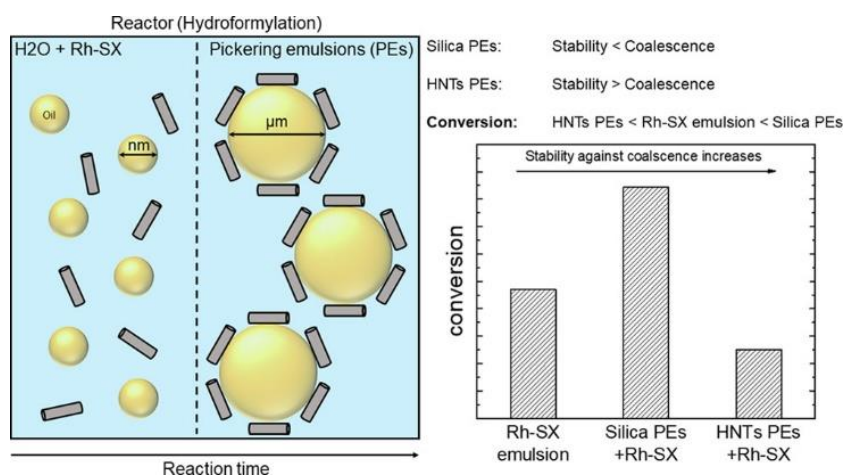
Many types of particles, either inorganic or organic, fulfill the partial wetting condition for stabilizing emulsions. Montmorillonites [31], polymeric latex [32], magnetic particles [33], carbon nanotubes [34] have proved to be efficient stabilizers of emulsions. The combination of particles of different chemical nature can even generate a composite with different properties from the individual components. As an illustration, Binks *et al.* [35] have mixed two types of silica particles with opposite wettability and used them as emulsifiers for water-toluene Pickering emulsion. It has been found that the transitional inversion of emulsions occurs from W/O to O/W with the addition of hydrophilic silica to systems stabilized by hydrophobic silica. Moreover, an increase in the proportion of hydrophilic silica mixtures with hydrophobic silica results in the deflocculation of water drops in the emulsions. Similarly, in a study of the

synergistic effect between silica NPs and organoclay on emulsion stability, Liu *et al.* [36] reported a high-temperature-resistant Pickering emulsion stabilized by organoclay and intermediate hydrophobic silica NPs. Because of the swelling and exfoliation ability, the organoclay NPs play a key role in the formation of networks in the continuous phase, while silica NPs adsorbed at the water-oil interface to form a rigid fence around the organoclay. The rheological properties of the resulting emulsions were found to be highly stable even after thermal rolling at 220 °C.

Normally, hard particles are widely used as emulsifiers for Pickering emulsions, but some Pickering emulsions have been achieved with soft particles, like microgels. Stock *et al.* [37] employed soft and hydrophilic poly(N-isopropylacrylamide) microgel particles (MGs) and hydrophobic silica NPs simultaneously stabilized emulsion. They revealed that the addition of silica particles enabled the formation of W/O emulsions with hydrophilic particles. Interestingly, the packing density of silica NPs at the interface between MGs is very dense, while the silica NPs adsorbed onto the surface of MGs in a loose packing.

The use of transition metal NPs has also been extensively explored notably for the heterogeneous catalysis. The stabilization of transition metal NPs is clearly crucial in their application because of the agglomeration problem. Employing solid particles with the ability of stabilizing emulsions allows to immobilize metal NPs as nanocatalysts with enhanced activity. A popular method for preparing particles composites is the chemical reduction of metal salts. Because of the coordination and electrostatic interaction between the heterocyclic cations in the NPs and metal salts, the *in situ* generated metal NPs can be stabilized by solid emulsifiers. For example, Yan *et al.* [38] used a Janus mesosilica nanosheets decorated with Pd NPs as interface active catalyst for the hydrogenation of nitrobenzene and NaHB<sub>4</sub>. Because of the perpendicular mesochannels of the silica NPs, the Pd NPs are uniformly loaded in the mesochannels to offer efficient passageway. Similarly, Li *et al.* [39] prepared Janus-type amphiphilic cellulose nanocrystal decorated with Pd NPs for catalysis, and the obtained Pickering emulsion system can be applied for both hydrogenation and Suzuki reaction.

Stehl *et al.* [40] illustrated the combination of surface-active rhodium catalyst (Rh-SX), and hydrophilic silica NPs or hollow halloysite nanotubes (HNTs) for the fabrication of emulsions, and studied the interconnections between catalyst and NPs (**Figure 2**). Rhodium NPs attachment at the interface occurs if the droplet size is on the order of micrometers. The ability of surface-active catalyst to adsorb onto the particle surface reduces the energy of attachment. The synergistic effect between rhodium catalysts and silica NPs allows to decrease the droplet size and improves the mechanical stability of the emulsion. The contact area between catalyst and reagents is insufficient at low emulsion stability, while the particles may block the transfer between catalyst and reagents at high emulsion stability. The authors have demonstrated that the intermediate stability of emulsion system contributes to the intensification of the hydroformylation process with the adjustment of particle properties, providing the highest conversion of 42 wt.%, nearly 3 times higher in comparison to the two other emulsions.



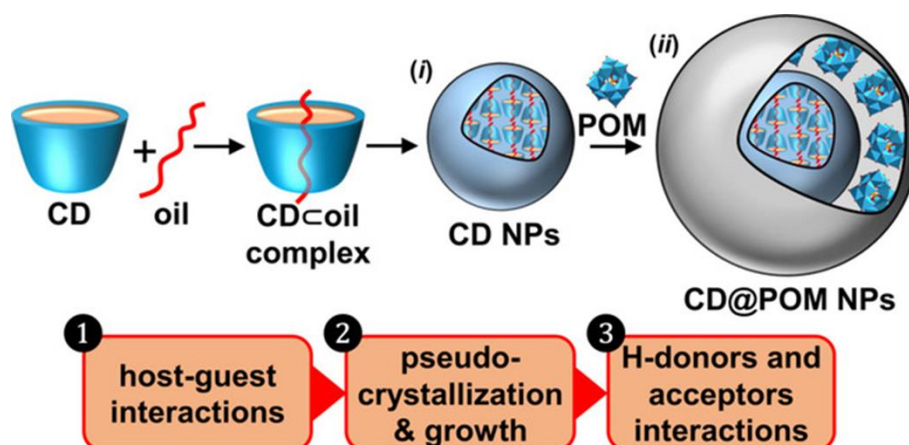
**Figure 2.** Schematic illustration of the proposed mechanism of the stabilization of the Pickering emulsions behavior during the hydroformylation. Left: The oil droplets stabilized by rhodium catalysts and hollow halloysite nanotubes are represented as yellow balls and grey tubes. The particles attach at the oil/water interface and stabilize the droplets against coalescence as micrometer-sized reactors. Right: Comparison of the conversion of 1-dodecene versus stability against coalescence in emulsion system formulated with silica and hollow halloysite nanotubes and without particles (Rh-SX emulsion) (Ref. 40 with permission of American Chemical Society).

Although carbon nanotubes have been already used for catalysis [41], their combination with metallic particles to stabilize emulsions and for catalytic applications is very promising.

Crossley *et al.* [42] have synthesized a family of recoverable catalysts that simultaneously stabilize emulsions by depositing palladium onto carbon nanotube-inorganic oxide hybrid NPs. The incorporation of solid catalysts at the interface between two phases exhibits excellent catalytic activity for a broad range of reaction. The hybrid particles localized at water/oil interface facilitate biphasic hydrodeoxygenation and condensation reactions. Zapata *et al.* [43] used the same strategy to prepare Pd or Pt metallized nanohybrids, which can be used to hydrogenate the aldol-condensation product at the water/oil interface in Pickering emulsions system. NPs as effective carriers for metal NPs can impart "smart" functions such as stimulus-responsive Pickering interfacial catalysis. Zeng *et al.* [44] successfully prepared gold NPs/amphiphilic core cross-linked supramolecular polymer particles (Au@CCSP) for stabilizing chloroform/water interface in order to produce emulsions with thermo-, light-, and amantadine hydrochloride guest-triggered demulsification, which also provided a good platform for the heterogeneously catalytic reduction reaction of p-nitroanisole by NaBH<sub>4</sub>.

Polyoxometalates (POMs), anionic metal oxide clusters (with several to tens of negative charges), have been extensively investigated for catalytic applications because of their tunable acidity, redox properties, thermal stability, and unique electrical and optical sensitivity [45]. However, the pristine POMs have difficulties in their separation and recycling during the catalysis process due to their hydrophilicity nature. Assembly of POMs with solid emulsifiers is revealed to be a successful example for preparing heterogeneous POM catalysts in biphasic reaction system, which is beneficial for increasing the mass transfer and facilitating catalyst recovery. Tang *et al.* [46] synthesized H<sub>3</sub>PW<sub>12</sub>O<sub>40</sub>-modified poly (1-vinyl-3-ethylimidazolium bromide) (PILs) combined to silica@polystyrene/polydivinylbenzene (PS/PDVB) to form Janus particles (JPs) (PA-PILs-JPs). The JPs are tailored for emulsification and catalysis and can be utilized to emulsify immiscible ionic liquid ([BMIM]BF<sub>4</sub>)/toluene emulsion. The obtained emulsion can be filled in column reactor to improve the acylation reaction of toluene with acetic anhydride. Excellent catalytic activity with a conversion of 95.3% and reusability have been demonstrated. The interaction between moleculars or particles can induce self-assembly for the fabrication of macroscopic supramolecular or supracolloids can be defined as

“colloidal tectonics” [47]. Leclercq *et al.* [11] and Pacaud *et al.* [48] developed self-assembled colloidal systems through the colloidal tectonics approach (**Figure 3**). The introduction of  $\text{PW}_{12}\text{O}_{40}^{3-}$  anions into an inclusion complex formed by the interaction between  $\beta$ -cyclodextrin (CD) and oil molecules allows the stabilization of emulsions by these core-shell NPs and to perform efficient catalytic activities as Pickering interfacial catalysis [49].



**Figure 3.** Schematic illustrations for the preparation of CD@POM NPs by self-assembly of complementary tectonics (CD, oil and POM): (i) Formation of CD NPs with CD and 1-decanol, (ii) POMs are deposited on the polar neutral interface of CD NPs (Ref. 38 with permission of Wiley).

## 2.2. Particle/surfactant interactions

Surfactants with diverse structures and abundant chemical properties have been extensively explored in various areas. The interaction of NPs with surfactants has received considerable interest owing to their simple preparation and improved properties. One of the advantages of using surfactants to combine with NPs is to modify its surface characteristic, especially its hydrophilic/hydrophobic properties.

### 2.2.1. Conventional surfactants

Clays are natural, low cost, biocompatible and applicable nanoparticles which have attracted much attention in recent decades for a wide range of applications. The combination of clay nanoparticles and surfactants can synergistically exhibit significant improvement in the

surface-active properties. Wang *et al.* [50] exploited the strong synergistic effect between nonionic surfactant Span 80 and NPs (layered double hydroxide particles or Laponite particles) to stabilize emulsions. The adsorption of Span 80 on the layered double hydroxide particles renders them more hydrophobic and enable them to stabilize W/O emulsions, while emulsions stabilized by Laponite-Span 80 are always O/W type. In the hybrid system, both NPs and Span-80 synergistically work together to increase the dilatational viscoelasticity modulus of the O/W interface, leading to a gel-like particle layer locates at the interface to prevent the coalescence of droplets.

Besides, Tan *et al.* [51] used tetramethylammonium chloride (TMAC)/Laponite hybrid particles as stabilizers for alkenyl succinic anhydride (ASA)-in-oil emulsion *via* the adsorption of TMAC on the surface of NPs. The presence of TMAC neutralizes the effective charge of NPs and decreases the apparent viscosity. Moreover, the addition of TMAC reduces the interfacial tension between ASA and Laponite aqueous dispersion. Thus, the hybrid significantly reduces the emulsion droplet size and enhances the creaming stability of emulsions. The addition of surfactant in laponite-stabilized emulsion allows the formation of a dense network structures and the increase of viscosity in the continuous phase which is responsible for the improvement of the emulsion stability. Zheng *et al.* [52] pointed out a correlation of the rheological behavior of the resulting emulsions with the type of surfactants. Three types of surfactants (*i.e.* dodecyltrimethylammonium bromide (DTAB), Pluronic F68 (F68), and sodium dodecyl sulfate (SDS)) can adsorb onto the surface of laponite particles through electrostatic interactions and hydrophobicity. A higher stability of laponite/surfactant Pickering emulsion can be achieved because of the formation of a network structure. Especially, differences in the rheology measurements can be observed between the three types of surfactants stabilized emulsion. The emulsions of laponite/SDS and laponite/DTAB showed a yield stress and shear-thinning, while laponite-stabilized emulsions and laponite/F68-stabilized emulsion behaved as Newtonian fluids.

An investigation was performed on the fabrication of emulsions from solutions of octadecylamine surfactant in oil and aqueous suspensions of laponite instead of suspending

particles and surfactant in the same phase as previously described [53]. The results suggested that the synergistic interaction occurred through the adsorption of surfactant from the oil phase onto the particles at liquid/liquid interface can reduce the average droplet size because of the enhanced particle adsorption at the O/W interface.

Like for clay NPs, several studies have been performed on synergistical effects of silica NPs and surfactants. Worthen *et al.* [54] reported the preparation of O/W emulsions with a combination of silica NPs and zwitterionic caprylamidopropyl betaine surfactant. The weak interaction between surfactant and nanoparticle promotes synergism in the fabrication of Pickering emulsions. At low adsorption of surfactant on the surface of silica NPs, a large fraction of surfactant freely adsorbs at the oil-water interface to reduce the interfacial tension, while the NPs provide a steric barrier to droplet coalescence, resulting in smaller droplets and slower creaming rates. Wei *et al.* [55] investigated the effects of different types of cationic surfactants on the properties of emulsions stabilized by silica NPs. These modified silica NPs showed excellent emulsification properties compared to pure surfactants or hydrophilic silica NPs. The presence of the electrostatic interaction between silica NPs and surfactants exhibits a competitive adsorption with the surfactant molecules at the O/W interface. The modified NPs is not spontaneously adsorbed at the oil/water interface, which may be explained by the large size of particles in comparison to the small surfactant molecules.

While Binks *et al.* [56] investigated the behavior of emulsion prepared by the synergic interactions of negatively charged silica and cationic surfactant CTAB. The silica surface become increasingly hydrophobic because the surfactant adsorption can effectively reduce the water-oil interfacial tension, thus preventing droplets from coalescing. The most stable emulsions can be obtained when particles have negligible charge and lead to flocculation. In addition to the wettability control of the nanoparticle-surfactant hybrid, a synergistic effect can be engineered by placing a surfactant, bearing responsive properties (such as pH, temperature, magnetic field, redox, CO<sub>2</sub>...). Jiang *et al.* [57] obtained CO<sub>2</sub>/N<sub>2</sub>-switchable Pickering emulsions by using a trace amount of N'-dodecyl-N,N-dimethylacetamide surfactant combination with silica NPs. Hydrophilic silica can be partially hydrophobized *in situ* by

adsorption of the surfactant through electrostatic interactions and therefore able to stabilize emulsion. At controlled temperatures, the surfactants can be switched to its active form, N<sup>+</sup>-dodecyl-N,N-dimethylacetamidinium bicarbonate (amidinium/cationic), by exposure to water and CO<sub>2</sub> and switched back to the inactive form (amidine/neutral) by bubbling N<sub>2</sub> or air through the solution. Both switchable surface-active particles and emulsions can be obtained by using the same trigger. Yu *et al.* [58] reported switchable Pickering emulsions stabilized with silica NPs and a trace amount of redox-switchable ferrocene surfactant (FcCOC<sub>10</sub>N) (10<sup>-5</sup> M). The silica and surfactant act synergistically to form emulsion with long-term stability. It is noteworthy that the surfactant concentration is reduced at least 100 times which would reduce discharge to the environment. Similar redox-responsive Pickering emulsion was also observed by Jiang *et al.* [59]. A trace amount of ferrocene azine surfactant (Fc<sup>+</sup>A) in combination with SiO<sub>2</sub> NPs by electrostatic interaction increases the hydrophobicity of SiO<sub>2</sub> NPs, and the as-obtained emulsifiers can significantly improve the stability of the emulsion. The synergy between Fc<sup>+</sup>A and SiO<sub>2</sub> NPs does not only improve the stability of emulsion, but also reduces the amount of surfactants dramatically.

Other types of stimuli-responsive emulsions have been studied by using combination of surfactant and silica NPs. Liu *et al.* [60] investigated the synergistic effect of fumed silica NPs and surfactant for the generation of pH-responsive emulsions with a wide pH range. Stable emulsions can be formed with the silica NPs and the N-(2-((2-aminoethyl) amino) ethyl) octadecenamide surfactant at pH of 2~12, completely coinciding with the pH range in which the highest flocculation occurs due to the introduction of the surfactant. Zhang *et al.* [61] used conventional surfactant myristylamidopropyl amine oxide (C<sub>14</sub>PAO) modified hydrophilic SiO<sub>2</sub> NPs through CO<sub>2</sub>-controllable electrostatic attraction, which served as CO<sub>2</sub>-switchable Pickering emulsifier. Jia *et al.* [62] prepared the oil/water emulsion stabilized with amphiphilic sodium benzenesulfonate (SBS) molecules and hydrophilic AlOOH nanoparticles complexes. The addition of SBS strongly increases the wettability of AlOOH NPs at the interface and generates emulsion. The obtained emulsions have shear, temperature and electrolyte tolerances, and can be applied to enhanced oil recovery. Hu *et al.* [63] observed that the *in situ* surface



modification of cellulose nanocrystals (CNCs) by the adsorption of small amount of surfactants could stabilize emulsion. The type and concentration of surfactant can be used to control the continuous phase of the emulsion. The results showed that double phase inversion (from O/W to W/O emulsion, followed by W/O to O/W emulsion) occurs with the increase of didecyldimethylammonium bromide (DMAB) concentration in CNC emulsion.

### 2.2.2. Bio-based surfactants

More recently, there has been an increasing demand for “bio-sourced” in a range of industrial applications, especially in cosmetics, food and pharmaceuticals, which limit the use of synthetic surfactants [64, 65]. Therefore, various bio-based surfactants have been explored as promising alternatives to replace their conventional counterparts (*e.g.*, tweens and spans) in emulsion systems, like glycolipids [66], lipopeptides [67], and fatty acids [68]. The combination of particles and natural surfactants may modulate the physical properties of NPs and generate new functional composite materials. Pi *et al.* [69] investigated the formation of crude oil-in-seawater Pickering emulsion co-stabilized by positively charged silica NPs and anionic rhamnolipid. The *in-situ* adsorption of rhamnolipid onto the silica surface endowed a steric barrier to prevent droplet coalescence. In comparison with the emulsion stabilized by either silica or rhamnolipid alone, the silica and rhamnolipid acted synergistically to form emulsion with smaller droplet size and higher stability. Zhao *et al.* [70] found that O/W emulsions were synergistically stabilized by the complex formation of silica NPs and sodium alginate derivative surfactant. They showed that the stability and viscoelastic properties of the Pickering emulsions increased when the molecular weight of sodium alginate derivative increased. Moreover, emulsions tend to be more stable with the increase of silica concentration because of the enhancement of 3D structure rigidity.

Santini *et al.* [71] investigated the water/hexane emulsions stabilized by the formation of palmitic acid-silica NPs complexes. The adsorption of surfactant at the particle surface leads to the formation of dense and persistent layers at the interface, which prevent the droplet coalescence. The study demonstrated that the most stable emulsions can be obtained only when

the amount of surfactant leads to the formation of single surfactant layers onto the particles surface.

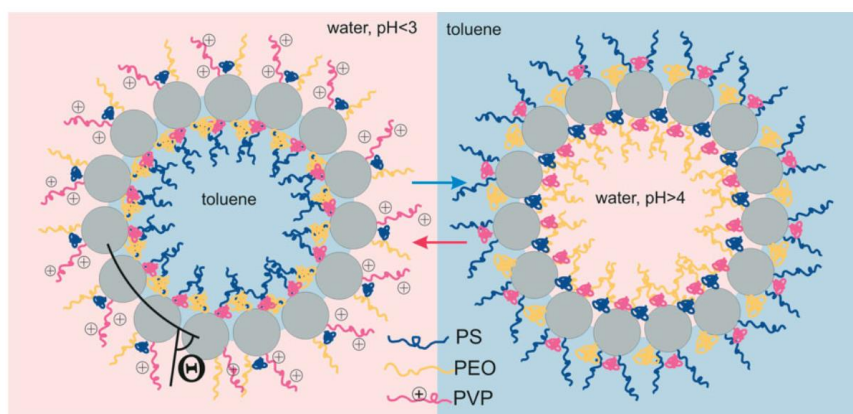
## 2.3. Particle/polymer interactions

Polymers possess some unique properties, such as light weight, stability and tunable thermal, have been extensively explored in material science [72, 73]. However, it remained difficult to find suitable polymer for the formation of Pickering emulsion. The synergism of polymers and particles remarkably improved the physical stability of emulsion and restructured their rheology and interfacial structure. Especially, polymers adsorbed on the particles surface can act as “soft” and “dynamic” building units, which can be controlled the self-assembly or disassembly process *via* tuning the surrounding environment and generate new functional composite materials [74].

### 2.3.1. Synthetic polymer

The combination of particle with polymers allows the development of stimuli-responsive (*e.g.* light, temperature and pH) Pickering emulsion system. For example, a dual-responsive (pH and magnetic) Pickering emulsion stabilized by nanocomposites (PDMNC) made of Fe<sub>3</sub>O<sub>4</sub> nanoparticle and poly[2-(dimethylamino) ethyl methacrylate] (PDMAEMA) [75]. The emulsification/demulsification of emulsion can be controlled by the synergistic effect from magnetic force, surface wettability and surface charge of the PDMNC. The surface wettability of the PDMNC was evaluated through water contact angle measurement, showing a decrease in the contact angle by increasing the pH from 3 to 11 because the hydrophobicity of PDMAEMA significantly increased when the deprotonation of surface amine groups occurred. This remote-switchable Pickering emulsions can be potentially used in oil recovery system. Generally, pH-responsive phase inversion Pickering emulsion make use of particles that have functional groups that respond sharply to small changes in environment. Motornov *et al.* [76] grafted mixed copolymer brushes (Poly(styrene-*b*-2-vinylpyridine-*b*-ethylene oxide)) on silica NPs to fabricate stimuli-responsive colloidal system (**Figure 4**). The balance between

hydrophobic polystyrene (PS) and hydrophilic polar fragments (charged poly (2-vinylpyridine) (P2VP) and polyethylene oxide (PEO)) can be regulated by an external trigger. At  $\text{pH} < 4$ , the polar component enhanced the hydrophilicity and drove the particles to form O/W type emulsion. At  $\text{pH} > 4$ , the deprotonated P2VP components increased the hydrophobic properties of the copolymer, leading to emulsion inversion to W/O type.

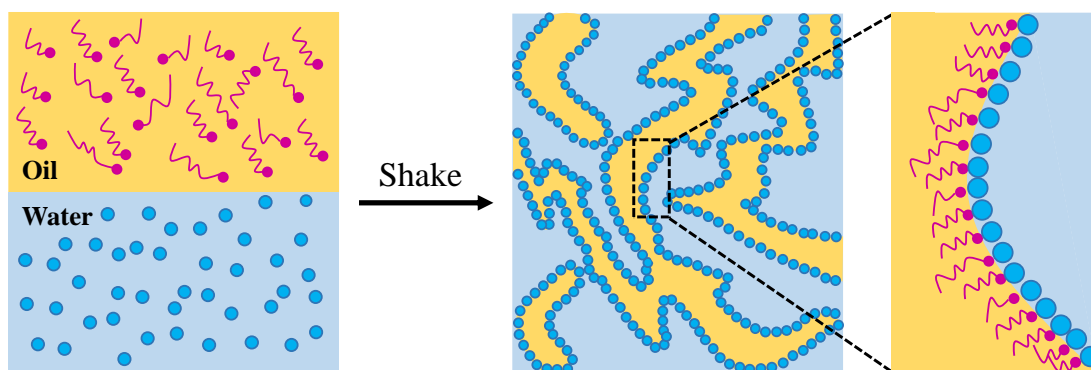


**Figure 4.** Schematic illustration of structure of the O/W and W/O pH-responsive Pickering emulsion. At  $\text{pH} < 3$ , O/W Pickering emulsion were formed, while the W/O Pickering emulsion were obtained at  $\text{pH} > 4$ . (Ref 76 with permission from Wiley)

In addition to the development of stimuli-responsive Pickering emulsion, the most obvious advantage of combining particles with polymers is the preparation of materials by Pickering emulsion polymerization method. Zhou *et al.* [77] modified silica NPs with ethacryloxypropyltrimethoxysilane (MPTMS) to stabilize the temperature-responsive Pickering emulsion. The morphology of PS/SiO<sub>2</sub> microspheres can be regulated via tuning SiO<sub>2</sub> concentrations and initiator sorts. At low SiO<sub>2</sub> particles concentration, hollow spheres can be obtained when water-solute initiator potassium persulfate was applied. Upon increasing the concentration of SiO<sub>2</sub> particles, the core/shell structure microspheres can be formed with the densely packed SiO<sub>2</sub> particles film when oil-solute initiator azobisisobutyronitrile was used. The facile Pickering emulsion polymerization method hold great potential for the development of material science.

Yet another interesting example of the combination of particle and polymers is given by Huang *et al.* [78]. Bicontinuous jammed emulsions (bijels) can be formed with sub-micrometre

domains by using carboxylated NPs and amine-terminated polymer (**Figure 5**). The colloidal particles were bound to each other at the water/oil interface to create characteristic channel diameter (10  $\mu\text{m}$  or less). This protocol allowed the bijels system to be achieved by using different solvents, particles and functionalized polymers.

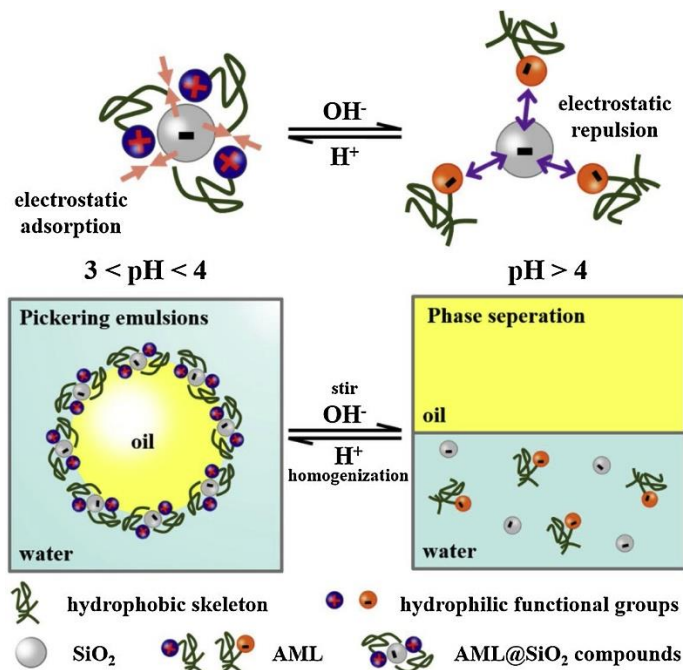


**Figure 5.** Schematic illustration of formation of bijels system prepared with particles and polymers irreversibly bound at the oil–water interface.

### 2.3.2. Biopolymer

Biopolymers are materials intentionally made from substances derived from plants or living organisms, such as protein and polysaccharides [79, 80]. The development of Pickering emulsion stabilized with biopolymer have received growing interest because the increasing demand for biodegradability and biocompatibility in food, personal care and medical applications [81, 82]. However, the formation of stable Pickering emulsion based on biopolymers are limited because normally the nature of biopolymer is very hydrophilic. The surface modification strategies is required to modify the wettability of biopolymer. The fusion of particles with biopolymers is considered as a facile alternative to chemical surface modification process for fabricating composites with enhanced performance. As an illustration, Lu *et al.* [83] reported that the surface of silica NPs can be *in situ* hydrophobized by the electrostatic adsorption of sustainable amphoteric lignin (AML) and enable them to stabilize pH-responsive in a narrow pH range from 3 to 4 (**Figure 6**). The positively charged phenylpropane backbone of AML was introduced to improve the interfacial activity of the negatively charged  $\text{SiO}_2$  particles because of the electrostatic interaction, which enhanced the

hydrophobicity and let the compounds adsorb at the oil/water interface. Above  $\text{pH} > 4$ , only a small amount of AML can be adsorbed onto the  $\text{SiO}_2$  surface due to their strong electrostatic repulsion leading to unstable emulsion.



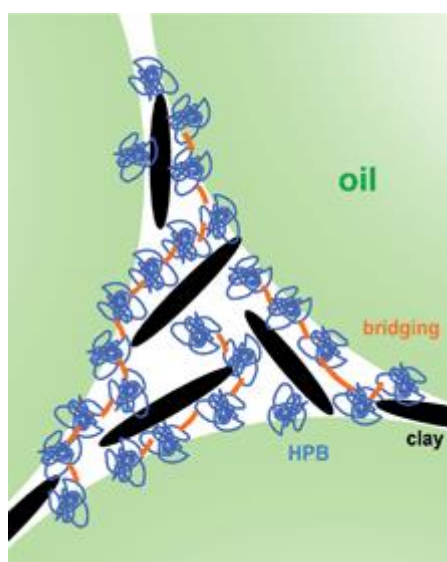
**Figure 6.** Schematic illustration of pH-responsive mechanism of emulsions stabilized by AML@ $\text{SiO}_2$  compounds. At  $3 < \text{pH} < 4$ , the positively charged AML molecule adsorbed at the surface of negatively charged silica by electrostatic adsorption. Upon increasing pH, phase separation is caused by both negatively charged AML and silica. (Ref 83 with permission from Elsevier)

Additionally, physical adsorption resulting from electrostatic interactions is a facile and feasible way for developing synergistic effect between solid particles and polymers. Huan *et al.* [84] investigated the combination of two oppositely charged nanopolysaccharides as emulsifiers for oil/water Pickering emulsions. The long-term stability of the emulsions under environmental stresses (pH and ionic strength) was enhanced as a result of the interfacial adsorption and distribution of cellulose.

A combination of protein and food-grade biopolymer particles (cellulose or starch) have been reported by Murray *et al.* [85]. The adsorbed film strength is increased in correlation with an increase of the stability according to the measurement of interfacial shear viscosity. The synergistic effect between protein and particles is responsible for the enhanced incorporation of

particles into the adsorbed layer, thus leading to the increase of the interfacial jamming of particles at the interface. In a similar way, Zembyla *et al.* [86] used a polyphenol-whey protein (WPI) complex between hydrophobic polyphenol particles and hydrophilic biopolymers (proteins). The results suggested that the main factors affecting complex formation and strength of the film is the electrostatic attraction between oppositely-charged polyphenol particles and proteins at the interface. The same phenomenon has been demonstrated by Jin *et al.* [87] with the use of soy protein to modify montmorillonite, from highly ordered to highly intercalated or fully exfoliated structures. The protein-coated clay took full advantage of the electrostatic attraction and hydrogen bonding at the interface, more than 90 % of protein bound with the clay at a mass ratio of 4:1.

Reger *et al.* [88] investigated the stabilization of emulsions using the *in situ* formed composite of hydrophobin H Star Protein B (HPB) and clay (Laponite XLG). On the basis of synergy interaction of two stabilizers, the hydrophobin-sandwiched clay particles act as sticky particles and form a three-dimensional network in the emulsions, which is favorable for the formation of gel-like emulsions (**Figure 7**). Especially, this clay–hydrophobin network does not only enhance the elastic properties of the gels but also improves the stability of emulsions.

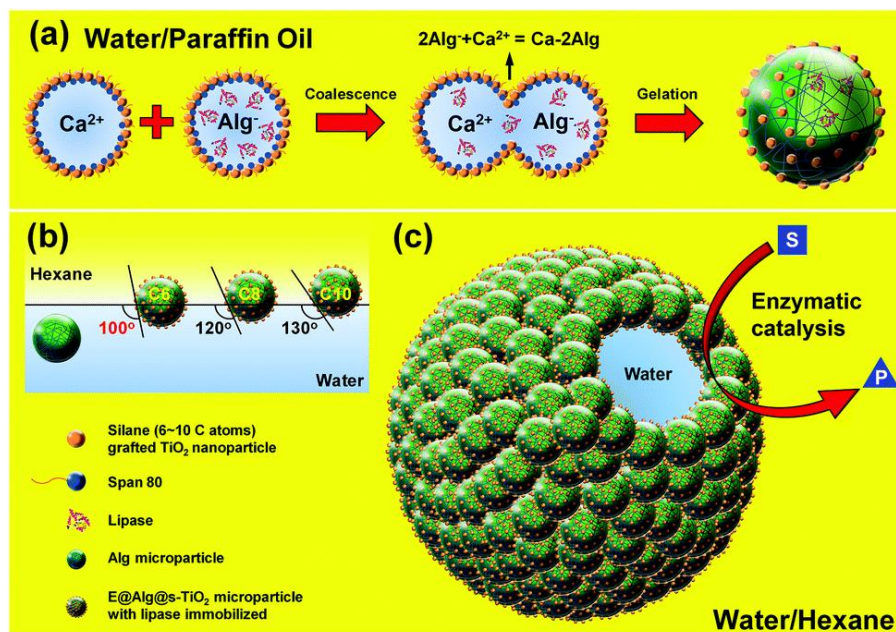


**Figure 7.** Schematic illustration of the self-supporting three-dimensional hydrophobin–clay network. The HPB molecules, clay, and the interaction between HPB are represented as a blue linear loop, black oval and orange line. (Ref 88 with permission from The Royal Society of Chemistry)

Han *et al.* [89] fabricated food-grade Pickering emulsions using all-natural cellulose nanofibrils (CNF) and nanocrystals (CNCs). Synergistic stabilization and tunable structures of Pickering emulsions were investigated by varying CNF concentration at a fixed CNCs concentration. Increasing CNF concentration, a dense network was formed in water phase to limit the motion of oil droplets, thus increasing the viscosity and stability of the emulsions. The synergism between nanocellulose exists and plays a crucial role in the properties of Pickering emulsion.

## 2.4. Particle/enzyme interaction

As the core of biocatalysis, enzymatic reaction opens the door to chemical industry for its higher efficiency and specificity as well as eco-friendly reaction conditions with less pollution and byproduct [90, 91]. The lipase, one of the most important enzymes, has been extensively explored for catalyzing a wide range of biochemical reactions (hydrolysis, transesterification/esterification, alcoholysis, or acidolysis). However, the application of free lipase is limited by its deficient activity, stability, and recyclability [92]. In particular, enzymes commonly present activity in aqueous media while the mass transfer of such systems is limited by the insufficient interfacial area in biphasic aqueous-organic reaction system. The combination of solid emulsifiers with enzyme is an emerging method for fabricating biohybrids that act as efficient interfacial biocatalysts that simultaneously stabilize emulsions and catalyze reactions at the water/oil interface. For example, enzymes have been immobilized in/on mesoporous silica [93], polymer [94], metal–organic frameworks (MOFs) [95], graphene oxide nanosheets [96], and Janus particles [97] for organic reactions at the water/oil interface. In such way, Yang *et al.* [98] prepared W/O emulsions stabilized with lipase-loaded alginate (Alg) microparticles with a coating of silanized titania NPs (E@Alg@s-TiO<sub>2</sub>). The wettability of E@Alg@s-TiO<sub>2</sub> can be adjusted by changing the chain length of grafted silane, thus endowing the formation of emulsion (**Figure 8**). The capsules containing the “immobilized” lipase are present on the surface of emulsion droplet and possess greater catalytic activity for the esterification of 1-hexanol and hexanoic acid in comparison with the free dispersion of lipase.



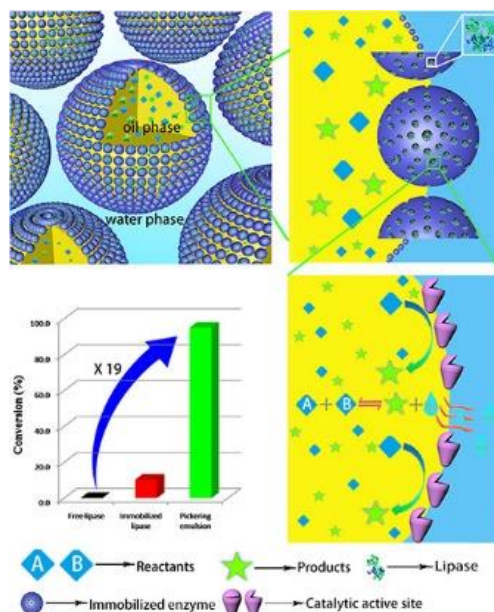
**Figure 8.** Schematic representation of emulsion stabilized with enzyme-immobilized surface-active alginate microparticles for interfacial biocatalysis: (a) E@Alg@s- $\text{TiO}_2$  microparticles is prepared through Alg gelation via coalescence of water/paraffin oil emulsion, (b) The wettability of E@Alg@s- $\text{TiO}_2$  microparticles is tuned by adjusting the chain length of grafted silane, (c) enzymatic catalysis at water/hexene interface. (Ref 98 with permission from Wiley)

Another example is illustrated with the enzymatic hydrolysis and esterification reactions performed in emulsions stabilized by the combination of lipase-coated silica NPs and surfactant N,N-dimethyldodecylamine [99]. In comparison with its traditional free lipase counterpart, the particle layer coated with the adsorbed lipase located at emulsion droplets interfaces maximizes the interfacial areas and improves mass transfer between the two phases, leading to a great improvement in catalytic performances.

The lipase has been also immobilized with clay particles by Li *et al.* [100] for further emulsion stabilization. The results showed that the immobilized lipase presented greater stability than the free lipase which might be attributed to a decline in the rate of denaturation of the enzyme as a result of fixation in the hydrophilic environment. It has been shown that the catalytic activity of emulsion stabilized by lipase/clay hybrid was more efficient and stable because of the three-dimensional structure of the enzyme for catalysis. Especially, there was a high level of activity after seven cycles, validating its ease of recovery and robust catalytic stability.



Dong *et al.* [101] used lipase AYS (*Candida rugosa*)-located mesoporous carbon nanospheres to stabilize emulsion, and studied the catalytic performances in phytosterol esterification/transesterification reaction system (**Figure 9**). The advantage of this method is that the presence of an oil-water interface to assist “lid” opening of lipase that allows to improve the catalytic efficiency. Moreover, the lipase-carbon nanosphere composite was easily recyclable because of the high mechanical and chemical stability of the carbon nanosphere.



**Figure 9.** Schematic illustration of conversion of phytosterol esters in O/W Pickering emulsion stabilized with lipase@MCS, and with the catalysis-lipase immobilized on the surface. Under stirring, the byproduct  $H_2O$  was removed automatically and thus would “push” the reaction forward. The conversion of phytosterol esters in Pickering emulsion system is 19-fold higher than free lipase one-phase system (Ref 101 with permission from the American Chemical Society).

## 2.5. Interfacial interaction with different types of particles

Considering that the properties of hybrid materials are strongly connected to the nature of the components and their interconnection, the fabrication of emulsifiers with various types of particles have been investigated to stabilize emulsions. Thus, different types of interfacial interactions may occur which such a design principle that leads to stabilization or destabilization of emulsions. For example, the addition of tannic acid (TA) to an emulsion stabilized by cellulose nanocrystals (CNC) and methylcellulose has been studied by Hu *et al.*

[102]. The emulsions prepared with the mixtures of CNCs and polymer can be transformed without oil leakage into solid dry emulsions *via* freeze-drying. These dry emulsion exhibit droplet coalescence within the solid matrix and thus cannot be redispersed in water. TA as an additional stabilizing agent imparts dispersibility to the dried emulsions thanks to the binding/adsorption of TA on MC-coated CNCs. The result showed that the synergistic interaction of cellulose nanocrystals, methylcellulose, and TA creates a dense, insoluble shell and stabilizes the emulsion during freeze-drying and redispersion processes. Jin *et al.* [103] investigated the formation of protein–polyphenol–polysaccharide nanocomplexes, and located at triglyceride oil/water interface to act as emulsifier. The study indicates that the interactions between ternary complexes would be dominated by hydrophobic interactions and hydrogen bonds. Their synergy in the formation of elastic film on the droplet surface leads to the decrease of the amount of emulsifier. The results showed that highly stable emulsions were achieved with the addition of 0.1 wt.% nanocomplexes, even at wide pH range from 1.5 to 7.5.

Wei *et al.* [104] prepared Pickering emulsion stabilized with zein colloidal particles (ZCPs), propylene glycol alginate (PGA), and rhamnolipid (Rha) and assessed how the stability, microstructure, rheology properties and *in vitro* gastrointestinal digestion are influenced by the addition sequence and stabilizers composition. They found that emulsions tend to be more stable when PGA was added first and then Rha, while the capacity of delaying lipolysis is improved with the coexistence of ZCPs, PGA, and Rha.

Compared to emulsions stabilized by surfactant–polymer systems, the emulsions studied by Sharma *et al.* [105] provide remarkably stable viscoelastic behavior at high pressure and high temperature conditions. Indeed, the addition of NPs provides a steric resistance against pressure induced droplet flocculation. Such property lets indicate its suitable use for oil field applications.

Interfacial interactions can be adjusted on demand with switchable Pickering emulsions. As example, Xu *et al.* [106] reported switchable emulsions with positively charged alumina NPs and anionic surfactant sodium dodecyl sulfate (SDS) and CO<sub>2</sub>/N<sub>2</sub>-responsive surfactant

N'-dodecyl-N,N-dimethylacetamide (DDAA). The hydrophilic alumina NPs are *in situ* hydrophobized by the adsorption of SDS molecules on their surface. Once the emulsion is formed, some CO<sub>2</sub> is bubbled. DDAA switches to the cationic amidinium form and forms ion pairs with the SDS molecules. It results in the destabilization of the emulsion.

### 3. Physicochemical properties of Pickering emulsions

Whatever the synergy nature involved in the stabilization of Pickering emulsions, the design of the synergistical combination of materials is crucial in order to finely tune the physicochemical properties of the emulsions: droplet size, stability, emulsion type, phase inversion, *etc...*

#### 3.1. Droplet size of Pickering emulsions

When several components are combined into a synergistic composite designed for emulsion stabilization, the size of the droplets can be modified in comparison with individual components. In this purpose, Jiang *et al.* [107] prepared a paraffin oil / water emulsion with silica particles in combination with Span 80 and Tween 80 surfactants for wood impregnation. Based on the partially hydrophobized silica particles by the surfactants on the surface, the stability of the obtained emulsions has been improved and the droplet size has been decreased. The synergistic effect of the hydrophobicity of paraffin oil combined with the nano-effect of the silica particles allow the authors to perform wood impregnation and the properties of the impregnated wood benefit from the reduced water absorption, improved mechanical properties and thermal stability.

The combination of different type of particles allows the stabilization of emulsion as proposed by Wang *et al.* [108] silica / calcite particles mixture. It has been showed that the increase of silica content in the particles mix decreases the stability and the droplet size of the emulsions. Because the silica NPs were too hydrophilic, they can easily be desorbed from the interfaces, while the density of the particles at the interfaces of the Pickering emulsions

decreased, the stability of the emulsions also decreased. Moreover, they demonstrated that larger silica particles were more easily adsorbed at the O/W interface and had more notable effect on the emulsion stability. This can be explained by the higher adsorption energy of a particle at the oil-water interface.

### 3.2. Stability of Pickering emulsions

Pickering emulsions present a superior stability compared to their surfactant-stabilized counterparts. Their high stability is one of the significant advantages for their use in a variety of industries spanning fields, such as food storage and bitumen emulsification. However, only temporary stability may be required in others cases, such as liquid phase heterogeneous catalysis and enhanced oil recovery. However, the use of Pickering emulsions stabilized with a single stabilizer is limited for practical applications because complex function is necessary. The overall performance of solid emulsifier is expected to achieve further improvements based on the synergistic effects by integrating the advantages of different components.

Monoolein is a lipid based on a glycerol backbone functionalized with a hydrocarbon attached through an ester bond. With a hydrophilic-lipophilic balance (HLB) of 3.8, the molecule is considered as amphiphilic. Monoolein is insoluble in water but highly soluble in oil which is interesting for drug delivery, emulsion stabilization [109]. Pichot *et al.* [110] investigated the stability of O/W emulsions in the presence of both monoolein and colloidal particles. The results showed that monoolein plays a key role in the initial “delay” of the coalescence phenomena and induces further droplet break-up by rapidly covering the created interface and reducing interfacial tension. Thus it allows the silica particles to assemble at the oil/water interface and provide long-term stability of the emulsion.

Gao *et al.* [111] evaluate the synergistic effect of the addition of polysaccharide combined with ultrasound treatment on the stability of low-salt myofibrillar protein. Both neutral polysaccharide guar gum and cationic polysaccharide chitosan are studied. Because of the formation of protein-polysaccharide agglomerates induced by high energy ultrasound, the thickness of the interface film and electrostatic repulsion is increased, resulting in higher

stability emulsion.

Wang *et al.* [112] investigated the formation of Pickering emulsion gel using the negatively charged palygorskite NPs (PAL) and cationic surfactant cetyltrimethylammonium bromide (CTAB). The emulsion ration was higher, and the stability under various environmental factors was better. The researchers demonstrate that the self-assembly of CTAB-PAC in the continuous phase can generate a three-dimensional network structure.

Yang *et al.* [113] revealed the synergistic interaction between stearyl trimethyl ammonium chloride modified montmorillonite NPs (STAC/MMT) and Tween 85 on nano-emulsion stability. It has been demonstrated that the emulsion prepared by STAC/MMT and Tween 85 had a better static stability and centrifugal stability. The addition of surfactant can reduce the oil-water interfacial tension of the emulsion and change the wetting properties of the particles, thus enhancing the stability of the emulsion. Surprisingly, the oil phase composition (Vitamin E-to-mix oil phase ratio) has important effect on emulsion stability because the viscosity of oil phase increased as the Vitamin E ratio increased, and the interaction between solid particles and oil phases. The emulsion stability can be also increased by the use of nanogel as stabilizer. Atarian *et al.* [114] have prepared sunflower oil / water emulsions stabilized with chitosan (CS)-stearic acid (SA) nanogels. Such nanogels are formed by the connection between the amine groups of CS and the carboxylic acid groups of SA. The authors revealed that the emulsion stability was significantly increased with higher SA/CS ratios because of the reduction of positive charges and the increase hydrophobicity of CS. This is due to the increase of the amide linkages by increasing the SA content. Especially, the emulsions stabilized by CS-SA nanogels present more oxidative stability compared with the emulsions stabilized by Tween 80.

It has been demonstrated that starch can be used to stabilize emulsions but also as co-stabilizer [23]. Cazotti *et al.* [115] revealed that the *in situ* surface modification of starch NPs (SNP) by the adsorption of styrene oxide (STO) could effectively stabilize Pickering mini-emulsions. The obtained PS latex particles were nearly one-to-one copy in size to the initial monomer droplets, confirming the successful stabilization of the mini-emulsion by SNP-STO.

Their work indicated a synergistic effect between the low water solubility of styrene and SNP-STO because of the interaction between the aromatic rings present on both styrene and modified SNP-STO. Song *et al.* [116] prepared sunflower oil/water emulsions by using modified starch particle and small molecular surfactants (*e.g.* sodium dodecyl sulfate, cetyltrimethylammonium bromide and Tween 20) as stabilizers. The authors observed that the addition of starch particles provides an interfacial film around each oil droplets and hinder the access of free radicals in the chain reaction indicating a decreasing rate of oxidation. In addition, the unabsorbed particles and surfactants were present at the continuous phase, increasing the viscosity of the emulsion system and decreasing the diffuse of pro-oxidants. The results imply that starch particles are compatible with anionic surfactants, and can enhance the physical and oxidative stabilities, which is promising for future applications of food dispersions to deliver functional ingredients into emulsions.

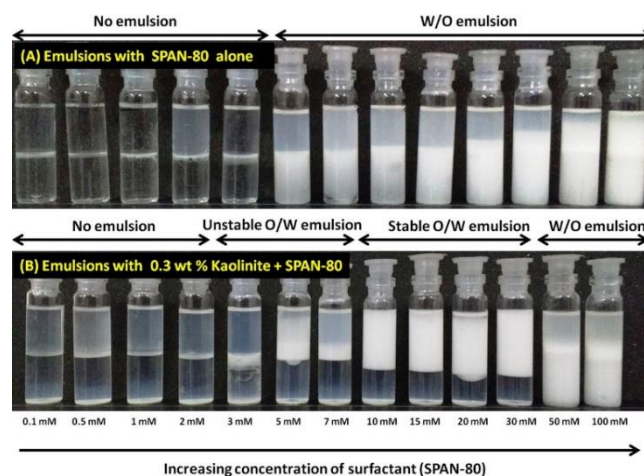
Hu *et al.* [117] prepared gel-like Pickering emulsions with hybrid  $\beta$ -cyclodextrin/short linear glucan NPs ( $\beta$ -CD/SLG). The results demonstrated that the homogeneously distributed  $\beta$ -CD in hybrid  $\beta$ -CD/SLG NPs plays important role in enhanced water dispersity, accelerated adsorption, and reduced interface tension during the emulsification process, while the addition of SLG fractions strongly ensured the emulsions with constant creaming index values for long-term storage.

Guo *et al.* [118] stabilized a trigger-responsive Pickering emulsion with silica NPs and commercial N,N-dimethyl-N-dodecyl amine surfactant ( $C_{12}$ -A). In this procedure,  $C_{12}$ -A was transformed into  $C_{12}$ -CO<sub>2</sub> with positive charge after exposure to CO<sub>2</sub>. The surface of silica NPs was modified with  $C_{12}$ -CO<sub>2</sub> to render it hydrophobic through electrostatic attraction. The resulting emulsion can be maintained stable for more than 6 months with CO<sub>2</sub>, and then be quickly destabilized after bubbling N<sub>2</sub> or by adding NaOH.

### 3.3. Emulsion types and phase inversion of Pickering emulsion

The emulsion type is determined by the wettability of the solid particle. O/W emulsions are stabilized by hydrophilic particles while W/O emulsions are stabilized by hydrophobic

particles. The natural NPs (such as silica, TiO<sub>2</sub> and clay) are typically too hydrophilic to form stable emulsion. The surface of these particles can be modified by grafting of functionalized substances according to well-established protocols. The wettability of NPs can be adjusted with a balance between the functional substances and the NPs properties. In particular, NPs can be shuttled between a hydrophilic and a hydrophobic state through the compatible interactions between surfactant and particles. The synergistic interaction between CaCO<sub>3</sub> NPs and sodium dodecyl sulfate (SDS) in emulsification process were investigated by Cui *et al.* [119]. With the increased surfactant content, a phase inversion was observed from O/W → W/O → O/W. The results suggested that the adsorption of surfactant on particle surfaces initially increases their hydrophobicity, and thus, induces the first inversion (O/W → W/O). The further adsorption of surfactant forms a bilayer that renders particles more hydrophilic again and induces the second phase inversion (W/O → O/W). Also, the threshold amount of surfactant concentration must be reached for some NPs / surfactants system.

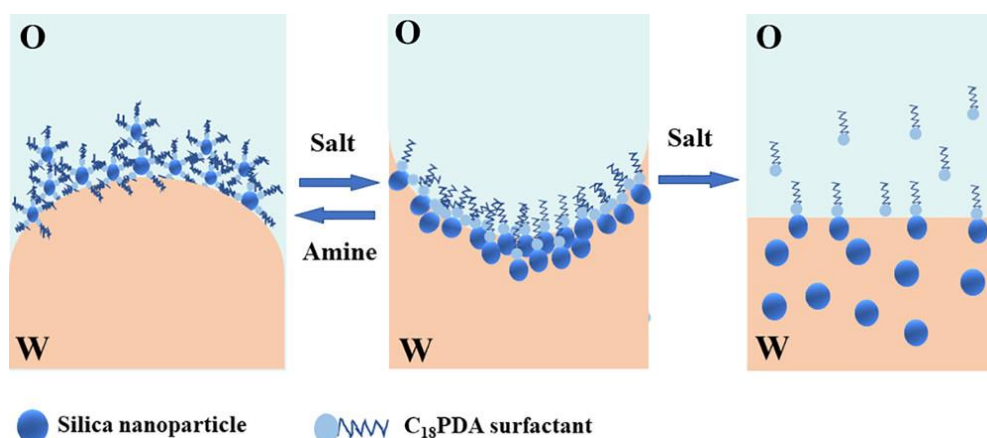


**Figure 10.** (A) W/O emulsions stabilized solely by pure SPAN-80. (B) Emulsions formed when a combination with varying quantity of SPAN-80 and fixed quantity of kaolinite (0.3 wt.%) was used. Photographs were taken one hour after emulsion preparation. (Ref 120 with permission from Elsevier)

In this direction, Nallamilli *et al.* [120] prepared decane / water emulsion stabilized by a combination of nonionic surfactant Span-80 and kaolinite NPs. They observed no stable emulsions formed at SPAN-80 concentrations < 3 mM, while stable W/O emulsions are formed above 5 mM (**Figure 10**). When emulsions formed by a combination with different quantity of

SPAN-80 and fixed quantity of kaolinite (0.3 wt.%), no emulsions were stable at concentration below 3 mM, unstable O/W emulsions formed at concentration between 5 mM and 7 mM, stable O/W emulsions formed at concentration between 10 mM and 30 mM. Interesting, a phase inversion from O/W to W/O occurs at high SPAN-80 concentrations. This phase inversion was attributed to the competitive adsorption of excess SPAN-80 on droplet while the bilayer-covered particles remain dispersed.

The addition of salt can modify the surfactant / NPs equilibrium as demonstrated by Liu *et al.* [121] with a Pickering emulsion stabilized by the adsorption of N-(2-((2-aminoethyl) amino) ethyl)octadecenamamide ( $C_{18}$ PDA) surfactant onto silica surfaces with  $Na_2CO_3$  addition. Under low surfactant concentration, the attractive interaction between silica NPs and surfactant is slightly reduced as the hydration repulsive forces increase with the increase of salt concentration that renders the particles hydrophilic (formation of O/W emulsions). Therefore, with different surfactant concentrations and salt addition, the silica-stabilized emulsions undergo phase inversion from O/W to W/O or vice versa (**Figure 11**). Under high salt concentration, silica NPs are observed to be partially dispersed in the water phase because of the increased interaction energies and the significantly decreased degree of flocculation, which induces the destabilization of emulsions.

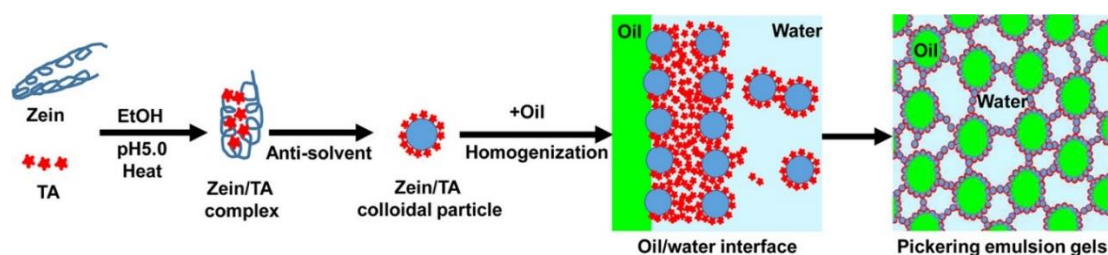


**Figure 11.** Schematic illustrations of the relationship between silica flocculation induced by  $C_{18}$ PDA and the corresponding emulsion formation. W/O emulsion stabilized with silica and  $C_{18}$ PDA, O/W emulsion is formed when the attraction between the silica NPs and  $C_{18}$ PDA is decreased by salinity. (c) No emulsion is formed at high salinity because the attractive interaction between silica and  $C_{18}$ PDA is largely reduced (Ref 121 with permission from Elsevier).



### 3.4. Rheology properties of Pickering emulsions

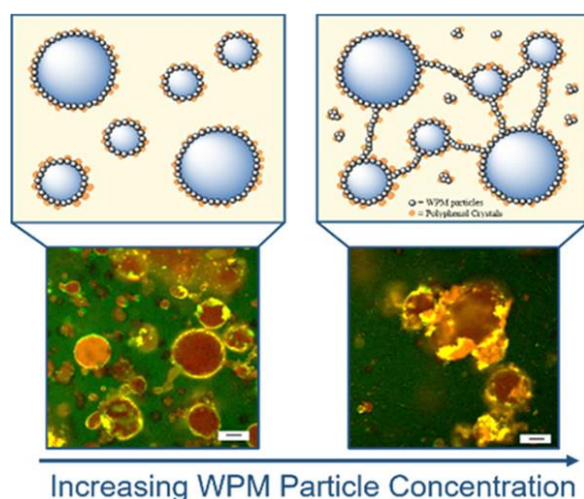
Understanding the rheological properties of Pickering emulsions is critical for their application, especially in related food processing, which required outstanding stability during storage, freeze-thawing, and heating processes [122]. Zou *et al.* [123] prepared edible emulsions stabilized by a zein/tannic acid complex colloidal particle (ZTP). Based on an antisolvent approach and hydrogen bonding interaction between zein and tannic acid (TA), the ZTP colloidal particles can be formed with near-neutral and enhanced interfacial reactivity. These interaction triggers cross-links between the ZTP particles to form a continuous network between the oil droplets, rendering the fabrication of stable emulsion gels (**Figure 12**). Lay-by-lay interfacial architecture on the emulsion droplets surface is observed, which suggested the formation of hierarchical interface microstructure by modulating the noncovalent interactions between TA and zein.



**Figure 12.** Schematic illustration of the preparation of emulsions gels stabilized with zein/tannic acid complex colloidal particles. The synthesis of zein/TA complex is performed at pH 5.0, then zein particles are coated by TA via an antisolvent method to form zein/TA colloidal particles. These particles are then used to form Pickering emulsion gels. (Ref 123 with permission from the American Chemical Society)

Bai *et al.* [124] studied the parameters that affect the depletion effect in emulsion stabilized by two types of nanocellulose. The addition of CNF changed the viscosity and viscoelastic properties of water phase, which generates an attraction between droplets. Therefore, three regimes of concentration-dependent depletion stabilization were presented, including (1) creaming of non-flocculated droplets at low cellulose nanofibrils concentration, (2) flocculation at intermediate cellulose nanofibrils content and, (3) stabilization of the emulsions with characteristic micron-sized droplets at the highest cellulose nanofibrils concentrations.

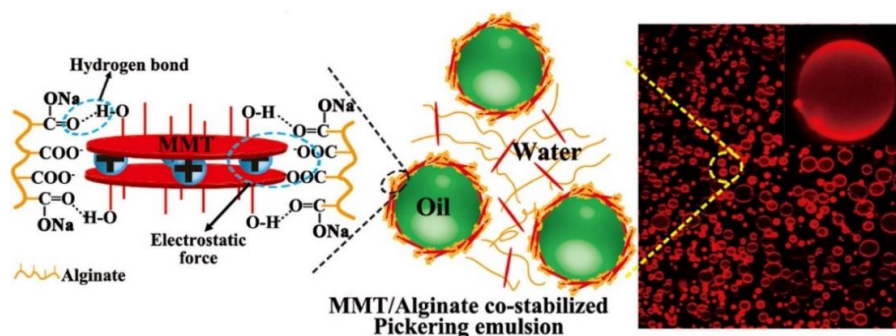
Zembyla *et al.* [125] stabilized emulsions with the formation of particle-particle complex at the W/O interface (**Figure 13**). A kind of double Pickering stabilization occurs: polyphenol particles adsorb at the interface from the oil side and whey protein microgel (WPM) particles adsorb at the interface from the aqueous side. In this case, the results showed that the synergistic interactions between particle-particle complex result in the formation of viscoelastic film on the oil-water interface, allowing the formation of stable droplets fully covered by a dense and uniform monolayer of microgel particles. The authors also studied the effect of whey protein particles concentration, and demonstrated that the WPM can act as a “colloidal glue” between the water droplet and polyphenol crystals at higher concentration, giving a significant improvement in the stability of emulsion.



**Figure 13.** Schematic representation of the influence of whey protein microgel (WPM) concentration in the particle-particle complex-stabilized emulsion. At low concentration of WPM, both polyphenol crystals and WPM particles coexist at the interface of the droplets; at high concentration of WPM, the WPM particles tend to aggregate with polyphenol crystals at the interface and between the water droplets. (Ref 124 with permission from the American Chemical Society)

Wang *et al.* [126] demonstrated synergistic stabilization of a novel Pickering emulsion by two negatively charged particles: alginate and montmorillonite (MMT). The adsorption of alginate molecular chains on the surface of MMT occurs through hydrogen bonding and electrostatic interaction, which not only enhances the dispersion of MMT NPs, but also improves the stability of the emulsion (**Figure 14**). Moreover, the viscoelasticity of the

emulsion was increased with the addition of alginate, thus rendering a gel-like continuous phase around the droplets which prevents the coalescence of droplets.



**Figure 14.** Scheme of MMT/Alginate co-stabilized emulsion. Alginate molecular chains are adsorbed on the surface of MMT via hydrogen bonding and electrostatic interaction, providing a three-dimensional network in the continuous phase. (Ref 125 with permission from Elsevier)

#### 4. Mechanism of synergism at the Pickering emulsion

Recently, many efforts have been directed to prepare NPs-based composite, aiming not only to improve the compatibility of NPs with other components but also to take advantage of the multifunctionality and enhanced properties of NPs for better emulsifiers. In particular, in order to combine substances of interest with NPs, the interactions should be carefully chosen based on the physicochemical properties. However, few mechanisms were proposed to explain the synergistic interaction between NPs and their co-stabilizer for efficient composite emulsifiers to stabilize emulsions.

##### 4.1. Wettability alteration

It is well known that the surface activity of solid particles mainly depends on the surface wettability. These two factors are important for the preparation of Pickering emulsions. Native NPs without modification may not act as emulsifiers or, at the best, stabilize emulsion with low efficiency. The adsorption of surfactants or NPs - through electrostatic attraction or hydrogen bonding interaction - onto the solid surface can efficiently modify the wettability of NPs. So, the modified particles preferentially stay at the oil/water interfaces and correspondingly bring out stable emulsion. As illustration, Binks *et al.* [127] developed a route for the fabrication of

O/W emulsions, through the combination of hydrophilic silica particles and the dissolved adipate esters in the aqueous phase. The *in situ* hydrophobization of silica particles with oil molecules is attributed to the formation of H-bonds between the carbonyl group of oil molecules and the hydroxyl group on particle surfaces, which enable them to stabilize emulsion.

Yan *et al.* [128] prepared CO<sub>2</sub>-responsive Pickering emulsion stabilized by biosourced maleopimaric acid glycidyl methacrylate ester 3-(dimethylamino)-propylamine imide (MPAGN) surfactant and silica NPs. After CO<sub>2</sub> bubbling, the nonionic MPAGN was transformed into the active cationic form, which can adsorb onto the surface of negatively charged silica NPs via electrostatic interactions. More interestingly, the destabilization of emulsions can be achieved with N<sub>2</sub> bubbling because the electrostatic interaction vanishes between NPs and surfactant.

Binks *et al.* [129] prepared emulsions stabilized by a mixture of oppositely charged silica NPs and alumina-coated silica NPs. It has been determined that the mixture of two particles types at certain amount leads to heteroaggregation and the decrease of net charge, which are capable of forming stable O/W emulsion with excellent coalescence stability. Moreover, the increased viscosity of the aqueous phase also plays an important role in the stability of emulsion. Similar results have also been reported for two types of oppositely charged polystyrene latex particles, in which the mixture of two particles are able to form emulsion with excellent stability [130]. Dechézelles *et al.* [131] developed alumina-functionalized ordered SBA-15 particles, which can be used to produce water/toluene emulsions. The results indicated that the emulsion stability comes from a synergetic effect coming from the mesopores, stabilization through interparticle capillary attractions, and the presence of a rough surface composed of alumina/silica phases.

An investigation was performed on the influence of the adsorption of anionic (SDS), cationic (CTAB), and nonionic (C<sub>12</sub>E<sub>5</sub>) surfactants on the surface of anionic silica NPs [132]. CTAB gives good adsorption and decreases the effective charge of the complex. It is noteworthy that the increase of CTAB concentration induces the aggregation of silica and a subsequent

destabilization of the emulsion. The combination of SDS molecules and silica NPs gives a supercharged system by increasing the effective charge of silica, which contributes to the increasing electric repulsion between particles. The effective charge on the particles does not show any appreciable change when nonionic surfactant is added, and the interaction between SDS and silica NPs result in the formation of very stable internally nanostructured emulsions with a mean diameter of 400 nm.

In addition to using electrostatic interaction effect, weak interaction such as hydrogen bonding is popular in the fabrication of Pickering emulsion for enhanced properties. Sieben *et al.* [133] described that raw kaolinite NPs, with *in-situ* addition of oleic acid, were utilized to achieve oil/water Pickering emulsion with better stability and higher emulsion volume. The synergistic interaction of kaolinite and oleic acid can change the wettability of the particles due to the hydrogen bonds and electrostatic interactions.

The mechanism of the synergism between the surfactant and silica NPs was explained by Bazazi *et al.* [134]. They used hydrophilic silica nanoparticles dispersion in combination with span micellar solution as emulsifier to *in-situ* generate double emulsion. The dynamic interfacial tension (IFT) measurement was used to understand the span-silica interaction. They found that the association between span and silica is attributed to the hydrophobic interaction and hydrogen bonding. The swollen span micellar solution form microemulsion, while the silica NPs gradually became surface-active by the adsorption of span and form a core-shell emulsion.

Xie *et al.* [135] developed a dual-responsive emulsion micro-reactor by combining light-sensitive titania (TiO<sub>2</sub>) and superparamagnetic iron oxide (Fe<sub>3</sub>O<sub>4</sub>) NPs as emulsifiers. The co-adsorption of partially hydrophobic TiO<sub>2</sub> and partially hydrophilic Fe<sub>3</sub>O<sub>4</sub> NPs at oil/water interface is triggered by van der Waals forces, which formed the liquid oil film between the squeezing interfaces thins. Under a desired position and time in a non-intrusive way, the obtained emulsion provides a smart platform for chemical reaction with responsive ability.

## 4.2. Increment in viscoelasticity

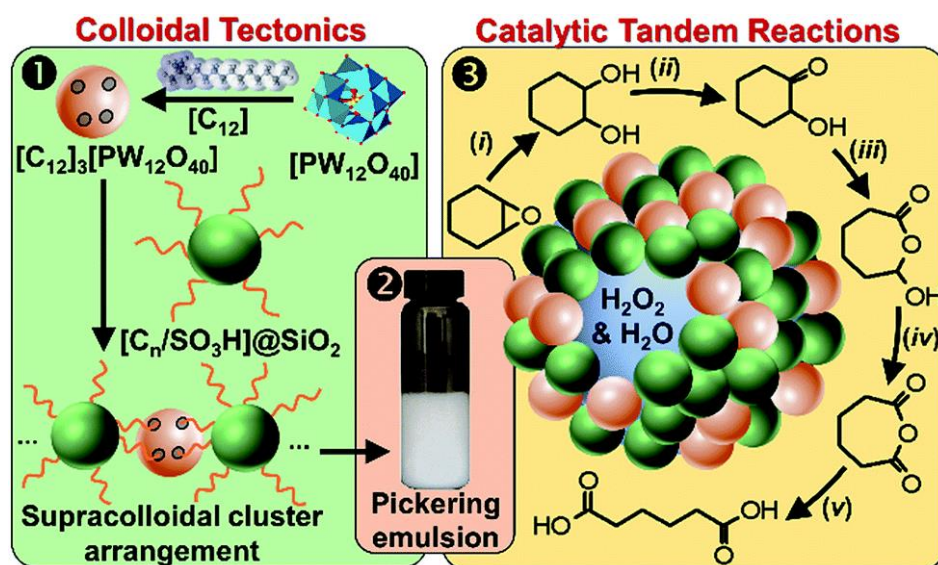
The viscoelastic behavior of emulsions can be adjusted in order to make them suitable with some applications such as cosmetic or oil recovery. Pi *et al.* [136] successfully fabricated oil-in-sea water emulsion stabilized with the mixture of xanthan gum (XG) and silica NPs. XG and silica NPs act synergistically to increase the viscoelasticity of the continuous phase and form a thick layer at the droplet surface. The latter prevents the coalescence and the creaming of droplets, which contribute to the formation of emulsion with smaller droplet size and greater stability. Notably, the required amount of XG and silica NPs for effective oil dispersion is significantly low thanks to the synergy of XG and silica NPs, which would reduce the potential adverse environmental impacts. The synergistic interaction between silica NPs and an oil-soluble amine surfactant has been studied by Whitby *et al.* [137] to form emulsion. They studied the synergistic interaction between silica NPs and an oil-soluble amine surfactant for the formation of viscoelastic composite layer at the O/W interface. The results showed that the adsorption of surfactant on the surface of the silica can reduce the surficial tension, as well as increase the particle hydrophobicity. The synergy between silica and surfactant contribute to the increase in the dilational viscoelasticity, and by the formation of networking between surfactant-coated particles, which produce an interfacial layer with non-Laplacian rheology.

## 4.3. *In situ* formation of Pickering interfacial catalyst

Pickering interfacial catalysis (PIC) concept appears as a promising solution to improve the catalytic performance of biphasic reaction system and to enhance mass transfer between substrates with opposite polarity [49]. In a PIC system, NPs can simultaneously act as emulsifiers and interfacial catalysts located at the oil/water interface. Hybrid NPs present better performance in various applications, particularly in the field of heterogeneous catalysts. These multifunctional catalysts can promote tandem or cascade reactions, where two or more individual reactions are combined in a single process. Especially, the development of PIC systems based on two types of NPs relying on the colloidal tectonics approach [138]. This approach is to determine how to use attractive forces to control molecular self-assembly and

produce new colloidal system with predetermined functions. In the case of catalytic system, the colloidal tectonics approach allows the formation of intermediate systems between homogeneous and heterogeneous mixtures from macroscopic and microscopic point of view, thus combining the properties of homogeneous and heterogeneous catalysis.

Stabilization of emulsion by the combination of dodecyltrimethylammonium phosphotungstate NPs  $[C_{12}]_3[PW_{12}O_{40}]$  and silica particles functionalized with alkyl and sulfonic acid groups  $[C_n/SO_3H]@SiO_2$ , based on the colloidal tectonics approach (**Figure 15**) has been studied by Yang *et al.* [139]. Especially, the porous  $[C_{12}]_3[PW_{12}O_{40}]$  NPs allow the accommodation of  $C_{18}$  chains belonging to  $[C_{18}/SO_3H]@SiO_2$ , leading to their interlocking. The synergistic interaction between two stabilizers determines the droplet size and the emulsion stability. Such emulsions show high efficiency for the conversion of cycloalkene oxides into diacids with aqueous  $H_2O_2$  combining the advantages of biphasic catalysis and homogeneous catalysis without their limitations.



**Figure 15.** Schematic illustrations of catalytic tandem reaction for the adipic acid synthesis by using  $[C_{18}/SO_3H]@SiO_2$  and  $[C_{12}]_3[PW_{12}O_{40}]$  nanoparticles both as catalyst and emulsifier. The self-assembly of two NPs driven by partial penetration of the alkyl chains of  $[C_{18}/SO_3H]@SiO_2$  into  $[C_{12}]_3[PW_{12}O_{40}]$ . (Ref 139 with permission from the Royal Society of Chemistry)

Recently, PIC concept has been adapted into Pickering interfacial biocatalysis (PIB), in which biocatalysts and solid emulsifiers are combined. Sun *et al.* [140] developed a PIB system based on recyclable enzyme–polymer composites that acted as both catalytic sites and

stabilizers at water/oil interface. The combination of enzyme and polymer preserves the enzyme structure, and the resulted emulsion system presents a significantly larger interfacial area. Moreover, the presence of biocatalysts at the interface let to a 270-fold improvement of the catalytic performance in comparison with a conventional biphasic system.

#### 4.4. Film formation

Dried or solid O/W emulsions have received significant interest for different applications such as drug delivery, food industries, paints and cosmetics. O/W emulsions can be dried by freeze/spray-drying for the preparation of oil powders. This process allows to obtain powders without oil leakage and to increase the shelf life of dispersed oil which is convenient for storage and transportation. Narukulla *et al.* [141] employed tannic acid (TA) and polyacryloyl hydrazide (PAHz)-Ag NPs to stabilize emulsions. The presence of TA reduces the concentration of PAHz, decreases the droplet size and enhances the emulsion stability. Especially, the obtained emulsions exhibit both freeze drying and re-dispersibility with containing nearly 98% oil. The synergy effect between TA and PAHz-Ag NPs is mainly due to the hydrogen bonding interaction and hydrophobic interaction with oil droplets. The as-obtained Pickering emulsions show increased stability.

Gao *et al.* [142] prepared emulsions with superior stability, through *in situ* modification of protein particles with small molecular weight surfactant sodium stearate (SS). The results presented an enhanced adsorption and targeted accumulation of zein particles at the interface with increasing SS concentration. Partial unfolding of zein particles modified by SS above its critical complexation concentration triggered the aggregation and close packing of particles at the oil/water interface, thus significantly improving the surface particle coverage and promoting efficient packing of zein particle at the interface. Moreover, protein-based oil gels without oil leakage were obtained by one-step freeze-drying of the zein-stabilized emulsions.

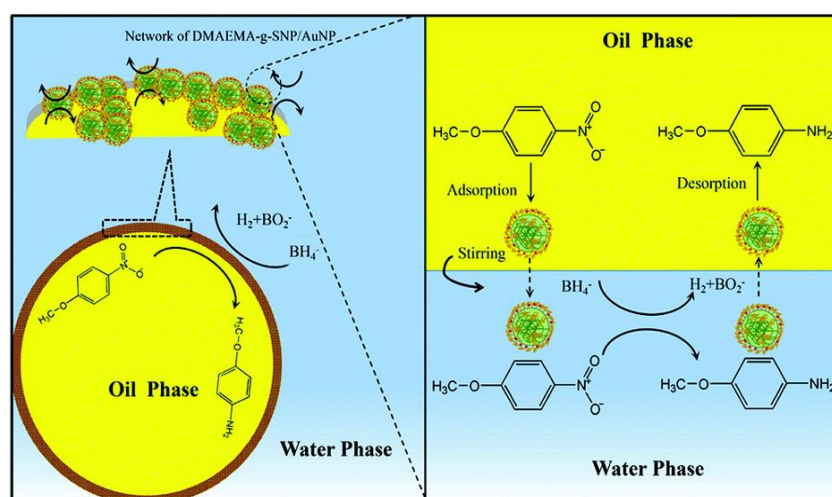


## 5. Applications of Pickering emulsions

The choice of each component of multi-compositional NPs as emulsifiers gives the opportunity to offer multiple applications, such as catalysis, photocatalysis, biomedical, etc. In the following section, it is discussed the combination of particles with different substances used to form “smart” emulsions for various applications.

### 5.1. Catalysis

Biphasic conditions are often required for catalytic reactions, and the use of emulsions for catalysis provide larger interfacial areas when compared to traditional reaction systems. Among them, many attempts have been performed to use metal NPs into a composite to achieve synergistic functionalities.



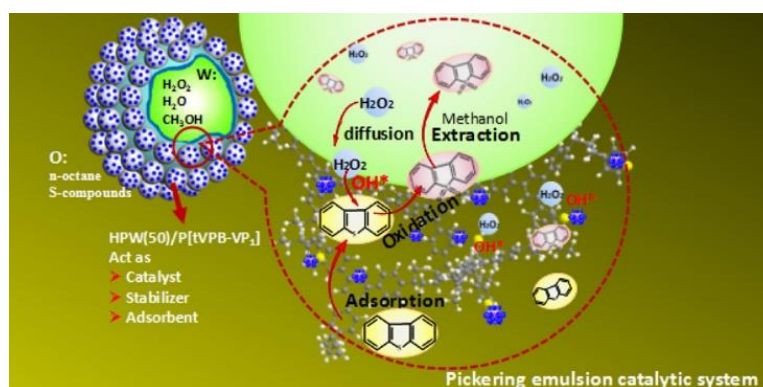
**Figure 16.** Schematic representation of emulsion stabilized by starch-based NPs and gold NPs. Demulsification occurs under acidic condition with the tertiary amines protonation that renders the surface hydrophilic and allows the NPs to desorb from the oil–water interface. Under basic condition, the deprotonation of amines makes the surface more hydrophobic and the re-adsorption at the interface takes place. (Ref 143 with permission from the Royal Society of Chemistry)

Qi *et al.* [143] utilized starch-based NPs and gold NPs as multifunctional emulsifiers (D-g-SNP/AuNP) to stabilize pH-responsive emulsion (**Figure 16**). The obtained emulsions act as catalytic micro-reactors for catalytic hydrogenation of *p*-nitroanisole to *p*-anisidine. The yield

obtained by the D-g-SNP/AuNP stabilized O/W emulsion was as high as 95%, outperforming the monophasic system or planar interface system. These excellent catalytic performances are due to the hydrophobic catalyst surface and the enhanced contact region, which facilitates the adsorption of the reactants onto the catalyst surface and the increased mass transfer frequency.

Xue *et al.* [144] have employed graphene-based NPs/palladium NPs (Pd/GO-Si) to form emulsions for the selective hydrogenation of cinnamaldehyde (CAL) to hydrocinnamaldehyde (HCAL). The graphene modified by organic silicane permits to enhance the lipophilicity of the surface, and promotes the adsorption of reactants at the Pd/GO-Si-stabilized emulsion interface. Based on the synergistic effect of graphene-based NPs and Pd NPs, the system presents high catalytic activity with yield of 83 % in 20 mins. The catalyst has been conveniently recycled for at least four times with no significant reduction in activity.

Xia *et al.* [145] synthesized amphiphilic catalysts HPW/P[tVPB-VP1] by loading phosphotungstic acid (HPW) NPs onto pyridine-based polymer (P[tVPB-VPx]) NPs. Different from the traditional amphiphilic catalysts, the polymer network structure of P[tVPB-VPx] ensures the absorption of dibenzothiophene (DBT) (**Figure 17**). The as-obtained amphiphilic HPW(50)/P[tVPB-VP1] presents ultra-fast and deep oxidative desulfurization rate, giving complete conversion of DBT from within 15 min at 60 °C. The satisfying results are explained by the catalyst that can assemble at the oil-water interface, which provides a fastest reaction dynamics.



**Figure 17.** Schematic illustration for simultaneous oxidation and extraction desulfurization in emulsion catalyzed by HPW(50)/P[tVPB-VP1] which also acts as emulsifiers and adsorbent. (Ref 145 with permission from the American Chemical Society)

The influence of particle wettability and concentration on the enzymatic catalytic reaction has been studied by Rodriguez *et al.* [146]. They compared the catalytic performance of aldoxime dehydratase in the enzymatic dehydration of n-octanaloxime to n-octanenitrile in both emulsion type (W/O and O/W). This study highlight that the emulsion type can affect the conversion of catalytic reaction.

Janus particles – in reference of the double-faced Roman god - have been extensively investigated in recent years because of their asymmetric structures or functionality and diverse potential applications. Dou and Wang [147] synthesized carbon-silica Janus particles containing phosphotungstic active component as solid emulsifiers for Pickering emulsion. Such system showed an excellent catalytic performance for oxidative desulfurization (99.86% obtained under the optimal condition). Here, the existence of phosphotungstic component acts as the active centers for the oxidation, whereas the considerable large interface between the extractant and oil promotes the extraction process and the contact area of catalyst and reactants.

## 5.2. Photocatalysis

One important issue in the synthesis of photocatalytic material is to increase photoactive material absorption in the visible light range and hot-electron transport to the reaction sites. Li *et al.* [148] provided a novel method to form emulsions through unmodified TiO<sub>2</sub> particles (**Figure 18**). In dye-contained wastewater, the adsorption of dye molecules (reactive brilliant red X<sub>3</sub>B, methyl orange, Congo red, and orange G) with characteristic sulfonate groups on the surface of TiO<sub>2</sub> particles leads to enhanced hydrophobicity of the particle surface and stabilize emulsion. The results show that the prepared system significantly enhances the efficiency of the photocatalytic degradation of the dyes in comparison with the non-emulsified system. The material also shows a good recyclability for re-use under long-time irradiation.



**Figure 18.** Schematic representation of photocatalytic dye degradation in O/W Pickering emulsion stabilized by commercial  $\text{TiO}_2$  NPs. The dye molecules attached on the surface of  $\text{TiO}_2$  and tuned its wettability to be an emulsifier. (Ref 148 with permission from Elsevier)

Chen *et al.* [149] prepared imprinted photocatalyst ZnO/GO-MIPs via Pickering emulsion polymerization technique and the *in situ* assembly of ZnO/graphene oxide on the synthetic molecular receptors (MIPs). The obtained ZnO/GO-MIPs catalysts could efficiently photoreduce Cr(VI) at the solid-water interface, and its efficiency was attributed to the synergistic catalytic effect between solid MIP core and the aqueous phase.

### 5.3. Enhanced oil recovery

Pickering emulsion have been applied in petroleum industry because of their attractive rheology characteristics. The utilization of NPs stabilized emulsion in the flooding and oil recovery process offer significant advantages to surfactants or polymers stabilized emulsion, such as excellent stability at high pressure and high temperature conditions, low cost, and environment friendliness [150]. Additionally, introducing surfactants onto the surface of NPs can also optimize rheological performance at extreme reservoir conditions by reducing the interfacial tension and altering the wettability of porous media [151].

Pei *et al.* [152] used silica NPs and hexadecyltrimethylammonium bromide (CTAB) co-stabilized emulsion flooding to enhance heavy oil recovery. The use of positively charged

CTAB molecules allowed for the hydrophobization of negatively charged silica particles, changing the wettability of silica NPs to promote their interfacial attachment at the interface. The synergistic interaction between nanoparticle and surfactant leads to the decrease of NPs concentration in the continuous aqueous phase, which results in the decrease of emulsion viscosity. The obtained emulsion flooding gives a great potential for enhanced oil recovery in waterflooded heavy oil reservoirs, with the permeability ranging from 500 mD to 2000 mD and the crude oil viscosity being lower than 1000 mPa.s. Another example regarding the use of silica and surfactant is given by Lee *et al.* [153]. The combination of silica, dodecyltrimethylammonium bromide (DTAB), and alcohol propoxy sulfate (Alfoterra S23-7S-90) can generate a structurally stable colloidal layer based on its optimal synergy effects. The results of sandpack flooding, Berea sandstone core flooding, and slim tube sandpack flooding experiments show that the colloidal solution could generate emulsion *in situ* at the pore scale and improve the oil recovery by 27% compared with the brine flooding case.

Liu *et al.* [154] prepared surface-active nanofluid by using silica nanoparticles and nonionic surfactant laurel monoanolamide, inducing the Pickering emulsions with *in-situ* mobility control. Chemical enhanced oil recovery factor of 29.2% and cumulative oil recovery of 70.9% suggested that surface-active nanofluid is the approach with great potential in industrial oilfield application.

Zhao *et al.* [155] reported on similar studies about crude oil/water Pickering emulsion stabilized by glucose-based cationic nonionic surfactant (GBDD)-modified halloysite nanotubes (H-GDBB). The emulsion type has been inverted from O/W to W/O and finally to O/W with the increase of GBDD concentration. Especially, H-GDBB nanofluid flooding could not only “peel off” the oil droplets on the rock surface through “wedge” adsorption pressure, but also form emulsion and reduce the displacement flow resistance and improve the oil recovery. Yet another interesting example of a surfactant-polymer-nanoparticle (SPN) based O/W Pickering emulsion system for application in enhanced oil recovery is given by Kumar *et al.* [156], where silica NPs show synergetic effect in presence of sodium dodecyl benzene sulfonate and carboxy methyl cellulose with the decrease of interfacial tension and droplet size

of emulsion in comparison with its surfactant-polymer or surfactant counterparts. It is found that adsorption of surfactant on the surface of silica modify its wettability as well as decrease the interfacial energy at the oil/water interface, while the consistent high viscosity values with addition of polymer had a significant effect on the rheological stability of emulsion. The investigation of the application of nanofluid injections revealed that the additional oil recovery of more than 24% could be achieved by injection of 0.5 pore volume of SPN-3 (at concentration of polymer, surfactant and NPs at 1.5 %, 825 ppm and 0.25 wt.% respectively) Pickering emulsion system after conventional water flooding.

#### 5.4. Biomedical

NPs-stabilized emulsions are very promising materials for biomedical applications because they have well-defined microstructures and they can be formulated with biocompatible NPs. Moreover, Pickering emulsions can be dried to make powdered composites materials, as well as destabilized to make coatings and adhesives by evaporating the volatile components to have a film of active ingredients on a solid surface. Sarkars *et al.* [157] prepared emulsion with lactoferrin nanogel particles (LFN) or a composite layer of LFN and inulin NPs (INP). The results showed that both LFN and INP are located at the interface because of the electrostatic attraction between oppositely charged LFN and INP at neutral and gastric pH. The presence of the secondary interfacial layer of INP provides a protective coating to the emulsion and further delay gastric digestion. This is mainly attributed to the formation of strong particle-particle composite layers at pH = 3, and INP exhibited effective steric barrier that slows down the access of pepsin to the LFN.

Sihler *et al.* [158] prepared inverse Pickering emulsions stabilized by silica NPs and various polymeric surfactants, with outstanding stability and narrow droplet size distribution. Silica particles are *in situ* hydrophobized by the adsorption of surfactant on the surface *via* van der Waals interaction and hydrogen bonding. The silica particles do not only form the shell of the emulsion droplets but some of them are obviously rendered hydrophilic and form a three-dimensional network in the inner of the droplets. The high flexibility of the system has potential

for biomedical applications like capsule cell interactions for drug delivery or diagnostics.

Sarkar *et al.* [159] developed emulsions stabilized by a composite layer of whey protein isolate (WPI) and cellulose nanocrystals (CNCs). The results of transmission electron microscopy, zeta potential, interfacial shear viscosity and theoretical surface coverage suggested both CNCs and WPI located at the O/W interface because of the electrostatic attraction between WPI and CNCs at pH 3. At an optimum concentration of CNCs, the formation of strong protein-particle composite adsorbed layers slows the access of pepsin to the protein interface, thus inhibiting droplet coalescence in the gastric phase. There are possibilities that the formation of network by the CNC in the continuous phase reduced the kinetics of proteolysis, or the formation of rigid CNC shell on the protein-coated droplets.

## 5.5. Cosmetics and personal care product

NPs-stabilized emulsions are significantly used in the formation of many cosmetic and personal care products because they show superior stability compared to emulsions stabilized by surfactants and polymer molecules. Recently, Rincón-Fontán *et al.* [160] investigated the synergic effect between mica and corn steep liquor-based biosurfactant extract to stabilize emulsions containing water and a non-aqueous soluble antioxidant (vitamin E). Both ingredients present a synergistic effect to form Pickering emulsion. The presence of biosurfactant extract improves the emulsion volume up to 70 % after 22 days, whereas the containing of 10 % mica component was able to increase the emulsion stability after 30 days of experiment. All the components have been proved to absorb UV light, giving antioxidant and sunscreen properties that suggests potential applications in cosmetic and pharmaceutical industry.

Sadeghpour *et al.* [161] improved the hydrophobicity of silica NPs by simple adsorption of oleic acid to their surfaces. Hydrophobic oils (long-chain alkanes, liquid paraffin, and liquid-crystalline) can be stabilized by the combination of silica and oleic acid with extremely small droplet size. Small angle X-ray scattering confirmed that the oleic acid-coated silica NPs were not aggregated. The sample procedure, the biocompatible materials, and the obtained emulsion

with high stability and small droplet size, were valuable for biological and body-care applications.

## 6. Conclusion

Pickering emulsions stabilized with hybrid nanomaterial offer novel properties that gives opportunities to use them or to integrate them in various industrial applications (food, cosmetics, oil recovery, catalysis, and pharmaceuticals...). In this review, we have summarized the considerable progress of the fabrication and application of the Pickering emulsion, with synergies between NPs and functional substances happening at the oil/water interface, which are not possible in most single nanoparticles system. Many efforts have been made to integrate particles into different composites, such as the *in situ* modification with small surfactant or polymer to tune the wettability of particles through electrostatic attraction and hydrogen bonding interaction. However, there is considerable room to explore new functions and materials, especially using particles in combination with emerging bio-sourced materials such as biopolymer, biosurfactant and enzyme. In this regard, intriguing hybrid materials with fantastic properties can be further developed and implemented in food and biocatalysis field. Especially, there has been booming interest in the development of switchable Pickering emulsion (emulsification/demulsification or phase inversion), which are triggered by surface wettability change response to the external controllable stimuli. With the increasingly demand of stimuli-responsive Pickering emulsion in various application (such as enhanced oil recovery and catalyst/product recovery), the construction of the more advanced emulsifiers endowed with stimuli responsiveness or bifunctionality need to be further systematically explored and require the in-depth study. The use of bijels system to carry out biphasic catalysis is a promising way to precise control of the reactions happened at the interface between the two immiscible phases. Moreover, the upcoming research and development in the bijels system should focus on the continuous flow reactors to addresses the limitation of the conventional batch reactors for the demand of industrial. Further investigation of novel hybrid nanomaterial is closely dependent on a better understanding of the mechanism, especially the interaction derived from



the interface between particles and functional substances, will undoubtedly help precise design and improve the value of the hybrid nanomaterials. This will inspire ideas and catalyze more directions to harness the Pickering emulsion to a wider scope of application.

## 7. References

- [1] A. Gupta, H.B. Eral, T.A. Hatton, P.S. Doyle, Nanoemulsions: formation, properties and applications, *Soft Matter*, 12 (2016) 2826-2841.
- [2] M. Lechuga, M. Fernandez-Serrano, E. Jurado, J. Nunez-Olea, F. Rios, Acute toxicity of anionic and non-ionic surfactants to aquatic organisms, *Ecotoxicology and Environmental Safety*, 125 (2016) 1-8.
- [3] P.J. Reeve, H.J. Fallowfield, The toxicity of cationic surfactant HDTMA-Br, desorbed from surfactant modified zeolite, towards faecal indicator and environmental microorganisms, *Journal of Hazardous Materials*, 339 (2017) 208-215.
- [4] Y.-Y. Li, B. Wang, M.-G. Ma, B. Wang, Review of recent development on preparation, properties, and applications of cellulose-based functional materials, *International Journal of Polymer Science*, (2018).
- [5] M.A. Hussein, A.A. Mohammed, M.A. Atiya, Application of emulsion and Pickering emulsion liquid membrane technique for wastewater treatment: an overview, *Environmental Science and Pollution Research*, 26 (2019) 36184-36204.
- [6] R. Roellig, C. Plikat, M.B. Ansorge-Schumacher, Efficient and selective carboligation with whole-cell biocatalysts in Pickering emulsion, *Angewandte Chemie International Edition*, 58 (2019) 12960-12963.
- [7] F. Gautier, M. Destribats, R. Perrier-Cornet, J.-F. Dechezelles, J. Giermanska, V. Heroguez, S. Ravaine, F. Leal-Calderon, V. Schmitt, Pickering emulsions with stimuable particles: from highly- to weakly-covered interfaces, *Physical Chemistry Chemical Physics*, 9 (2007) 6455-6462.
- [8] L. Leclercq, V. Nardello-Rataj, Pickering emulsions based on cyclodextrins: A smart solution for antifungal azole derivatives topical delivery, *European Journal of Pharmaceutical Sciences*, 82 (2016) 126-137.
- [9] J. Zhou, X. Qiao, B.P. Binks, K. Sun, M. Bai, Y. Li, Y. Liu, Magnetic Pickering Emulsions Stabilized by Fe<sub>3</sub>O<sub>4</sub> Nanoparticles, *Langmuir*, 27 (2011) 3308-3316.
- [10] N. Zou, X. Lin, M. Li, L. Li, C. Ye, J. Chen, T. Qiu, Ionic Liquid@Amphiphilic Silica Nanoparticles: Novel Catalysts for Converting Waste Cooking Oil to Biodiesel, *ACS Sustainable Chemistry & Engineering*, 8 (2020) 18054-18061.
- [11] L. Leclercq, R. Company, A. Muehlbauer, A. Mouret, J.-M. Aubry, V. Nardello-Rataj, Versatile Eco-friendly Pickering Emulsions Based on Substrate/Native Cyclodextrin Complexes: A Winning Approach for Solvent-Free Oxidations, *ChemSusChem*, 6 (2013) 1533-1540.
- [12] L.K. Maansson, F. Peng, J.J. Crassous, P. Schurtenberger, A microgel-Pickering emulsion route to colloidal molecules with temperature-tunable interaction sites, *Soft Matter*, 16 (2020) 1908-1921.
- [13] B. Yang, L. Leclercq, J.-M. Clacens, V. Nardello-Rataj, Acidic/amphiphilic silica nanoparticles: new eco-friendly Pickering interfacial catalysis for biodiesel production, *Green Chemistry*, 19 (2017) 4552-4562.
- [14] L. Zhang, G. Zhang, J. Ge, P. Jiang, L. Ding, pH-and thermo-responsive Pickering emulsion stabilized by silica nanoparticles and conventional nonionic copolymer surfactants, *Journal of Colloid and Interface Science*, 616 (2022) 129-140.
- [15] Z. Li, Y. Shi, A. Zhu, Y. Zhao, H. Wang, B.P. Binks, J. Wang, Light-responsive, reversible

- emulsification and demulsification of oil-in-water pickering emulsions for catalysis, *Angewandte Chemie*, 133 (2021) 3974-3979.
- [16] N. Sun, Q. Li, D. Luo, P. Sui, Q. Jiang, J. Liu, A. Li, W. Si, Y. Ma, Dual-responsive pickering emulsion stabilized by Fe<sub>3</sub>O<sub>4</sub> nanoparticles hydrophobized in situ with an electrochemical active molecule, *Colloids and Surfaces A: Physicochemical and Engineering Aspects*, 608 (2021) 125588.
- [17] S. Yu, D. Zhang, J. Jiang, W. Xia, Redox-responsive Pickering emulsions stabilized by silica nanoparticles and ferrocene surfactants at a very low concentration, *ACS Sustainable Chemistry & Engineering*, 7 (2019) 15904-15912.
- [18] G. Douyère, L. Leclercq, V. Nardello-Rataj, From polyethyleneimine hydrogels to Pickering-like smart “On/Off” emulgels switched by pH and temperature, *Journal of Colloid and Interface Science*, 628 (2022) 807-819.
- [19] J. Tang, P.J. Quinlan, K.C. Tam, Stimuli-responsive Pickering emulsions: recent advances and potential applications, *Soft Matter*, 11 (2015) 3512-3529.
- [20] Y. Yang, Z. Fang, X. Chen, W. Zhang, Y. Xie, Y. Chen, Z. Liu, W. Yuan, An overview of pickering emulsions: solid-particle materials, classification, morphology, and applications, *Frontiers in Pharmacology*, 8 (2017) 287/281-287/220.
- [21] D. Gonzalez Ortiz, C. Pochat-Bohatier, J. Cambedouzou, M. Bechelany, P. Miele, Current Trends in Pickering Emulsions: Particle Morphology and Applications, *Engineering*, (2020).
- [22] J. Wu, G.-H. Ma, Recent Studies of Pickering Emulsions: Particles Make the Difference, *Small*, 12 (2016) 4633-4648.
- [23] F. Zhu, Starch based Pickering emulsions: Fabrication, properties, and applications, *Trends in Food Science & Technology*, 85 (2019) 129-137.
- [24] J. Xiao, Y. Li, Q. Huang, Recent advances on food-grade particles stabilized Pickering emulsions: Fabrication, characterization and research trends, *Trends in Food Science & Technology*, 55 (2016) 48-60.
- [25] J. Wang, M. Yu, C. Yang, Colloidal TiO<sub>2</sub> nanoparticles with near-neutral wettability: An efficient Pickering emulsifier, *Colloids and Surfaces A: Physicochemical and Engineering Aspects*, 570 (2019) 224-232.
- [26] D. Li, Y. He, S. Wang, On the Rotation of the Janus CuO/CuS Colloids Formed at a Pickering Emulsion Interface, *The Journal of Physical Chemistry C*, 113 (2009) 12927-12929.
- [27] I. Fuchs, D. Avnir, Induction of Amphiphilicity in Polymer@Silica Particles: Ceramic Surfactants, *Langmuir*, 29 (2013) 2835-2842.
- [28] Y. Cui, M. Threlfall, J.S. van Duijneveldt, Optimizing organoclay stabilized Pickering emulsions, *Journal of Colloid and Interface Science*, 356 (2011) 665-671.
- [29] A. Sharkawy, M.F. Barreiro, A.E. Rodrigues, Chitosan-based Pickering emulsions and their applications: A review, *Carbohydrate Polymers*, 250 (2020) 116885.
- [30] M.A. Creighton, W. Zhu, F. van Krieken, R.A. Petteruti, H. Gao, R.H. Hurt, Three-Dimensional Graphene-Based Microbarriers for Controlling Release and Reactivity in Colloidal Liquid Phases, *ACS Nano*, 10 (2016) 2268-2276.
- [31] J. Dong, A.J. Worthen, L.M. Foster, Y. Chen, K.A. Cornell, S.L. Bryant, T.M. Truskett, C.W. Bielawski, K.P. Johnston, Modified Montmorillonite Clay Microparticles for Stable Oil-in-Seawater Emulsions, *ACS Applied Materials & Interfaces*, 6 (2014) 11502-11513.
- [32] J.I. Amalvy, S.P. Armes, B.P. Binks, J.A. Rodrigues, G.F. Unali, Use of sterically-stabilised

- polystyrene latex particles as a pH-responsive particulate emulsifier to prepare surfactant-free oil-in-water emulsions, *Chemical Communications*, (2003) 1826-1827.
- [33] X. Qiao, J. Zhou, B.P. Binks, X. Gong, K. Sun, Magnetorheological behavior of Pickering emulsions stabilized by surface-modified Fe<sub>3</sub>O<sub>4</sub> nanoparticles, *Colloids and Surfaces A: Physicochemical and Engineering Aspects*, 412 (2012) 20-28.
- [34] M.P. Godfrin, A. Tiwari, A. Bose, A. Tripathi, Phase and Steady Shear Behavior of Dilute Carbon Black Suspensions and Carbon Black Stabilized Emulsions, *Langmuir*, 30 (2014) 15400-15407.
- [35] B.P. Binks, S.O. Lumsdon, Transitional Phase Inversion of Solid-Stabilized Emulsions Using Particle Mixtures, *Langmuir*, 16 (2000) 3748-3756.
- [36] L. Liu, X. Pu, H. Tao, K. Chen, W. Guo, D. Luo, Z. Ren, Pickering emulsion stabilized by organoclay and intermediately hydrophobic nanosilica for high-temperature conditions, *Colloids and Surfaces A: Physicochemical and Engineering Aspects*, 610 (2021) 125694.
- [37] S. Stock, F. Jakob, S. Röhl, K. Gräff, M. Kühnhammer, N. Hondow, S. Micklethwaite, M. Kraume, R. von Klitzing, Exploring water in oil emulsions simultaneously stabilized by solid hydrophobic silica nanospheres and hydrophilic soft PNIPAM microgel, *Soft matter*, 17 (2021) 8258-8268.
- [38] S. Yan, H. Zou, S. Chen, N. Xue, H. Yang, Janus mesoporous silica nanosheets with perpendicular mesochannels: affording highly accessible reaction interfaces for enhanced biphasic catalysis, *Chemical Communications*, 54 (2018) 10455-10458.
- [39] D.-d. Li, J.-z. Jiang, C. Cai, Palladium nanoparticles anchored on amphiphilic Janus-type cellulose nanocrystals for Pickering interfacial catalysis, *Chemical Communications*, 56 (2020) 9396-9399.
- [40] D. Stehl, N. Milojevic, S. Stock, R. Schomaecker, R. von Klitzing, Synergistic Effects of a Rhodium Catalyst on Particle-Stabilized Pickering Emulsions for the Hydroformylation of a Long-Chain Olefin, *Industrial & Engineering Chemistry Research*, 58 (2019) 2524-2536.
- [41] N.M. Briggs, J.S. Weston, B. Li, D. Venkataramani, C.P. Aichele, J.H. Harwell, S.P. Crossley, Multiwalled Carbon Nanotubes at the Interface of Pickering Emulsions, *Langmuir*, 31 (2015) 13077-13084.
- [42] S. Crossley, J. Faria, M. Shen, D.E. Resasco, Solid Nanoparticles that Catalyze Biofuel Upgrade Reactions at the Water/Oil Interface, *Science*, 327 (2010) 68-72.
- [43] P.A. Zapata, J. Faria, M. Pilar Ruiz, D.E. Resasco, Condensation/Hydrogenation of Biomass-Derived Oxygenates in Water/Oil Emulsions Stabilized by Nanohybrid Catalysts, *Topics in Catalysis*, 55 (2012) 38-52.
- [44] T. Zeng, A. Deng, D. Yang, H. Li, C. Qi, Y. Gao, Triple-Responsive Pickering Emulsion Stabilized by Core Cross-linked Supramolecular Polymer Particles, *Langmuir*, 35 (2019) 11872-11880.
- [45] S.-S. Wang, G.-Y. Yang, Recent Advances in Polyoxometalate-Catalyzed Reactions, *Chemical Reviews*, 115 (2015) 4893-4962.
- [46] X. Tang, Y. Hou, Q.B. Meng, G. Zhang, F. Liang, X.-M. Song, Heteropoly acids-functionalized Janus particles as catalytic emulsifier for heterogeneous acylation in flow ionic liquid-in-oil Pickering emulsion, *Colloids and Surfaces A: Physicochemical and Engineering Aspects*, 570 (2019) 191-198.
- [47] L. Leclercq, Get beyond limits: From colloidal tectonics concept to the engineering of eco-friendly catalytic systems, *Frontiers in Chemistry*, 6 (2018) 168.
- [48] B. Pacaud, L. Leclercq, J.-F. Dechezelles, V. Nardello-Rataj, Hybrid Core-Shell Nanoparticles by "Plug and Play" Self-Assembly, *Chemistry – A European Journal*, 24 (2018) 17672-17676.

- [49] M. Pera-Titus, L. Leclercq, J.M. Clacens, F. De Campo, V. Nardello-Rataj, Pickering interfacial catalysis for biphasic systems: from emulsion design to green reactions, *Angewandte Chemie*, 54 (2015) 2006-2021.
- [50] J. Wang, F. Yang, J. Tan, G. Liu, J. Xu, D. Sun, Pickering Emulsions Stabilized by a Lipophilic Surfactant and Hydrophilic Plate-like Particles, *Langmuir*, 26 (2010) 5397-5404.
- [51] H. Tan, W. Liu, D. Yu, H. Li, M.A. Hubbe, B. Gong, W. Zhang, H. Wang, G. Li, ASA-in-water emulsions stabilized by laponite nanoparticles modified with tetramethylammonium chloride, *Chemical Engineering Science*, 116 (2014) 682-693.
- [52] B. Zheng, B. Zheng, A.J. Carr, X. Yu, D.J. McClements, S.R. Bhatia, Emulsions stabilized by inorganic nanoclays and surfactants: Stability, viscosity, and implications for applications, *Inorganica Chimica Acta*, 508 (2020) 119566.
- [53] C.P. Whitby, D. Fornasiero, J. Ralston, Effect of oil soluble surfactant in emulsions stabilised by clay particles, *Journal of Colloid and Interface Science*, 323 (2008) 410-419.
- [54] A.J. Worthen, L.M. Foster, J. Dong, J.A. Bollinger, A.H. Peterman, L.E. Pastora, S.L. Bryant, T.M. Truskett, C.W. Bielawski, K.P. Johnston, Synergistic Formation and Stabilization of Oil-in-Water Emulsions by a Weakly Interacting Mixture of Zwitterionic Surfactant and Silica Nanoparticles, *Langmuir*, 30 (2014) 984-994.
- [55] X.-Q. Wei, W.-J. Zhang, L. Lai, P. Mei, L.-M. Wu, Y.-Q. Wang, Different cationic surfactants-modified silica nanoparticles for Pickering emulsions, *Journal of Molecular Liquids*, 291 (2019) 111341.
- [56] B.P. Binks, J.A. Rodrigues, W.J. Frith, Synergistic Interaction in Emulsions Stabilized by a Mixture of Silica Nanoparticles and Cationic Surfactant, *Langmuir*, 23 (2007) 3626-3636.
- [57] J. Jiang, Y. Zhu, Z. Cui, B.P. Binks, Switchable Pickering Emulsions Stabilized by Silica Nanoparticles Hydrophobized In Situ with a Switchable Surfactant, *Angewandte Chemie International Edition*, 52 (2013) 12373-12376.
- [58] S. Yu, D. Zhang, J. Jiang, W. Xia, Redox-Responsive Pickering Emulsions Stabilized by Silica Nanoparticles and Ferrocene Surfactants at a Very Low Concentration, *ACS Sustainable Chemistry & Engineering*, 7 (2019) 15904-15912.
- [59] Q. Jiang, N. Sun, Q. Li, W. Si, J. Li, A. Li, Z. Gao, W. Wang, J. Wang, Redox-Responsive Pickering Emulsions Based on Silica Nanoparticles and Electrochemical Active Fluorescent Molecules, *Langmuir*, 35 (2019) 5848-5854.
- [60] L. Liu, X. Pu, Y. Zhou, J. Zhou, D. Luo, Z. Ren, Smart Pickering water-in-oil emulsion by manipulating interactions between nanoparticles and surfactant as potential oil-based drilling fluid, *Colloids and Surfaces A: Physicochemical and Engineering Aspects*, (2019) Ahead of Print.
- [61] Y. Zhang, X. Ren, S. Guo, X. Liu, Y. Fang, CO<sub>2</sub>-Switchable Pickering Emulsion Using Functionalized Silica Nanoparticles Decorated by Amine Oxide-Based Surfactants, *ACS Sustainable Chemistry & Engineering*, 6 (2018) 2641-2650.
- [62] H. Jia, J. He, Y. Xu, T. Wang, L. Zhang, B. Wang, X. Jiang, X. Li, X. Zhang, K. Lv, Synergistic effects of AIOOH and sodium benzenesulfonate on the generation of Pickering emulsions and their application for enhanced oil recovery, *Colloids and Surfaces A: Physicochemical and Engineering Aspects*, (2022) 128333.
- [63] Z. Hu, S. Ballinger, R. Pelton, E.D. Cranston, Surfactant-enhanced cellulose nanocrystal Pickering emulsions, *Journal of Colloid and Interface Science*, 439 (2015) 139-148.

- [64] M. Nitschke, S.G.V.A.O. Costa, *Biosurfactants in food industry*, *Trends in Food Science & Technology*, 18 (2007) 252-259.
- [65] D.J. McClements, C.E. Gumus, *Natural emulsifiers - Biosurfactants, phospholipids, biopolymers, and colloidal particles: Molecular and physicochemical basis of functional performance*, *Advances in Colloid and Interface Science*, 234 (2016) 3-26.
- [66] S.A. Onaizi, M. Alsulaimani, M.K. Al-Sakkaf, S.A. Bahadi, M. Mahmoud, A. Alshami, *Crude oil/water nanoemulsions stabilized by biosurfactant: Stability and pH-Switchability*, *Journal of Petroleum Science and Engineering*, 198 (2021) 108173.
- [67] N.G. Ganesan, M.A. Miastkowska, J. Pulit-Prociak, P. Dey, V. Rangarajan, *Formulation of a stable biocosmetic nanoemulsion using a Bacillus lipopeptide as the green-emulsifier for skin-care applications*, *Journal of Dispersion Science and Technology*, (2022) 1-13.
- [68] Z. Hu, S. Ballinger, R. Pelton, E.D. Cranston, *Surfactant-enhanced cellulose nanocrystal Pickering emulsions*, *Journal of Colloid and Interface Science*, 439 (2015) 139-148.
- [69] G. Pi, L. Mao, M. Bao, Y. Li, H. Gong, J. Zhang, *Preparation of oil-in-seawater emulsions based on environmentally benign nanoparticles and biosurfactant for oil spill remediation*, *ACS Sustainable Chemistry & Engineering*, 3 (2015) 2686-2693.
- [70] X. Zhao, G. Yu, J. Li, Y. Feng, L. Zhang, Y. Peng, Y. Tang, L. Wang, *Eco-friendly pickering emulsion stabilized by silica nanoparticles dispersed with high-molecular-weight amphiphilic alginate derivatives*, *ACS Sustainable Chemistry & Engineering*, 6 (2018) 4105-4114.
- [71] E. Santini, E. Guzman, M. Ferrari, L. Liggieri, *Emulsions stabilized by the interaction of silica nanoparticles and palmitic acid at the water-hexane interface*, *Colloids and Surfaces A: Physicochemical and Engineering Aspects*, 460 (2014) 333-341.
- [72] A. Sharkawy, M.F. Barreiro, A.E. Rodrigues, *Chitosan-based Pickering emulsions and their applications: A review*, *Carbohydrate polymers*, 250 (2020) 116885.
- [73] N. Ghavidel, P. Fatehi, *Recent Developments in the Formulation and Use of Polymers and Particles of Plant-based Origin for Emulsion Stabilizations*, *ChemSusChem*, 14 (2021) 4850-4877.
- [74] Y. Wang, L. Zhu, H. Zhang, H. Huang, L. Jiang, *Formulation of pH and temperature dual-responsive Pickering emulsion stabilized by chitosan-based microgel for recyclable biocatalysis*, *Carbohydrate Polymers*, 241 (2020) 116373.
- [75] L.E. Low, C.W. Ooi, E.S. Chan, B.H. Ong, B.T. Tey, *Dual (magnetic and pH) stimuli-reversible Pickering emulsions based on poly (2-(dimethylamino) ethyl methacrylate)-bonded Fe<sub>3</sub>O<sub>4</sub> nanocomposites for oil recovery application*, *Journal of Environmental Chemical Engineering*, 8 (2020) 103715.
- [76] M. Motornov, R. Sheparovych, R. Lupitskiy, E. MacWilliams, O. Hoy, I. Luzinov, S. Minko, *Stimuli-responsive colloidal systems from mixed brush-coated nanoparticles*, *Advanced Functional Materials*, 17 (2007) 2307-2314.
- [77] H. Zhou, T. Shi, X. Zhou, *Preparation of polystyrene/SiO<sub>2</sub> microsphere via Pickering emulsion polymerization: Synergistic effect of SiO<sub>2</sub> concentrations and initiator sorts*, *Applied Surface Science*, 266 (2013) 33-38.
- [78] C. Huang, J. Forth, W. Wang, K. Hong, G.S. Smith, B.A. Helms, T.P. Russell, *Bicontinuous structured liquids with sub-micrometre domains using nanoparticle surfactants*, *Nature Nanotechnology*, 12 (2017) 1060-1063.
- [79] X. Yan, C. Ma, F. Cui, D.J. McClements, X. Liu, F. Liu, *Protein-stabilized Pickering emulsions:*

- Formation, stability, properties, and applications in foods, *Trends in Food Science & Technology*, 103 (2020) 293-303.
- [80] Y. Chu, Y. Sun, W. Wu, H. Xiao, Dispersion Properties of Nanocellulose: A Review, *Carbohydrate Polymers*, 250 (2020) 116892.
- [81] X. Yan, C. Ma, F. Cui, D.J. McClements, X. Liu, F. Liu, Protein-stabilized Pickering emulsions: Formation, stability, properties, and applications in foods, *Trends in Food Science & Technology*, 103 (2020) 293-303.
- [82] F. Cui, S. Zhao, X. Guan, D.J. McClements, X. Liu, F. Liu, T. Ngai, Polysaccharide-based Pickering emulsions: Formation, stabilization and applications, *Food Hydrocolloids*, 119 (2021) 106812.
- [83] S. Lu, D. Yang, M. Wang, M. Yan, Y. Qian, D. Zheng, X. Qiu, Pickering emulsions synergistic-stabilized by amphoteric lignin and SiO<sub>2</sub> nanoparticles, Stability and pH-responsive mechanism, *Colloids and Surfaces A: Physicochemical and Engineering Aspects*, (2019) Ahead of Print.
- [84] S. Huan, Y. Zhu, W. Xu, D.J. McClements, L. Bai, O.J. Rojas, Pickering emulsions via interfacial nanoparticle complexation of oppositely charged nanopolysaccharides, *ACS Applied Materials & Interfaces*, 13 (2021) 12581-12593.
- [85] B.S. Murray, K. Durga, A. Yusoff, S.D. Stoyanov, Stabilization of foams and emulsions by mixtures of surface active food-grade particles and proteins, *Food Hydrocolloids*, 25 (2011) 627-638.
- [86] M. Zembyla, B.S. Murray, S.J. Radford, A. Sarkar, Water-in-oil Pickering emulsions stabilized by an interfacial complex of water-insoluble polyphenol crystals and protein, *Journal of Colloid and Interface Science*, 548 (2019) 88-99.
- [87] M. Jin, Q. Zhong, Structure Modification of Montmorillonite Nanoclay by Surface Coating with Soy Protein, *Journal of Agricultural and Food Chemistry*, 60 (2012) 11965-11971.
- [88] M. Reger, T. Sekine, T. Okamoto, K. Watanabe, H. Hoffmann, Pickering emulsions stabilized by novel clay-hydrophobin synergism, *Soft Matter*, 7 (2011) 11021-11030.
- [89] Y. Han, R. Chen, Z. Ma, Q. Wang, X. Wang, Y. Li, G. Sun, Stabilization of Pickering emulsions via synergistic interfacial interactions between cellulose nanofibrils and nanocrystals, *Food Chemistry*, 395 (2022) 133603.
- [90] I. Oroz-Guinea, E. Garcia-Junceda, Enzyme catalysed tandem reactions, *Current Opinion in Chemical Biology*, 17 (2013) 236-249.
- [91] R.A. Sheldon, P.S. van, Enzyme immobilisation in biocatalysis: why, what and how, *Chemical Society Reviews*, 42 (2013) 6223-6235.
- [92] A.M. Klivanov, Why are enzymes less active in organic solvents than in water?, *Trends in Biotechnology*, 15 (1997) 97-101.
- [93] Y. Jiang, X. Liu, Y. Chen, L. Zhou, Y. He, L. Ma, J. Gao, Pickering emulsion stabilized by lipase-containing periodic mesoporous organosilica particles: A robust biocatalyst system for biodiesel production, *Bioresource Technology*, 153 (2014) 278-283.
- [94] Z. Wang, M.C.M. van Oers, F.P.J.T. Rutjes, J.C.M. van Hest, Polymersome Colloidosomes for Enzyme Catalysis in a Biphasic System, *Angewandte Chemie International Edition*, 51 (2012) 10746-10750.
- [95] J. Shi, X. Wang, S. Zhang, L. Tang, Z. Jiang, Enzyme-conjugated ZIF-8 particles as efficient and stable Pickering interfacial biocatalysts for biphasic biocatalysis, *Journal of Materials Chemistry B*, 4 (2016) 2654-2661.
- [96] J. Zhao, D. Yang, J. Shi, J. Li, S. Zhang, Y. Wu, Z. Jiang, Robust and recyclable 2D nanobiocatalysts

- for biphasic reactions in Pickering emulsions, *Industrial & Engineering Chemistry Research*, 57 (2018) 8708-8717.
- [97] J. Wang, R. Huang, W. Qi, R. Su, Z. He, Oriented Enzyme Immobilization at the Oil/Water Interface Enhances Catalytic Activity and Recyclability in a Pickering Emulsion, *Langmuir*, 33 (2017) 12317-12325.
- [98] X. Yang, Y. Wang, R. Bai, H. Ma, W. Wang, H. Sun, Y. Dong, F. Qu, Q. Tang, T. Guo, B.P. Binks, T. Meng, Pickering emulsion-enhanced interfacial biocatalysis: tailored alginate microparticles act as particulate emulsifier and enzyme carrier, *Green Chemistry*, 21 (2019) 2229-2233.
- [99] S. Yu, D. Zhang, J. Jiang, Z. Cui, W. Xia, B.P. Binks, H. Yang, Biphasic biocatalysis using a CO<sub>2</sub>-switchable Pickering emulsion, *Green Chemistry*, 21 (2019) 4062-4068.
- [100] D. Li, M. Shen, G. Sun, H. Jin, P. Cai, Z. Wang, Y. Jin, J. Chen, S. Ding, Facile immobilization of lipase based on Pickering emulsion via a synergistic stabilization by palygorskite-enzyme, *Clay Minerals*, 54 (2019) 293-298.
- [101] Z. Dong, M. Zheng, Z. Liu, J. Shi, H. Tang, X. Xiang, F. Huang, Carbon Nanoparticle-Stabilized Pickering Emulsion as a Sustainable and High-Performance Interfacial Catalysis Platform for Enzymatic Esterification/Transesterification, *ACS Sustainable Chemistry & Engineering*, 7 (2019) 7619-7629.
- [102] Z. Hu, H.S. Marway, H. Kasem, R. Pelton, E.D. Cranston, Dried and Redispersible Cellulose Nanocrystal Pickering Emulsions, *ACS Macro Letters*, 5 (2016) 185-189.
- [103] W. Jin, B. Li, W. Jin, B. Li, W. Jin, J. Zhu, Y. Jiang, P. Shao, Q. Huang, P. Shao, Gelatin-Based Nanocomplex-Stabilized Pickering Emulsions: Regulating Droplet Size and Wettability through Assembly with Glucomannan, *Journal of Agricultural and Food Chemistry*, 65 (2017) 1401-1409.
- [104] Y. Wei, D. Zhou, A. Mackie, S. Yang, L. Dai, L. Zhang, L. Mao, Y. Gao, Stability, interfacial structure, and gastrointestinal digestion of  $\beta$ -carotene-loaded pickering emulsions co-stabilized by particles, a biopolymer, and a surfactant, *Journal of Agricultural and Food Chemistry*, 69 (2021) 1619-1636.
- [105] T. Sharma, G.S. Kumar, B.H. Chon, J.S. Sangwai, Thermal stability of oil-in-water pickering emulsion in the presence of nanoparticle, surfactant, and polymer, *Journal of Industrial and Engineering Chemistry*, 22 (2015) 324-334.
- [106] M. Xu, W. Zhang, X. Pei, J. Jiang, Z. Cui, B.P. Binks, CO<sub>2</sub>/N<sub>2</sub> triggered switchable Pickering emulsions stabilized by alumina nanoparticles in combination with a conventional anionic surfactant, *RSC Advances*, 7 (2017) 29742-29751.
- [107] J. Jiang, J. Cao, W. Wang, H. Shen, Preparation of a synergistically stabilized oil-in-water paraffin Pickering emulsion for potential application in wood treatment, *Holzforschung*, 72 (2018) 489-497.
- [108] S. Wang, Y. He, Y. Zou, Study of Pickering emulsions stabilized by mixed particles of silica and calcite, *Particuology*, 8 (2010) 390-393.
- [109] C.V. Kulkarni, W. Wachter, G. Iglesias-Salto, S. Engelskirchen, S. Ahualli, Monoolein: a magic lipid?, *Physical Chemistry Chemical Physics*, 13 (2011) 3004-3021.
- [110] R. Pichot, F. Spyropoulos, I.T. Norton, Mixed-emulsifier stabilised emulsions: Investigation of the effect of monoolein and hydrophilic silica particle mixtures on the stability against coalescence, *Journal of Colloid and Interface Science*, 329 (2008) 284-291.
- [111] T. Gao, X. Zhao, R. Li, A. Bassey, Y. Bai, K. Ye, S. Deng, G. Zhou, Synergistic effects of polysaccharide addition-ultrasound treatment on the emulsified properties of low-salt myofibrillar



- protein, *Food Hydrocolloids*, 123 (2022) 107143.
- [112] S. Wang, Y. Shen, X. Chen, L. Dong, H. Yu, M. Bao, Y. Li, Cationic surfactant-modified palygorskite particles as effective stabilizer for Pickering emulsion gel formation, *Applied Clay Science*, 219 (2022) 106439.
- [113] Z. Yang, W. Wang, G. Wang, X. Tai, Optimization of low-energy Pickering nanoemulsion stabilized with montmorillonite and nonionic surfactants, *Colloids and Surfaces A: Physicochemical and Engineering Aspects*, (2019) Ahead of Print.
- [114] M. Atarian, A. Rajaei, M. Tabatabaei, A. Mohsenifar, H. Bodaghi, Formulation of Pickering sunflower oil-in-water emulsion stabilized by chitosan-stearic acid nanogel and studying its oxidative stability, *Carbohydrate Polymers*, 210 (2019) 47-55.
- [115] J.C. Cazotti, S.E. Smeltzer, N.M.B. Smeets, M.A. Dube, M.F. Cunningham, Starch nanoparticles modified with styrene oxide and their use as Pickering stabilizers, *Polymer Chemistry*, 11 (2020) 2653-2665.
- [116] X. Song, F. Zheng, F. Ma, H. Kang, H. Ren, The physical and oxidative stabilities of Pickering emulsion stabilized by starch particle and small molecular surfactant, *Food Chemistry*, 303 (2020) 125391.
- [117] Y. Hu, C. Qiu, Z. Jin, Y. Qin, C. Zhan, X. Xu, J. Wang, Pickering emulsions with enhanced storage stabilities by using hybrid  $\beta$ -cyclodextrin/short linear glucan nanoparticles as stabilizers, *Carbohydrate Polymers*, (2019) Ahead of Print.
- [118] S. Guo, Y. Zhang, CO<sub>2</sub>/N<sub>2</sub>-switchable high internal phase Pickering emulsion stabilized by silica nanoparticles and low-cost commercial N,N-dimethyl-N-dodecylamine, *Colloids and Surfaces A: Physicochemical and Engineering Aspects*, 562 (2019) 119-126.
- [119] Z.G. Cui, K.Z. Shi, Y.Z. Cui, B.P. Binks, Double phase inversion of emulsions stabilized by a mixture of CaCO<sub>3</sub> nanoparticles and sodium dodecyl sulphate, *Colloids and Surfaces A: Physicochemical and Engineering Aspects*, 329 (2008) 67-74.
- [120] T. Nallamilli, M.G. Basavaraj, Synergistic stabilization of Pickering emulsions by in situ modification of kaolinite with non ionic surfactant, *Applied Clay Science*, 148 (2017) 68-76.
- [121] L. Liu, X. Pu, Y. Zhou, X. Wu, D. Luo, Z. Ren, Phase Inversion of Pickering Emulsions by Electrolyte for Potential Reversible Water-in-Oil Drilling Fluids, *Energy Fuels*, 34 (2020) 1317-1328.
- [122] Abdullah, J. Weiss, T. Ahmad, C. Zhang, H. Zhang, A review of recent progress on high internal-phase Pickering emulsions in food science, *Trends in Food Science & Technology*, 106 (2020) 91-103.
- [123] Y. Zou, J. Guo, S.-W. Yin, J.-M. Wang, X.-Q. Yang, Pickering Emulsion Gels Prepared by Hydrogen-Bonded Zein/Tannic Acid Complex Colloidal Particles, *Journal of Agricultural and Food Chemistry*, 63 (2015) 7405-7414.
- [124] L. Bai, S. Huan, W. Xiang, O.J. Rojas, Pickering emulsions by combining cellulose nanofibrils and nanocrystals: phase behavior and depletion stabilization, *Green Chemistry*, 20 (2018) 1571-1582.
- [125] M. Zembyla, A. Lazidis, B.S. Murray, A. Sarkar, Water-in-Oil Pickering Emulsions Stabilized by Synergistic Particle-Particle Interactions, *Langmuir*, 35 (2019) 13078-13089.
- [126] L. Wang, M. Hasanzadeh Kafshgari, M. Meunier, Optical properties and applications of plasmonic-metal nanoparticles, *Advanced Functional Materials*, 30 (2020) 2005400.

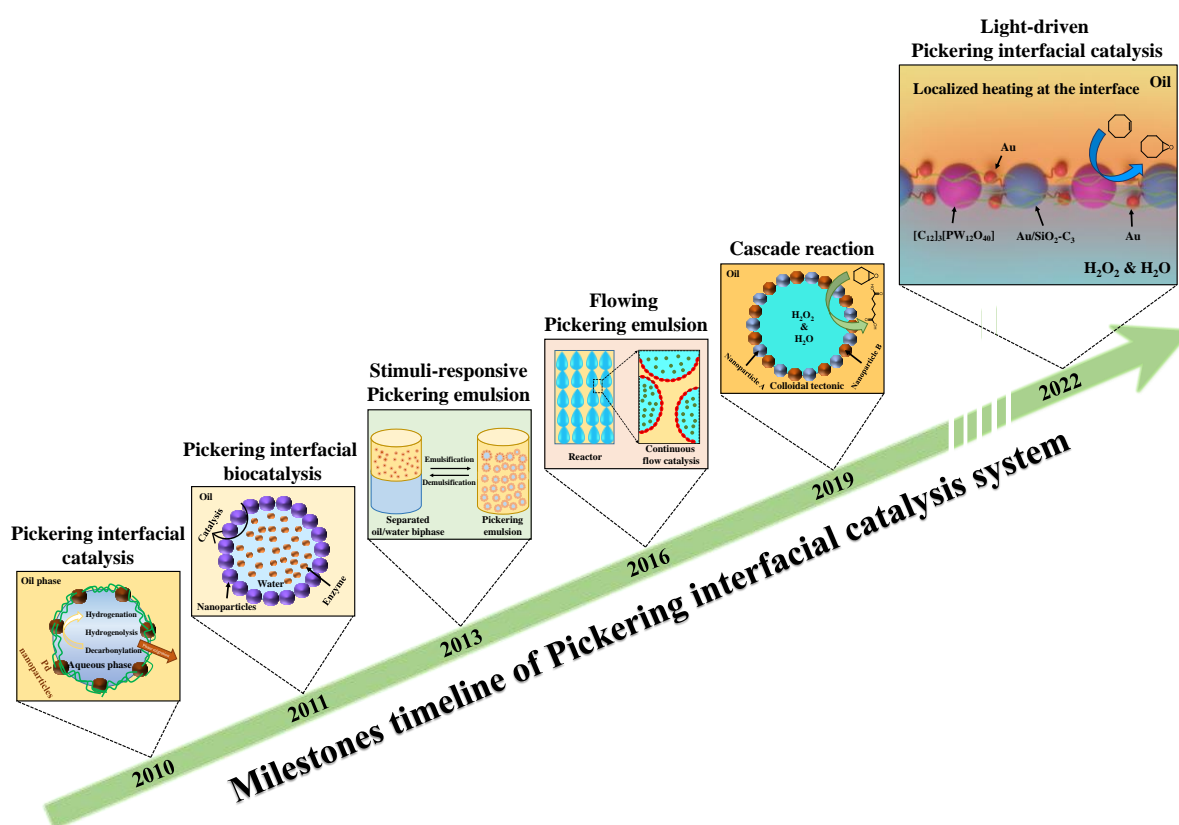
- [127] B.P. Binks, D. Yin, Pickering emulsions stabilized by hydrophilic nanoparticles: in situ surface modification by oil, *Soft Matter*, 12 (2016) 6858-6867.
- [128] X. Yan, Z. Zhai, J. Xu, Z. Song, S. Shang, X. Rao, CO<sub>2</sub>-Responsive Pickering Emulsions Stabilized by a Bio-based Rigid Surfactant with Nanosilica, *Journal of Agricultural and Food Chemistry*, 66 (2018) 10769-10776.
- [129] B.P. Binks, W. Liu, J.A. Rodrigues, Novel Stabilization of Emulsions via the Heteroaggregation of Nanoparticles, *Langmuir*, 24 (2008) 4443-4446.
- [130] T. Nallamilli, B.P. Binks, E. Mani, M.G. Basavaraj, Stabilization of Pickering Emulsions with Oppositely Charged Latex Particles: Influence of Various Parameters and Particle Arrangement around Droplets, *Langmuir*, 31 (2015) 11200-11208.
- [131] J.-F. Dechezelles, C. Ciotonea, C. Catrinescu, A. Ungureanu, S. Royer, V. Nardello-Rataj, Emulsions Stabilized with Alumina-Functionalized Mesoporous Silica Particles, *Langmuir*, 36 (2020) 3212-3220.
- [132] S. Ahualli, G.R. Iglesias, W. Wachter, M. Dulle, D. Minami, O. Glatter, Adsorption of Anionic and Cationic Surfactants on Anionic Colloids: Supercharging and Destabilization, *Langmuir*, 27 (2011) 9182-9192.
- [133] P.G. Sieben, F. Wypych, R.A. de Freitas, Oleic acid as a synergistic agent in the formation of kaolinite-mineral oil Pickering emulsions, *Applied Clay Science*, 216 (2022) 106378.
- [134] P. Bazazi, S.H. Hejazi, Spontaneous Formation of Double Emulsions at Particle-Laden Interfaces, *Journal of Colloid and Interface Science*, 587 (2021) 510-521.
- [135] C.-Y. Xie, S.-X. Meng, L.-H. Xue, R.-X. Bai, X. Yang, Y. Wang, Z.-P. Qiu, B.P. Binks, T. Guo, T. Meng, Light and Magnetic Dual-Responsive Pickering Emulsion Micro-Reactors, *Langmuir*, 33 (2017) 14139-14148.
- [136] G. Pi, Y. Li, M. Bao, L. Mao, H. Gong, Z. Wang, Novel and Environmentally Friendly Oil Spill Dispersant Based on the Synergy of Biopolymer Xanthan Gum and Silica Nanoparticles, *ACS Sustainable Chemistry & Engineering*, 4 (2016) 3095-3102.
- [137] C.P. Whitby, D. Fornasiero, J. Ralston, L. Liggieri, F. Ravera, Properties of Fatty Amine-Silica Nanoparticle Interfacial Layers at the Hexane-Water Interface, *The Journal of Physical Chemistry C*, 116 (2012) 3050-3058.
- [138] L. Leclercq, Get beyond limits: from colloidal tectonics concept to the engineering of eco-friendly catalytic systems, *Frontiers in Chemistry*, 6 (2018) 161-168.
- [139] B. Yang, L. Leclercq, V. Schmitt, M. Pera-Titus, V. Nardello-Rataj, Colloidal tectonics for tandem synergistic Pickering interfacial catalysis: oxidative cleavage of cyclohexene oxide into adipic acid, *Chemical Science*, 10 (2019) 501-507.
- [140] Z. Sun, U. Glebe, H. Charan, A. Boeker, C. Wu, Enzyme-Polymer Conjugates as Robust Pickering Interfacial Biocatalysts for Efficient Biotransformations and One-Pot Cascade Reactions, *Angewandte Chemie International Edition*, 57 (2018) 13810-13814.
- [141] R. Narukulla, U. Ojha, T. Sharma, Enhancing the stability and redispersibility of o/w Pickering emulsion through polyacryloyl hydrazide-tannic acid synergy, *Colloids and Surfaces A: Physicochemical and Engineering Aspects*, 568 (2019) 204-215.
- [142] Z.-M. Gao, X.-Q. Yang, N.-N. Wu, L.-J. Wang, J.-M. Wang, J. Guo, S.-W. Yin, Protein-Based Pickering Emulsion and Oil Gel Prepared by Complexes of Zein Colloidal Particles and Stearate, *Journal of Agricultural and Food Chemistry*, 62 (2014) 2672-2678.

- [143] L. Qi, Z. Luo, X. Lu, Facile synthesis of starch-based nanoparticle stabilized Pickering emulsion: its pH-responsive behavior and application for recyclable catalysis, *Green Chemistry*, 20 (2018) 1538-1550.
- [144] B. Xue, T. Xu, D. Li, J. Xu, Y. Li, F. Wang, J. Zhu, A Pickering emulsion of a bifunctional interface prepared from Pd nanoparticles supported on silicane-modified graphene oxide: an efficient catalyst for water-mediated catalytic hydrogenation, *Catalysis Science & Technology*, 10 (2020) 1096-1105.
- [145] R. Xia, W. Lv, K. Zhao, S. Ma, J. Hu, H. Wang, H. Liu, Catalyst, Emulsion Stabilizer, and Adsorbent: Three Roles In One for Synergistically Enhancing Interfacial Catalytic Oxidative Desulfurization, *Langmuir*, 35 (2019) 3963-3971.
- [146] A.M. Bago Rodriguez, L. Schober, A. Hinzmann, H. Gröger, B.P. Binks, Effect of Particle Wettability and Particle Concentration on the Enzymatic Dehydration of n-Octanaloxime in Pickering Emulsions, *Angewandte Chemie*, 133 (2021) 1470-1477.
- [147] S.-Y. Dou, R. Wang, The C-Si Janus nanoparticles with supported phosphotungstic active component for Pickering emulsion desulfurization of fuel oil without stirring, *Chemical Engineering Journal*, 369 (2019) 64-76.
- [148] Q. Li, T. Zhao, M. Li, W. Li, B. Yang, D. Qin, K. Lv, X. Wang, L. Wu, X. Wu, J. Sun, One-step construction of Pickering emulsion via commercial TiO<sub>2</sub> nanoparticles for photocatalytic dye degradation, *Applied Catalysis B: Environmental*, 249 (2019) 1-8.
- [149] Z. Chen, Y. Luo, C. Huang, X. Shen, In situ assembly of ZnO/graphene oxide on synthetic molecular receptors: Towards selective photoreduction of Cr (VI) via interfacial synergistic catalysis, *Chemical Engineering Journal*, 414 (2021) 128914.
- [150] Y. Zhou, D. Yin, W. Chen, B. Liu, X. Zhang, A comprehensive review of emulsion and its field application for enhanced oil recovery, *Energy Science & Engineering*, 7 (2019) 1046-1058.
- [151] M. Khalil, G. Aulia, E. Budianto, B. Mohamed Jan, S.H. Habib, Z. Amir, M.F. Abdul Patah, Surface-Functionalized Superparamagnetic Nanoparticles (SPNs) for Enhanced Oil Recovery: Effects of Surface Modifiers and Their Architectures, *ACS Omega*, 4 (2019) 21477-21486.
- [152] H. Pei, Z. Shu, G. Zhang, J. Ge, P. Jiang, Y. Qin, X. Cao, Experimental study of nanoparticle and surfactant stabilized emulsion flooding to enhance heavy oil recovery, *Journal of Petroleum Science and Engineering*, 163 (2018) 476-483.
- [153] J. Lee, T. Babadagli, Optimal design of pickering emulsions for heavy-oil recovery improvement, *Journal of Dispersion Science and Technology*, 41 (2020) 2048-2062.
- [154] R. Liu, J. Lu, W. Pu, Q. Xie, Y. Lu, D. Du, X. Yang, Synergetic effect between in-situ mobility control and micro-displacement for chemical enhanced oil recovery (CEOR) of a surface-active nanofluid, *Journal of Petroleum Science and Engineering*, 205 (2021) 108983.
- [155] T. Zhao, J. Chen, Y. Chen, Y. Zhang, J. Peng, Study on synergistic enhancement of oil recovery by halloysite nanotubes and glucose-based surfactants, *Journal of Dispersion Science and Technology*, (2020) Ahead of Print.
- [156] N. Kumar, T. Gaur, A. Mandal, Characterization of SPN Pickering emulsions for application in enhanced oil recovery, *Journal of Industrial and Engineering Chemistry*, 54 (2017) 304-315.
- [157] A. Sarkar, V. Ademuyiwa, S. Stublely, N.H. Esa, F.M. Goycoolea, X. Qin, F. Gonzalez, C. Olvera, Pickering emulsions co-stabilized by composite protein/ polysaccharide particle-particle interfaces: Impact on in vitro gastric stability, *Food Hydrocolloids*, 84 (2018) 282-291.

- [158] S. Sihler, A. Schrade, Z. Cao, U. Ziener, Inverse Pickering Emulsions with Droplet Sizes below 500 nm, *Langmuir*, 31 (2015) 10392-10401.
- [159] A. Sarkar, S. Zhang, B. Murray, J.A. Russell, S. Boxal, Modulating in vitro gastric digestion of emulsions using composite whey protein-cellulose nanocrystal interfaces, *Colloids and Surfaces B: Biointerfaces*, 158 (2017) 137-146.
- [160] M. Rincon-Fontan, L. Rodriguez-Lopez, X. Vecino, J.M. Cruz, A.B. Moldes, Study of the synergic effect between mica and biosurfactant to stabilize Pickering emulsions containing Vitamin E using a triangular design, *Journal of Colloid and Interface Science*, 537 (2019) 34-42.
- [161] A. Sadeghpour, F. Pirolt, O. Glatter, Submicrometer-Sized Pickering Emulsions Stabilized by Silica Nanoparticles with Adsorbed Oleic Acid, *Langmuir*, 29 (2013) 6004-6012.



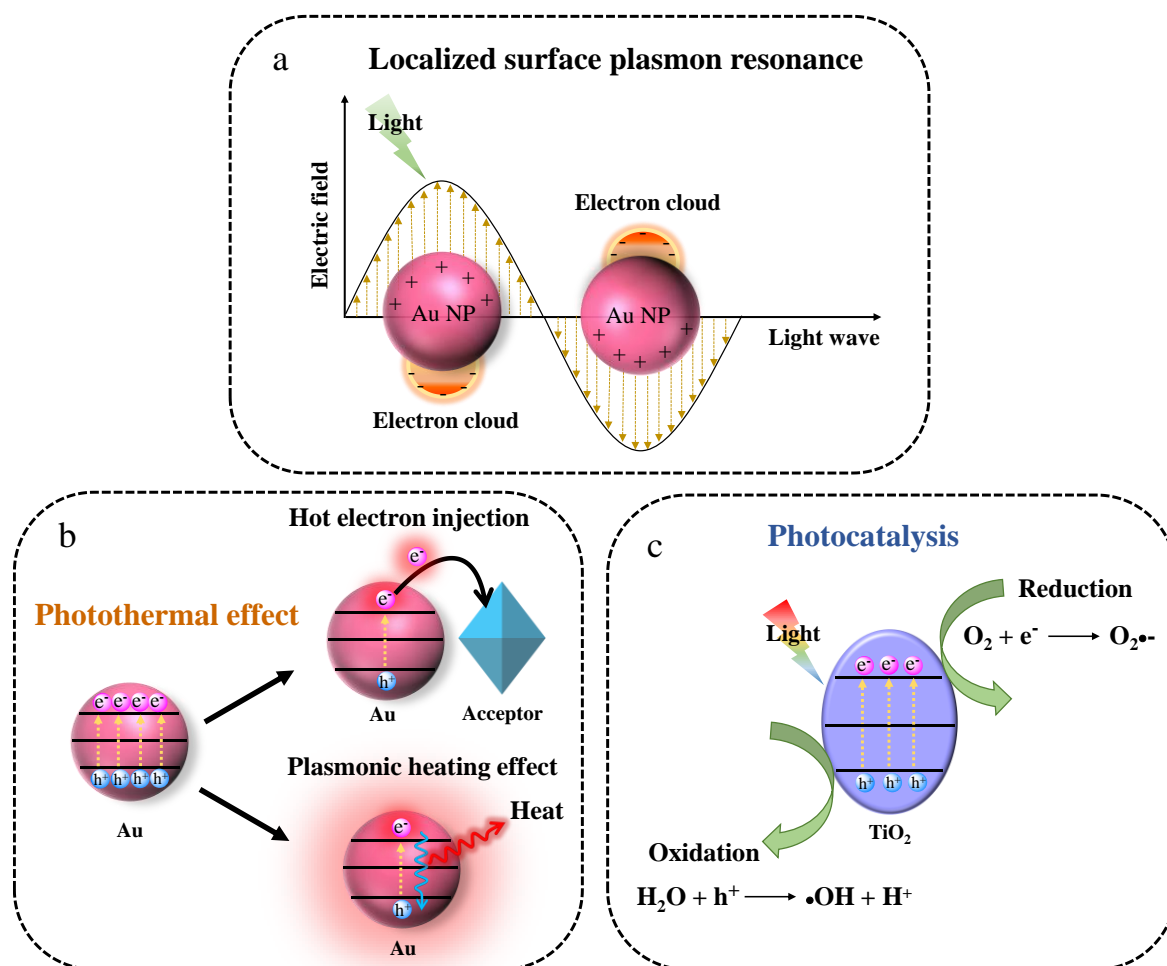
# Chapter II. Light-driven Pickering interfacial catalysis for oxidation of cyclooctene at room temperature





## 1. Introduction

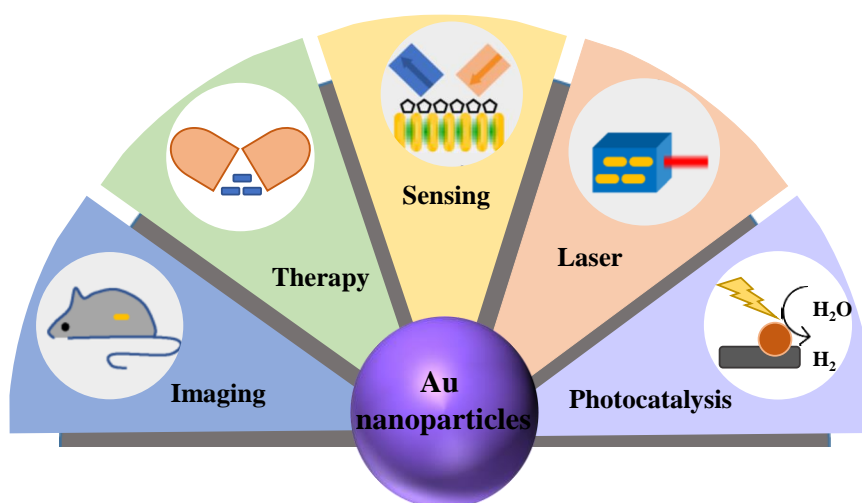
Owing to their localized surface plasmon resonance (LSPR) properties, noble metal NPs based on silver and gold can effectively enhance the spectral absorption to generate hot electrons and photothermal effect by hyperthermia [1-3]. These characteristics allow an efficient conversion of light-to-energy and energy transfer to the microenvironment around the NP surface (**Figure 1a**). Among noble metal particles, Au NPs (NPs) are most commonly used as plasmonic materials and catalysts due to their low reactivity, easy fabrication and facile application. Moreover, they are used for target therapy by local heating in biological applications [4, 5].



**Figure 1.** (a) Schematic illustration of localized surface plasmon resonance in Au NPs. (b) Scheme describing the transfer of hot charge carriers to the surroundings and relaxation of charge carriers into heat. (c) Schematic illustration of photocatalytic mechanism of TiO<sub>2</sub> under light irradiation.



Semiconductors can be used as photocatalysts (**Figure 1c**) for oxidation reactions, including  $\text{TiO}_2$  [6],  $\text{WO}_3$  [7] and  $\text{ZnO}$  [8]. While electron–hole pairs are generated from photocatalysts, LSPR can serve as an additional energy input through converting light energy into a hot carrier [9] (**Figure 1b**). Depending on the different decay pathways of plasmonic energy, the mechanisms of hot carriers in the chemical reaction are proposed as follows: (1) optically excited hot electrons can inject into the electron-accepting states of nearby surface and can take part in the reaction; (2) photo-induced hot carriers play a negligible role in activating the surface adsorbed reactants, but convert energy into heat through energy exchange between electrons and phonons; (3) both hot carrier-driven reactant activation and photothermal heating exist and can act synergistically to drive the chemical reactions.



**Figure 2.** Applications of Au NPs, including imaging, therapy, sensing, laser and plasmonic catalysis.

The plasmonic properties of Au NPs are dictated by their size, shape and composition, as well as by the surrounding conditions such as the pH, concentration and ionic environment. They are used in a great deal of applications including optical devices, biological sensing, and photocatalysis [10–12] (**Figure 2**). For example, Au nanospheres [13], nanorods [14] and nanoshells [15] have strong absorption in near-infrared light region to generate both hot electrons and hyperthermia effects. Hou *et al.* [16] prepared monodisperse and uniform theranostic agents based on core/shell/shell  $\text{Fe}_3\text{O}_4@\text{SiO}_2@\text{Au}$ -PEG NPs by a seed growth method. Because of their excellent superparamagnetic and plasmonic properties, the obtained

NPs were used as contrast agents for magnetic resonance and computed tomography dual imaging, and high photothermal therapies. Inspired by LSPR properties that enable a significant and rapid increase of the local temperature at the nanometer scale, Au NPs have also found a broad range of applications in the chemical industry as plasmonic catalysts for oxidation [17], reduction [18], hydrogenation reactions [19], and so on [20, 21].

In general, most of catalytic reactions are driven by thermal energy. However, in a conventional heating approach, the thermal energy generated by external heating during the chemical reaction cannot be precisely localized on the catalyst surface, and heat dissipates into the surroundings, resulting in energy loss. High operating temperature can result in negative side effects such as undesired selectivity for products in partial-oxidation reactions and catalyst deactivation. The integration of plasmonic NPs in a catalytic system can be remarkably beneficial for the design of new catalyst systems [22, 23]. Ideally, the heating of the catalytic system can be performed in the presence of photothermal agent *via* remote light irradiation [24-26]. When photothermal transformation gets close to the catalytic centers, heating can become much more effective. Compared to conventional external heating, plasmon-driven catalysis utilizes hot electrons and/or a temperature gradient on the catalyst surface under light irradiation to accelerate the catalytic activity, and makes the catalytic process greener [27, 28]. Moreover, the reaction pathways can be shifted by injecting hot carriers into specific chemical bonds, thus changing the reaction selectivity. Indeed, several studies have reported photoassisted-improved catalytic process under light irradiation using plasmonic particles based materials, like hybrid Ag@SBA-15 [29], Pt-decorated graphene oxide [30] and Au coated Fe<sub>3</sub>O<sub>4</sub>@SiO<sub>2</sub> [31]. The results from these studies clearly demonstrate the possibility of using plasmonic noble metal NPs as energy converters to drive catalytic reaction at moderate bulk temperature.

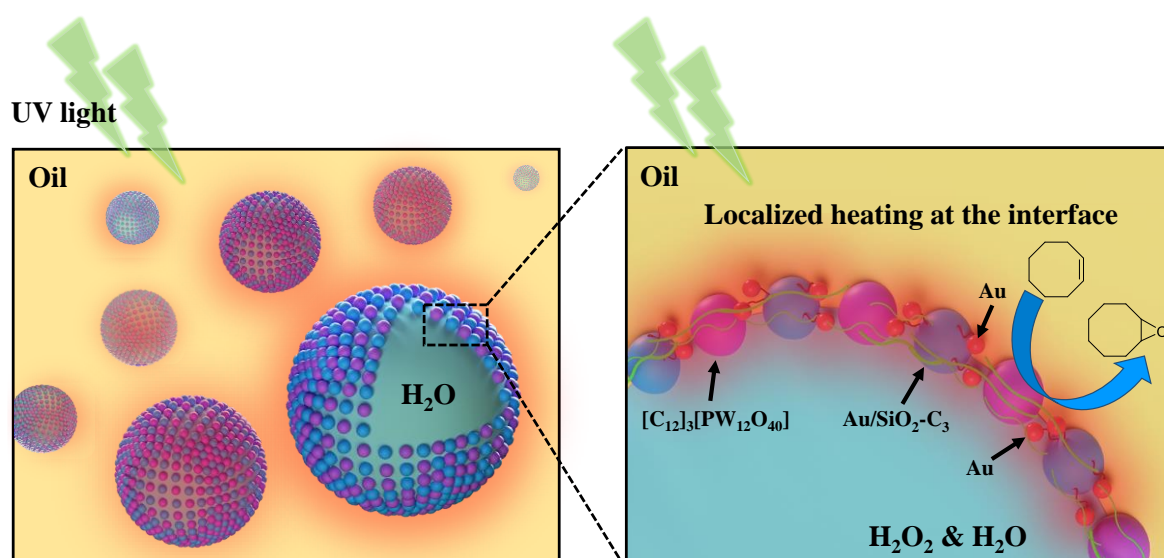
Organic-aqueous biphasic catalysis systems are common when performing reactions between immiscible reagents and catalysts, such as oxidation, biomass conversion, Suzuki coupling, and polymerization [32-34]. Despite their benefits, conventional biphasic systems often suffer from low reaction efficiency because of high mass/heat transfer resistances due to limited organic/aqueous interfacial area [35]. To address this limitation, Pickering interfacial

catalysis (PIC) is a promising strategy to improve the efficiency of biphasic chemical reactions [36-39]. In PIC systems, the solid NPs act both as catalyst and emulsifier at the organic/aqueous interface, which increases the interfacial area for mass transport, thus promoting catalytic efficiency [40, 41]. The first example of catalytic reaction in Pickering emulsion was reported by Crossley *et al.* [42]. Pd/carbon nanotube-inorganic oxide hybrid NPs not only showed interfacial activity for stabilizing Pickering emulsions, but also enhanced the reaction efficiency for the biphasic hydrodeoxygenation of phenolic compounds (98% conversion of glutaraldehyde in emulsion and 58% in single aqueous phase), and hydrogenation and etherification of aldehydes. Later, a variety of interfacial-active catalysts were developed for PIC, ranging from acid/base to oxidation/epoxidation catalysts, as reviewed by Pera-Titus *et al.* [43]. Until now, improvements have been reported on PIC systems, but high reaction temperature and long reaction time are still required [44, 45], which cause excessive energy and cost. For example, Fan *et al.* [46] used amphiphilic silica NPs functionalized with alkyl chains and alkyl sulfonic groups to stabilize Pickering emulsion for the etherification of glycerol with dodecanol at 150 °C for 16 h. Thus, it is necessary to develop a suitable strategy to conduct interfacial reactions at milder conditions.

Polyoxometalates (POMs) are anionic metal oxide clusters based on high-valent transition metals (such as M, Mo, W, V and Nb) that have been developed and applied for various reactions, including transesterification, hydrolysis, Friedel-Crafts alkylation and oxidation of olefins, alcohols, alkanes, *etc.* [47-49]. POMs exist in numerous types of structures. For example, the phosphomolybdate,  $[\text{PMo}_{12}\text{O}_{40}]^{3-}$ , and the silicotungstate,  $[\text{SiW}_{12}\text{O}_{40}]^{4-}$ , anions have the same structure as  $[\text{PW}_{12}\text{O}_{40}]^{3-}$ , display the so-called Keggin ionic type with the generic formula  $[\text{YM}_{12}\text{O}_{40}]$ , where Y is the heteroatom (normally P, Si, or B), and M is the addenda atom (such as Mo or W). The studies have focused mainly on the Keggin-type heteropolyanions because of their high availability and stability, and they can be used as efficient catalysts for the selective oxidation of substrates using  $\text{H}_2\text{O}_2$  as oxidant [50-52]. However, their hydrophilic nature limits their application because of complex separation and recycling. As a way out, different approaches have been proposed for heterogenizing POM catalysts. In particular, POM-

based  $[C_{12}]_3[PW_{12}O_{40}]$  catalysts resulting from the attractive interaction (ionic type) between dodecyltrimethylammonium chains and phosphotungstate anions have proven to be excellent candidates for stabilizing Pickering emulsion with high catalytic activity for the oxidation of olefins [53, 54]. In a recent work, Yang *et al.* [55] used the colloidal tectonics approach to prepare emulsions stabilized by the interaction between  $[C_{12}]_3[PW_{12}O_{40}]$  and amphiphilic silica NPs. The self-assembly of dual NPs resulted in their synergistic and superior performance for the cleavage of olefins.

Bearing these facts in mind, we have developed catalytic nanomaterials for light-driven oxidation of olefins in a PIC system. The system combines amphiphilic silica NPs loaded with Au NPs, acting as on-site heaters/plasmon activators, and  $[C_{12}]_3[PW_{12}O_{40}]$  NPs acting as catalysts (**Figure 3**). The physicochemical properties, stability and plasmonic effects of the emulsion stabilized with dual NPs have been systematically investigated. Then, the catalytic activity has been evaluated for the plasmon-assisted catalytic oxidation of cyclooctene using  $H_2O_2$  as oxidant under light irradiation. More importantly, the synergistic catalysis and on-site heater/plasmon activators for the oxidation of cyclooctene afforded much higher yield at milder conditions which cannot be achieved by the sole use of  $[C_{12}]_3[PW_{12}O_{40}]$  NPs.



**Figure 3.** Schematic illustration of the PIC system designed in this study using self-assembled amphiphilic silica NPs loaded with Au NPs, acting as on-site heaters/plasmon activators, and  $[C_{12}]_3[PW_{12}O_{40}]$  NPs, acting as catalyst, under light irradiation.

## 2. Experimental part

### 2.1. Materials

Reagent-grade  $\text{HAuCl}_4 \cdot 3\text{H}_2\text{O}$  (99.9%), sodium citrate (99%),  $\text{NaBH}_4$  (98%), (3-aminopropyl)triethoxysilane (APTES, 99%), sodium hydroxide (NaOH, 99%) and trimethoxy(propyl)silane (97%) were purchased from Aldrich (USA). Aerosil<sup>®</sup>200 was a generous gift from Evonik Industries AG (Germany). Hydrogen peroxide (50%) was supplied by VWR International (France). Cyclooctene (95%) was procured from TCI (Japan). Toluene (99%) and heptane (99%) were supplied by Sigma-Aldrich.  $\text{CDCl}_3$  (99.8%) was purchased from Euriso-top (France). All the aqueous solutions were prepared using Millipore water produced by a water purification system with a water resistivity higher than 18.2  $\text{M}\Omega \text{ cm}$  (Barnstead, Thermo Scientific, USA).

### 2.2. Synthesis of amphiphilic silica NPs ( $\text{SiO}_2\text{-C}_3$ )

In a typical procedure [56], a suspension of Aerosil<sup>®</sup>200 was prepared by adding 0.5 g Aerosil<sup>®</sup>200 in 200 mL water/ethanol solution (1/1 v/v, pH = 9.8). Then, 0.91 mL (5 mmol) of trimethoxy(propyl)silane ( $\text{C}_3$ ) was slowly added into the suspension under vigorous stirring. Furthermore, 0.105 mL (0.5 mmol) of APTES was added to the suspension. The reaction mixture was stirred at room temperature for 1 h, followed by heating at 80 °C for 1 h. The NPs were collected by centrifugation, and were washed with water and ethanol six times. Ultimately, the amphiphilic  $\text{SiO}_2\text{-C}_3$  NPs were dried at 80 °C overnight.

### 2.3. Synthesis of Au NPs

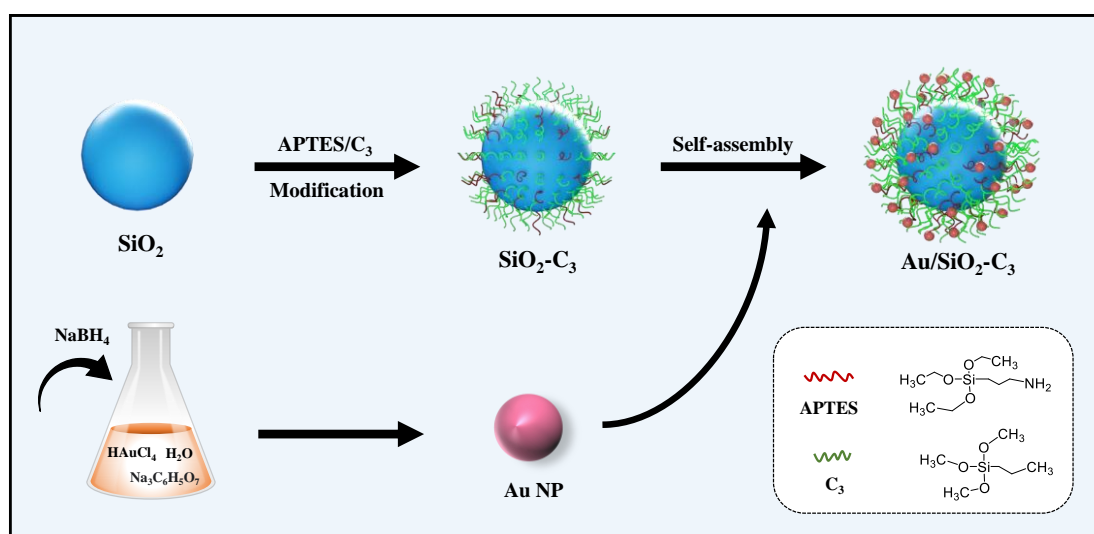
Au NPs were obtained using the protocol reported by Turkevich *et al.* [57]. In brief, 95 mL of an aqueous solution of  $\text{HAuCl}_4 \cdot 3\text{H}_2\text{O}$  (1 wt.%) was prepared, and then 2 mL of an aqueous solution of sodium citrate (38.8 mM) was added under vigorous stirring. After 1 min, 1 mL of a freshly prepared  $\text{NaBH}_4$  aqueous solution (10 mM) was added to the mixture which took a reddish color. The Au dispersion was stored under darkness at 4 °C.

## 2.4. Synthesis of Au-loaded amphiphilic silica NPs (Au/SiO<sub>2</sub>-C<sub>3</sub>)

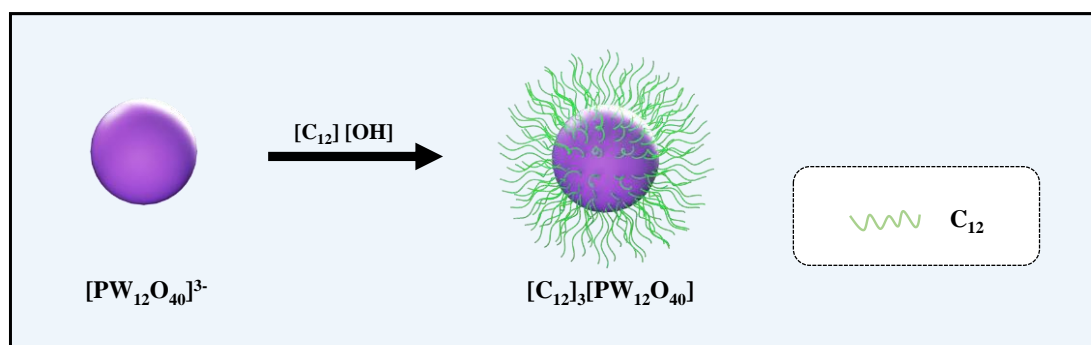
Au NPs were immobilized on the surface of amphiphilic SiO<sub>2</sub>-C<sub>3</sub> NPs by self-assembly method [58]. Firstly, 3 mL of a Au NPs dispersion (obtained in section 2.3) were added to 3 mL of an ethanolic dispersion of SiO<sub>2</sub>-C<sub>3</sub> NPs (1.5 wt.%) under vigorous stirring. The Au/SiO<sub>2</sub>-C<sub>3</sub> NPs was collected by centrifugation and washed with deionized water three times. The NPs were collected and then dried in an oven at 80 °C overnight. A scheme of the protocol for preparing Au/SiO<sub>2</sub>-C<sub>3</sub> NPs is provided in **Figure 4**.

## 2.5. Synthesis of amphiphilic POM NPs ([C<sub>12</sub>]<sub>3</sub>[PW<sub>12</sub>O<sub>40</sub>])

Amphiphilic POM NPs were prepared by the protocol described in ref. [55]. Briefly, 100 mL of an aqueous solution of dodecyltrimethylammonium bromide [C<sub>12</sub>][Br] (0.2 M) was eluted on a hydroxide ion exchange resin to obtain an aqueous solution of [C<sub>12</sub>][OH]. An aqueous solution of H<sub>3</sub>PW<sub>12</sub>O<sub>40</sub> (around 6.5 mmol, 10<sup>-4</sup> M) was added dropwise to the aqueous [C<sub>12</sub>][OH] solution (0.3 mM) until pH 7 at 25 °C under dry Ar and vigorous magnetic stirring (1,500 rpm). The colorless precipitate of tri(dodecyltrimethylammonium) phosphotungstate was obtained after a few minutes. The resulting [C<sub>12</sub>]<sub>3</sub>[PW<sub>12</sub>O<sub>40</sub>] NPs were collected and washed with water to remove impurities, and then lyophilized (**Figure 5**).



**Figure 4.** Schematic representation of the synthesis protocol of amphiphilic silica SiO<sub>2</sub>-C<sub>3</sub>, Au, and Au/SiO<sub>2</sub>-C<sub>3</sub> NPs.



**Figure 5.** Schematic representation of the synthesis protocol of amphiphilic [C<sub>12</sub>]<sub>3</sub>[PW<sub>12</sub>O<sub>40</sub>] NPs.

## 2.6. Physicochemical characterization of NPs

The Au and Au/SiO<sub>2</sub>-C<sub>3</sub> NPs were visualized by high-resolution transmission electron microscopy (HRTEM) using a JEOL JSM-6360LV microscope at a voltage of 200 kV.

The UV-Vis spectra of Au and Au/SiO<sub>2</sub>-C<sub>3</sub> NPs were recorded with a Nano Photometer N60 spectrometer (IMPLEN, Germany).

The nanoparticle size distribution and zeta potential of the different particle dispersions were obtained using Zetasizer (Nano ZS ZEN 3600, Malvern, UK) equipped with a He-Ne laser at 632.8 nm, using 0.1 wt.% particles dispersed in water at room temperature (a few drop of ethanol was added inside to wet hydrophobic NPs).

Fourier transform infrared spectroscopy (FT-IR) was performed using a Nicolet 380 FTIR Spectrometer equipped with an attenuated total reflector (Thermo Electron, USA).

Thermogravimetric analyses (TGA) were performed on a Q500 (TA Instruments, USA). In a typical test, at least 10 mg of sample was heated from 30 to 900 °C at a rate of 10 °C/min under nitrogen atmosphere (60 mL (STP)/min).

Contact angle measurement was performed by the sessile drop method (DSA 100 Krüss GmbH, Germany) by depositing a small drop of 4 µL of water onto the pellet with 100 mg NPs compressed at 1800 bar during 10 min.

The Au loading in the Au/SiO<sub>2</sub>-C<sub>3</sub> NPs was quantified by Agilent 5110 vertical dual view inductively coupled plasma optical emission spectrometer (ICP-OES) equipped with an

OneNeb nebulizer, a quartz double pass spray chamber and a quartz torch (Agilent). In a typical test, 50 mg samples were weighed and 1ml HF/1ml HCl/1ml HNO<sub>3</sub> were added and heated at 110 °C in closed teflon tubes for 24 h. Then, 30 ml of ultrapure water were added. The cleared solutions were filtered at 0.45 μm and diluted for the ICP-OES analysis.

X-ray photoelectron spectroscopy (XPS) was performed using a Kratos AXIS Ultra DLD spectrometer using a monochromatic Al K $\alpha$  radiation (1486.6 eV) operating at 225 W (15 mA, 15kV). High-resolution spectra were collected using an analysis area of  $\approx 300 \mu\text{m} \times 700 \mu\text{m}$  and a 20 eV pass energy.

## 2.7. Preparation of emulsions

Typically, 1.0 wt.% Au/SiO<sub>2</sub>-C<sub>3</sub> and 1.8 wt.% [C<sub>12</sub>]<sub>3</sub>[PW<sub>12</sub>O<sub>40</sub>] were dispersed in 1.5 mL of oil phase and ultrasound for 5 min, followed by the addition of 1.5 mL of water in a 5 mL glass vial. Emulsions were formed using Ultraturrax T10 basic (IKA, Germany) at room temperature and 11,500 rpm for 2 min.

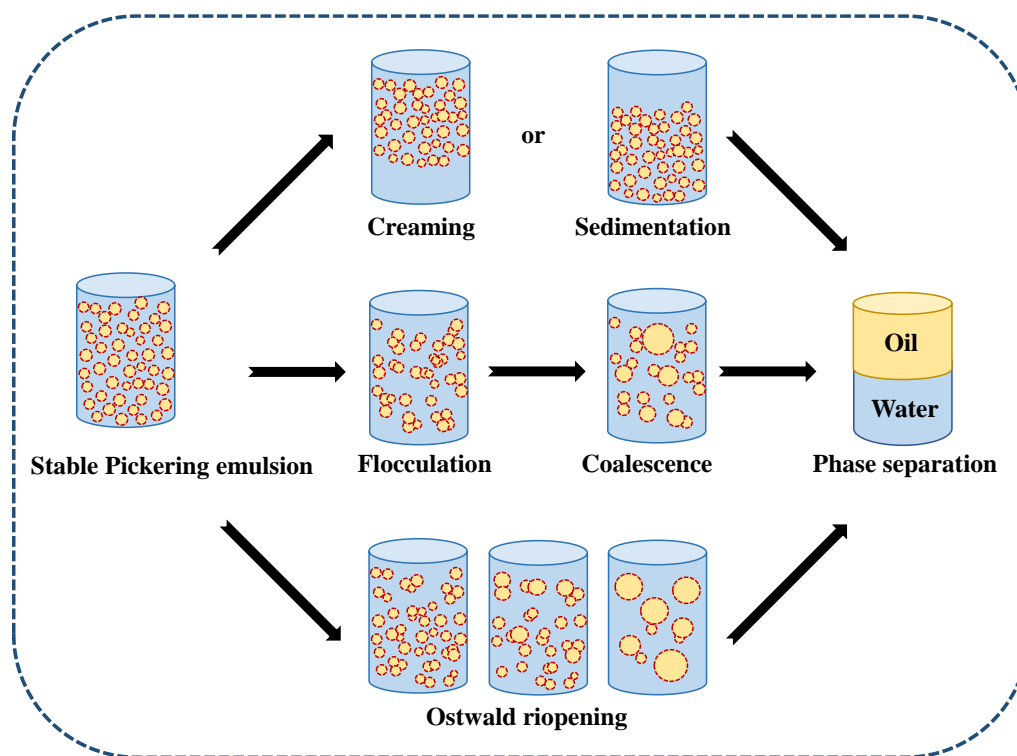
## 2.8. Emulsion characterization

Optical micrographs were taken using a VHX-900 F digital microscope equipped with a VH-Z100UR/W/T lens (Keyence, France). The emulsions were diluted with the continuous phase before observation, and photographs from different locations of the emulsion drop were taken to represent the general view of the emulsion droplets. The images were analyzed using ImageJ software (National Institutes of Health, USA) to measure the droplet diameter. The log-normal distribution function was obtained after statistical analysis of the micrographs using OriginPro 8<sup>®</sup> (OriginLab, USA).

The emulsion stability was characterized at 60 °C by static multiple light scattering (SMLS) using a Turbiscan Lab (Formulaction, France) operating with a near-infrared light source ( $\lambda = 880 \text{ nm}$ ). Transmission mode was used to analyze from clear to turbid dispersions while backscattering mode was used to analyze opaque and concentrated dispersions [59-61]. The light intensity of emulsion usually changes slightly, indicating a low change of droplet



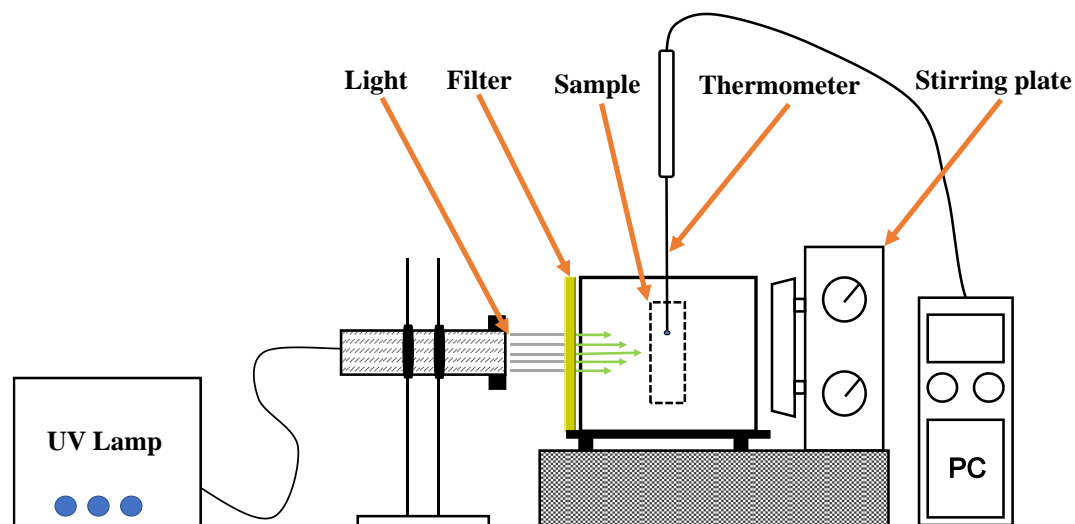
concentration and higher stability. More specifically, the  $\Delta BS$  intensity decreases for larger particle sizes (coalescence and flocculation) or at lower particle concentrations (sedimentation and creaming) when the particle size is larger than the incident wavelength. The decrease in  $\Delta BS$  at the top layer of an emulsion indicates a decrease in the top concentration and clarification of upper layer. In contrast, an increase of  $\Delta T$  at the top layer reflects the clarification process. Moreover, the backscattering light is more sensitive for detecting emulsion droplets because they have high obscuration which can reflect the backscattering light [62]. Meanwhile, transmission light is suitable to evaluate the diluted emulsion phase [63]. Several emulsion instability phenomena such as creaming, sedimentation, flocculation, coalescence and Ostwald ripening are depicted in **Figure 6**. Although gravitational separation can sometimes happen due to the difference in the density of the two immiscible phases, coalescence involving collision of two or more small droplets to form a single larger droplet can be considered as the parent instability mechanism [64-66].



**Figure 6.** Schematic representation of destabilization mechanisms of emulsions, where the yellow dots represent the droplets and the blue background indicates the continuous phase.

## 2.9. Photothermal conversion measurements

The photothermal conversion experiments were carried out under light irradiation using a Hg-Xe lamp (LightningCure LC8, Hamamatsu, Japan) incorporating a filter (A9616-09) inside to select the irradiation light (**Figure 7**). A thermal insulation was made with PS foam at the outside of the cuvette to limit heat dissipation. A 495-nm long-pass filter was placed between the sample and the light source (**Figure A-2**). The UV light irradiance distribution was dependent on the distance from the light output end to the target surface. The longer the distance from the light source to the target sample, the lower the power density and the larger beam size can be obtained. The light source was placed at 2 cm from the surface of the cuvette rendering a maximum power of 355 mW measured using an 843-R optical power meter (Newport Corporation). The beam size focused to around 6.7 mm with the maximum power density of 1 W/cm<sup>2</sup>. The temperature change of the solution was recorded using a data logger thermometer YC-727U (Maximum Electronic Co., LTD). The thermometer was kept outside the irradiation area to avoid photoheating of the iron-made probe. A magnetic stirrer was used for gentle stirring. In the photothermal conversion test, 1 mL of Au NPs dispersion or Au/SiO<sub>2</sub>-C<sub>3</sub> emulsion were irradiated with light. The temperature change of the prepared sample was recorded every 20 s.



**Figure 7.** Scheme of the experimental setup used for measuring temperature changes under light irradiation mediated by NPs. Nomenclature: **Light** indicates UV lamp irradiation; **filter** indicates the 495 nm long-pass filter; **sample** indicates the aqueous solution or emulsion sample in a quartz cuvette (1 mL), and **thermometer** connected to computer for recording the temperature change; **stirring plate** was set at 120 rpm to keep the sample homogeneous.

### 2.10. Plasmon-assisted catalytic tests

In a typical catalytic test, 1.5 mL of toluene containing cyclooctene (2 mol/L) and 1.5 mL of water containing 1.2 equiv. H<sub>2</sub>O<sub>2</sub> (50%) were added to a 5-mL glass vial, followed by [C<sub>12</sub>]<sub>3</sub>[PW<sub>12</sub>O<sub>40</sub>] (50 mg) and Au/SiO<sub>2</sub>-C<sub>3</sub> (30 mg) at room temperature. The final dispersion was emulsified using an Ultraturrax at 11,500 rpm for 2 min. Then, 1 mL of the obtained emulsion was added into a 2-mL cuvette, and it was gently stirred at 120 rpm under light irradiation (495 nm wavelength) at a given power density for the desired period of time. The temperature change inside the emulsion was recorded every 20 s.

After the reaction, the system was demulsified by centrifugation, the upper oil phase was separated by decantation, and it was dissolved in CDCl<sub>3</sub>, whereas C<sub>2</sub>Cl<sub>4</sub>H<sub>2</sub> was used as internal standard for analysis. Then, 50 μL of the oil phase, 50 μL (0.5 mol/L) of the internal standard solution and 400 μL of deuterated CDCl<sub>3</sub> were added in a NMR tube. The yield was measured by <sup>1</sup>H NMR on an Advance 300 Bruker spectrometer at 300.12 MHz.

For catalyst reuse experiments, the mixed NPs were collected by centrifugation and dried at 80 °C. The emulsification protocol describe above was repeated and the subsequent catalytic run was carried out.

For control experiments, the catalytic reaction was performed at the same emulsification and reaction conditions described above, but under heating in an oil bath (IKA, RCT standard, heat output 600 W), and the temperature was set as the corresponding maximum temperature reached with the light-driven experiment. Another catalytic reaction was carried out at identical conditions at room temperature in a dark environment, i.e. without light irradiation.

The laser-driven catalytic experiments were carried out with the same setup and identical catalytic reaction conditions, but changing the light source. For pulsed laser tests, a 532 nm pulsed laser Surelite II (Continuum, USA) operating in 10 Hz repetition rate and 10 ns pulse width was employed to investigate the plasmon-assisted oxidation of olefins in emulsion. The average power is set to around 500 mW and the beam size of the laser focused to around 10 mm, while the average power density of the pulsed laser is around 100 mW/cm<sup>2</sup>.

### 3. Results and discussion

#### 3.1 Synthesis and characterization of NPs

##### 3.1.1. Dynamic light scattering measurements

The dynamic properties of the NPs in aqueous solution were characterized using dynamic light scattering (DLS) [67-69]. **Table 1** shows the results of the mean particle size and zeta potential of the as-prepared NPs. The Au NPs have a hydrodynamic diameter around 13 nm, with a zeta potential of  $-34.7$  mV. It is also observed that the hydrodynamic diameter of bare SiO<sub>2</sub> NPs is around 90 nm, with a negative surface charge of  $-38$  mV. After surface modification, the surface charge of SiO<sub>2</sub>-C<sub>3</sub> NPs becomes strongly positive ( $+42.6$  mV), which can be attributed to protonated amine groups on silica surface. By comparing the surface charge of SiO<sub>2</sub>-C<sub>3</sub> and Au/SiO<sub>2</sub>-C<sub>3</sub>, the overall charge of Au/SiO<sub>2</sub>-C<sub>3</sub> NPs decreases slightly ( $+40.3$  mV), suggesting that the silica surface is not fully covered with Au NPs [70]. The hydrodynamic diameter of the SiO<sub>2</sub>-C<sub>3</sub> NPs is about 200 nm in water. This observation points out partial aggregation of NPs. The average hydrodynamic diameter of Au/SiO<sub>2</sub>-C<sub>3</sub> NPs remains approximately the same as SiO<sub>2</sub>-C<sub>3</sub> NPs. Finally, [C<sub>12</sub>]<sub>3</sub>[PW<sub>12</sub>O<sub>40</sub>] NPs display a hydrodynamic diameter of 48 nm, with a negative surface charge of  $-31.7$  mV.

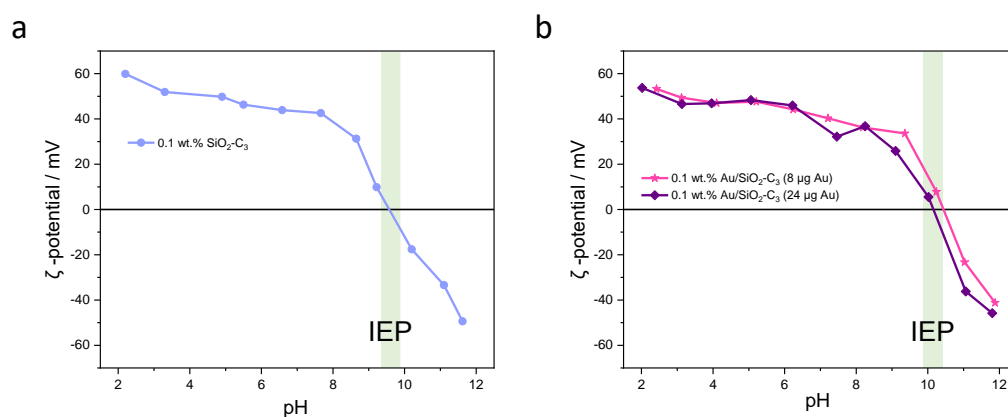
**Table 1** Main physicochemical properties of the NPs prepared in this study

	Au	SiO <sub>2</sub>	SiO <sub>2</sub> -C <sub>3</sub>	Au/SiO <sub>2</sub> -C <sub>3</sub>	[C <sub>12</sub> ] <sub>3</sub> [PW <sub>12</sub> O <sub>40</sub> ]
D <sub>h</sub> (nm) <sup>a</sup>	13	90	190	207	48
ζ (mV) <sup>b</sup>	-34.7	-38	42.6	40.3	-31.7

<sup>a</sup> Hydrodynamic diameter of NPs measured by DLS. <sup>b</sup> Determined for 0.1 wt.% NPs suspensions in water at 25 °C in neutral pH.

To better understand the interaction between water and the dispersed particles, a series of zeta potential measurements were carried out as a function of the pH. As shown in **Figure 8a**, the surface charge of SiO<sub>2</sub>-C<sub>3</sub> NPs evolves from positive to negative with a zeta potential

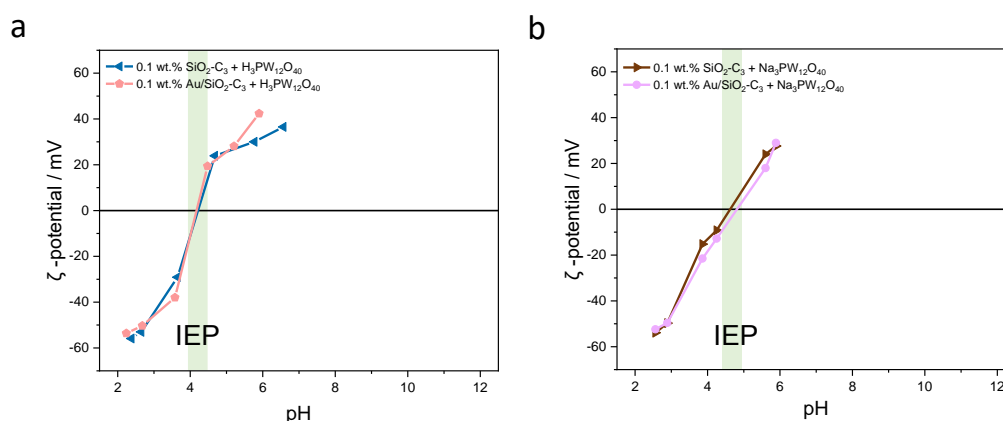
ranging from +59.9 mV to  $-49.4$  mV by increasing the pH from 2 to 12 with an isoelectric point (IEP) at around pH 10. The positive charge is attributed to the presence of amine groups on the silica surface, which tend to be fully protonated and form  $-\text{NH}_3^+$  at low pH. By comparing the surface charge of  $\text{SiO}_2\text{-C}_3$  and  $\text{Au/SiO}_2\text{-C}_3$  at pH 2 (**Figure 8b**), the zeta potential exhibits a slightly higher value in the former case (+59.9 mV vs. +53.3 mV). This observation points out the presence of free amine groups after decoration with Au NPs. Above pH 10, the amine groups are fully deprotonated and a negative zeta potential is observed (up to  $-41.2$  mV at pH 12). Compared to  $\text{SiO}_2\text{-C}_3$  NPs,  $\text{Au/SiO}_2\text{-C}_3$  NPs display a lower surface charge value over the pH because of the presence of Au NPs on the surface. When more Au NPs are grafted on the silica surface (the amount of Au increases from 8 to 24  $\mu\text{g}$ ), the surface charge value slightly decreases. The  $\text{SiO}_2\text{-C}_3$  and  $\text{Au/SiO}_2\text{-C}_3$  NPs dispersions are stable below pH 8 and above 12, since zeta potential values are outside the range  $\pm 30$  mV [71].



**Figure 8.** Evolution of the zeta potential as a function of the pH for dispersions of  $\text{SiO}_2\text{-C}_3$  and  $\text{Au/SiO}_2\text{-C}_3$  NPs in water at 25 °C (IEP = isoelectric point). pH adjusted using different concentration of HCl and NaOH ( $1$  to  $10^{-4}$  M) aqueous solution. (a) 0.1 wt.%  $\text{SiO}_2\text{-C}_3$  dispersion in deionized water; (b) 0.1 wt.%  $\text{Au/SiO}_2\text{-C}_3$  dispersion at variable Au loading.

In order to develop a PIC system, the surface of silica NPs was decorated with Keggin-type  $\text{H}_3\text{PW}_{12}\text{O}_{40}$ , and the zeta potential was measured to assess the electrostatic interactions between  $\text{Au/SiO}_2\text{-C}_3$  and  $\text{H}_3\text{PW}_{12}\text{O}_{40}$  (**Figure 9a**). In the preparations,  $\text{H}_3\text{PW}_{12}\text{O}_{40}$  solution was used to adjust the pH of the  $\text{Au/SiO}_2\text{-C}_3$  dispersion. The surface charge of  $\text{Au/SiO}_2\text{-C}_3$  +  $\text{H}_3\text{PW}_{12}\text{O}_{40}$  mixture is negative ( $-53.6$  mV) at pH 2.2. Compared to  $\text{Au/SiO}_2\text{-C}_3$  NPs in the acid

pH range, the addition of  $\text{H}_3\text{PW}_{12}\text{O}_{40}$  affects the surface charge of  $\text{Au}/\text{SiO}_2\text{-C}_3$  NPs. The protonation of  $-\text{NH}_2$  groups by addition of  $\text{H}_3\text{PW}_{12}\text{O}_{40}$  results in the formation of ammonium POM, that is  $[-\text{CH}_2\text{NH}_3]_3[\text{PW}_{12}\text{O}_{40}]$  [72-74]. As the  $\text{H}_3\text{PW}_{12}\text{O}_{40}$  concentration increases from 0.001 to 14  $\mu\text{mol/L}$  (pH from 6.5 to 2.4), the surface charge of  $\text{SiO}_2\text{-C}_3$  NPs evolves from positive to negative (from +36.5 to -55.9 mV), while the IEP is reached at pH 4, indicating that the amine groups on the silica surface have been fully covered with  $[-\text{PW}_{12}\text{O}_{40}]^{3-}$  anions. Above pH 4, an excess of free amine groups leads to a positive charge. This phenomenon could indicate that  $[\text{PW}_{12}\text{O}_{40}]^{3-}$  ions are coated on the surface of  $\text{SiO}_2\text{-C}_3$  NPs and induces the formation of  $\text{SiO}_2\text{-C}_3/\text{H}_3\text{PW}_{12}\text{O}_{40}$  complex. Moreover, the adsorption of  $[\text{PW}_{12}\text{O}_{40}]^{3-}$  on the surface of  $\text{Au}/\text{SiO}_2\text{-C}_3$  NPs is favorable for catalysis in a Pickering emulsion system.

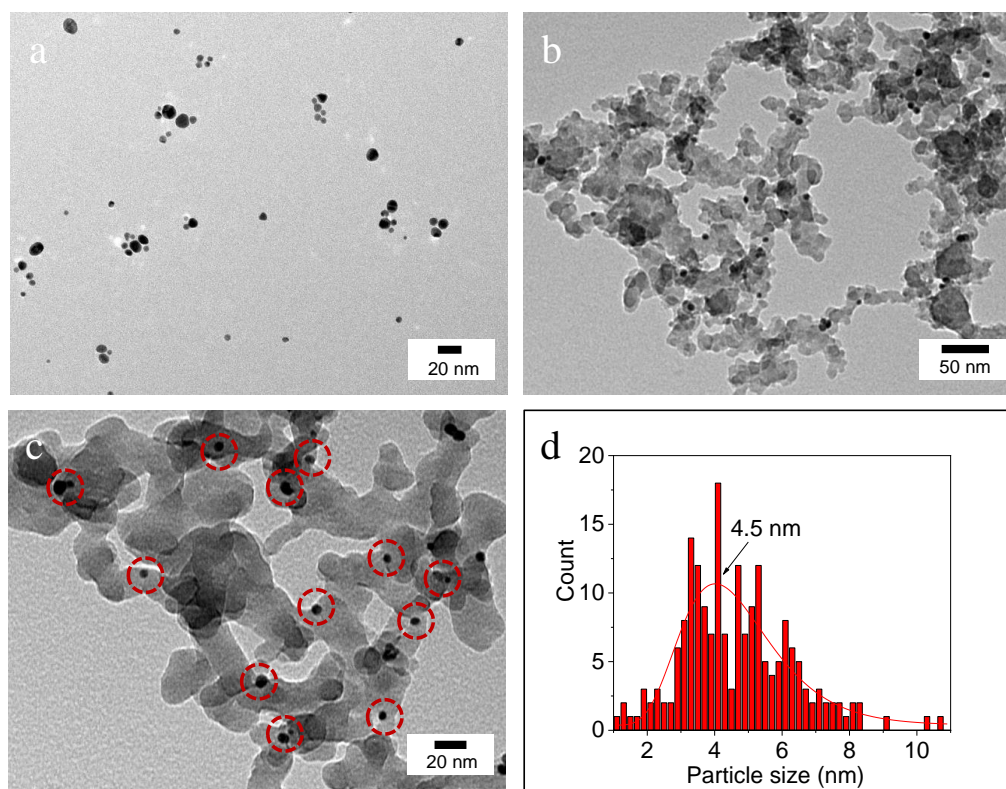


**Figure 9.** Evolution of the zeta potential as a function of the pH for 0.1 wt.%  $\text{SiO}_2\text{-C}_3$  and  $\text{Au}/\text{SiO}_2\text{-C}_3$  NPs (8  $\mu\text{g}$  Au loading amount) dispersion in water at 25  $^\circ\text{C}$ . (a) pH adjusted with  $\text{H}_3\text{PW}_{12}\text{O}_{40}$  solution (1 to  $10^{-4}$  M); (b) pH adjusted with  $\text{Na}_3\text{PW}_{12}\text{O}_{40}$  solution (1 to  $10^{-4}$  M).

$\text{Na}_3\text{PW}_{12}\text{O}_{40}$  is Keggin type polyoxotungstate sodium salt that can be adsorbed on the silica surface. It is noteworthy that the interaction of  $\text{SiO}_2\text{-C}_3$  NPs with  $\text{Na}_3\text{PW}_{12}\text{O}_{40}$  is similar to that of  $\text{H}_3\text{PW}_{12}\text{O}_{40}$  alone because  $[\text{PW}_{12}\text{O}_{40}]^{3-}$  induces the formation of  $\text{H}^+$  in water (**Figure 9b**). The surface of  $\text{Au}/\text{SiO}_2\text{-C}_3$  NPs in water is positive (+40.3 mV) at neutral pH. The higher the  $\text{Na}_3\text{PW}_{12}\text{O}_{40}$  concentration, the lower the  $\text{Au}/\text{SiO}_2\text{-C}_3$  surface charge. It indicates the effective adsorption of  $[\text{PW}_{12}\text{O}_{40}]^{3-}$  on the surface of  $\text{Au}/\text{SiO}_2\text{-C}_3$ . As the  $\text{Na}_3\text{PW}_{12}\text{O}_{40}$  concentration continues to increase, multiple-layer adsorption of  $[\text{PW}_{12}\text{O}_{40}]^{3-}$  on  $\text{Au}/\text{SiO}_2\text{-C}_3$  may be formed [75, 76]. Above pH 4, the zeta potential of  $\text{Au}/\text{SiO}_2\text{-C}_3$  NPs turns positive.

### 3.1.2. Transmission electron microscopy characterization

The surface architecture and morphology of the different NPs were characterized by TEM (**Figure 10**). Au NPs present a uniform spherical structure (**Figure 10a**). The immobilization of Au NPs on SiO<sub>2</sub>-C<sub>3</sub> NPs is confirmed in **Figure 10b and c**, although the amount of Au NPs visible is low. The TEM image indicates that Au/SiO<sub>2</sub>-C<sub>3</sub> particles are spherical with large size polydispersity, which is consistent with the DLS measurement. Au NPs (highlighted by red circles) are well dispersed on the silica surface. Image analysis indicates a size of Au NPs around 4.5 nm (**Figure 10d**). Based on the ICP analysis, the loading of Au is about 0.13 wt.%.

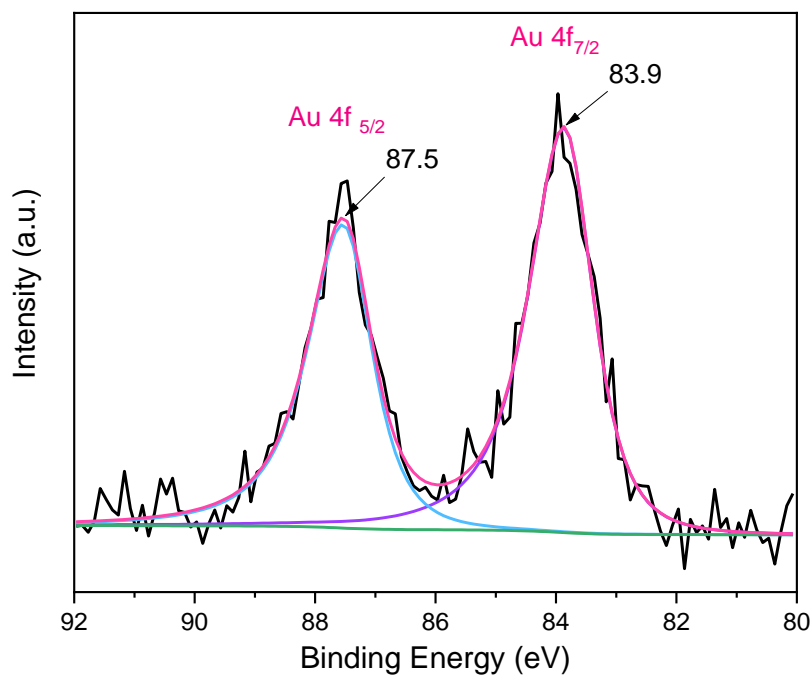


**Figure 10.** TEM micrograph of (a) Au NPs, (b and c) Au/SiO<sub>2</sub>-C<sub>3</sub> NPs and (d) the particle size distributions of the Au NPs.

### 3.1.3. X-ray photoelectron spectroscopy analysis

XPS was performed to evaluate the surface composition and oxidation state of Au in Au/SiO<sub>2</sub>-C<sub>3</sub>. Typically, the binding energy of Au (4f<sub>7/2</sub>) component for a standard metallic gold film (Au<sup>0</sup>) is observed at 84.0 eV. However, the binding energy of Au 4f can vary depending on

the particle size of Au NPs the support. It can be seen in **Figure 11** that the binding energy of the Au ( $4f_{7/2}$ ) component for Au/SiO<sub>2</sub>-C<sub>3</sub> is measured to be 83.9 eV, confirming that the Au surface is mainly in the metallic state. This negative peak shift in the binding energy could be attributed to the metal-support (Au/SiO<sub>2</sub>) interaction and chemical environment [77, 78].

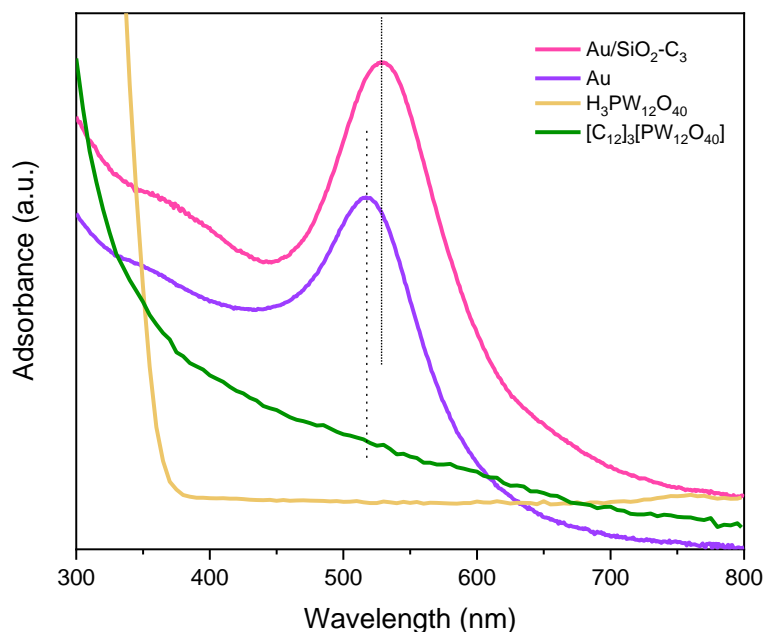


**Figure 11.** XPS Au 4f scan of Au/SiO<sub>2</sub>-C<sub>3</sub> NPs.

### 3.1.4. UV-vis spectroscopy

As displayed in **Figure 12**, Au NPs exhibit a significant surface plasmon resonance characteristic band at around 518 nm [79, 80]. Most notably, the spectrum of Au/SiO<sub>2</sub>-C<sub>3</sub> shows a band at around 528 nm that is slightly shifted compared with that of Au NPs. This can be explained by the variation in the distances between Au NPs and the change of dielectric constant due to the silica environment [81]. However, pure H<sub>3</sub>PW<sub>12</sub>O<sub>40</sub> and [C<sub>12</sub>]<sub>3</sub>[PW<sub>12</sub>O<sub>40</sub>] only display the UV-light absorption properties.

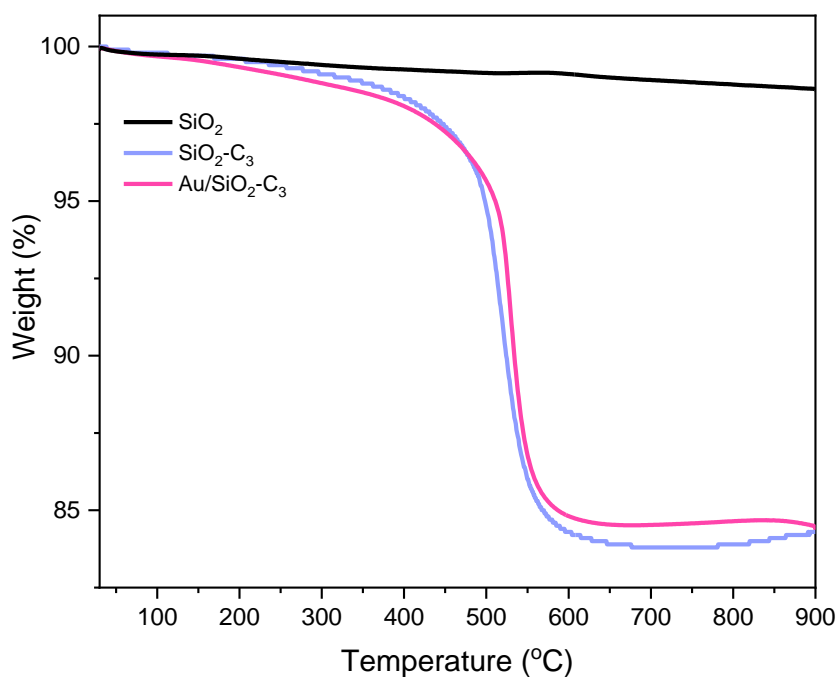




**Figure 12.** UV-vis spectra of Au, Au/SiO<sub>2</sub>-C<sub>3</sub>, H<sub>3</sub>PW<sub>12</sub>O<sub>40</sub> and [C<sub>12</sub>]<sub>3</sub>[PW<sub>12</sub>O<sub>40</sub>] dispersion. The spectra were measured using deionized water for Au NPs, H<sub>3</sub>PW<sub>12</sub>O<sub>40</sub> and [C<sub>12</sub>]<sub>3</sub>[PW<sub>12</sub>O<sub>40</sub>], and SiO<sub>2</sub>-C<sub>3</sub> for Au/SiO<sub>2</sub>-C<sub>3</sub> NPs, respectively, which were used as references.

### 3.1.5. Thermostability

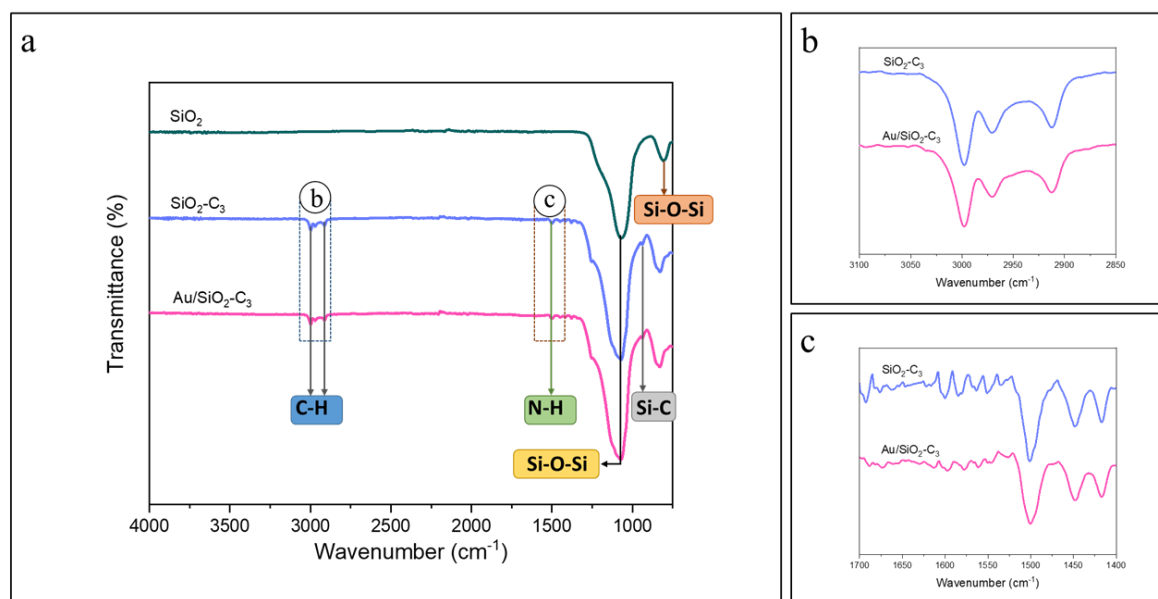
The stability of the different particles was investigated by thermogravimetric analysis. As shown in **Figure 13**, SiO<sub>2</sub> NPs show high thermal stability with a weight loss of 0.4% from 30 to 200 °C, which is attributed to water desorption. The total weight loss is observed to be 1.5% for the bare SiO<sub>2</sub> in the whole range of 30-900 °C due to condensation of silanol groups in the temperature range 200-900 °C [56]. Both SiO<sub>2</sub>-C<sub>3</sub> and Au/SiO<sub>2</sub>-C<sub>3</sub> NPs show almost no weight loss (1.0%) from 30 to 200 °C. For SiO<sub>2</sub>-C<sub>3</sub> NPs, a weight loss of 15.3% between 400 °C and 600 °C is observed that can be assigned to the decomposition of amine groups and C<sub>3</sub> chains, but with no significant weight change between 600 to 900 °C. Au/SiO<sub>2</sub>-C<sub>3</sub> NPs exhibit a similar trend with a weight change about 14.5% between 400 to 600 °C. This observation supports the excellent stability of the obtained Au/SiO<sub>2</sub>-C<sub>3</sub> NPs.



**Figure 13.** Thermogravimetric profiles of SiO<sub>2</sub>, SiO<sub>2</sub>-C<sub>3</sub> and Au/SiO<sub>2</sub>-C<sub>3</sub> NPs. Experimental conditions: 10-20 mg samples for each analysis, 10 °C/min from 30 to 900 °C and N<sub>2</sub> as atmosphere.

### 3.1.6. Fourier transform infrared spectroscopy

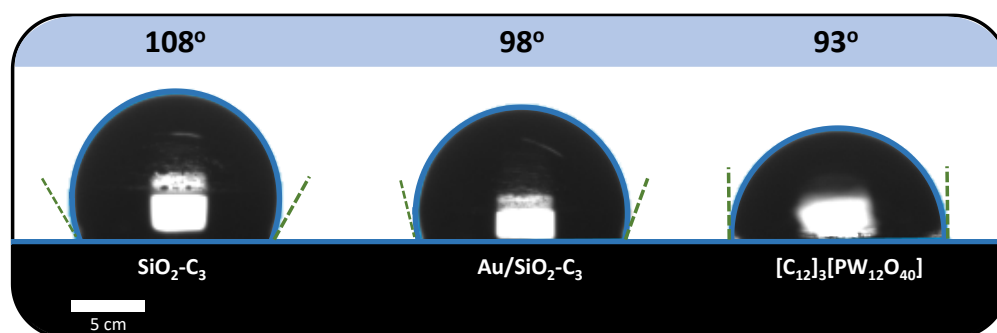
To confirm the presence of alkyl chains and amine groups on the silica surface, the FT-IR spectra of SiO<sub>2</sub>, SiO<sub>2</sub>-C<sub>3</sub> and Au/SiO<sub>2</sub>-C<sub>3</sub> NPs were measured. As shown in **Figure 14**, two bands at 1070 and 810 cm<sup>-1</sup> can be attributed to asymmetric and stretching vibrations of Si-O-Si bonds, respectively. After surface modification with C<sub>3</sub> chains and amine groups, characteristic bands appear at 2993 and 2904 cm<sup>-1</sup> that can be attributed to -CH<sub>2</sub> stretching vibrations in the C<sub>3</sub> chain. The absorption band at 1505 cm<sup>-1</sup> (bending vibration of -NH) confirms the grating of APTES on the silica surface. Characteristic bands appear at 930 cm<sup>-1</sup> can be assigned to stretching modes of Si-C groups. The Au NPs coating does not affect the spectrum of Au/SiO<sub>2</sub>-C<sub>3</sub> NPs compared to SiO<sub>2</sub>-C<sub>3</sub> NPs. These results prove the successful functionalization of Au/SiO<sub>2</sub>-C<sub>3</sub> NPs.



**Figure 14.** FT-IR spectra (transmittance mode) of  $\text{SiO}_2$ ,  $\text{SiO}_2\text{-C}_3$  and  $\text{Au/SiO}_2\text{-C}_3$  NPs. (a) Complete spectra. (b) and (c) Magnification of the spectra.

### 3.1.7. Water contact angle analysis

The surface wettability of the particles was characterized by water contact angle analysis. The hydrophilic  $\text{SiO}_2$  NPs show no measurable contact angle because of instantaneous water absorption [82]. In contrast, as shown in **Figure 15**, the water contact angle of  $\text{SiO}_2\text{-C}_3$  is  $108^\circ$ , indicating that  $\text{C}_3$  moieties successfully modify the silica surface.  $\text{Au/SiO}_2\text{-C}_3$  NPs are less hydrophobic ( $98^\circ$ ) than  $\text{SiO}_2\text{-C}_3$  because of the hydrophilicity of the grafted Au NPs.  $[\text{C}_{12}]_3[\text{PW}_{12}\text{O}_{40}]$  NPs are less hydrophobic ( $93^\circ$ ). According to the Bancroft rule [83], emulsion stabilized with these NPs are expected to be water-in-oil.

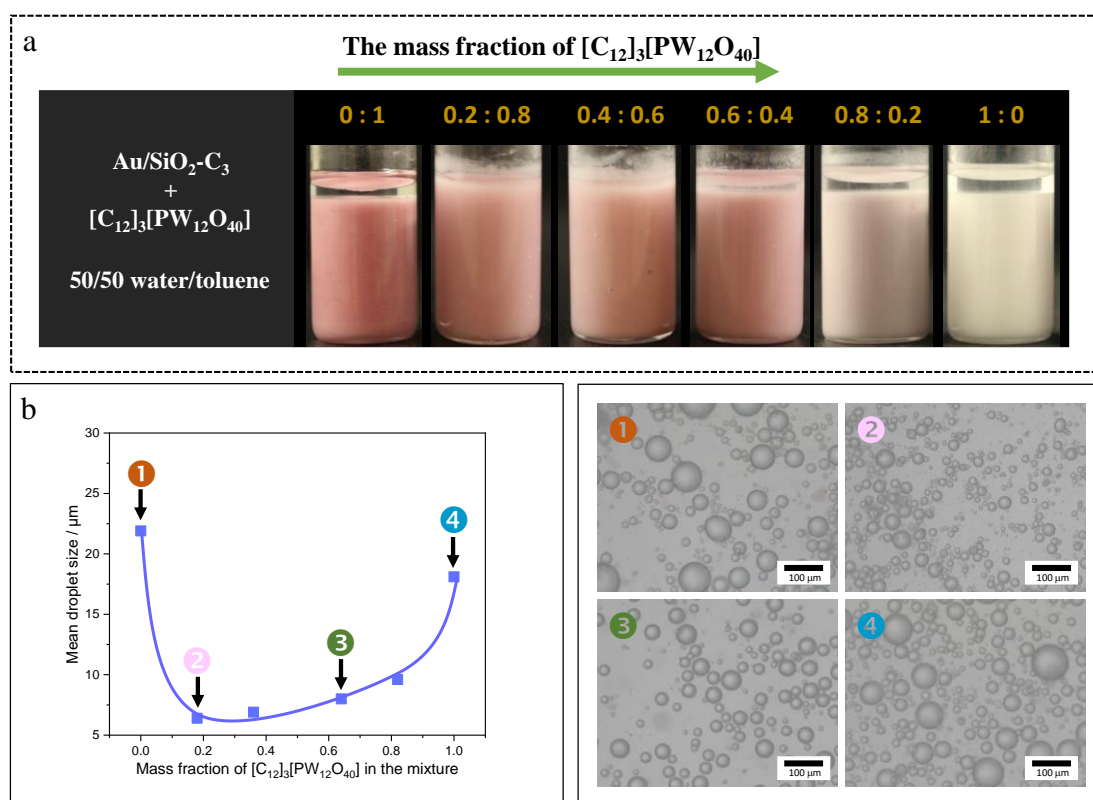


**Figure 15.** Photographs of water droplets deposited on compressed NPs and corresponding contact angles measured with water.

## 3.2. Physicochemical properties of the Pickering emulsions

### 3.2.1. Synergistic effect between Au/SiO<sub>2</sub>-C<sub>3</sub> and polyoxometalates (POMs) nanoparticles

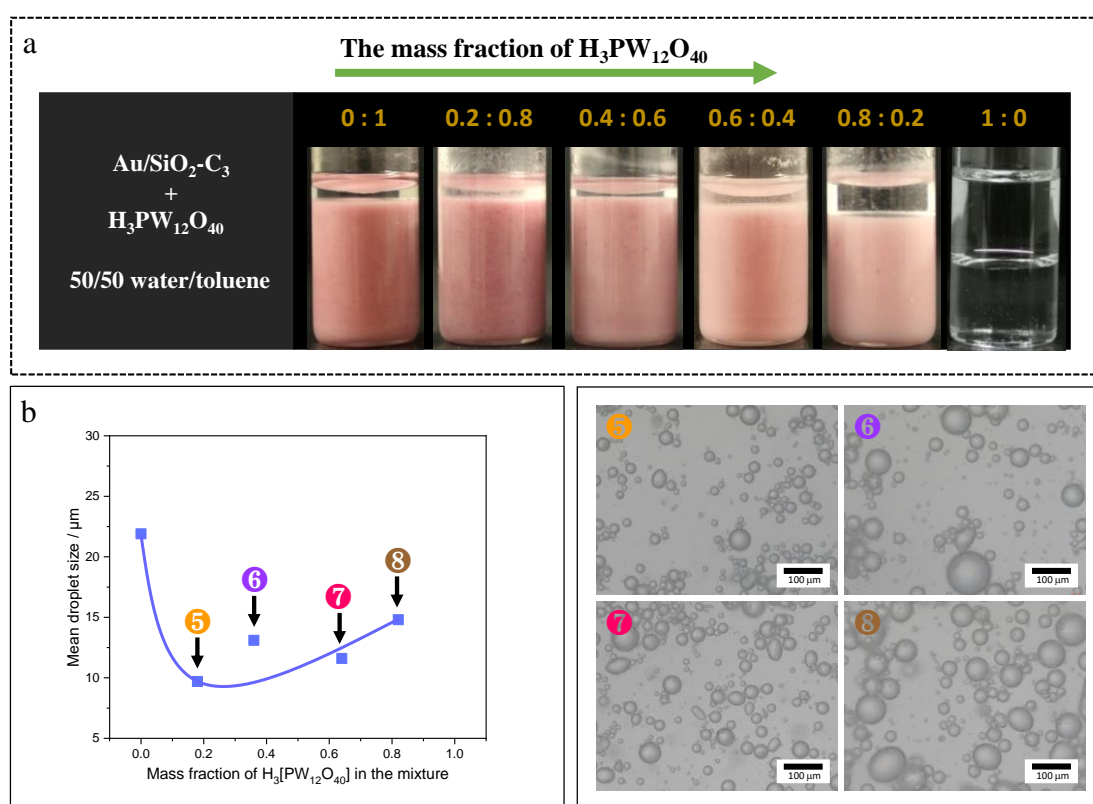
The emulsification properties of Au/SiO<sub>2</sub>-C<sub>3</sub> NPs + POMs (here, POM correspond to [C<sub>12</sub>]<sub>3</sub>[PW<sub>12</sub>O<sub>40</sub>] or H<sub>3</sub>PW<sub>12</sub>O<sub>40</sub> NPs) for a 50 : 50 (v/v) water/toluene biphasic system were investigated with different mass fractions of POM. The emulsions were observed by optical microscopy to assess the emulsion type and the evolution of the average droplets size with the POM mass fraction (Figure 16, Figure 17, Table A-1 and A-2).



**Figure 16.** (a) Photographs of emulsion droplets stabilized by Au/SiO<sub>2</sub>-C<sub>3</sub> NPs + [C<sub>12</sub>]<sub>3</sub>[PW<sub>12</sub>O<sub>40</sub>] NPs at variable mass fractions; (b) Evolution of the average droplet size as a function of the [C<sub>12</sub>]<sub>3</sub>[PW<sub>12</sub>O<sub>40</sub>] mass fraction for emulsions stabilized by Au/SiO<sub>2</sub>-C<sub>3</sub> NPs + [C<sub>12</sub>]<sub>3</sub>[PW<sub>12</sub>O<sub>40</sub>] NPs (the guided line is added manually). The inset present the micrographs of water-in-oil emulsions. *Emulsification conditions: 1.5 mL toluene, 1.5 mL water, 80 mg NPs (2.8 wt.%), emulsification at 11,500 rpm for 2 min.*

A water-in-oil emulsion is obtained using [C<sub>12</sub>]<sub>3</sub>[PW<sub>12</sub>O<sub>40</sub>] NPs, and the average droplet size is 18 μm. In parallel, Au/SiO<sub>2</sub>-C<sub>3</sub> NPs can stabilize a water-in-oil emulsion with an average

droplet size of 22  $\mu\text{m}$ . In this case, the color of the emulsion becomes pink due to the presence of Au NPs. In contrast, the droplet size of the emulsions stabilized with Au/SiO<sub>2</sub>-C<sub>3</sub> NPs + [C<sub>12</sub>]<sub>3</sub>[PW<sub>12</sub>O<sub>40</sub>] NPs are 2–4 times smaller compared to the average droplet size of the emulsion stabilized by Au/SiO<sub>2</sub>-C<sub>3</sub> NP or [C<sub>12</sub>]<sub>3</sub>[PW<sub>12</sub>O<sub>40</sub>] NPs alone. The emulsion droplets have smaller and more uniform by changing the mass ratio between Au/SiO<sub>2</sub>-C<sub>3</sub> NPs + [C<sub>12</sub>]<sub>3</sub>[PW<sub>12</sub>O<sub>40</sub>] NPs, suggesting a synergistic effect between both NPs. The combination of Au/SiO<sub>2</sub>-C<sub>3</sub> NPs and [C<sub>12</sub>]<sub>3</sub>[PW<sub>12</sub>O<sub>40</sub>] NPs shows almost zero zeta potential (−3 mV), indicating that both NPs show electrostatic interaction or neutralization to produce a complex.



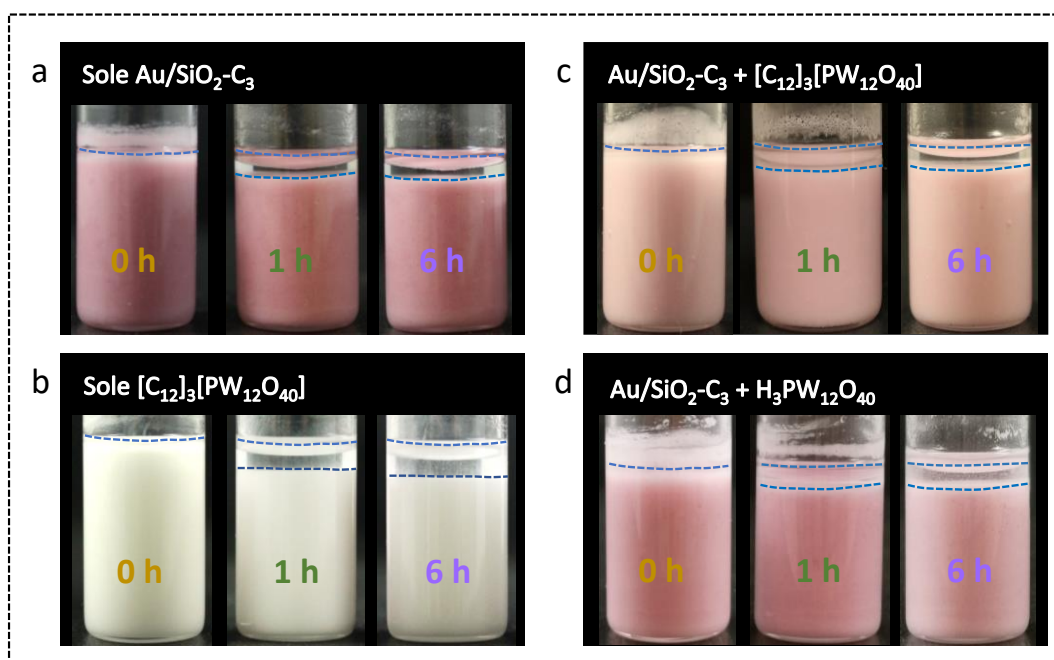
**Figure 17.** (a) Photographs of emulsion droplets stabilized by Au/SiO<sub>2</sub>-C<sub>3</sub> NPs + H<sub>3</sub>PW<sub>12</sub>O<sub>40</sub> NPs at variable mass fractions; (b) Evolution of the average droplet size as a function of the H<sub>3</sub>PW<sub>12</sub>O<sub>40</sub> mass fraction for emulsions stabilized by Au/SiO<sub>2</sub>-C<sub>3</sub> NPs + H<sub>3</sub>PW<sub>12</sub>O<sub>40</sub> NPs (the guided line is added manually). The inset present the micrographs of water-in-oil emulsions. *Emulsification conditions: 1.5 mL toluene, 1.5 mL water, 80 mg NPs (2.8 wt.%), emulsification at 11,500 rpm for 2 min.*

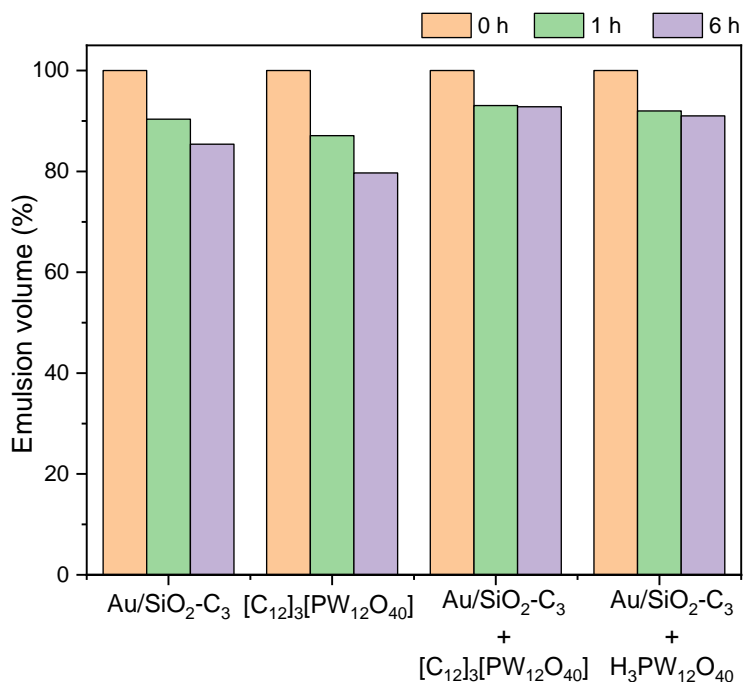
Opposing the above observations, the droplet size of emulsions stabilized by Au/SiO<sub>2</sub>-C<sub>3</sub> NPs + H<sub>3</sub>PW<sub>12</sub>O<sub>40</sub> NPs decreases first, and then increases with the H<sub>3</sub>PW<sub>12</sub>O<sub>40</sub> mass fraction in the mixture despite the lower total amount of solid particles in the system. This can be explained

by the pH induced change of surface charge of Au/SiO<sub>2</sub>-C<sub>3</sub> NPs [36]. The pH of the emulsion stabilized with mixed Au/SiO<sub>2</sub>-C<sub>3</sub> NPs + H<sub>3</sub>PW<sub>12</sub>O<sub>40</sub> was estimated by adding 1 wt.% emulsion to water, and the pH evolves from 3.6 to 4.3. Based on the results of zeta potential, the surface charge of Au/SiO<sub>2</sub>-C<sub>3</sub> is highly negative in the presence of H<sub>3</sub>PW<sub>12</sub>O<sub>40</sub>. This high surface charge value usually refers to the ability to form a relatively stable suspension.

### 3.2.2. Emulsion stability

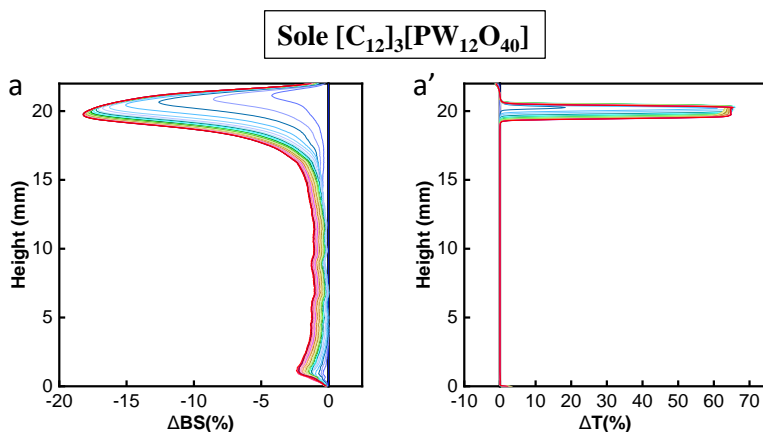
The emulsion stability was evaluated as a function of time for Au/SiO<sub>2</sub>-C<sub>3</sub> NPs and POM NPs, and for a mixture of both NPs (**Figure 18**). Combining both NPs, the emulsions are much more stable with no obvious collapse after 6 h at 60 °C compared to the emulsions prepared with only Au/SiO<sub>2</sub>-C<sub>3</sub> or POM NPs. To gain more insight into the stability of the emulsions, multiple light scattering measurements were performed using Turbiscan to monitor the change of transmission ( $\Delta T$ ) and backscattering ( $\Delta BS$ ) light intensity. Both the  $\Delta T$  and  $\Delta BS$  intensities are a function of the volume of the emulsion phase at a specific height and droplet size of the sample.

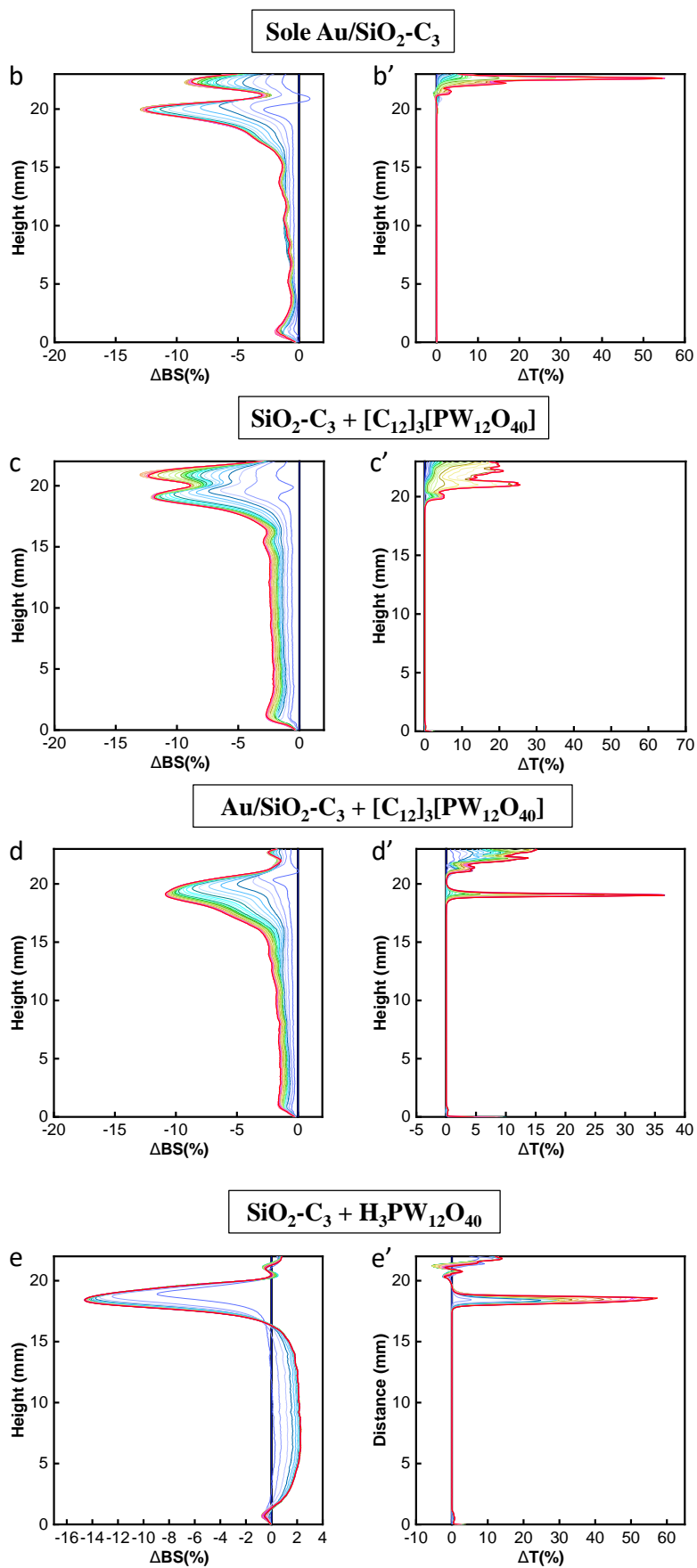




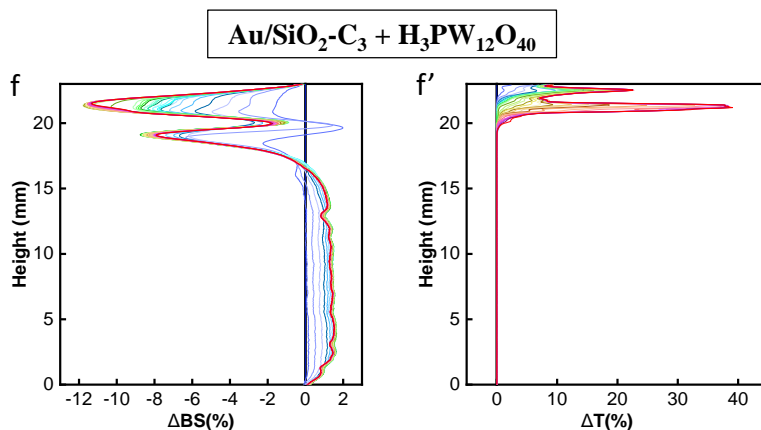
**Figure 18.** Photographs (a-d) and emulsion volume fractions (e) of water/toluene Pickering emulsion stabilized by Au/SiO<sub>2</sub>-C<sub>3</sub> NPs, [C<sub>12</sub>]<sub>3</sub>[PW<sub>12</sub>O<sub>40</sub>] NPs, and a 40/60 wt.% combination of Au/SiO<sub>2</sub>-C<sub>3</sub> NPs + POM NPs at 60 °C. *Emulsification conditions: 1.5 mL toluene, 1.5 mL water, 80 mg (2.8 wt.%) NPs, 11,500 rpm for 2 min.*

The obtained curves represent the variation of  $\Delta$ BS and  $\Delta$ T from the bottom of the sample to the top, with the curve color changing from blue to red from 0 to 6 h (**Figure 19**). The  $\Delta$ BS value of the top layer of [C<sub>12</sub>]<sub>3</sub>[PW<sub>12</sub>O<sub>40</sub>] NPs drops sharply as the  $\Delta$ T signal dramatically increases, which suggests that the top of the emulsion is clarified due to gravity-induced migration. Moreover, the slight decrease in  $\Delta$ BS in the middle portion of the emulsion can be interpreted as an increase of the droplet size, which may be due to coalescence or flocculation.









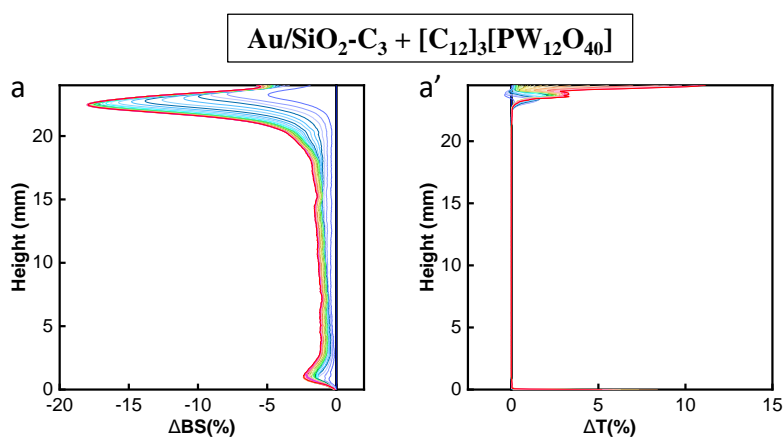
**Figure 19.** Backscattering ( $\Delta$ BS) and transmission ( $\Delta$ T) signals vs. sample height and time at 60 °C for water/toluene (1/1 v/v) Pickering emulsions stabilized by [C<sub>12</sub>]<sub>3</sub>[PW<sub>12</sub>O<sub>40</sub>] NPs (a and a'), Au/SiO<sub>2</sub>-C<sub>3</sub> NPs (b and b'), and a 40/60 wt.% combination of SiO<sub>2</sub>-C<sub>3</sub> NPs + [C<sub>12</sub>]<sub>3</sub>[PW<sub>12</sub>O<sub>40</sub>] NPs (c and c'), Au/SiO<sub>2</sub>-C<sub>3</sub> NPs + [C<sub>12</sub>]<sub>3</sub>[PW<sub>12</sub>O<sub>40</sub>] NPs (d and d'), SiO<sub>2</sub>-C<sub>3</sub> NPs + H<sub>3</sub>PW<sub>12</sub>O<sub>40</sub> (e and e') and Au/SiO<sub>2</sub>-C<sub>3</sub> NPs + H<sub>3</sub>PW<sub>12</sub>O<sub>40</sub> (f and f') from 0 h (blue curve) to 6 h (red curve). *Emulsification conditions: 80 mg NPs, 1.5 mL water, 1.5 mL toluene, emulsified at 11500 rpm for 2 min.*

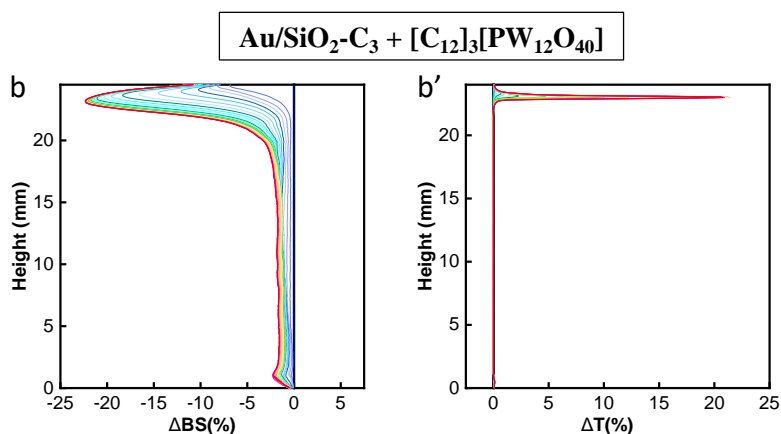
For the emulsion stabilized by Au/SiO<sub>2</sub>-C<sub>3</sub> NPs, the slight variation of  $\Delta$ BS suggests good stability. Moreover, the  $\Delta$ T signal stays almost unchanged over time (6 h), pointing out no apparent stratification. Compared with the emulsion stabilized solely by [C<sub>12</sub>]<sub>3</sub>[PW<sub>12</sub>O<sub>40</sub>] NPs or Au/SiO<sub>2</sub>-C<sub>3</sub> NPs, the emulsion stability in the presence of combined Au/SiO<sub>2</sub>-C<sub>3</sub> NPs + [C<sub>12</sub>]<sub>3</sub>[PW<sub>12</sub>O<sub>40</sub>] NPs is more pronounced, which can be observed by the changes in the backscattering and transmission results. The slight change of  $\Delta$ BS points out lower creaming. On the top of the emulsion, the lower  $\Delta$ BS and higher  $\Delta$ T represent the clarified layer induced by sedimentation and/or aggregation of droplets. The emulsion stabilized by Au/SiO<sub>2</sub>-C<sub>3</sub> NPs + H<sub>3</sub>PW<sub>12</sub>O<sub>40</sub> NPs exhibits a clear drop in  $\Delta$ BS at the upper layer of the emulsion, which is a clear evidence of creaming. A tiny change of  $\Delta$ BS is observed in the middle part of the emulsion that confirms emulsion stability. The addition of H<sub>3</sub>PW<sub>12</sub>O<sub>40</sub> to the system results in a pH decrease. The emulsions stabilized by Au/SiO<sub>2</sub>-C<sub>3</sub> NPs + POM NPs show higher emulsion volume, reflecting the excellent stability of the obtained emulsion.

Based on these results, we can conclude that the emulsion stability in the presence of Au/SiO<sub>2</sub>-C<sub>3</sub> NPs + POM NPs is higher than that of emulsions stabilized by solely NPs. This

observation can be explained by the formation of a compact interfacial layer by aggregation of NPs that is likely to protect the droplet surface and limit flocculation or coalescence of water droplets [84, 85]. The sharp drop of  $\Delta\text{BS}$  at the sample top should be attributed to demulsification due to severe gravity separation, which produces clarification at the top layer. Coalescence also occurs at the middle layer of the emulsion. Especially, the emulsion viscosity decreases at high temperature, which promotes the change in droplet size and particle migration. In the meantime, the high temperature promotes the collision of water droplets and accelerates emulsion destabilization [86]. Both  $\Delta T$  and  $\Delta\text{BS}$  signals rapidly change within the first 2 h and tend to be balanced over time. These results indicate that the layering process occurs immediately after emulsion preparation, and the sample can maintain long-term stability once equilibrium is reached.

Before testing the catalytic efficiency of the system, it is important to study the emulsion stability in the presence of the substrate or product (**Figure 20**). Indeed, the oil properties play a key role in emulsion stabilization because they directly affect the wetting of NPs. It can be clearly observed that the emulsion stabilized with cyclooctene solution (2 mol/L) used as oil is quite similar to the original emulsion (*i.e.* toluene). Moreover, the emulsion stabilized with cyclooctene oxide (2 mol/L) as oil possesses only a lower  $\Delta\text{BS}$  signal within the whole tested height and is almost unchanged over time, suggesting neither creaming nor phase separation. These results suggest high emulsion stability in the presence of the reactant and product.



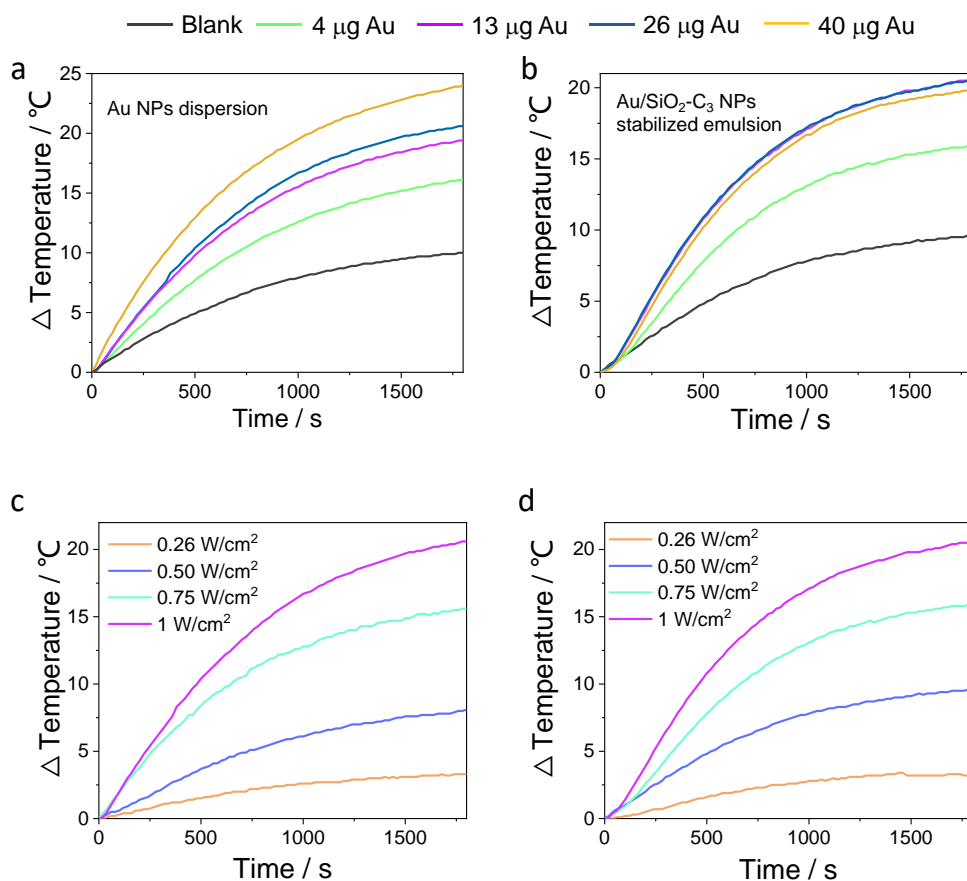


**Figure 20.** Backscattering ( $\Delta\text{BS}$ ) and transmission ( $\Delta\text{T}$ ) signals vs. sample height and time at 60 °C for water/toluene (containing substrate or product) emulsions stabilized by a 40/60 wt.% combination of Au/SiO<sub>2</sub>-C<sub>3</sub> NPs and [C<sub>12</sub>]<sub>3</sub>[PW<sub>12</sub>O<sub>40</sub>] NPs from 0 h (blue curve) to 6 h (red curve). Emulsification conditions: 80 mg NPs, 50/50 v/v, emulsified at 11500 rpm for 2 min, (a and a') using 2 mol/L cyclooctene (substrate) in toluene as oil phase and (b and b') using 2 mol/L cyclooctene oxide (product) in toluene as oil phase.

### 3.3. Study of plasmon-induced photothermal effect

Since both Au and Au/SiO<sub>2</sub>-C<sub>3</sub> NPs have a broad surface plasmon resonance peak at around 518 nm, it results in the absorption of light in the visible range (**Figure A-2 and A-3**). Au NPs absorb strongly light and can generate heat *via* localized photothermal effect. To investigate the photothermal properties of Au NPs, the temperature profile of Au NPs dispersion and Au/SiO<sub>2</sub>-C<sub>3</sub> NPs-stabilized emulsion generated by focalized light irradiation was performed (**Figure 21**). The photothermal curves exhibit a marked photothermal effect for Au NPs dispersion with the highest temperature increase (24 °C) vs. only 10 °C for water at the same conditions (**Figure 21a**). Increasing the amount of Au NPs (from 4 to 40 μg) leads to a  $\Delta\text{T}$  increase from 16.1 to 24 °C. The maximal temperature obtained for Au NPs dispersion at 40 μg is 48 °C. The temperature increases for Au/SiO<sub>2</sub>-C<sub>3</sub> NPs-stabilized emulsion and for pure Au NPs are similar. **Figure 21b** shows the photothermal profiles for the emulsion stabilized with variable Au NPs amount. The highest photothermal effect is observed for Au/SiO<sub>2</sub>-C<sub>3</sub>-stabilized emulsion with 13 μg Au ( $\Delta\text{T}$  increase of 20.6 °C), and the maximal temperature reached 47 °C. No significant temperature change was observed by further increasing the Au amount. In the emulsions system, the high viscosity of the medium might hinder heat diffusion

[87]. Besides, Au NPs are densely packed at the both inner and outer interface of the droplets, resulting in poor heat transfer into outer phase of the emulsion while the local temperature of the solid particle shell is expected to be much higher [88, 89]. Local heating remains the high-temperature zone in microscale which cannot be detected using a thermometer which is placed at the upper layer of emulsion.



**Figure 21.** Photothermal profiles of Au NPs dispersion and Au/SiO<sub>2</sub>-C<sub>3</sub>-stabilized emulsion. (a) Temperature profiles of ultrapure water and Au NPs dispersion at variable concentration as a function of light irradiation time at a power density of 1  $\text{W}/\text{cm}^2$ . (b) Temperature profiles of SiO<sub>2</sub>-C<sub>3</sub> NPs and Au/SiO<sub>2</sub>-C<sub>3</sub>-stabilized emulsion at variable Au concentration as a function of light irradiation time at a power density of 1  $\text{W}/\text{cm}^2$ . (c) Temperature profiles of Au NPs dispersion with different power density as a function of light irradiation time using 13  $\mu\text{g Au}$  NPs. (d) Temperature profiles of Au/SiO<sub>2</sub>-C<sub>3</sub>-stabilized emulsion with different power density as a function of light irradiation time using 13  $\mu\text{g Au}$  NPs.

Further investigations of the dependence of the photothermal effect on the power density for Au dispersion and Au/SiO<sub>2</sub>-C<sub>3</sub>-stabilized emulsion were performed. The photothermal curves present a strong power-dependent effect for Au NPs dispersion by increasing the power

density from 0.26 to 1 W/cm<sup>2</sup> (**Figure 21c**). Similar trends are observed for the emulsion (**Figure 21d**). The Au/SiO<sub>2</sub>-C<sub>3</sub>-stabilized emulsion displays an analogous power density dependence of photothermal performance, pointing out that Au NPs located at the droplet interface have a notable photothermal performance. It is worth to point out that the temperatures described above correspond to the global temperature of the system, and it is highly probable that the temperature near the surface of the Au NPs is much higher.

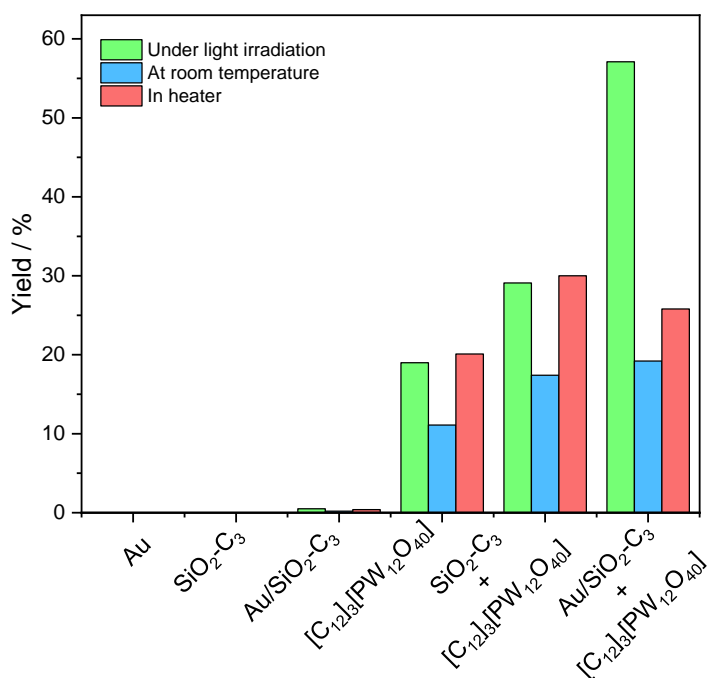
### 3.4. Catalytic performance

#### 3.4.1. Plasmon-driven interfacial activation

Given that the photothermal properties of the Au NPs on the Au/SiO<sub>2</sub>-C<sub>3</sub>-stabilized emulsion can be harnessed to increase temperature under light irradiation, we aim to effectively utilize the light-induced heat/hot electrons to improve the catalytic performance of [C<sub>12</sub>]<sub>3</sub>[PW<sub>12</sub>O<sub>40</sub>] NPs for oxidation reactions in a PIC system. Thus, the catalytic oxidation of cyclooctene in Pickering emulsion was chosen as a proof-of-concept to evaluate the catalytic activity of combined Au/SiO<sub>2</sub>-C<sub>3</sub> NPs + [C<sub>12</sub>]<sub>3</sub>[PW<sub>12</sub>O<sub>40</sub>] NPs under light irradiation. For comparison, control experiments were carried out at room temperature without light irradiation. To exclude the bulk thermal effect of light irradiation, the reaction was performed at the same conditions, but light was replaced by external heating. Indeed, the temperature in the emulsion increased only slightly (around 3 °C) under 0.26 W/cm<sup>2</sup> light irradiation during 60 min. Therefore, the oil bath temperature was set at 28 °C and dark experiments were performed at this temperature. The results of the cyclooctene oxidation under light irradiation, together with the control experiments are summarized in **Figure 22**.

Blank experiments were carried out with Au, SiO<sub>2</sub>-C<sub>3</sub> and Au/SiO<sub>2</sub>-C<sub>3</sub> NPs. SiO<sub>2</sub>-C<sub>3</sub> and Au/SiO<sub>2</sub>-C<sub>3</sub> NPs give stable water-in-oil emulsions with the catalytic system in the presence of H<sub>2</sub>O<sub>2</sub>. No conversion is observed for experiments both in the presence and absence of light at room temperature, and with external heating at 28 °C. These results point out that Au/SiO<sub>2</sub>-C<sub>3</sub> NPs alone are not catalytically active for the cyclooctene oxidation.

Using  $[C_{12}]_3[PW_{12}O_{40}]$  NPs, the cyclooctene oxide yield is only 19% under light, while 11% yield is achieved using  $[C_{12}]_3[PW_{12}O_{40}]$  NPs at the same conditions at room temperature. Furthermore, a thermal experiment at 28 °C catalyzed by  $[C_{12}]_3[PW_{12}O_{40}]$  NPs results in 20% yield of cyclooctene oxide at 95-100% selectivity which is only slightly higher than the yield obtained for the experiment performed under light at room temperature. These results point out that the presence of light does not improve the catalytic performance of  $[C_{12}]_3[PW_{12}O_{40}]$  NPs alone for cyclooctene oxidation.



**Figure 22.** Yield of cyclooctene oxide in the oxidation of cyclooctene over various NPs. Reaction conditions: 40  $\mu$ g Au NPs, 30 mg SiO<sub>2</sub>-C<sub>3</sub> NPs, 30 mg Au/SiO<sub>2</sub>-C<sub>3</sub> NPs, 50 mg  $[C_{12}]_3[PW_{12}O_{40}]$  NPs, 50 mg  $[C_{12}]_3[PW_{12}O_{40}]$  NPs + 30 mg SiO<sub>2</sub>-C<sub>3</sub> NPs, and 50 mg  $[C_{12}]_3[PW_{12}O_{40}]$  NPs + 30 mg Au/SiO<sub>2</sub>-C<sub>3</sub> NPs are used in the reaction, respectively; 1.5 mL water (containing 1.2 equiv. H<sub>2</sub>O<sub>2</sub>), 1.5 mL toluene (2 mol/L cyclooctene), emulsification at 11,500 rpm for 2 min, put 1 mL emulsion in the cuvette under the light (0.26 W/cm<sup>2</sup> power density), at room temperature (25 °C) and in heater (28 °C), respectively. Results based on <sup>1</sup>H NMR analysis.

Next, the reaction was performed by combining SiO<sub>2</sub>-C<sub>3</sub> and  $[C_{12}]_3[PW_{12}O_{40}]$  NPs. The results show a markedly higher yield of cyclooctene oxide after 60 min at the three reaction conditions compared to that of the reaction with their sole counterpart. The difference could be

attributed to the synergy effect of  $\text{SiO}_2\text{-C}_3$  and  $[\text{C}_{12}]_3[\text{PW}_{12}\text{O}_{40}]$  NPs at the water-oil interface, which can be explained by the smaller droplet size and higher emulsion volume compared to the emulsions stabilized by  $[\text{C}_{12}]_3[\text{PW}_{12}\text{O}_{40}]$  NPs (**Table A-4**), allowing higher interfacial area [90, 91].

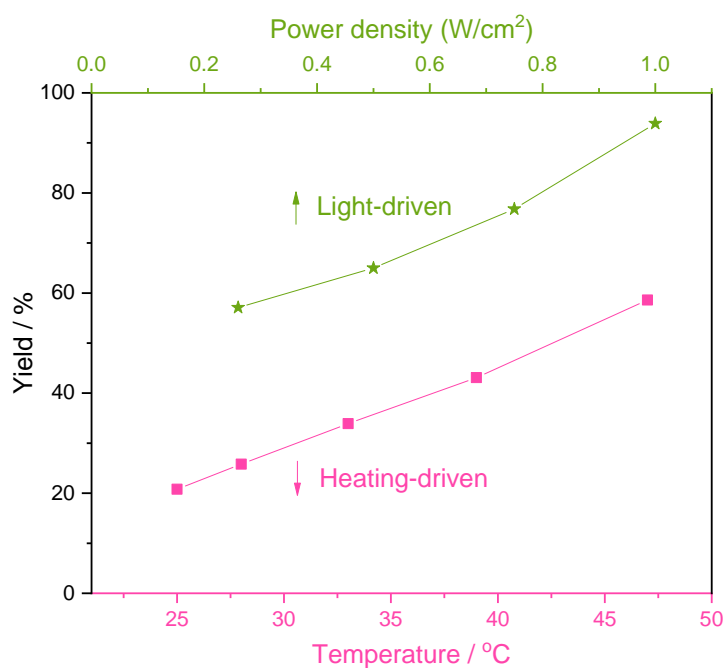
To assess the effect of plasmon-driven interfacial activation on the catalytic reaction, the reaction over  $\text{Au/SiO}_2\text{-C}_3 + [\text{C}_{12}]_3[\text{PW}_{12}\text{O}_{40}]$  NPs was conducted while keeping all variables unaltered (*i.e.* 60 min light irradiation, 50/50 v/v, 80 mg NPs). Strikingly, a high cyclooctene yield is obtained when  $\text{Au/SiO}_2\text{-C}_3$  and  $[\text{C}_{12}]_3[\text{PW}_{12}\text{O}_{40}]$  NPs are added.  $\text{Au/SiO}_2\text{-C}_3 + [\text{C}_{12}]_3[\text{PW}_{12}\text{O}_{40}]$  NPs give 21% yield within 60 min at room temperature. At the same time, a slight increase of yield to 26% is observed under thermal heating at 28 °C. Interesting, the catalytic performance of  $\text{Au/SiO}_2\text{-C}_3 + [\text{C}_{12}]_3[\text{PW}_{12}\text{O}_{40}]$  NPs is increased by focalized light irradiation, reaching 57% yield of cyclooctene oxide after 60 min. These results clearly show a positive impact of light irradiation on the reaction efficiency.

We infer from the results above that the enhanced catalytic efficiency might be attributed to local plasmon-driven heating/activation at the water-oil interface. Au NPs provide efficient conversion of light to heat/hot electrons under light irradiation, and then thermal energy dissipation to the microenvironment around NPs, enhancing the reaction rate. Therefore, it can be concluded that the large activity gap between the light-driven and conventional thermally-driven reactions should be attributed to the synergy effect of  $\text{Au/SiO}_2\text{-C}_3$  (the unique interfacial location of the Au NPs) and  $[\text{C}_{12}]_3[\text{PW}_{12}\text{O}_{40}]$  NPs at the water-oil interface.

### 3.4.2. Effect of power density

One important feature of Au NPs is that their LSPR properties can be tailored by tuning the power density of light irradiation. In this view, the catalytic performance of  $\text{Au/SiO}_2\text{-C}_3 + [\text{C}_{12}]_3[\text{PW}_{12}\text{O}_{40}]$  NPs was studied at variable power density (**Figure 23**). By increasing it from 0.26 to 1  $\text{W/cm}^2$ , the yield of cyclooctene oxide increases gradually from 57 to 94%. Control experiments were performed in an oil bath thermostated at the temperature reached in the emulsion during the experiment under light irradiation (from 28 to 47 °C for 60 min). Under

light irradiation, the yield is 1.6-4.5 times higher than thermal heating and room temperature. In previous studies, single  $[C_{12}]_3[PW_{12}O_{40}]$  NPs afford 98% yield of cyclooctene oxide after 3 h at 65 °C in emulsion system [54]. The TOF for light-driven system at a power density of 1  $W/cm^2$  is 188  $h^{-1}$ , whereas the TOF for emulsions stabilized by  $[C_{12}]_3[PW_{12}O_{40}]$  NPs alone is much lower (32  $h^{-1}$ ). The catalytic efficiency of the light-driven experiment is higher, implying a greater contribution of the temperature increase at the interface. The yield increases linearly with the light intensity. The gap between the reaction yield between the experiment with light irradiation and with thermal heating points out an important local heating at the water-oil interface.



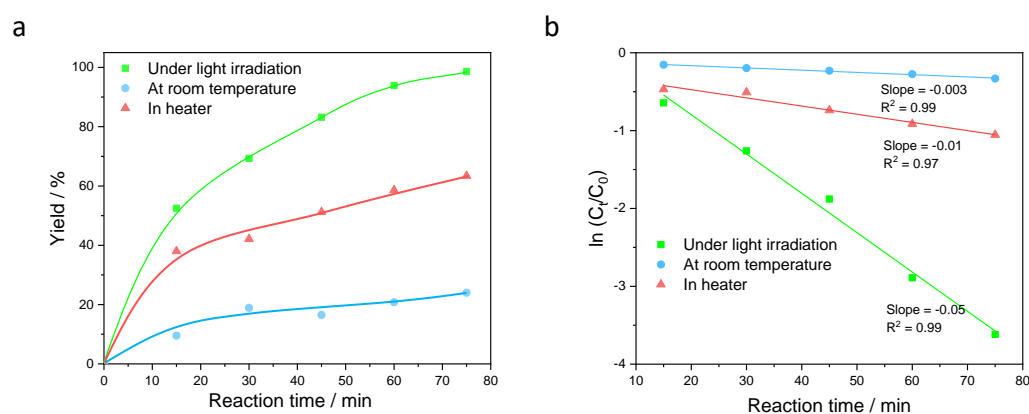
**Figure 23.** Yield of cyclooctene oxide over  $Au/SiO_2-C_3 + [C_{12}]_3[PW_{12}O_{40}]$  NPs under light irradiation at variable power density or upon heating at different temperatures. *Reaction conditions: 30 mg  $Au/SiO_2-C_3$  NPs, 50 mg  $[C_{12}]_3[PW_{12}O_{40}]$  NPs, 1.5 mL toluene (containing 2 mol/L cyclooctene) and 1.5 mL water (containing 1.2 equiv.  $H_2O_2$ ), emulsification at 11500 rpm for 2 min, 120 rpm, 60 min. Results based on  $^1H$  NMR.*

### 3.4.3. Effect of reaction time

The time-dependent yield of cyclooctene oxidation over  $[C_{12}]_3[PW_{12}O_{40}]$  and  $Au/SiO_2-C_3$  NPs is shown in **Figure 24a**. The reaction rate of the cyclooctene oxidation was compared for



experiments under light irradiation, room temperature and external heating. The thermal experiments were regulated at 47 °C with external heating, which corresponds to the highest temperature obtained with the emulsion stabilized by combined  $[C_{12}]_3[PW_{12}O_{40}]$  and Au/SiO<sub>2</sub>-C<sub>3</sub> NPs under 1 W/cm<sup>2</sup> light irradiation. The cyclooctene oxide yield under light reaches 99% within 75 min, while for conventional heating at 47 °C and at room temperature the yield is 63% and 24%, respectively. Based on the kinetic plots in **Figure 24b** and the kinetic equation  $\ln(C_t/C_0) = -kt$ , the catalytic oxidation of cyclooctene process follows a first order kinetics. The kinetic constant under light irradiation is  $k = 0.05 \text{ min}^{-1}$ , which is much larger than  $k = 0.01 \text{ min}^{-1}$  under conventional heating and  $k = 0.003 \text{ min}^{-1}$  at room temperature.

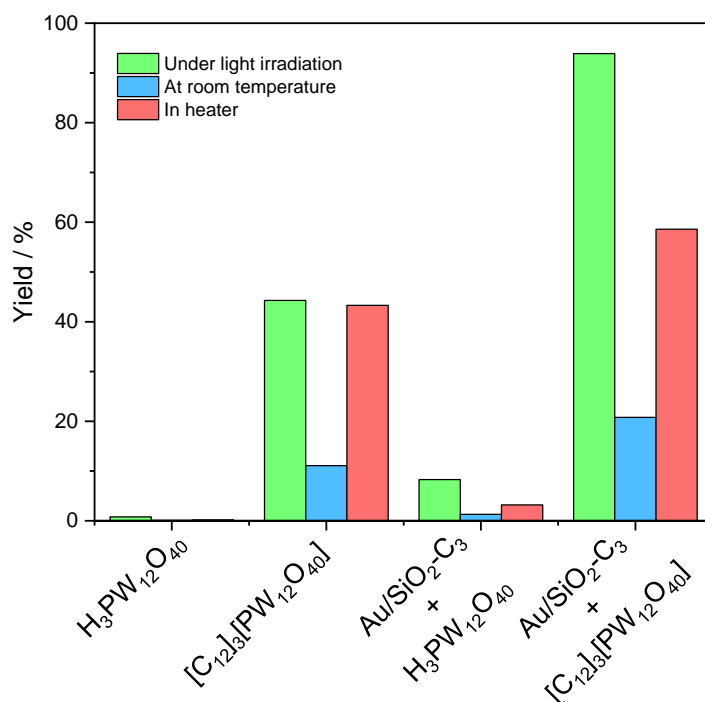


**Figure 24.** (a) Time-evolution of the yield of cyclooctene oxide for cyclooctene oxidation using  $[C_{12}]_3[PW_{12}O_{40}]$  and Au/SiO<sub>2</sub>-C<sub>3</sub> (60/40 wt.%) NPs under light irradiation, room temperature and external heating (the lines are a guide to the eye), (b) Kinetic plots under light irradiation, room temperature and external heating. *Reaction conditions: 30 mg Au/SiO<sub>2</sub>-C<sub>3</sub> NPs, 50 mg  $[C_{12}]_3[PW_{12}O_{40}]$  NPs, 1.5 mL toluene (containing 2 mol/L cyclooctene) and 1.5 mL water (containing 1.2 equiv. H<sub>2</sub>O<sub>2</sub>), emulsification at 11,500 rpm for 2 min, 120 rpm. Results based on <sup>1</sup>H NMR.*

### 3.4.4. Effect of the type of POM

Based on the above observations, it can be concluded that light-driven interfacial catalysis greatly impacts cyclooctene oxidation. To further demonstrate the advantage of interfacial catalysis in our reaction, control experiments were carried out by replacing  $[C_{12}]_3[PW_{12}O_{40}]$  NPs by water-soluble H<sub>3</sub>PW<sub>12</sub>O<sub>40</sub> (**Figure 25**). Under identical light irradiation conditions (1 W/cm<sup>2</sup>), Au/SiO<sub>2</sub>-C<sub>3</sub> NPs + H<sub>3</sub>PW<sub>12</sub>O<sub>40</sub>-stabilized emulsion gives only 8% yield within 60 min.

For experiments performed with no light irradiation or in the absence of Au/SiO<sub>2</sub>-C<sub>3</sub> NPs, the yield of cyclooctene is negligible. These results can be explained by the lack of interfacial contact between substrates and catalysts [55], and illustrate the benefits of the PIC system under light.

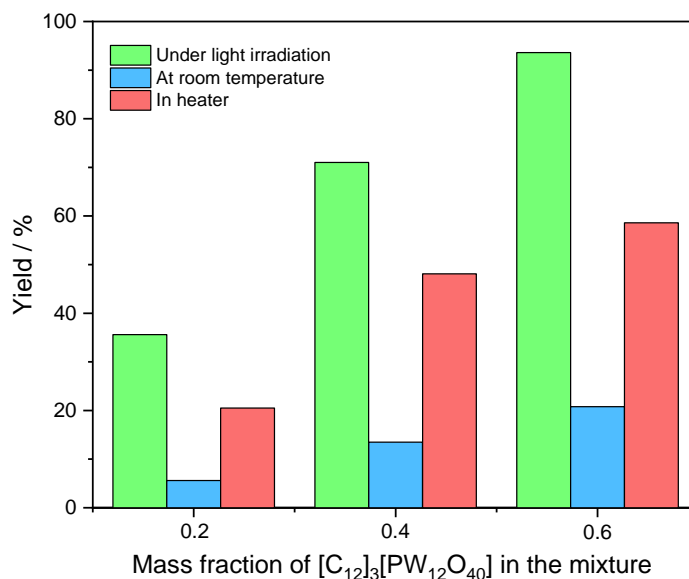


**Figure 25.** Results for cyclooctene oxidation using different types of POMs and combinations with Au/SiO<sub>2</sub>-C<sub>3</sub> NPs: only 50 mg H<sub>3</sub>PW<sub>12</sub>O<sub>40</sub>, only 50 mg [C<sub>12</sub>]<sub>3</sub>[PW<sub>12</sub>O<sub>40</sub>] NPs, or combination of 50 mg H<sub>3</sub>PW<sub>12</sub>O<sub>40</sub> + 30 mg Au/SiO<sub>2</sub>-C<sub>3</sub> NPs, and 50 mg [C<sub>12</sub>]<sub>3</sub>[PW<sub>12</sub>O<sub>40</sub>] + 30 mg Au/SiO<sub>2</sub>-C<sub>3</sub> NPs. *Reactions conditions: 1.5 mL toluene (containing 2 mol/L cyclooctene) and 1.5 mL water (containing 1.2 equiv. H<sub>2</sub>O<sub>2</sub>), emulsification at 11,500 rpm for 2 min, 120 rpm. Results based on <sup>1</sup>H NMR.*

It is noteworthy that the high yield of cyclooctene oxide achieved in cyclooctene oxidation might be attributed to several factors: 1) presence of catalytic sites [C<sub>12</sub>]<sub>3</sub>[PW<sub>12</sub>O<sub>40</sub>] at the water-oil interface leading to a large contact area between reactants and catalysts and favoring the mass transfer; 2) synergistic effect between Au/SiO<sub>2</sub>-C<sub>3</sub> NPs and [C<sub>12</sub>]<sub>3</sub>[PW<sub>12</sub>O<sub>40</sub>] NPs providing the interfacial location of catalytic sites and on-site heater during the reaction; 3) coverage of the droplet surface by a thicker layer of closely packed Au/SiO<sub>2</sub>-C<sub>3</sub> NPs + [C<sub>12</sub>]<sub>3</sub>[PW<sub>12</sub>O<sub>40</sub>] NPs responsible for emulsion stability [92, 93].

### 3.4.5. Effect of $[C_{12}]_3[PW_{12}O_{40}]$ concentration

The effect of catalyst amount on the catalytic activity was further studied (**Figure 26**). The yield of cyclooctene oxide under light irradiation was gradually increased from 36 to 94% while increasing the  $[C_{12}]_3[PW_{12}O_{40}]$  NP concentration from 0.5 to 1.8 wt.%.



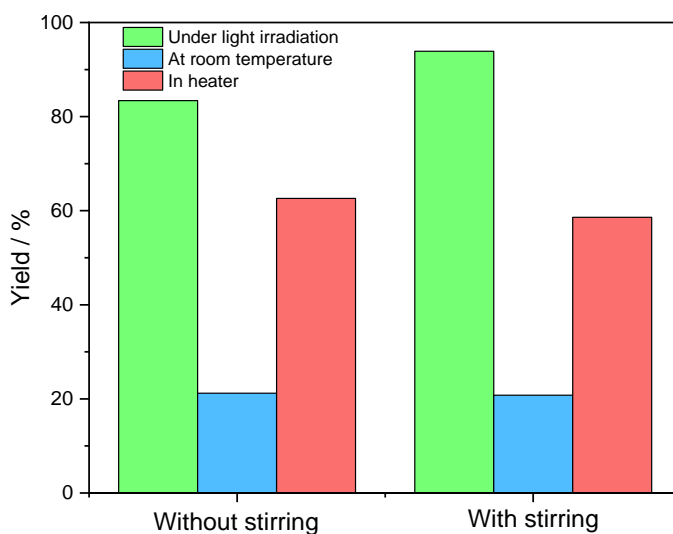
**Figure 26.** Evolution of the yield of cyclooctene oxide with the mass fraction of  $[C_{12}]_3[PW_{12}O_{40}]$  for the oxidation of cyclooctene using a combination of  $[C_{12}]_3[PW_{12}O_{40}]$  and  $Au/SiO_2-C_3$  NPs. *Reactions conditions: 80 mg NPs, 1.5 mL toluene (containing 2 mol/L cyclooctene) and 1.5 mL water (containing 1.2 equiv.  $H_2O_2$ ), emulsification at 11500 rpm for 2 min, 120 rpm. Results based on  $^1H$  NMR.*

By increasing the mass fraction between  $Au/SiO_2-C_3$  NPs +  $[C_{12}]_3[PW_{12}O_{40}]$  NPs, the average droplet size evolved from 6.4 to 8  $\mu m$  (**Table A-1**). The smaller droplet size provides much larger interfacial area where the catalytic NPs are localized, affording a high mass transfer rate.

### 3.3.6. Effect of stirring speed

Next, we studied the effect of the stirring speed on the catalytic performance (**Figure 27**). Without stirring, the combination of  $Au/SiO_2-C_3$  +  $[C_{12}]_3[PW_{12}O_{40}]$  NPs affords 63% yield of cyclooctene oxide within 60 min under thermal heating, which is almost equal to the yield

obtained using gentle stirring (59% yield within 60 min, 120 rpm). In parallel, the yield of cyclooctene oxide reaches 21% within 60 min at room temperature whatever irrespective of the stirring speed. Under light irradiation, the emulsion without stirring gives 83% yield within 60 min, which is higher than the value obtained under thermal heating. Interestingly, the yields with/without stirring are comparable (94%, within 60 min). The slight decrease of yield might be attributed to the inhomogeneity of light irradiation during the reaction.

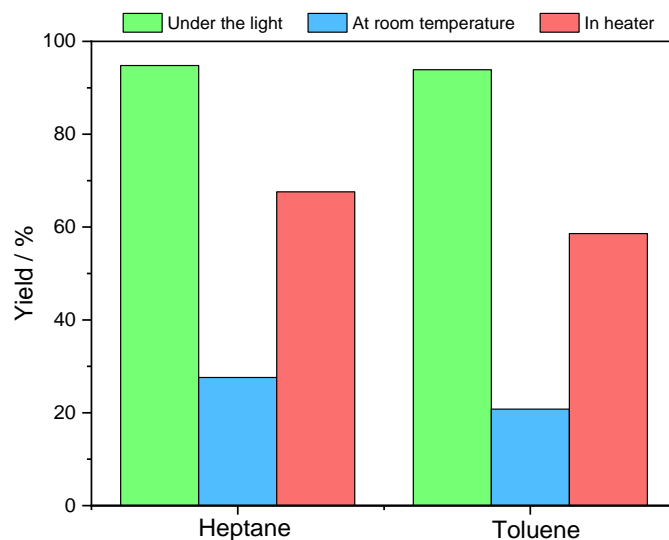


**Figure 27.** Yield of cyclooctene oxide with/without stirring under light irradiation, room temperature and external heating (47 °C). *Reactions conditions: 30 mg Au/SiO<sub>2</sub>-C<sub>3</sub> NPs, 50 mg [C<sub>12</sub>]<sub>3</sub>[PW<sub>12</sub>O<sub>40</sub>] NPs, 1.5 mL toluene (containing 2 mol/L cyclooctene) and 1.5 mL water (containing 1.2 equiv. H<sub>2</sub>O<sub>2</sub>), emulsification at 11,500 rpm for 2 min, 60 min, no stirring or 120 rpm. Results based on <sup>1</sup>H NMR.*

### 3.4.7. Effect of solvent

To demonstrate the versatility of the Au/SiO<sub>2</sub>-C<sub>3</sub> + [C<sub>12</sub>]<sub>3</sub>[PW<sub>12</sub>O<sub>40</sub>] NP system, the influence of different solvents was investigated. As shown in **Figure 28**, the yield of cyclooctene oxide reaches 95% in heptane within 60 min under light irradiation, which is 1.4 to 3.5 times higher than that obtained under conventional heating or at room temperature, respectively. The emulsion volume is 98% is for Au/SiO<sub>2</sub>-C<sub>3</sub> + [C<sub>12</sub>]<sub>3</sub>[PW<sub>12</sub>O<sub>40</sub>] NPs-stabilized

water/n-heptane emulsion with a mean droplet size of 13.7  $\mu\text{m}$ , suggesting preferential adsorption of particles at the water-oil interface (**Table A-3**). The results point out that n-heptane is also suitable for our reaction system.



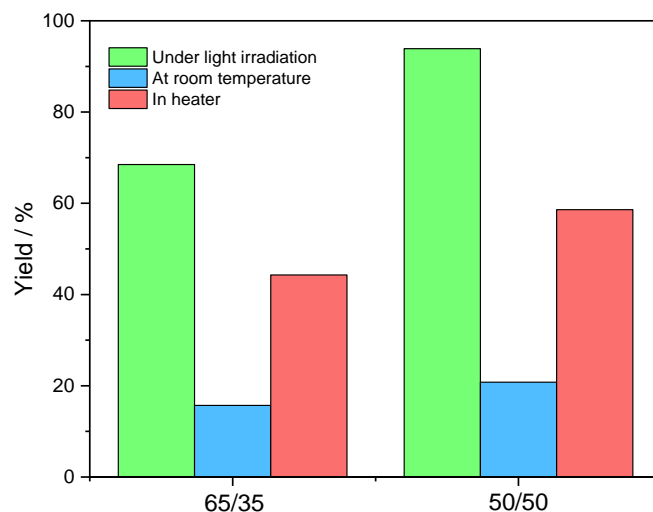
**Figure 28.** Results for cyclooctene oxidation with different organic solvents. *Reactions conditions: 30 mg Au/SiO<sub>2</sub>-C<sub>3</sub> NPs, 50 mg [C<sub>12</sub>]<sub>3</sub>[PW<sub>12</sub>O<sub>40</sub>] NPs, 1.5 mL organic solvents (containing 2 mol/L cyclooctene) and 1.5 mL water (containing 1.2 equiv. H<sub>2</sub>O<sub>2</sub>), emulsification at 11500 rpm for 2 min, 120 rpm, 60 min, 120 rpm. Results based on <sup>1</sup>H NMR.*

### 3.4.8. Effect of water/oil ratio

The effect of the water/oil ratio on the catalytic performance was also studied (**Figure 29**). Increasing the water/oil ratio from 50:50 to 65:35 substantially reduces the yield of cyclooctene oxide from 94% to 68% under light irradiation, whereas it decreases from 58% to 40% under external heating, and decreases from 21% to 15% at room temperature, respectively. Moreover, no emulsion is obtained when the water/oil ratio is further increased to 75:25. In contrast, the emulsion volume is 30% with excess oil by decreasing the water/oil ratio from 50:50 to 35:65, but this system is not suitable for catalysis.

To explain this behavior, we investigated the effect of the water/oil ratio on the emulsion properties (**Table A-3**). The combination of Au/SiO<sub>2</sub>-C<sub>3</sub> and [C<sub>12</sub>]<sub>3</sub>[PW<sub>12</sub>O<sub>40</sub>] NPs generates a stable emulsion for a water/oil ratio ranging from 50:50 to 65:35, with an increased emulsion

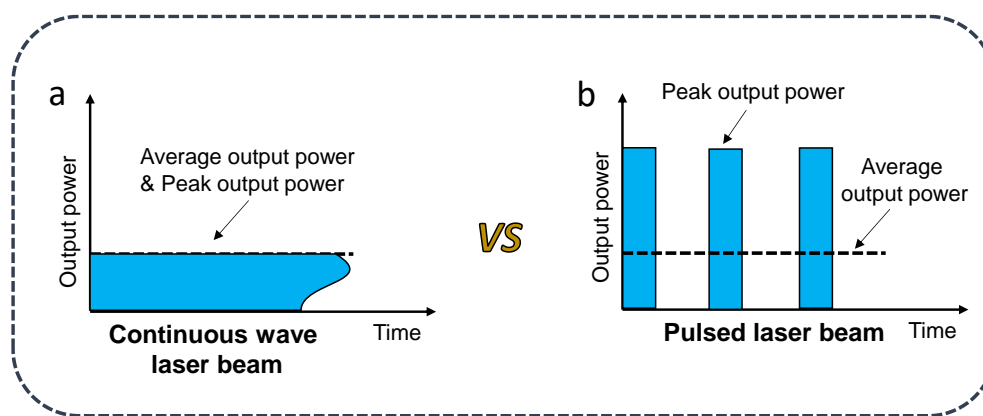
volume from 92% to 100%. Although full emulsification is obtained at 65:35 ratio, the viscosity is too high, which results in a lower yield. At 75:25 ratio, the particles disperse in the oil phase, resulting in no emulsion formation.



**Figure 29.** Evolution of cyclooctene oxide with different water/oil ratio under light irradiation, at room temperature and in the external heating (47 °C). *Reactions conditions: 30 mg Au/SiO<sub>2</sub>-C<sub>3</sub> NPs, 50 mg [C<sub>12</sub>]<sub>3</sub>[PW<sub>12</sub>O<sub>40</sub>] NPs, certain amount organic solvents (containing 2 mol/L cyclooctene) and certain amount water (containing 1.2 equiv. H<sub>2</sub>O<sub>2</sub>), emulsification at 11,500 rpm for 2 min, 120 rpm, 60 min, 120 rpm. Results based on <sup>1</sup>H NMR.*

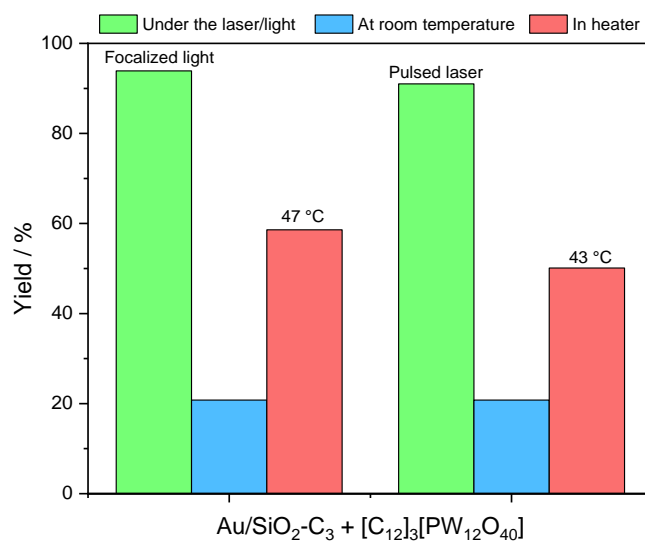
### 3.4.9. Effect of pulsed laser

The LSPR of noble metal NPs can be excited by UV, visible, near-infrared (NIR) light or laser, and is dictated by the size, shape and composition of plasmonic NPs [94-96]. One of the disadvantages of using UV lamps is the broad spectral range and most of their spectrum lies outside the absorption spectra of plasmonic noble metal NPs [97, 98]. Unlike UV light, lasers exhibit higher photonic efficiency, deeper penetration and sharper spectrum. Pulsed lasers can be utilized to create highly localized heating (**Figure 30**), to achieve significant temperature at nanoscale [99-101]. This is because of the short duration of the optical excitation compared to the time scale needed for heat to diffuse through the distance of the mean interparticle- spacing. Thus the significant temperature rise is localized at the nanoscale.



**Figure 30.** Schematic illustration of the output power of (a) continuous wave laser beam and (b) pulsed laser beam versus irradiation time.

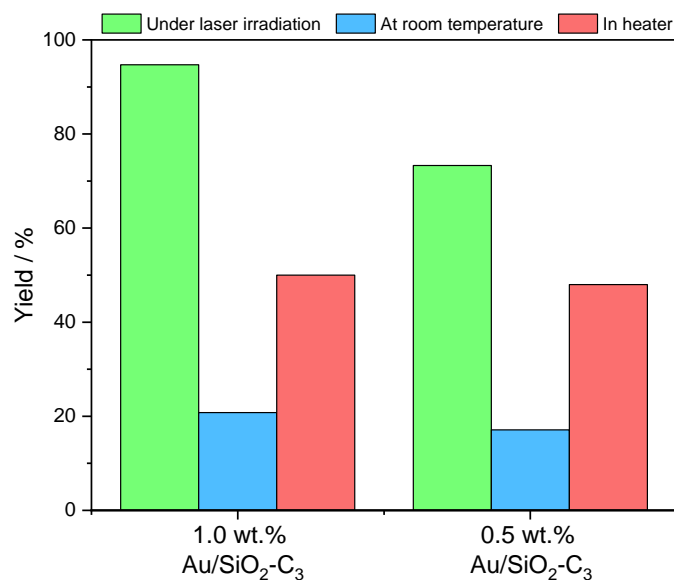
To study the catalytic performance of the particles under 532-nm pulsed laser, dedicated catalytic tests were conducted. As shown in **Figure 31**, cyclooctene is almost transformed to cyclooctene oxide within 60 min under pulsed laser irradiation, with 91% yield of cyclooctene oxide. Compared with the reaction conditions without pulsed laser irradiation at room temperature, the activity increases by more than 4.4 times.



**Figure 31.** Results for cyclooctene oxidation over Au/SiO<sub>2</sub>-C<sub>3</sub> + [C<sub>12</sub>]<sub>3</sub>[PW<sub>12</sub>O<sub>40</sub>] NPs under light or laser irradiation, room temperature and external heating. *Reactions conditions: 30 mg Au/SiO<sub>2</sub>-C<sub>3</sub> NPs, 50 mg [C<sub>12</sub>]<sub>3</sub>[PW<sub>12</sub>O<sub>40</sub>] NPs, 1.5 mL toluene (containing 2 mol/L cyclooctene) and 1.5 mL water (containing 1.2 equiv. H<sub>2</sub>O<sub>2</sub>), emulsification at 11,500 rpm for 2 min, 120 rpm, 60 min, 120 rpm. Results based on <sup>1</sup>H NMR.*

The pulsed laser irradiation-driven catalytic performance was further studied by comparing the reaction progress at constant temperature ( $T = 43\text{ }^{\circ}\text{C}$ ) corresponding at the highest temperature reached during the laser-driven catalytic reaction. The yield of cyclooctene oxide is 50%, which is still far smaller than the value measured for the experiment under pulsed laser irradiation.

The effect of Au/SiO<sub>2</sub>-C<sub>3</sub> concentration on the catalytic performance was further studied. H<sub>2</sub>O<sub>2</sub> might be in deficit since Au NPs can facilitate its decomposition. Therefore, 1.5 equiv. H<sub>2</sub>O<sub>2</sub> were added to the reaction system (instead of 1.2 equiv. H<sub>2</sub>O<sub>2</sub>). As depicted in **Figure 32**, under pulsed laser irradiation, decreasing the Au/SiO<sub>2</sub>-C<sub>3</sub> concentration from 1.0 to 0.5 wt.% results in a decline of the yield from 95% to 73%. Besides, the yield decreases slightly for the reaction performed under conventional heating and at room temperature at lower Au/SiO<sub>2</sub>-C<sub>3</sub> concentration. Overall, these results clearly demonstrate the key role of Au/SiO<sub>2</sub>-C<sub>3</sub> NPs in the laser-driven catalytic experiments.



**Figure 32.** Results for cyclooctene oxidation over Au/SiO<sub>2</sub>-C<sub>3</sub> and [C<sub>12</sub>]<sub>3</sub>[PW<sub>12</sub>O<sub>40</sub>] NPs under pulsed laser irradiation, room temperature and external heating. *Reactions conditions:* 30 mg or 15 mg Au/SiO<sub>2</sub>-C<sub>3</sub> NPs, 50 mg [C<sub>12</sub>]<sub>3</sub>[PW<sub>12</sub>O<sub>40</sub>] NPs, 1.5 mL toluene (containing 2 mol/L cyclooctene) and 1.5 mL water (containing 1.5 equiv. H<sub>2</sub>O<sub>2</sub>), emulsification at 11500 rpm for 2 min, 120 rpm, 60 min, 120 rpm. Results based on <sup>1</sup>H NMR.

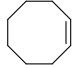
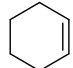
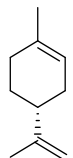
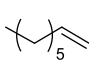


To understand the effect of Au/SiO<sub>2</sub>-C<sub>3</sub> NPs on the catalytic performance, the influence of the droplets size and emulsion properties was studied. The catalytic performance of Au/SiO<sub>2</sub>-C<sub>3</sub> + [C<sub>12</sub>]<sub>3</sub>[PW<sub>12</sub>O<sub>40</sub>] NPs is highly dependent on the emulsion properties (**Table A-3**). As the Au/SiO<sub>2</sub>-C<sub>3</sub> NPs concentration increases from 0.5 to 1.0 wt.%, the emulsion volume increases from 83% to 92% along with a droplets size decline from 11.3 to 8 μm. This suggests that a higher particle concentration leads to a denser shell, reducing coalescence and resulting in turn into the formation of a stable emulsion.

### 3.5. Scope of substrates

To assess the versatility of Au/SiO<sub>2</sub>-C<sub>3</sub> and [C<sub>12</sub>]<sub>3</sub>[PW<sub>12</sub>O<sub>40</sub>] NPs in the light-driven activated biphasic reaction, a variety of cyclic olefins were tested. The results are summarized in **Table 2**. Cyclohexene oxidation results mainly in 1,2-cyclohexanediol with 70% yield after 1 h under light irradiation (entry 2). In contrast, the yield is 57% at 47 °C. In both cases, no cyclohexene epoxide is observed due to fast ring opening in emulsion. In the case of limonene, 1,2-limonene oxide is obtained as main product together with carvone as minor product. Although the limonene conversion is slightly lower under light compared to the experiment at 47 °C (35% vs. 45% after 2 h), the yield of 1,2-limonene oxide is higher in the former case (29% vs. 11%) due to a much higher selectivity (83% vs. 24%). The oxidation of 1-octene shows 11% yield to 1,2-epoxyoctane after 2 h in the light-driven test, whereas it is only 3% yield at 47 °C. Compared to batch reaction counterparts, the light-driven reaction using our system exhibits an enhanced catalytic efficiency. In a previous study [54], conventional thermal experiments were performed with single [C<sub>12</sub>]<sub>3</sub>[PW<sub>12</sub>O<sub>40</sub>] NPs and the yield of 1,2-limonene oxide reached 79% after 6 h at 65 °C. The conversion of 1-octene into 1,2-epoxyoctane using [C<sub>12</sub>]<sub>3</sub>[PW<sub>12</sub>O<sub>40</sub>] NPs gave a yield of was 43% at 65 °C after 6 h. Linear olefins, such as 1-octene and limonene, are far less-reactive than olefins because of the inherent inactivity of substrates [102]. These results demonstrate the versatility of the Au/SiO<sub>2</sub>-C<sub>3</sub> and [C<sub>12</sub>]<sub>3</sub>[PW<sub>12</sub>O<sub>40</sub>] NPs-stabilized emulsion system for the light-driven oxidation of olefins.

**Table 2** Catalytic results for oxidation of olefins in water/toluene Pickering emulsion stabilized Au/SiO<sub>2</sub>-C<sub>3</sub> + [C<sub>12</sub>]<sub>3</sub>[PW<sub>12</sub>O<sub>40</sub>] NPs

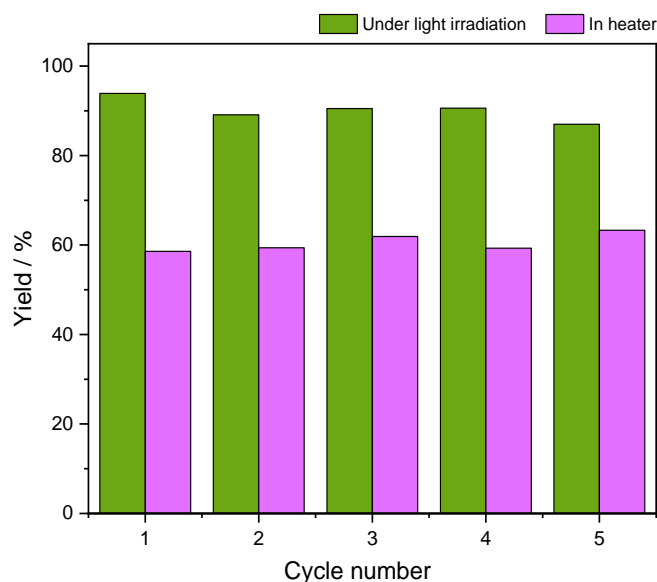
Substrate	t/h	Light irradiation		Heater (47 °C)	
		Conv. (%)	Yield (%)	Conv. (%)	Yield (%)
		94	94 <sup>a</sup>	61	58a
	1	70	70 <sup>b</sup>	57	57b
	2	35	29 <sup>c</sup> / 8.0 <sup>d</sup>	45	11 <sup>c</sup> / 6.5 <sup>d</sup>
	2	12	11 <sup>e</sup>	3	3 <sup>e</sup>

Reactions conditions: 30 mg Au/SiO<sub>2</sub>-C<sub>3</sub> NPs, 50 mg [C<sub>12</sub>]<sub>3</sub>[PW<sub>12</sub>O<sub>40</sub>] NPs, 1.5 mL toluene (containing 2 mol/L substrates) and 1.5 mL water (containing 1.2 equiv. H<sub>2</sub>O<sub>2</sub>), emulsification at 11500 rpm for 2 min, 60 min, 120 rpm. Results based on <sup>1</sup>H NMR for <sup>a</sup> cyclooctene oxide, <sup>b</sup> 1,2-cyclohexanediol, <sup>c</sup> 1,2-limonene oxide, <sup>d</sup> carvone and <sup>e</sup> 1,2-epoxyoctane.

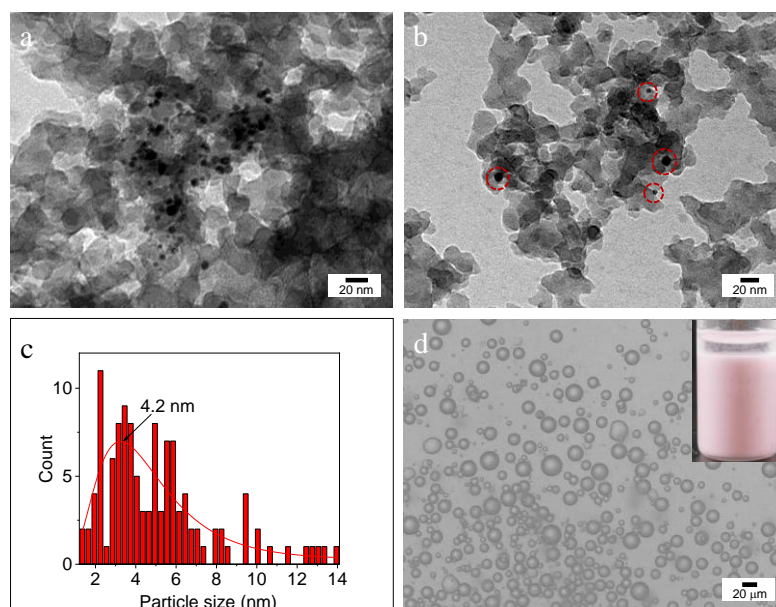
### 3.6. Reusability

Finally, the reusability of the Au/SiO<sub>2</sub>-C<sub>3</sub> + [C<sub>12</sub>]<sub>3</sub>[PW<sub>12</sub>O<sub>40</sub>] NP system was investigated. A loss of NPs is observed during emulsification and washing of NPs. The catalyst loss is one of the reasons for activity loss of the reaction system. To limit their loss, NPs were collected and dried after each catalytic reaction followed by centrifugation. It can be considered that there is no solid products in the catalytic system, other than catalytic NPs. Then, the catalysts were re-emulsified with fresh cyclooctene solution and water. As shown in **Figure 33**, Au/SiO<sub>2</sub>-C<sub>3</sub> + [C<sub>12</sub>]<sub>3</sub>[PW<sub>12</sub>O<sub>40</sub>] NPs can be reused for at least five runs without loss of catalytic activity. In parallel, the reusability of Au/SiO<sub>2</sub>-C<sub>3</sub> + [C<sub>12</sub>]<sub>3</sub>[PW<sub>12</sub>O<sub>40</sub>] NPs was investigated under conventional heating. No change was observed for the yield after five consecutive runs. This body of results demonstrate the absence of catalyst poisoning during the reaction. The TEM micrographs of the recovered Au/SiO<sub>2</sub>-C<sub>3</sub> + [C<sub>12</sub>]<sub>3</sub>[PW<sub>12</sub>O<sub>40</sub>] NPs show the presence of small Au NPs aggregates, and the microstructure of the hybrid particles does not change significantly compared to the fresh material (**Figure 34a and b**). The particle size distribution of Au NPs is

similar to that of fresh Au/SiO<sub>2</sub>-C<sub>3</sub> NPs (**Figure 34c**). The reused particles can still form stable emulsion (**Figure 34d and Table A-5**), resulting from a perfect interfacial activity of the NPs. Their facile recovery combined with their excellent stability make Au/SiO<sub>2</sub>-C<sub>3</sub> + [C<sub>12</sub>]<sub>3</sub>[PW<sub>12</sub>O<sub>40</sub>] NPs promising in catalytic reactions.



**Figure 33.** Catalytic performance of the reaction system with 40/60 wt.% Au/SiO<sub>2</sub>-C<sub>3</sub> and [C<sub>12</sub>]<sub>3</sub>[PW<sub>12</sub>O<sub>40</sub>] NPs in five consecutive runs. Results based on <sup>1</sup>H NMR.



**Figure 34.** (a and b) TEM images of recovered Au/SiO<sub>2</sub>-C<sub>3</sub> + [C<sub>12</sub>]<sub>3</sub>[PW<sub>12</sub>O<sub>40</sub>] NPs after the fifth run. (c) Particle size distribution of Au NPs in Au/SiO<sub>2</sub>-C<sub>3</sub> NPs after the fifth run. (d) Optical micrographs of the Pickering emulsion after the fifth run (the inset is a photograph of the emulsion).

### 3.7. Discussion

Reduction of energy consumption is key to develop more efficient processes. A question that emerges from the results presented in the above sections is to assess whether plasmonic heating under light irradiation can be used to activate chemical reactions more efficiently compared to the conventional thermal heating in PIC systems.

The determination of the theoretical energy ( $Q_{TH}$ ) that is required for a reaction mixture to reach a certain temperature can be calculated from equation (1) and the determination of energy input ( $Q_L$ ) for the energy supplied by the lamp is represented as equation (2) which is given in terms of power dissipation and the time of exposure. From these, the overall energy saving factor ( $\eta$ ) of the light irradiation compared to the theoretical minimum energy required can be calculated from equation (3):

$$Q_{TH} = mc_P\Delta T \quad (1)$$

$$Q_L = P_{avg}\Delta t \quad (2)$$

$$\eta = (Q_{TH} - Q_L)/Q_{TH} \quad (3)$$

where  $m$  is the mass of the biphasic system (g);  $c_P$  is the specific heat capacity of each phase ( $Jg^{-1}C^{-1}$ ); and  $\Delta T$  is the temperature change observed for the reaction ( $^{\circ}C$ ). Besides,  $P_{avg}$  is the average power output of the lamp (W),  $\Delta t$  is the light irradiation time (h) and  $\eta$  is the saving under plasmon heating compared to thermal heating (energy saving %).

In chemical reaction using a thermal batch reactor, we suppose the energy supplied from heating reaction mixture from low temperature to high temperature is equal to the cooling process from high temperature to low temperature. Therefore, the overall energy required  $Q_{TH}$  is represented as equation (4):

$$Q_{TH} = Q_{TH-heating} + Q_{TH-cooling} \quad (4)$$

where  $Q_{TH-heating}$  is the energy required from low temperature to high temperature and  $Q_{TH-cooling}$  is the energy required from high temperature to low temperature.

For example, if 10 mL water/toluene Pickering emulsion reaction mixture (1/1 v/v) is

carried out for 1 h in both conventional thermal heating and light irradiation systems, temperature required for catalytic system is 80 °C. We compute below the energy difference for heating/cooling a batch and a continuous flow reactor.

### Batch reactor:

#### 1) Energy delivered during conventional thermal heating method

a. Energy supplied for heating reaction mixture from room temperature to 80 °C

$$\begin{aligned}
 Q_{TH-heating} &= mc_P\Delta T = (m_Wc_{PW} + m_Tc_{PT})\Delta T \\
 &= (V_W\rho_Wc_{PW} + V_T\rho_Tc_{PT})\Delta T \\
 &= \left( \left( \frac{10}{2} \right) \times 1 \times 4.18 + \left( \frac{10}{2} \right) \times 0.87 \times 1.72 \right) \times (80 - 25) \\
 &= 1560 \text{ J}
 \end{aligned} \tag{5}$$

where  $m_W$  and  $m_T$  are the mass of water and toluene (g), respectively;  $c_{PW}$  and  $c_{PT}$  are the specific heat capacity of water and toluene, respectively ( $\text{Jg}^{-1}\text{C}^{-1}$ ); and  $\Delta T$  is the temperature change observed for the reaction.

b. Energy supplied for cooling reaction mixture from 80 °C to room temperature

$$Q_{TH-cooling} = Q_{TH-heating} = 1560 \text{ J} \tag{6}$$

c. Total energy supplied for conventional thermal heating method

$$Q_{TH} = Q_{TH-heating} + Q_{TH-cooling} = 1560 + 1560 = 3120 \text{ J} \tag{7}$$

#### 2) Energy delivered during light irradiation

a. Energy delivered during light irradiation for 1 h.

$$\begin{aligned}
 Q_L &= P_{avg}\Delta t = P_{density}S_{beam}\Delta t = P_{density}\pi(r^2)\Delta t \\
 &= 1 \times 3.14 \times (0.67/2)^2 \times 1 = 0.35 \text{ W/h} \\
 &= 0.35 \times 3600 = 1260 \text{ J}
 \end{aligned} \tag{8}$$

where  $P_{density}$  is the power density of the lamp ( $1 \text{ W/cm}^2$ ),  $S_{beam}$  represent the light beam area ( $\text{cm}^2$ ) and  $r$  is light beam radius (cm).

#### 3) Percentage of energy saved (%)

$$\eta = \frac{(Q_{TH} - Q_L)}{Q_{TH}} = \frac{(3120 - 1260)}{3120} \times 100 = 59\% \quad (9)$$

Starting from this point, the reaction conditions must be re-evaluated. For example, 10 mL/h water/toluene Pickering emulsion reaction mixture (1/1 v/v) is used for 1 h in both continuous flow reactor and light irradiation systems, and temperature required for catalytic system is also 80 °C.

### Continuous flow reactor:

#### 1) Energy delivered during conventional thermal heating method

a. Energy supplied for heating reaction mixture from room temperature to 80 °C

$$Q_{flow-heating} = mc_p\Delta T = Q_{TH-heating} = 1560 \text{ J} \quad (10)$$

b. Total energy supplied during conventional thermal heating method

$$Q_{flow} = Q_{flow-heating} + Q_{flow-cooling} = 1560 + 1560 = 3120 \text{ J} \quad (11)$$

c. Heat power ascribed to flowrate

$$\begin{aligned} P_{flow} &= P_{heating\ flow} + P_{cooling\ flow} \\ &= (10/3600) \times 1560 + (10/3600) \times 1560 = 8.7 \text{ W} \end{aligned} \quad (12)$$

d. Energy delivered for 1 h.

$$Q_{flow} = P_{flow} \times \Delta t = 8.7 \times 1 = 8.7 \text{ W/h} = 8.7 \times 3600 = 31192 \text{ J} \quad (13)$$

$$Q_{total-flow} = Q_{flow} + Q_{TH} = 31192 + 3120 = 34312 \text{ J} \quad (14)$$

#### 2) Energy delivered during light irradiation for 1 h

$$Q_{L-flow} = P_{avg} \times \Delta t = 0.35 \times 1 = 0.35 \text{ W/h} = 0.35 \times 3600 = 1260 \text{ J} \quad (15)$$

$$Q_{total-L} = Q_{L-flow} + Q_L = 1260 + 1260 = 2520 \text{ J} \quad (16)$$

#### 3) Percentage of energy saved (%)

$$\eta = \frac{(Q_{total-flow} - Q_{total-L})}{Q_{total-flow}} = \frac{(34312 - 2520)}{34312} \times 100 = 93\% \quad (17)$$

Based on the results above, we can conclude that light-driven heterogeneous catalytic reaction in PIC system is more efficient than conventional thermal heating reaction, with a

potential energy saving of about 50-90%. Indeed, it is not necessary to heat all the mass of substance to drive the reaction in heterogeneous catalysis. Plasmonic effect provides direct local heating at the surface of active sites, thus avoiding unnecessary heating of the whole reaction system. Moreover, plasmonic heating allows a rapid start-up and shutdown process with good credentials for continuous flow operations. Furthermore, the utilization of low cost, safe and environmentally friendly light emitting diodes (LEDs) could increase even more the benefits for plasmonic heating applications.

#### 4. Conclusions

In summary, we have designed a PIC system that benefits from the photothermal effect of plasmonic Au NPs and the catalytic properties of  $[\text{C}_{12}]_3[\text{PW}_{12}\text{O}_{40}]$  NPs for the oxidation of cyclooctene with  $\text{H}_2\text{O}_2$ . The combination of Au/SiO<sub>2</sub>-C<sub>3</sub> NPs with  $[\text{C}_{12}]_3[\text{PW}_{12}\text{O}_{40}]$  NPs does not only enhance the emulsion stability, but also allows selective photoactivation of the water/oil interface. As a result, combined Au/SiO<sub>2</sub>-C<sub>3</sub> and  $[\text{C}_{12}]_3[\text{PW}_{12}\text{O}_{40}]$  NPs catalyze the oxidation of olefins in emulsion under light irradiation. Compared to thermal-driven counterparts, light irradiation (1 W/cm<sup>2</sup>) affords higher catalytic activity. The synergistic effect of combined Au/SiO<sub>2</sub>-C<sub>3</sub> and  $[\text{C}_{12}]_3[\text{PW}_{12}\text{O}_{40}]$  NPs improves the catalytic process unlike for sole particles. We infer that Au/SiO<sub>2</sub>-C<sub>3</sub> NPs play a role of on-site heaters/activators at the water/oil interface in contact with the  $[\text{C}_{12}]_3[\text{PW}_{12}\text{O}_{40}]$  NPs. Thanks to the stabilization endowed by Au/SiO<sub>2</sub>-C<sub>3</sub> and  $[\text{C}_{12}]_3[\text{PW}_{12}\text{O}_{40}]$  NPs, the catalytic activity can be maintained for at least five catalytic runs. This work represents a first attempt of employing light for accelerating the catalytic efficiency by combining plasmon-driven photothermal effects of Au NPs and Pickering emulsions, opening an avenue for engineering remotely controlled heating processes instead of traditional heaters to carry out heterogeneous catalytic reactions.

## 5. References

- [1] L. Wang, M. Hasanzadeh Kafshgari, M. Meunier, Optical properties and applications of plasmonic-metal nanoparticles, *Advanced Functional Materials*, 30 (2020) 2005400.
- [2] J. Liu, H. He, D. Xiao, S. Yin, W. Ji, S. Jiang, D. Luo, B. Wang, Y. Liu, Recent advances of plasmonic nanoparticles and their applications, *Materials*, 11 (2018) 1833.
- [3] A. Sanchot, G. Baffou, R. Marty, A. Arbouet, R. Quidant, C. Girard, E. Dujardin, Plasmonic nanoparticle networks for light and heat concentration, *Acs Nano*, 6 (2012) 3434-3440.
- [4] P.K. Jain, X. Huang, I.H. El-Sayed, M.A. El-Sayed, Review of some interesting surface plasmon resonance-enhanced properties of noble metal nanoparticles and their applications to biosystems, *Plasmonics*, 2 (2007) 107-118.
- [5] M. Sharifi, F. Attar, A.A. Saboury, K. Akhtari, N. Hooshmand, A. Hasan, M.A. El-Sayed, M. Falahati, Plasmonic gold nanoparticles: Optical manipulation, imaging, drug delivery and therapy, *Journal of Controlled Release*, 311 (2019) 170-189.
- [6] X. Li, J.-L. Shi, H. Hao, X. Lang, Visible light-induced selective oxidation of alcohols with air by dye-sensitized TiO<sub>2</sub> photocatalysis, *Applied Catalysis B: Environmental*, 232 (2018) 260-267.
- [7] Y. Su, Z. Han, L. Zhang, W. Wang, M. Duan, X. Li, Y. Zheng, Y. Wang, X. Lei, Surface hydrogen bonds assisted meso-porous WO<sub>3</sub> photocatalysts for high selective oxidation of benzylalcohol to benzylaldehyde, *Applied Catalysis B: Environmental*, 217 (2017) 108-114.
- [8] K. Qi, B. Cheng, J. Yu, W. Ho, Review on the improvement of the photocatalytic and antibacterial activities of ZnO, *Journal of Alloys and Compounds*, 727 (2017) 792-820.
- [9] S. Luo, X. Ren, H. Lin, H. Song, J. Ye, Plasmonic photothermal catalysis for solar-to-fuel conversion: current status and prospects, *Chemical Science*, 12 (2021) 5701-5719.
- [10] J. Zheng, X. Cheng, H. Zhang, X. Bai, R. Ai, L. Shao, J. Wang, Gold nanorods: the most versatile plasmonic nanoparticles, *Chemical Reviews*, 121 (2021) 13342-13453.
- [11] X. Huang, P.K. Jain, I.H. El-Sayed, M.A. El-Sayed, Plasmonic photothermal therapy (PPTT) using gold nanoparticles, *Lasers in Medical Science*, 23 (2008) 217-228.
- [12] M. Hu, J. Chen, Z.-Y. Li, L. Au, G.V. Hartland, X. Li, M. Marquez, Y. Xia, Gold nanostructures: engineering their plasmonic properties for biomedical applications, *Chemical Society Reviews*, 35 (2006) 1084-1094.
- [13] A. Guo, Y. Fu, G. Wang, X. Wang, Diameter effect of gold nanoparticles on photothermal conversion for solar steam generation, *RSC Advances*, 7 (2017) 4815-4824.
- [14] M.A. Mackey, M.R.K. Ali, L.A. Austin, R.D. Near, M.A. El-Sayed, The Most Effective Gold Nanorod Size for Plasmonic Photothermal Therapy: Theory and In Vitro Experiments, *The Journal of Physical Chemistry B*, 118 (2014) 1319-1326.
- [15] H. Liu, D. Chen, L. Li, T. Liu, L. Tan, X. Wu, F. Tang, Multifunctional gold nanoshells on silica nanorattles: a platform for the combination of photothermal therapy and chemotherapy with low systemic toxicity, *Angewandte Chemie International Edition*, 50 (2011) 891-895.
- [16] X. Hou, X. Wang, R. Liu, H. Zhang, X. Liu, Y. Zhang, Facile synthesis of multifunctional Fe<sub>3</sub>O<sub>4</sub>@SiO<sub>2</sub>@Au magneto-plasmonic nanoparticles for MR/CT dual imaging and photothermal therapy, *RSC Advances*, 7 (2017) 18844-18850.
- [17] X. Huang, Y. Li, Y. Chen, H. Zhou, X. Duan, Y. Huang, Plasmonic and catalytic AuPd nanowheels



- for the efficient conversion of light into chemical energy, *Angewandte Chemie International Edition*, 52 (2013) 6063-6067.
- [18] G. Liu, Q. Xiong, Y. Xu, Q. Fang, K.C.-F. Leung, M. Sang, S. Xuan, L. Hao, Sandwich-structured MXene@ Au/polydopamine nanosheets with excellent photothermal-enhancing catalytic activity, *Colloids and Surfaces A: Physicochemical and Engineering Aspects*, 633 (2022) 127860.
- [19] L.C. de la Garza, N. Brodusch, R. Gauvin, A. Moores, Plasmon-Enhanced Hydrogenation of 1-Dodecene and Toluene Using Ruthenium-Coated Gold Nanoparticles, *ACS Applied Nano Materials*, 4 (2021) 1596-1603.
- [20] R. Ma, J. Sun, D.H. Li, J.J. Wei, Review of synergistic photo-thermo-catalysis: Mechanisms, materials and applications, *International Journal of Hydrogen Energy*, 45 (2020) 30288-30324.
- [21] Z. Tang, F. Zhu, J. Zhou, W. Chen, K. Wang, M. Liu, N. Wang, N. Li, Monolithic NF@ ZnO/Au@ ZIF-8 photocatalyst with strong photo-thermal-magnetic coupling and selective-breathing effects for boosted conversion of CO<sub>2</sub> to CH<sub>4</sub>, *Applied Catalysis B: Environmental*, 309 (2022) 121267.
- [22] J. Qiu, W.D. Wei, Surface plasmon-mediated photothermal chemistry, *The Journal of Physical Chemistry C*, 118 (2014) 20735-20749.
- [23] F. Wang, Y. Huang, Z. Chai, M. Zeng, Q. Li, Y. Wang, D. Xu, Photothermal-enhanced catalysis in core-shell plasmonic hierarchical Cu<sub>7</sub>S<sub>4</sub> microsphere@ zeolitic imidazole framework-8, *Chemical science*, 7 (2016) 6887-6893.
- [24] X. Chen, A. Yang, G. Wang, M. Wei, N. Liu, B. Li, L. Wu, Reinforced Catalytic Oxidation of Polyoxometalate@ Charge Transfer Complex by On-Site Heating from Photothermal Conversion, *Chemical Engineering Journal*, (2022) 137134.
- [25] Q. Yang, Q. Xu, S.H. Yu, H.L. Jiang, Pd Nanocubes@ ZIF-8: Integration of Plasmon-Driven Photothermal Conversion with a Metal-Organic Framework for Efficient and Selective Catalysis, *Angewandte Chemie*, 128 (2016) 3749-3753.
- [26] A. Pineda, L. Gomez, A.M. Balu, V. Sebastian, M. Ojeda, M. Arruebo, A.A. Romero, J. Santamaria, R. Luque, Laser-driven heterogeneous catalysis: efficient amide formation catalysed by Au/SiO<sub>2</sub> systems, *Green chemistry*, 15 (2013) 2043-2049.
- [27] C. Fasciani, C.J.B. Alejo, M. Grenier, J.C. Netto-Ferreira, J. Scaiano, High-temperature organic reactions at room temperature using plasmon excitation: decomposition of dicumyl peroxide, *Organic Letters*, 13 (2011) 204-207.
- [28] Y. Zhao, R.M. Sarhan, A. Eljarrat, Z. Kochovski, C. Koch, B. Schmidt, W. Koopman, Y. Lu, Surface-Functionalized Au-Pd Nanorods with Enhanced Photothermal Conversion and Catalytic Performance, *ACS Applied Materials & Interfaces*, 14 (2022) 17259-17272.
- [29] K. Fuku, R. Hayashi, S. Takakura, T. Kamegawa, K. Mori, H. Yamashita, The synthesis of size-and color-controlled silver nanoparticles by using microwave heating and their enhanced catalytic activity by localized surface plasmon resonance, *Angewandte Chemie*, 125 (2013) 7594-7598.
- [30] J.-J. Li, S.-C. Cai, X. Chen, D.-X. Yan, J. Chen, H.-P. Jia, Engineering rGO nanosheets-adsorption layer supported Pt nanoparticles to enhance photo-thermal catalytic activity under light irradiation, *Journal of Materials Chemistry A*, 7 (2019) 11985-11995.
- [31] M. Kang, Y. Kim, Au-coated Fe<sub>3</sub>O<sub>4</sub>@ SiO<sub>2</sub> core-shell particles with photothermal activity, *Colloids and Surfaces A: Physicochemical and Engineering Aspects*, 600 (2020) 124957.
- [32] T. Kitanosono, K. Masuda, P. Xu, S. Kobayashi, Catalytic organic reactions in water toward sustainable society, *Chemical Reviews*, 118 (2018) 679-746.

- [33] G. Cravotto, E. Borretto, M. Oliverio, A. Procopio, A. Penoni, Organic reactions in water or biphasic aqueous systems under sonochemical conditions. A review on catalytic effects, *Catalysis Communications*, 63 (2015) 2-9.
- [34] R.A. Sheldon, Green solvents for sustainable organic synthesis: state of the art, *Green Chemistry*, 7 (2005) 267-278.
- [35] F. Chang, C.M. Vis, W. Ciptonugroho, P.C. Bruijninx, Recent developments in catalysis with Pickering Emulsions, *Green Chemistry*, 23 (2021) 2575-2594.
- [36] B. Yang, G. Douyère, L. Leclercq, V. Nardello-Rataj, M. Pera-Titus, One-pot oxidative cleavage of cyclic olefins for the green synthesis of dicarboxylic acids in Pickering emulsions in the presence of acid phosphate additives, *Catalysis Science & Technology*, 10 (2020) 6723-6728.
- [37] X. Liu, Y. Mao, S. Yu, H. Zhang, K. Hu, L. Zhu, J. Ji, J. Wang, An efficient and recyclable Pickering magnetic interface biocatalyst: application in biodiesel production, *Green Chemistry*, 23 (2021) 966-972.
- [38] N. Zou, X. Lin, M. Li, L. Li, C. Ye, J. Chen, T. Qiu, Ionic liquid@amphiphilic silica nanoparticles: novel catalysts for converting waste cooking oil to biodiesel, *ACS Sustainable Chemistry & Engineering*, 8 (2020) 18054-18061.
- [39] B. Yang, L. Leclercq, J.-M. Clacens, V. Nardello-Rataj, Acidic/amphiphilic silica nanoparticles: new eco-friendly Pickering interfacial catalysis for biodiesel production, *Green Chemistry*, 19 (2017) 4552-4562.
- [40] Y. Xi, B. Liu, S. Wang, X. Huang, H. Jiang, S. Yin, T. Ngai, X. Yang, Growth of Au nanoparticles on phosphorylated zein protein particles for use as biomimetic catalysts for cascade reactions at the oil–water interface, *Chemical science*, 12 (2021) 3885-3889.
- [41] D. Dedovets, Q. Li, L. Leclercq, V. Rataj, J. Leng, S. Zhao, M. Pera-Titus, Multiphase Microreactors Based on Liquid–Liquid and Gas–Liquid Dispersions Stabilized by Colloidal Catalytic Particles, *Angewandte Chemie International Edition*, 61.
- [42] S. Crossley, J. Faria, M. Shen, D.E. Resasco, Solid nanoparticles that catalyze biofuel upgrade reactions at the water/oil interface, *Science*, 327 (2010) 68-72.
- [43] M. Pera-Titus, L. Leclercq, J.M. Clacens, F. De Campo, V. Nardello-Rataj, Pickering interfacial catalysis for biphasic systems: from emulsion design to green reactions, *Angewandte Chemie International Edition*, 54 (2015) 2006-2021.
- [44] X. Quan, H. Gu, C. Hu, Y. Zhang, Y. Li, W. Gao, C. Li, Sulfonated polydivinylbenzene bamboo-like nanotube stabilized Pickering emulsion for effective oxidation of olefins to 1, 2-diol, *Journal of Colloid and Interface Science*, 606 (2022) 158-166.
- [45] Y. Zhang, M. Zhang, H. Yang, Tuning biphasic catalysis reaction with a pickering emulsion strategy exemplified by selective hydrogenation of benzene, *ChemCatChem*, 10 (2018) 5224-5230.
- [46] Z. Fan, A. Tay, M. Pera-Titus, W.-J. Zhou, S. Benhabbari, X. Feng, G. Malcouronne, L. Bonneviot, F. De Campo, L. Wang, Pickering Interfacial Catalysts for solvent-free biomass transformation: Physicochemical behavior of non-aqueous emulsions, *Journal of colloid and interface science*, 427 (2014) 80-90.
- [47] Y. Zhou, Z. Guo, W. Hou, Q. Wang, J. Wang, Polyoxometalate-based phase transfer catalysis for liquid–solid organic reactions: a review, *Catalysis Science & Technology*, 5 (2015) 4324-4335.
- [48] S. Zhang, F. Ou, S. Ning, P. Cheng, Polyoxometalate-based metal–organic frameworks for heterogeneous catalysis, *Inorganic Chemistry Frontiers*, 8 (2021) 1865-1899.

- [49] W.-J. Cui, S.-M. Zhang, Y.-Y. Ma, Y. Wang, R.-X. Miao, Z.-G. Han, Polyoxometalate-Incorporated Metal-Organic Network as a Heterogeneous Catalyst for Selective Oxidation of Aryl Alkenes, *Inorganic Chemistry*, 61 (2022) 9421-9432.
- [50] K. Sato, M. Aoki, R. Noyori, A "green" route to adipic acid: Direct oxidation of cyclohexenes with 30 percent hydrogen peroxide, *Science*, 281 (1998) 1646-1647.
- [51] L. Leclercq, R. Company, A. Mühlbauer, A. Mouret, J.M. Aubry, V. Nardello-Rataj, Versatile Eco-friendly Pickering Emulsions Based on Substrate/Native Cyclodextrin Complexes: A Winning Approach for Solvent-Free Oxidations, *ChemSusChem*, 6 (2013) 1533-1540.
- [52] K. Kamata, K. Yonehara, Y. Sumida, K. Yamaguchi, S. Hikichi, N. Mizuno, Efficient epoxidation of olefins with  $\geq 99\%$  selectivity and use of hydrogen peroxide, *Science*, 300 (2003) 964-966.
- [53] L. Leclercq, A. Mouret, S. Renaudineau, V. Schmitt, A. Proust, V. Nardello-Rataj, Self-assembled polyoxometalates nanoparticles as pickering emulsion stabilizers, *The Journal of Physical Chemistry B*, 119 (2015) 6326-6337.
- [54] L. Leclercq, A. Mouret, A. Proust, V. Schmitt, P. Bauduin, J.M. Aubry, V. Nardello-Rataj, Pickering emulsion stabilized by catalytic polyoxometalate nanoparticles: A new effective medium for oxidation reactions, *Chemistry—A European Journal*, 18 (2012) 14352-14358.
- [55] B. Yang, L. Leclercq, V. Schmitt, M. Pera-Titus, V. Nardello-Rataj, Colloidal tectonics for tandem synergistic Pickering interfacial catalysis: oxidative cleavage of cyclohexene oxide into adipic acid, *Chemical Science*, 10 (2019) 501-507.
- [56] B. Yang, Pickering interfacial catalysis for oxidative cleavage by  $H_2O_2$  in biphasic systems, in, *Lille 1*, 2017.
- [57] J. Turkevich, P.C. Stevenson, J. Hillier, A study of the nucleation and growth processes in the synthesis of colloidal gold, *Discussions of the Faraday Society*, 11 (1951) 55-75.
- [58] S.L. Westcott, S.J. Oldenburg, T.R. Lee, N.J. Halas, Formation and Adsorption of Clusters of Gold Nanoparticles onto Functionalized Silica Nanoparticle Surfaces, *Langmuir*, 14 (1998) 5396-5401.
- [59] X. Zhang, Y. Wu, Y. Li, B. Li, Y. Pei, S. Liu, Effects of the interaction between bacterial cellulose and soy protein isolate on the oil-water interface on the digestion of the Pickering emulsions, *Food Hydrocolloids*, 126 (2022) 107480.
- [60] H. Jia, J. He, Y. Xu, T. Wang, L. Zhang, B. Wang, X. Jiang, X. Li, X. Zhang, K. Lv, Synergistic effects of  $AlOOH$  and sodium benzenesulfonate on the generation of Pickering emulsions and their application for enhanced oil recovery, *Colloids and Surfaces A: Physicochemical and Engineering Aspects*, 638 (2022) 128333.
- [61] K. Huang, R. Liu, Y. Zhang, X. Guan, Characteristics of two cedarwood essential oil emulsions and their antioxidant and antibacterial activities, *Food Chemistry*, 346 (2021) 128970.
- [62] M. Yue, M. Huang, Z. Zhu, T. Huang, M. Huang, Effect of ultrasound assisted emulsification in the production of Pickering emulsion formulated with chitosan self-assembled particles: Stability, macro, and micro rheological properties, *LWT*, 154 (2022) 112595.
- [63] L.E. Low, S.P. Siva, Y.K. Ho, E.S. Chan, B.T. Tey, Recent advances of characterization techniques for the formation, physical properties and stability of Pickering emulsion, *Advances in colloid and interface science*, 277 (2020) 102117.
- [64] C.L. Harman, M.A. Patel, S. Guldin, G.-L. Davies, Recent developments in Pickering emulsions for biomedical applications, *Current Opinion in Colloid & Interface Science*, 39 (2019) 173-189.
- [65] Y. Chevalier, M.-A. Bolzinger, Emulsions stabilized with solid nanoparticles: Pickering emulsions,

- Colloids and Surfaces A: Physicochemical and Engineering Aspects, 439 (2013) 23-34.
- [66] H. Fan, A. Striolo, Mechanistic study of droplets coalescence in Pickering emulsions, *Soft Matter*, 8 (2012) 9533-9538.
- [67] G. Douyère, L. Leclercq, V. Nardello-Rataj, From polyethyleneimine hydrogels to Pickering-like smart “On/Off” emulgels switched by pH and temperature, *Journal of Colloid and Interface Science*, 628 (2022) 807-819.
- [68] J. Jiang, S. Yu, W. Zhang, H. Zhang, Z. Cui, W. Xia, B.P. Binks, Charge-Reversible Surfactant-Induced Transformation Between Oil-in-Dispersion Emulsions and Pickering Emulsions, *Angewandte Chemie International Edition*, 60 (2021) 11793-11798.
- [69] F. Yang, J. Yang, S. Qiu, W. Xu, Y. Wang, Tannic acid enhanced the physical and oxidative stability of chitin particles stabilized oil in water emulsion, *Food Chemistry*, 346 (2021) 128762.
- [70] E. Skrzyńska, J. Ftouni, A.-S. Mamede, A. Addad, M. Trentesaux, J.-S. Girardon, M. Capron, F. Dumeignil, Glycerol oxidation over gold supported catalysts – “Two faces” of sulphur based anchoring agent, *Journal of Molecular Catalysis A: Chemical*, 382 (2014) 71-78.
- [71] G. Douyère, L. Leclercq, V. Nardello-Rataj, Cross-linked poly (4-vinylpyridine) particles for pH- and ionic strength-responsive “on-off” Pickering emulsions, *Colloids and Surfaces A: Physicochemical and Engineering Aspects*, 631 (2021) 127705.
- [72] C. Li, Y. Pi, S. Liu, J. Feng, X. Zhang, S. Li, R. Tan, Phosphotungstate-Functionalized Mesoporous Janus Silica Nanosheets for Reaction-Controlled Pickering Interfacial Catalysis, *ACS Sustainable Chemistry & Engineering*, 9 (2021) 13501-13513.
- [73] Y. Leng, J. Wang, D. Zhu, M. Zhang, P. Zhao, Z. Long, J. Huang, Polyoxometalate-based amino-functionalized ionic solid catalysts lead to highly efficient heterogeneous epoxidation of alkenes with H<sub>2</sub>O<sub>2</sub>, *Green Chemistry*, 13 (2011) 1636-1639.
- [74] F. Bentaleb, O. Makrygenni, D. Brouri, C. Coelho Diogo, A. Mehdi, A. Proust, F. Launay, R. Villanneau, Efficiency of polyoxometalate-based mesoporous hybrids as covalently anchored catalysts, *Inorganic Chemistry*, 54 (2015) 7607-7616.
- [75] Z. Cui, C.M. Li, PtRu catalysts supported on heteropolyacid and chitosan functionalized carbon nanotubes for methanol oxidation reaction of fuel cells, *Physical Chemistry Chemical Physics*, 13 (2011) 16349-16357.
- [76] E. Asenath Smith, W. Chen, How to prevent the loss of surface functionality derived from aminosilanes, *Langmuir*, 24 (2008) 12405-12409.
- [77] P. Kumar, M.C. Mathpal, S. Ghosh, G.K. Inwati, J.R. Maze, M.-M. Duvenhage, W. Roos, H. Swart, Plasmonic Au nanoparticles embedded in glass: Study of TOF-SIMS, XPS and its enhanced antimicrobial activities, *Journal of Alloys and Compounds*, 909 (2022) 164789.
- [78] A. Zwijnenburg, A. Goossens, W.G. Sloof, M.W. Craje, A.M. van der Kraan, L. Jos de Jongh, M. Makkee, J.A. Moulijn, XPS and Mössbauer characterization of Au/TiO<sub>2</sub> propene epoxidation catalysts, *The Journal of Physical Chemistry B*, 106 (2002) 9853-9862.
- [79] S.M. Demers, C.R. Shirazinejad, J.L.A. Garcia, J.R. Matthews, J.H. Hafner, Ultraviolet analysis of gold nanorod and nanosphere solutions, *The Journal of Physical Chemistry C*, 121 (2017) 5201-5207.
- [80] S.S. Shankar, S. Bhargava, M. Sastry, Synthesis of gold nanospheres and nanotriangles by the Turkevich approach, *Journal of Nanoscience and Nanotechnology*, 5 (2005) 1721-1727.
- [81] J. Chen, X. Li, X. Wu, J.T. Pierce, N. Fahrudin, M. Wu, J.X. Zhao, Au-silica nanowire nanohybrid

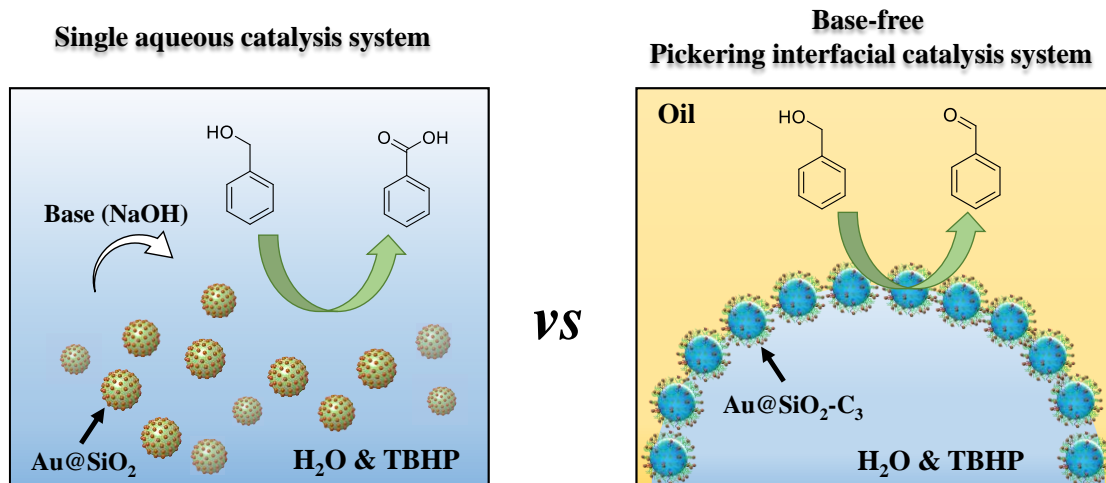
- as a hyperthermia agent for photothermal therapy in the near-infrared region, *Langmuir*, 30 (2014) 9514-9523.
- [82] J.-F.o. Dechézelles, C. Ciotonea, C. Catrinescu, A. Ungureanu, S.b. Royer, V.r. Nardello-Rataj, Emulsions stabilized with alumina-functionalized mesoporous silica particles, *Langmuir*, 36 (2020) 3212-3220.
- [83] W.D. Bancroft, The theory of emulsification, V, *The Journal of Physical Chemistry*, 17 (2002) 501-519.
- [84] L. Bai, S. Huan, W. Xiang, O.J. Rojas, Pickering emulsions by combining cellulose nanofibrils and nanocrystals: Phase behavior and depletion stabilization, *Green chemistry*, 20 (2018) 1571-1582.
- [85] S. Arditty, C. Whitby, B. Binks, V. Schmitt, F. Leal-Calderon, Some general features of limited coalescence in solid-stabilized emulsions, *The European Physical Journal E*, 11 (2003) 273-281.
- [86] J. Su, Q. Guo, Y. Chen, W. Dong, L. Mao, Y. Gao, F. Yuan, Characterization and formation mechanism of lutein pickering emulsion gels stabilized by  $\beta$ -lactoglobulin-gum arabic composite colloidal nanoparticles, *Food Hydrocolloids*, 98 (2020) 105276.
- [87] C.-H. Chou, C.-D. Chen, C.C. Wang, Highly efficient, wavelength-tunable, gold nanoparticle based optothermal nanoconvertors, *The Journal of Physical Chemistry B*, 109 (2005) 11135-11138.
- [88] K. Jiang, D.A. Smith, A. Pinchuk, Size-dependent photothermal conversion efficiencies of plasmonically heated gold nanoparticles, *The Journal of Physical Chemistry C*, 117 (2013) 27073-27080.
- [89] R. Bielas, T. Hornowski, K. Paulovičová, M. Rajňák, A. Józefczak, The effect of magnetic particles covering the droplets on the heating rate of Pickering emulsions in the AC magnetic field, *Journal of Molecular Liquids*, 320 (2020) 114388.
- [90] A.M. Bago Rodriguez, L. Schober, A. Hinzmann, H. Gröger, B.P. Binks, Effect of Particle Wettability and Particle Concentration on the Enzymatic Dehydration of n-Octanaloxime in Pickering Emulsions, *Angewandte Chemie*, 133 (2021) 1470-1477.
- [91] H. Zhao, J. Li, L. Wang, C. Li, S. Zhang, Pickering emulsion stabilized by dual stabilizer: A novel reaction/separation system for methacrolein synthesis, *Chemical Engineering Science*, 229 (2021) 116038.
- [92] M. Kargar, K. Fayazmanesh, M. Alavi, F. Spyropoulos, I.T. Norton, Investigation into the potential ability of Pickering emulsions (food-grade particles) to enhance the oxidative stability of oil-in-water emulsions, *Journal of Colloid and Interface Science*, 366 (2012) 209-215.
- [93] S. Lv, H. Zhou, L. Bai, O.J. Rojas, D.J. McClements, Development of food-grade Pickering emulsions stabilized by a mixture of cellulose nanofibrils and nanochitin, *Food Hydrocolloids*, 113 (2021) 106451.
- [94] H. Xiang, Y. Chen, Energy-converting nanomedicine, *Small*, 15 (2019) 1805339.
- [95] J. Liu, F. Zhai, H. Zhou, W. Yang, S. Zhang, Nanogold flower-inspired nanoarchitectonics enables enhanced light-to-heat conversion ability for rapid and targeted chemo-photothermal therapy of a tumor, *Advanced Healthcare Materials*, 8 (2019) 1801300.
- [96] M. Gondal, M. Sayeed, A. Alarfaj, Activity comparison of  $\text{Fe}_2\text{O}_3$ , NiO,  $\text{WO}_3$ ,  $\text{TiO}_2$  semiconductor catalysts in phenol degradation by laser enhanced photo-catalytic process, *Chemical Physics Letters*, 445 (2007) 325-330.
- [97] T. Kumpulainen, J. Pekkanen, J. Valkama, J. Laakso, R. Tuokko, M. Mäntysalo, Low temperature nanoparticle sintering with continuous wave and pulse lasers, *Optics & Laser Technology*, 43 (2011)

570-576.

- [98] F. Glaser, C. Kerzig, O.S. Wenger, Multi-photon excitation in photoredox catalysis: concepts, applications, methods, *Angewandte Chemie International Edition*, 59 (2020) 10266-10284.
- [99] P. Keblinski, D.G. Cahill, A. Bodapati, C.R. Sullivan, T.A. Taton, Limits of localized heating by electromagnetically excited nanoparticles, *Journal of Applied Physics*, 100 (2006) 054305.
- [100] M. Nazemi, S.R. Panikkanvalappil, C.-K. Liao, M.A. Mahmoud, M.A. El-Sayed, Role of Femtosecond Pulsed Laser-Induced Atomic Redistribution in Bimetallic Au–Pd Nanorods on Optoelectronic and Catalytic Properties, *ACS nano*, 15 (2021) 10241-10252.
- [101] A.B.S. Bakhtiari, D. Hsiao, G. Jin, B.D. Gates, N.R. Branda, An efficient method based on the photothermal effect for the release of molecules from metal nanoparticle surfaces, *Angewandte Chemie*, 121 (2009) 4230-4233.
- [102] A. Mouret, L. Leclercq, A. Mühlbauer, V. Nardello-Rataj, Eco-friendly solvents and amphiphilic catalytic polyoxometalate nanoparticles: a winning combination for olefin epoxidation, *Green Chemistry*, 16 (2014) 269-278.



# Chapter III. Grafting of ultra-small Au nanoparticles on silica particles as catalysts for alcohol oxidation at the water/oil interface







## 1. Introduction

The oxidation of alcohols into their corresponding carbonyl compounds is an important reaction to produce fine chemicals [1-3]. In particular, the selective oxidation of primary alcohols into aldehydes has attracted more and more interest because of their critical role in the fragrance industry [4]. Many reactions have been established using stoichiometric oxygen donors such as chromate or permanganate, but these reagents are expensive and toxic [5, 6]. Nitroxyl radicals such as 2,2,6,6-tetramethyl-piperidine-1-oxyl (TEMPO) in combination with a stoichiometric oxidant such as sodium hypochlorite can significantly enhance the oxidation efficiency using oxygen and nitric acid [7-9]. However, nitric acid is highly corrosive and produces waste. Considering the increasing concern to design green processes, it is highly desirable to develop a green alternative for efficient alcohol oxidation.

So far, a remarkable number of metal NPs have been extensively studied for selective oxidation of alcohols under mild conditions, especially based on Pd [10], Cu [11], Co [12], and Ru [13] NPs, with different oxidants such as aqueous H<sub>2</sub>O<sub>2</sub> [14], *tert*-Butyl hydroperoxide (TBHP) [15] and air/molecular oxygen [16]. Recently, the unexpectedly high activity of Au NPs for CO oxidation has motivated its use for the liquid-phase oxidation of alcohols [17-19]. Unlike supported Pd and Pt catalysts, Au NPs with ultra-small size exhibit very high selectivity and are less prone to metal leaching, over-oxidation, and self-poisoning [20, 21]. The remarkable catalytic performance of Au strongly depends on the NP size, which can be controlled by the preparation method and the support nature [22]. Thus, silica [23], graphite [24], titanium dioxide [25], nanoceria [26], and alumina [27] have been used as supports for Au NPs, which were used as active heterogeneous catalysts for benzyl alcohol oxidation Corma *et al.* [28] reported that Au nanoclusters deposited on metal oxides show a high catalytic activity for the oxidation of various alcohols. Besides, the combination of Au with a second type of metal to form a bimetallic catalyst can promote benzyl alcohol oxidation due to a synergistic effect between both metals [29]. However, basic promoters such as NaOH and K<sub>2</sub>CO<sub>3</sub> are often needed for oxidation of alcohol [30, 31], but they suffer from cumbersome post-processing

problems, since they generate salt after neutralization, which is incompatible with the Green Chemistry principles. In parallel, the low solubility of organic molecules in water and the small reaction interface lead to low catalytic efficiency. To improve the interface activity, co-solvent [32], surfactant [33] and continuous-flow microreactors [34, 35] have been used, but additives or complex equipment is required to boost the solid/liquid contact on the catalyst surface [36-38]. Therefore, developing a novel catalytic system providing a green and base-free reaction platform still remains a major challenge.

Pickering interfacial catalysis (PIC), as a new and efficient interfacial catalytic system, has been developed to improve and boost the reaction activity of biphasic reactions [39-41]. Unlike traditional biphasic reactions, PIC systems show the following inherent advantages: (1) large interfacial area to decrease the diffusion-related limitation in biphasic reaction; (2) improved catalytic activity/selectivity driven by the solubility difference in the organic/aqueous phase; (3) facile emulsification/ demulsification; (4) increased ecological benefits. Surface wettability of solid NPs plays a crucial role in the formation and stabilization of Pickering emulsions [42-44]. In pioneering studies, Li *et al.* [45] prepared phosphotungstate-functionalized mesoporous Janus silica nanosheets by selectively decorating ammonium phosphotungstate (PW) on the one side of silica nanosheets. PW-functionalized silica materials displayed excellent catalytic activity and selectivity in the oxidation of benzyl alcohol by the formation of H<sub>2</sub>O<sub>2</sub>-switchable Pickering emulsions. Jing *et al.* [46] reported novel amphiphilic Pb@amZSM-5 nanoreactors by *in situ* reduction of Pb NPs (1.5 nm) on the surface of ultra-small amphiphilic zeolites (amZSM-5). The as-prepared Pb@amZSM-5 nanoreactors showed excellent amphiphilicity for stabilizing Pickering emulsions with uniform droplets around 50 μm and exhibited high catalytic activity for the selective oxidation of alcohols using air as oxidant without base.

The higher catalytic activity of Au NPs in benzyl alcohol oxidation is often observed in the presence of base promoters (such as hydroxides and carbonates) [47, 48]. A striking example is the selective oxidation of benzyl alcohol into benzoic acid using hydrogen peroxide in an Au-based catalytic microcapillary reactor [49]. The Au NPs immobilization into fused silica capillary tubing were used as microreactors, which provide the shortened diffusion path

of the reagents. Under optimized conditions (80 °C, resident time = 639 s), the conversion of benzyl alcohol over 100% can be achieved with high selectivity of benzoic acid, using a substrate:H<sub>2</sub>O<sub>2</sub>:base = 1:10:3 ratio. Benzyl alcohol oxidation in the presence of ceria supported Au NPs (Au–CeO<sub>2</sub>) with the addition of K<sub>2</sub>CO<sub>3</sub> as oxidant was also studied by Nozaki *et al.* [50], the catalysts Au–CeO<sub>2</sub> was synthesized using amorphous alloy as a precursor and followed by directly alloying Au with Ce–Al alloy, which exhibited excellent catalytic activity for the oxidation of benzyl alcohol to benzaldehyde. However, the addition of K<sub>2</sub>CO<sub>3</sub> are necessary in these systems to obtain good catalytic performance. Indeed, the presence of hydroxide ions can assist the dehydrogenation of the alcohol in the catalytic oxidation process, thus accelerating the catalytic activity. Also, the subsequent oxidation of benzaldehyde is boosted at high pH environment, leading to the high yield of benzoic yield in aqueous solvents.

Herein we have synthesized surface-active NPs behaving both as catalyst and emulsifier to precisely localize catalytic sites at the water-oil interface and conduct the base-free oxidation of benzyl alcohol using aqueous H<sub>2</sub>O<sub>2</sub> as oxidant. Specifically, we prepared Au@SiO<sub>2</sub>-C<sub>3</sub> NPs composed of a hydrophobic silica core and highly dispersed Au NPs immobilized on the silica surface. The Au@SiO<sub>2</sub>-C<sub>3</sub> NPs were used to formulate a stable Pickering emulsion platform for interfacial catalysis. Unlike hydrophilic Au@SiO<sub>2</sub> NPs and single-phase catalysis, Au@SiO<sub>2</sub>-C<sub>3</sub> NPs exhibited higher catalytic performance for the selective oxidation of benzyl alcohol in PIC system. We show that the interfacial location of the Au NPs plays a key role in achieving outstanding catalytic activity.

## 2. Experimental section

### 2.1. Materials

Reagent-grade HAuCl<sub>4</sub> · 3H<sub>2</sub>O (99.9 %), NaBH<sub>4</sub>, (3-aminopropyl)triethoxysilane (APTES), sodium hydroxide, trimethoxy(propyl)silane (C<sub>3</sub>) (97%), *tert*-Butyl hydroperoxide (70%) (TBHP) were purchased from Aldrich (USA). Aerosil<sup>®</sup>200 was a generous gift from Evonik Industries AG (Germany). Benzyl alcohol (99%) was procured from TCI (Japan). CDCl<sub>3</sub>

(99.8%) was supplied by Euriso-top (France). Tetrakis(hydroxymethyl)phosphonium chloride (THPC) solution (80% in H<sub>2</sub>O) and 1,1,2,2-tetrachloroethane were obtained from Sigma. All the water solutions were prepared using Millipore water produced in a water purification device with a water resistivity higher than 18.2 MΩ cm (Barnstead, Thermo Scientific, USA).

## 2.2. Synthesis of ultra-small Au NPs

In a typical synthesis of ultra-small Au NPs [51], 45.5 mL of water were added into a 100-mL round-bottomed flask at room temperature and stirred at 500 rpm. Then, 1.5 mL of an aqueous solution of NaOH (0.2 mol/L) and the reducing agent THPC (1 mL of a solution composed of 1.2 mL of 80% THPC aqueous solution diluted to 100 mL with water) were added into the flask. After the addition of THPC for two min, 2 mL of solution containing 20 mg fresh HAuCl<sub>4</sub> (dark-aged for 15 min before use) were added to the flask, resulting in the formation of an orange-brown hydrosol. The as-prepared ultra-small Au NP dispersion was stored in a refrigerator at 4 °C under darkness.

## 2.3. Synthesis of amphiphilic silica NPs (SiO<sub>2</sub>-C<sub>3</sub>)

Amphiphilic silica NPs were prepared by a typical procedure described before [52]. Briefly, 0.5 g of Aerosil<sup>®</sup>200 were dispersed in 200 mL of water/ethanol solution (1/1 v/v, pH 9.8) in an ultrasonic for 30 min and stirred for further 30 min at 500 rpm. Subsequently, 5 mmol of trimethoxy(propyl)silane (C<sub>3</sub>) were slowly added into the suspension and stirred for another 5 min. Then, 0.5 mmol of APTES were added dropwise into the reaction system, and the mixture was stirred at room temperature for another 1 h, followed by heating to 80 °C for 1 h. The resulting SiO<sub>2</sub>-C<sub>3</sub> NPs were collected by centrifugation and washed six times with water and ethanol at 5000 rpm for 10 min to remove residual organosilane, and then dried at 80 °C overnight.

## 2.4. Synthesis of ultra-small Au grafted amphiphilic silica NPs (Au/SiO<sub>2</sub>-C<sub>3</sub>)

Ultra-small Au NPs were immobilized on the surface of amphiphilic SiO<sub>2</sub>-C<sub>3</sub> NPs by the self-assembly method [53]. In a typical preparation, 3 mL of ultra-small Au NP dispersion (see

section 2.3) were slowly added to 3 mL of SiO<sub>2</sub>-C<sub>3</sub> ethanolic dispersion (1.5 wt.%) at room temperature under stirring at 800 rpm. After centrifugation, washing with water and ethanol, drying in an oven at 80 °C overnight, the Au/SiO<sub>2</sub>-C<sub>3</sub> NPs were obtained.

### 2.5. Synthesis of Au-loaded amphiphilic silica NPs (Au@SiO<sub>2</sub>-C<sub>3</sub>)

Au@SiO<sub>2</sub>-C<sub>3</sub> NPs were prepared by the *in situ* method [54, 55]. In a typical preparation, 0.5 g of SiO<sub>2</sub>-C<sub>3</sub> NPs were dispersed in 200 mL of ethanol under sonication for 10 min, and stirred for 2 h at room temperature. Then, 18 mL of an aqueous HAuCl<sub>4</sub> solution (14 mg HAuCl<sub>4</sub>, 2 mmol/L) were added and stirred for 2 h. Then, 38 mL of freshly prepared NaBH<sub>4</sub> aqueous solution (20 mg NaBH<sub>4</sub>, 14 mmol/L) were added and the color of the solution turned orange-brown immediately. After 1 h, the obtained NPs were collected by centrifugation, followed by washing with water and ethanol to remove impurities, and dried at 80 °C overnight to obtain the Au@SiO<sub>2</sub>-C<sub>3</sub> NPs.

### 2.6. Synthesis of Au-loaded hydrophilic silica NPs (Au@SiO<sub>2</sub>)

The Au@SiO<sub>2</sub> NPs were synthesized by the one-pot method [56]. In a typical preparation, 0.5 g of Aerosil®200 NPs were dispersed in 200 mL of distilled water under sonication for 10 min at room temperature. Then, 211 µL of APTES were added into the solution under vigorous stirring at 80 °C for 3 h. Next, 10 mg of HAuCl<sub>4</sub> were dissolved in 1 mL of water, and the solution was added to the dispersion under stirring. A NaOH solution was used to set the pH in the range 5-7. After stirring for 1 h at 80 °C, 1 mL of the reducing agent solution containing 10 mg NaBH<sub>4</sub> was added into the solution, and the color of dispersion turned into brown-orange immediately. The mixture was kept for further 2 h under heating. The Au@SiO<sub>2</sub> NPs were separated by centrifugation, washed with distilled water and ethanol for six times, and dried at 80 °C overnight.

### 2.7. NPs characterization

The size distribution and zeta potential of the different NPs were measured by dynamic light scattering (DLS) measurements using a Zetasizer Nano ZS ZEN 3600 (Malvern, UK).

The transmission electron microscopic (TEM) images were collected on a FEI Tecnai G2 F20s-twin D573 field emission transmission electron microscope operating at 200 kV.

The Fourier transform infrared (FT-IR) spectra were recorded on a Thermo Nicolet AVATAR spectrometer in the range 400-4000  $\text{cm}^{-1}$ .

Thermogravimetric analysis (TGA) was carried out on a TGA Q500 thermal analyzer from 30 to 900  $^{\circ}\text{C}$  in  $\text{N}_2$  flow using a heating rate of 10  $^{\circ}\text{C}/\text{min}$  and 10-20 mg sample.

The Au content was measured using an Agilent's 5110 vertical dual view inductively coupled plasma optical emission spectrometer (ICP-OES) equipped with an OneNeb nebulizer, a quartz double pass spray chamber and a quartz torch (Agilent). 50 mg dried samples were weight, and 1mL HF / 1mL HCl / 1mL  $\text{HNO}_3$  were added and heated at 110  $^{\circ}\text{C}$  in closed Teflon tubes for 24 h. Then, 30 mL of ultrapure water were added. The solutions were filtered at 0.45  $\mu\text{m}$  and diluted for ICP-OES analysis.

X-ray photoelectron spectroscopy (XPS) was performed on a Kratos AXIS Ultra DLD spectrometer using monochromatic Al K $\alpha$  radiation (1486.6 eV) operating at 225 W (15 mA, 15kV). The spectra were collected using an analysis area of  $\approx 300 \mu\text{m} \times 700 \mu\text{m}$  and a 20 eV pass energy.

The water contact angles were characterized using a water static contact angle meter (Kruss DSA25S, Germany) equipped with a charge-coupled camera. Typically, a drop of water (4  $\mu\text{L}$ ) was placed on the pellets made by compressing the particles power at 1800 bar pressure for 10 min.

## 2.8. Emulsion preparation

Typically, 1.8 wt.% Au@SiO<sub>2</sub>-C<sub>3</sub> NPs were weighted in a glass vessel before adding 1.5 mL of oil phase and 1.5 mL of water at room temperature. Emulsions were formed using Ultraturrax T10 homogenizer (IKA, Germany) at a stirring rate of 11,500 rpm for 2 min.

## 2.9. Emulsion characterization

Optical microphotographs of the emulsions were recorded on a VHX-900 F digital microscope equipped with 100X to 1000X magnification lens VH-Z100UR/W/T (Keyence, France). The droplet diameter was measured using ImageJ software (National Institutes of Health, USA). The droplet size distribution was obtained by treatment of experimental data with log-normal function (OriginPro 8<sup>®</sup>, USA). The volume fraction of the emulsion phase was monitored after the freshly prepared emulsion was suspended for a certain time using ImageJ software.

### 2.10. Catalytic tests

The oxidation of benzyl alcohol with TBHP was carried out in a 10-mL sealed glass vial. In a typical test, 75 mg of Au@SiO<sub>2</sub>-C<sub>3</sub> NPs were dispersed in 1.5 mL of toluene containing benzyl alcohol (0.1 mol/L), followed by the addition of 1.5 mL of water containing TBHP (42  $\mu$ L, 70%, 2.0 equiv.). The mixture was emulsified using an Ultraturrax at 11,500 rpm for 2 min and then sealed and heated at 80  $^{\circ}$ C for a certain time under magnetic stirring (500 rpm). After the reaction, the emulsion was cooled down to room temperature and centrifuged. The upper layer oil phase containing the product was collected by decantation and analyzed and quantified by <sup>1</sup>H NMR. Nuclear magnetic resonance (NMR) measurements were conducted on a Bruker Avance-500 spectrometer. CDCl<sub>3</sub> was used as solvent for the oil phase, whereas C<sub>2</sub>H<sub>2</sub>Cl<sub>4</sub> was used as internal standard. For the recyclability tests, the Au@SiO<sub>2</sub>-C<sub>3</sub> NPs were washed five times with ethanol and water and dried in an oven overnight. Freshly prepared 1.5 mL of toluene containing benzyl alcohol (0.1 mol/L) and 1.5 mL of water containing TBHP (2.0 equiv.) were added into the recycled Au@SiO<sub>2</sub>-C<sub>3</sub> NPs for the next run.

Catalytic tests in toluene were carried out in 3 mL of toluene and 75 mg of Au@SiO<sub>2</sub>-C<sub>3</sub> NPs, followed by the addition of benzyl alcohol (16  $\mu$ L) and TBHP (2.0 equiv.). The mixture was sealed and transferred to an oil bath for reaction at 80  $^{\circ}$ C for 3 h. After the reaction, the mixture was centrifuged to separate the solution from the catalyst, and the collected organic phase was analyzed by <sup>1</sup>H NMR.



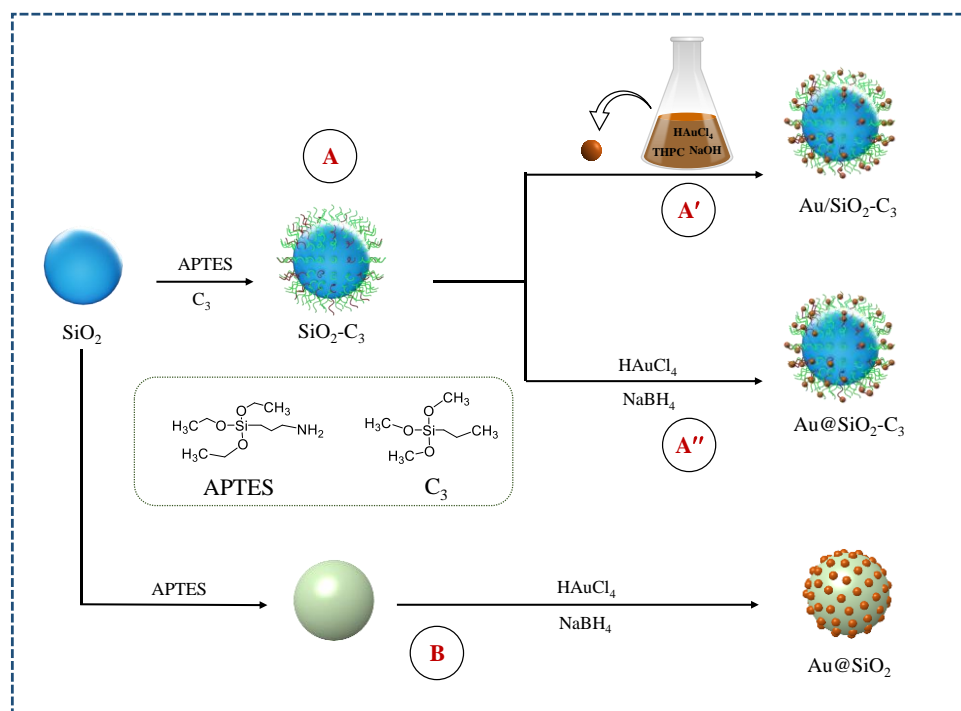
In the case of single water phase catalytic reaction, the pH of deionized water was adjusted to pH 9-11 using an aqueous NaOH solution. In a typical test, 75 mg of Au@SiO<sub>2</sub> NPs were dispersed in 3 mL of water, followed by the addition of benzyl alcohol (32 μL) and TBHP (2.0 equiv.). The resulting dispersion was stirred at 80 °C for 3 h. After reaction, the system was cool down, and the solution was centrifuged to separate the aqueous phase. An excess amount of an aqueous HCl solution was added to neutralize the base and decrease the solubility of products in water. The products were extracted with CH<sub>2</sub>Cl<sub>2</sub> for five times, and the obtained solution was dried over MgSO<sub>4</sub> to remove trace water. The solvent was then evaporated, and the products were identified and quantified by <sup>1</sup>H NMR.

### 3. Results and discussion

#### 3.1. Synthesis and characterization of NPs

##### 3.1.1. Preparation of nanoparticles

A schematic illustration of the synthesis procedure of amphiphilic NPs is presented in **Scheme 1**. Briefly, C<sub>3</sub> chains and APTES were covalently grafted on silica by silanization. Then, ultra-small Au NPs were immobilized on the surface of the NPs to prepare the interfacially-active catalyst. Both the self-assembled and *in-situ* reduction method were used to generate Au NPs. The final Au-loaded samples were denoted as Au/SiO<sub>2</sub>-C<sub>3</sub> (method A') and Au@SiO<sub>2</sub>-C<sub>3</sub> (method A''), respectively. Besides, the hydrophilic catalyst was synthesized by grafting APTES on the silica surface by silanization. The Au NPs were immobilized on the silica surface by adsorption of HAuCl<sub>4</sub> on amine groups, followed by reduction, and were labeled as Au@SiO<sub>2</sub> (method B).



**Scheme 1.** Schematic representation of the synthesis protocol of Au/SiO<sub>2</sub>-C<sub>3</sub> NPs (method A'), Au@SiO<sub>2</sub>-C<sub>3</sub> NPs (method A'') and Au@SiO<sub>2</sub> NPs (method B).

Zeta potential measurements were performed to measure the surface charge of the silica NPs before and after surface functionalization. To examine the dynamic properties of the obtained NPs in dispersion, we measured the hydrodynamic diameter by DLS. The mean size and surface charge of the obtained NPs are listed in **Table 1**.

**Table 1** Main physicochemical characteristics of the NPs

	Au	SiO <sub>2</sub>	SiO <sub>2</sub> -C <sub>3</sub>	Au/SiO <sub>2</sub> -C <sub>3</sub>	Au@SiO <sub>2</sub> -C <sub>3</sub>	Au@SiO <sub>2</sub>
D <sub>h</sub> (nm) <sup>a</sup>	2.3	90	190	210	254	210
ζ (mV) <sup>b</sup>	-35.7	-38	42.6	40.2	35.6	32.7

<sup>a</sup> Hydrodynamic diameter of NPs measured by DLS. <sup>b</sup> Determined for 0.1 wt.% NPs dispersion in water at 25 °C in neutral pH.

In method A', ultra-small Au NP (2.3 nm) aqueous dispersion is obtained by reduction of chloroauric acid with THPC. The bare silica NPs has a hydrodynamic diameter around 90 nm with a negative charge of -38 mV. In contrast, the surface charge and structure of SiO<sub>2</sub>-C<sub>3</sub> NPs are significantly affected by surface modification. The SiO<sub>2</sub>-C<sub>3</sub> NPs exhibit a mean size of 190 nm with a zeta potential of +42.6 mV at pH 7. The positive surface charge of SiO<sub>2</sub>-C<sub>3</sub> NPs is

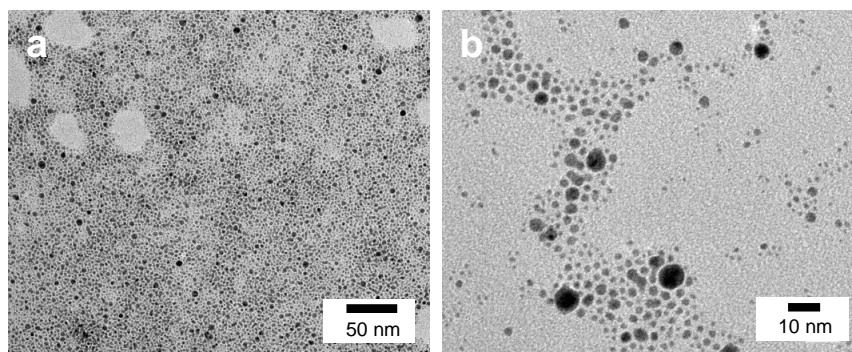
ascribed to the protonated amine groups ( $-\text{NH}_3^+$ ) on the silica surface ( $\text{pH } 7 > \text{isoelectric point}$ ) [57]. Then, Au NPs ( $-35.7 \text{ mV}$ ) were immobilized on the  $\text{SiO}_2\text{-C}_3$  NPs by electrostatic interaction. The hydrodynamic diameter ( $210 \text{ nm}$ ) of the obtained  $\text{Au/SiO}_2\text{-C}_3$  NPs keeps almost unchanged compared to  $\text{SiO}_2\text{-C}_3$  NPs, while the surface charge of  $\text{Au/SiO}_2\text{-C}_3$  NPs ( $-40.2 \text{ mV}$ ) decreases slightly due to the negatively charged Au NPs.

In method A'', the  $\text{Au@SiO}_2\text{-C}_3$  NPs were prepared by *in situ* grafting the Au NPs on  $\text{SiO}_2\text{-C}_3$  NPs. Unlike  $\text{SiO}_2\text{-C}_3$  NPs, the charge of  $\text{Au@SiO}_2\text{-C}_3$  NPs also decreases slightly ( $+35.6 \text{ mV}$ ). This can be explained by the negative Au NPs immobilized on the positive amine groups *via* electrostatic attraction, thus inducing a decrease of the effective surface charge.

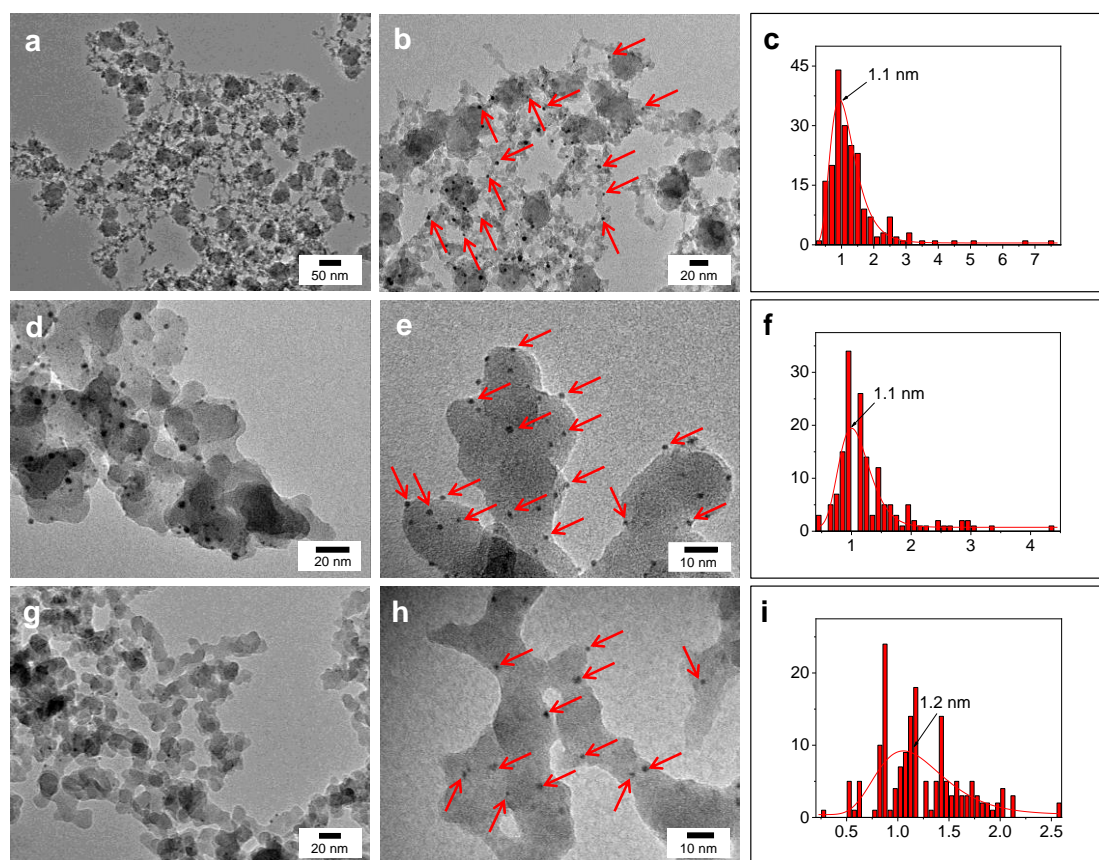
The  $\text{Au@SiO}_2$  NPs show an average diameter of  $210 \text{ nm}$ , with a surface charge of  $+32.7 \text{ mV}$ . The hydrodynamic diameter is larger than that measured by TEM, suggesting partial aggregation of NPs due to polymerization of APTES [56, 58].

### 3.1.2. Transmission electron microscopy characterization

To identify the morphology structure of the as-prepared samples, TEM micrographs were measured on the different NPs (**Figure 1-2**). As displayed in **Figure 1a and b**, the ultra-small Au NPs are spherical and have a broad particle size distribution. **Figure 2a-b** indicate the successful immobilization of Au NPs on  $\text{SiO}_2\text{-C}_3$  NPs. The size distribution (**Figure 2c**) of Au NPs lies in the range of  $0.3\text{-}7 \text{ nm}$  with an average diameter of  $1.1 \text{ nm}$ . As depicted in **Figures 2d-e**, the Au NPs synthesized by the *in-situ* method are uniform and well dispersed on  $\text{SiO}_2\text{-C}_3$ . Au NPs show a narrow size distribution around  $1.1 \text{ nm}$  (**Figure 2f**). The  $\text{Au@SiO}_2\text{-C}_3$  NPs present an irregular spherical morphology. Aggregation of  $\text{Au@SiO}_2$  NPs is visible in **Figure 2g**. The larger NP clusters suggest strong interaction between the amine groups on the silica surface. Au NPs on  $\text{Au@SiO}_2$  are dispersed uniformly and show an average size ( $1.2 \text{ nm}$ ), which is similar to the size of Au NPs immobilized on  $\text{Au@SiO}_2\text{-C}_3$  NPs.



**Figure 1.** TEM image of the as-prepared ultra-small Au NPs (a and b).

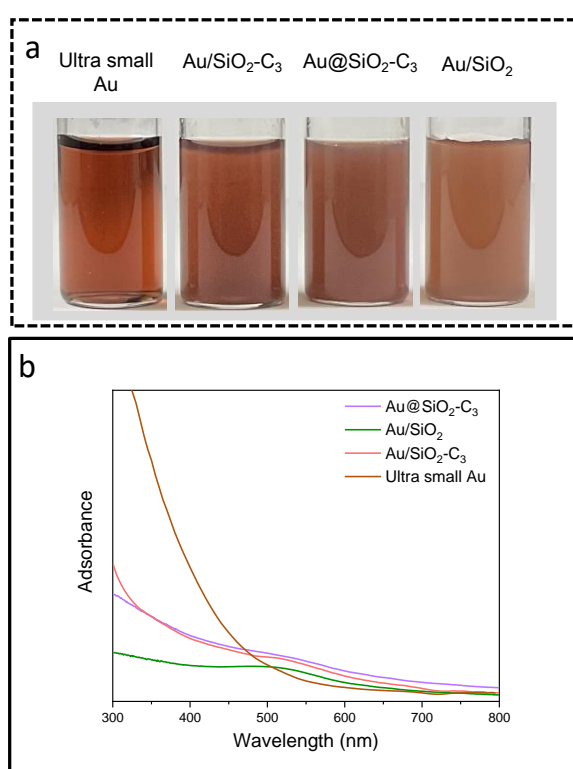


**Figure 2.** TEM image of the as-prepared samples and the corresponding Au size distribution. (a-d) ultra-small Au NPs, and Au/SiO<sub>2</sub>-C<sub>3</sub>, (e-h) Au@SiO<sub>2</sub>-C<sub>3</sub>, (i-l) Au@SiO<sub>2</sub> NPs.

Overall, using a simple synthetic pathway, we can coat the silica surface with uniform and mono-dispersed Au NPs without modifying the structure of silica particles. The Au loading on Au@SiO<sub>2</sub>-C<sub>3</sub> NPs is about 0.46 wt.% based on ICP analysis, while the Au loading on Au@SiO<sub>2</sub> is 0.36 wt.%.

### 3.1.3. UV-vis spectroscopy

The UV-*vis* spectra of the ultra-small Au, Au/SiO<sub>2</sub>-C<sub>3</sub>, Au@SiO<sub>2</sub>-C<sub>3</sub> and Au@SiO<sub>2</sub> NPs are shown in **Figure 3a-b**. The spectra of ultra-small Au do not exhibit any plasmonic absorbance, while Au/SiO<sub>2</sub>-C<sub>3</sub>, Au@SiO<sub>2</sub>-C<sub>3</sub> and Au@SiO<sub>2</sub> NPs show very weak plasmonic absorbance around 520 nm (**Figure 3b**). The weak plasmonic absorbance of the NPs can be explained by the variation of distances between Au NPs due to the silica environment. The presence of a weak plasmon feature further evidences that Au NPs possess ultra-small size.

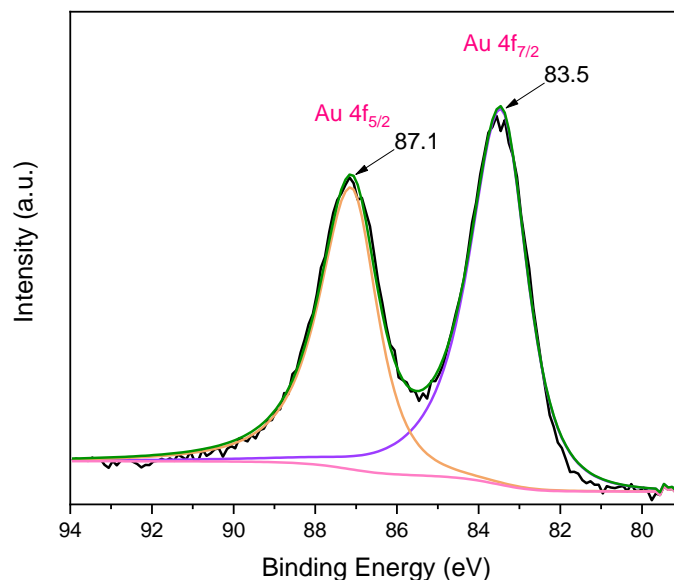


**Figure 3.** (a) Photographs of dispersions, (b) UV spectra of ultra-small Au, Au/SiO<sub>2</sub>-C<sub>3</sub>, Au@SiO<sub>2</sub>-C<sub>3</sub>, and Au@SiO<sub>2</sub> NPs. The spectra were measured using deionized water for ultra-small Au NPs, and SiO<sub>2</sub>-C<sub>3</sub> for Au/SiO<sub>2</sub>-C<sub>3</sub>, Au@SiO<sub>2</sub>-C<sub>3</sub>, and Au@SiO<sub>2</sub> NPs, respectively, which were used as reference.

### 3.1.4. X-ray photoelectron spectroscopy analysis

The Au state on the as-prepared Au@SiO<sub>2</sub>-C<sub>3</sub> NPs was investigated by XPS (**Figure 4**), suggesting that the Au<sup>3+</sup> precursors is fully reduced to yield Au<sup>0</sup> NPs. The binding energy of Au 4f<sub>7/2</sub> for Au@SiO<sub>2</sub>-C<sub>3</sub> NPs is about 83.5 eV, which moves approximately 0.5 eV towards

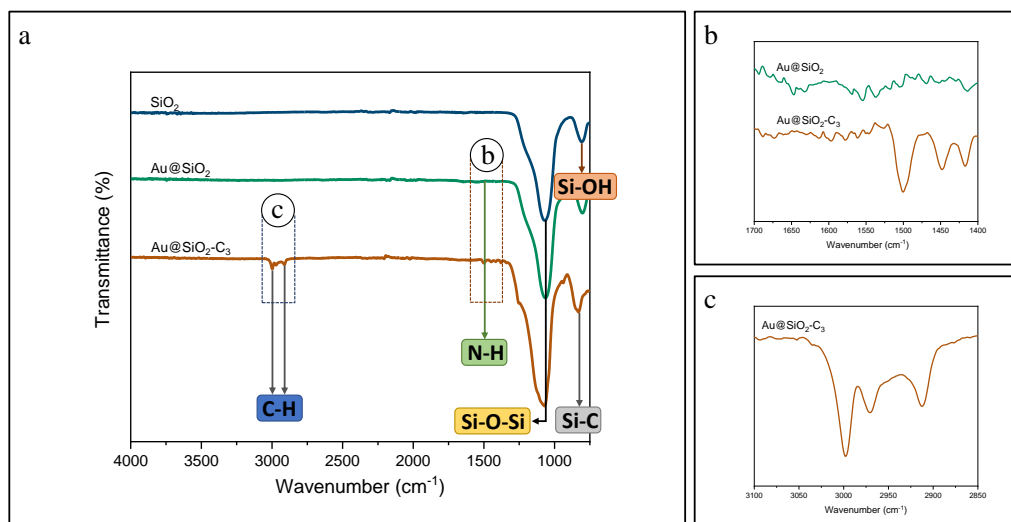
lower binding energy relative to the binding energy (84.0 eV) of Au 4f<sub>7/2</sub> compared to a metallic Au film (Au<sup>0</sup>) [59]. This observation can be explained by the interaction between Au and SiO<sub>2</sub>-C<sub>3</sub>, which modifies the electron density of Au [60, 61].



**Figure 4.** XPS spectra of Au 4f core level for Au@SiO<sub>2</sub>-C<sub>3</sub> NPs.

### 3.1.5. Fourier transform infrared spectroscopy

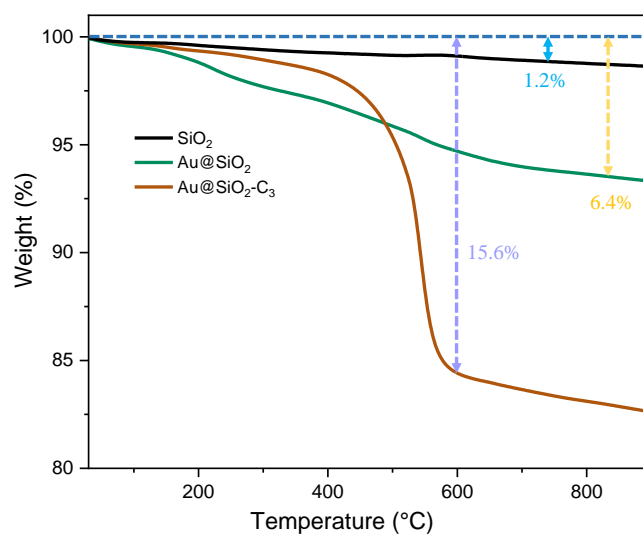
FT-IR spectroscopy was used to assess composition of the NPs (**Figure 5**). The Aerosil<sup>®</sup>200 silica NPs show a characteristic band at 1076 cm<sup>-1</sup> due to the Si-O vibration. For both Au@SiO<sub>2</sub> and Au@SiO<sub>2</sub>-C<sub>3</sub> NPs, a band appears around 1505 cm<sup>-1</sup> corresponding to the bending vibration of N-H groups. This observation indicates the successful grafting of amine groups on the silica surface. For Au@SiO<sub>2</sub>-C<sub>3</sub> NPs, two bands of 2993 and 2904 cm<sup>-1</sup> can be assigned to the stretching vibrations of -CH<sub>2</sub> groups. After Au NPs deposition, the spectra of Au@SiO<sub>2</sub>-C<sub>3</sub> and Au@SiO<sub>2</sub> NPs remain unchanged.



**Figure 5.** FT-IR spectra of Aerosil<sup>®</sup>200 silica, Au@SiO<sub>2</sub>, Au@SiO<sub>2</sub>-C<sub>3</sub> NPs. (a) The whole spectra. (b and c) The main transmittance peaks have been highlighted for more clarity.

### 3.1.6. Thermostability

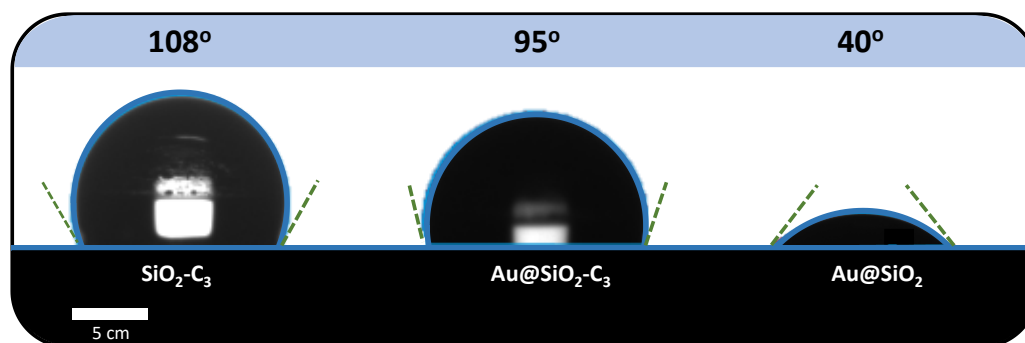
To confirm the thermal stability of the as-prepared NPs, thermogravimetric analysis was performed (**Figure 6**). SiO<sub>2</sub> NPs show high thermal stability with weight loss of only 0.4% from 30 to 200 °C, which can be attributed to the water desorption. From 200 to 900 °C, a slight weight loss is observed due to silica dehydroxylation [62]. The TGA curve of Au@SiO<sub>2</sub>-C<sub>3</sub> NPs presents two stages: i) a weight loss of 0.5% below 150 °C due to absorbed moisture, pointing out the hydrophobic properties of the NPs; ii) a weight loss of 13.8% between 400 to 600 °C that can be attributed to the decomposition of alkyl chains. Besides, the weight loss observed for Au@SiO<sub>2</sub> (1.2%) between 30-200 °C corresponds to the desorption of adsorbed water. The main weight loss (4.1%) corresponds to the decomposition of amine groups between 200-600 °C. These results demonstrate that the as-prepared particles have good thermal stability in the range of 30 to 400 °C, and that the functional groups are grafted on the surface of silica particles.



**Figure 6.** Thermogravimetric profiles of SiO<sub>2</sub>, Au@SiO<sub>2</sub> and Au@SiO<sub>2</sub>-C<sub>3</sub> NPs. Experimental conditions: 10-20 mg samples for each analysis, 10 °C /min from 30 to 900 °C and N<sub>2</sub> as atmosphere.

### 3.1.7. Water contact angle analysis

The surface wettability of particles plays an important role in the formation and stability of Pickering emulsion. The near-neutral wettability (contact angle around 90°) can promote efficient positioning of particles at the water-oil interface, providing a steric barrier against droplet coalescence. The surface wettability of silica particles can be adjusted *via* surface functionalization. The water contact angle of SiO<sub>2</sub>-C<sub>3</sub>, Au@SiO<sub>2</sub>-C<sub>3</sub> and Au@SiO<sub>2</sub> NPs was measured (**Figure 7**).



**Figure 7.** The water contact angle of SiO<sub>2</sub>-C<sub>3</sub>, Au@SiO<sub>2</sub>-C<sub>3</sub>, and Au@SiO<sub>2</sub>.

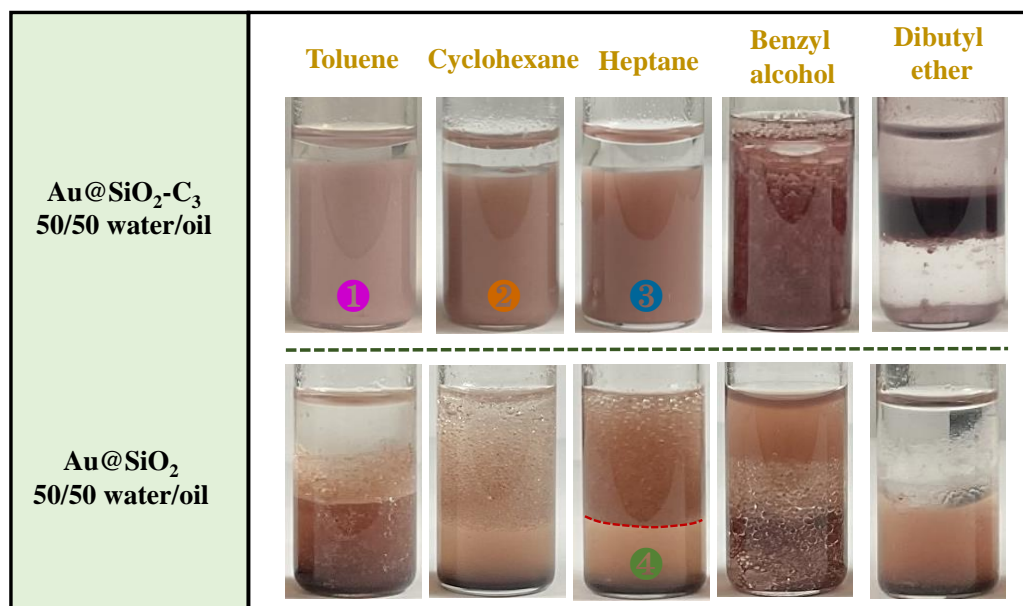


Bare silica is too hydrophilic to measure the water contact angle. The water contact angle of  $\text{SiO}_2\text{-C}_3$  NPs is around  $108^\circ$ , whereas  $\text{Au@SiO}_2\text{-C}_3$  NPs have near-neutral wettability ( $95^\circ$ ) and  $\text{Au@SiO}_2$  NPs has a contact angle around  $40^\circ$ .  $\text{Au@SiO}_2\text{-C}_3$  NPs are more hydrophobic because of the alkyl chains grafted on the silica surface.

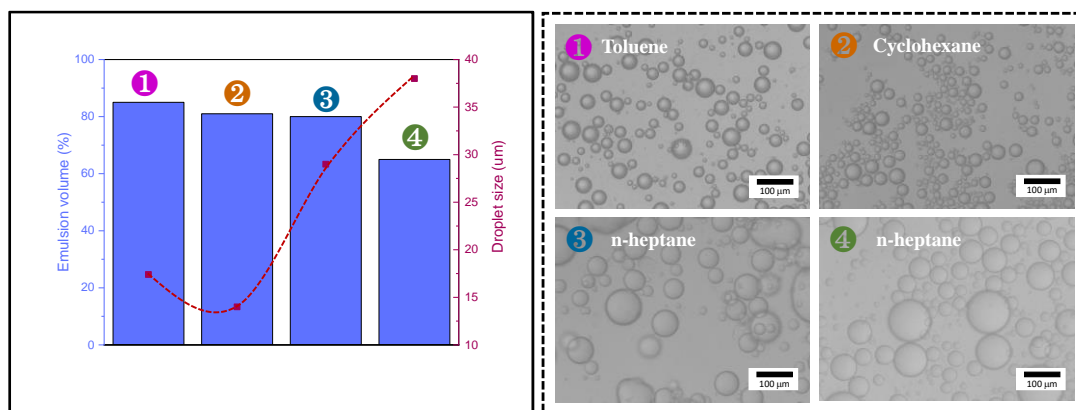
### 3.2. Physicochemical properties of the Pickering emulsions

#### 3.2.1. Influence of the organic solvents

The emulsifying properties of the NPs for water/oil biphasic systems was investigated. Since the nature of oil is of great importance for the NP wettability and emulsion stabilization, the influence of the different oils on the emulsion stability was studied (**Figure 8 and Table A-6**). Amphiphilic  $\text{Au@SiO}_2\text{-C}_3$  NPs can generate well-defined water-in-oil emulsion with toluene (emulsion volume up to 85%), n-heptane (81%) and cyclohexane (80%). However, no emulsion is obtained with benzyl alcohol and dibutyl ether. The optical microscopy images show that the as-prepared emulsions with three types of oils have uniform droplets (**Figure 9**), and an average size of  $17\ \mu\text{m}$  (toluene),  $14\ \mu\text{m}$  (cyclohexane) and  $29\ \mu\text{m}$  (n-heptane).



**Figure 8.** (a) Photographs of Pickering emulsion stabilized by  $\text{Au@SiO}_2\text{-C}_3$  and  $\text{Au@SiO}_2$  NPs. Conditions: 1.5 mL oil, 1.5 mL water, 75 mg NPs (2.7 wt.%), emulsified at 11,500 rpm for 2 min.



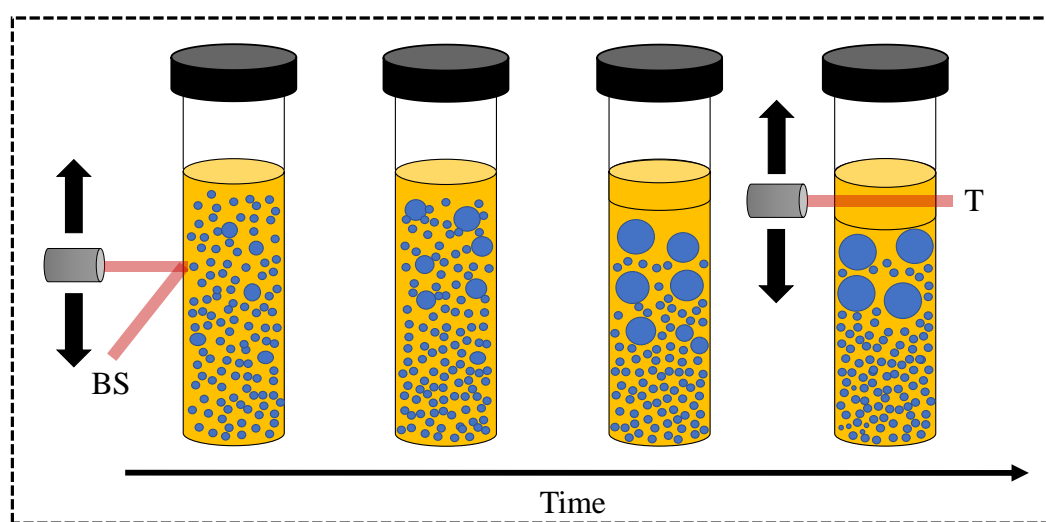
**Figure 9.** Emulsion volume fraction, mean droplet size and typical optical micrograph of a Pickering emulsion stabilized by Au@SiO<sub>2</sub>-C<sub>3</sub> and Au@SiO<sub>2</sub> NPs. Conditions: 1.5 mL toluene, 1.5 mL water, 75 mg NPs (2.7 wt.%), emulsified at 11,500 rpm for 2 min.

For comparison, the emulsification properties of Au@SiO<sub>2</sub> were also investigated. The photographs of the emulsion and the corresponding optical microscopy images are displayed in **Figure 8 and 9**. The droplet of n-heptane/H<sub>2</sub>O emulsions stabilized by Au@SiO<sub>2</sub> NPs have an average size of 38 μm with the emulsion volume fraction of 65%. No emulsion is observed with Au@SiO<sub>2</sub> for cyclohexane, toluene, benzyl alcohol and dibutyl ether. This significant difference between Au@SiO<sub>2</sub>-C<sub>3</sub> and Au@SiO<sub>2</sub> NPs can be attributed to their distinct surface wettability. Thus, Au@SiO<sub>2</sub>-C<sub>3</sub> NPs can be used as emulsifiers for preparing Pickering emulsions. Moreover, such small droplets can remarkably enhance the catalytic performance of the nanoreactors in biphasic reaction because of short diffusion distances [63].

### 3.2.2. Emulsion stability

To investigate the stability of the obtained emulsions, we performed light scattering experiments using Turbiscan Lab Expert. The backscattering and transmission profiles of laser irradiation (880 nm) were measured along the height of glass vial. It is worth noting that the delta backscattering ( $\Delta$ BS) profile represents the emulsion coalescence, creaming and sedimentation process over the time, while the delta transmission ( $\Delta$ T) profiles can be used to analyze the formation of a clarified serum layer (**Figure 10**). Considering that  $\Delta$ BS intensity is a function of the volume of the emulsion phase at a specific height and droplet size in the glass vial, the  $\Delta$ BS intensity decreases either with the droplet size or by decreasing the droplet

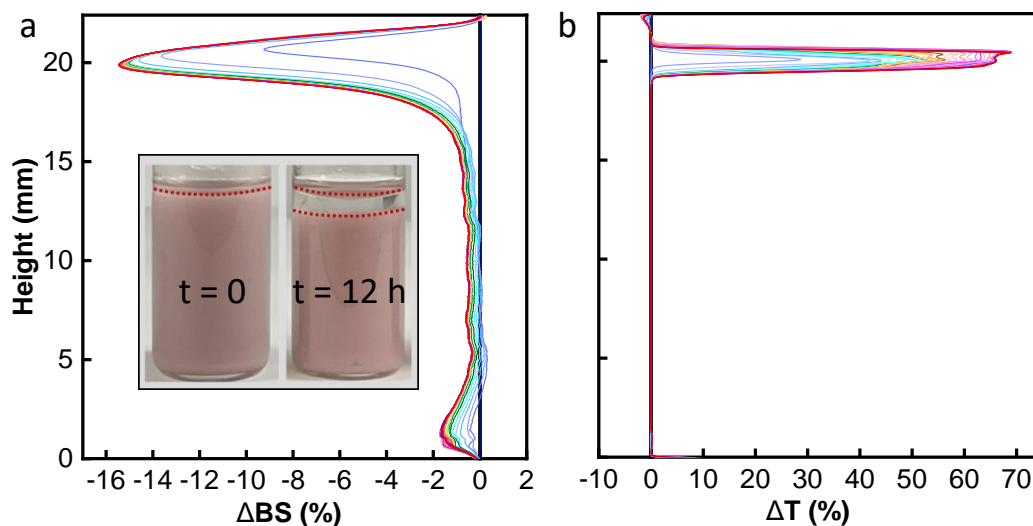
concentration, since the average emulsion droplet size is larger than the incident wavelength. The sharp decrease in  $\Delta BS$  at the top layer of the emulsion suggests a decrease in the top concentration and clarification of the layer. In such case,  $\Delta BS$  is more representative than  $\Delta T$  for characterizing emulsion destabilization because of the ability of emulsion droplets to scatter light beam [64, 65]. The variation of  $\Delta BS$  and  $\Delta T$  over the time as a function of the height of the vial reflects the moving trend of droplets and predicates the stability of Pickering emulsions.



**Figure 10.** Schematic representation of time-evolution of the clarification and sedimentation process (BS is backscattered light and T is transmitted light, while the blue dots represent the water droplets and yellow backgrounding indicates the continuous oil phase).

The evolution of  $\Delta BS$  and  $\Delta T$  intensities over time for the emulsion stabilized with Au@SiO<sub>2</sub>-C<sub>3</sub> NPs is shown in **Figure 11**.  $\Delta BS$  of the Au@SiO<sub>2</sub>-C<sub>3</sub> NPs emulsion is sharply reduced at the top layer of the sample over the time, but no obvious variation is observed in the sample height range of 0 to 18 mm (**Figure 11a**).  $\Delta T$  intensity at the top layer of the sample increases sharply during the first 2 h (**Figure 11b**) and keeps constant after 3 h. This indicates that the main instability at the top layer of the emulsion is a clarification phenomenon, and serious gravity migration may occur at the top layer. As mentioned previously, the droplet size is larger than the wavelength of light source, thus, the slight decrease of  $\Delta BS$  in the middle part of the sample is attributed to the variation of the droplet size. A growth of the droplet size (caused by flocculation and coalescence) can lead to global variations in the middle of the sample, while emulsion droplets migration (sedimentation processes) leads to local variations

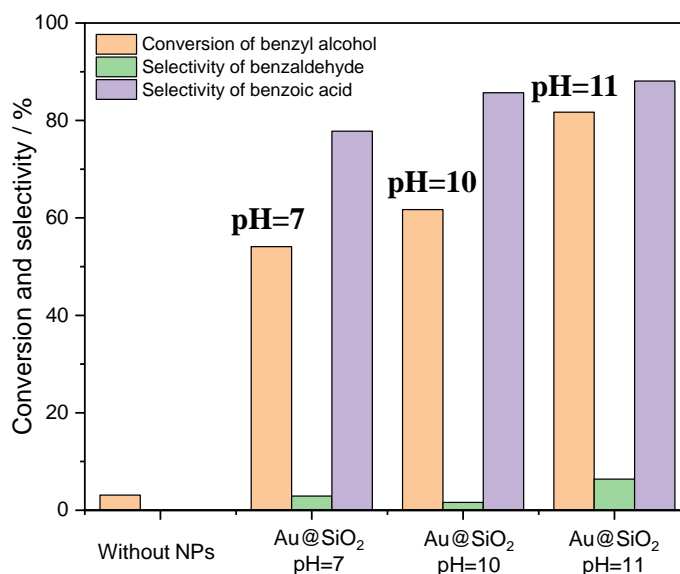
of the concentration at the top layer of the samples. Especially, the high temperature at 60 °C could also accelerate emulsion destabilization. Overall, these results clearly state that the as-prepared Au@SiO<sub>2</sub>-C<sub>3</sub> NPs can form stable emulsions at high temperature, and flocculation and coalescence are the main destabilization processes of emulsion.



**Figure 11.** (a) Delta backscattering ( $\Delta$ BS) and (b) delta transmission ( $\Delta$ T) signals vs. sample height and time at 60 °C for water/toluene (1/1 v/v) Pickering emulsions stabilized by Au@SiO<sub>2</sub>-C<sub>3</sub> from 0 h (blue curve) to 12 h (red curve). Reaction conditions: 75 mg NPs, 1.5 mL water, 1.5 mL toluene, emulsified at 11500 rpm for 2 min.

### 3.3. Catalytic performance

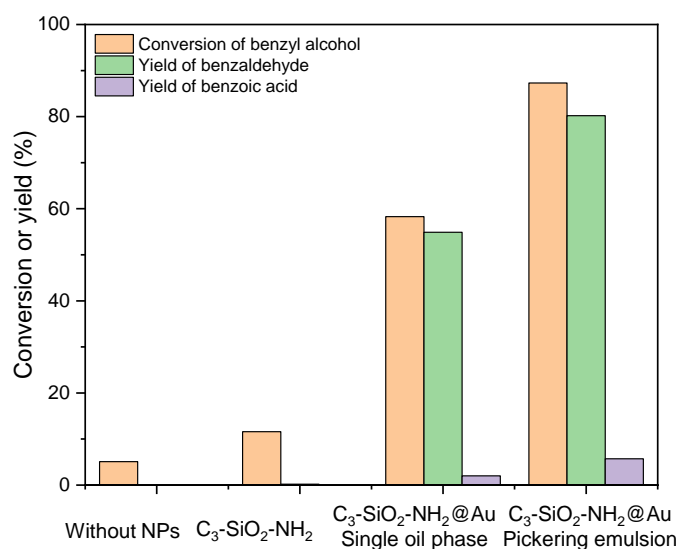
The oxidation of benzyl alcohol was first carried out in water over Au@SiO<sub>2</sub> NPs with/without base (NaOH) (**Figure 12**). As expected, a blank test shows negligible conversion. Au@SiO<sub>2</sub> NPs allow 54% conversion and 78% selectivity to benzoic acid without base and low selectivity (3%) toward benzaldehyde. The catalytic performance of Au@SiO<sub>2</sub> NPs depends on the pH of the reaction system. Increasing the pH from 7 to 11 substantially enhances the benzyl alcohol conversion from 54% to 82%, with concomitant increase of the selectivity to benzoic acid from 78% to 88%.



**Figure 12.** Effect of pH on benzyl alcohol conversion and selectivity catalyzed by Au@SiO<sub>2</sub> NPs in water. Reaction conditions: 2.7 wt.% Au@SiO<sub>2</sub> NPs, 3 mL water, 32  $\mu$ L benzyl alcohol, 2.0 equiv. TBHP, NaOH solution is used to adjust the pH, 11,500 rpm for 2 min, 80  $^{\circ}$ C, 3 h, 500 rpm.

To compare the catalytic activity of the conventional base-assisted system with that of base-free PIC system, Au@SiO<sub>2</sub>-C<sub>3</sub>-stabilized emulsions were employed as a platform to create an efficient and recyclable water/oil biphasic system. The catalytic results are provided in **Figure 13** together with results of blank tests over SiO<sub>2</sub>-C<sub>3</sub> NPs and with TBHP but without catalyst. As expected, benzyl alcohol can be hardly converted without catalyst with only 5% conversion. SiO<sub>2</sub>-C<sub>3</sub> NPs give low catalytic conversion (7%) with 2% selectivity to benzaldehyde although a stable emulsion can be formed. It indicates that SiO<sub>2</sub>-C<sub>3</sub> NPs are not catalytically active for the reaction. In contrast, Au@SiO<sub>2</sub>-C<sub>3</sub> NPs provide high conversion (87%) within 3 h in the presence of a Pickering emulsion with 92% and 6% selectivity to benzaldehyde and benzoic acid, respectively.

To assess the benefits of interfacial catalysis, we explored the catalytic performance of Au@SiO<sub>2</sub>-C<sub>3</sub> NPs in toluene. Au@SiO<sub>2</sub>-C<sub>3</sub> NPs show 58% conversion with 94% and 3% selectivity to benzaldehyde and benzoic acid, respectively.

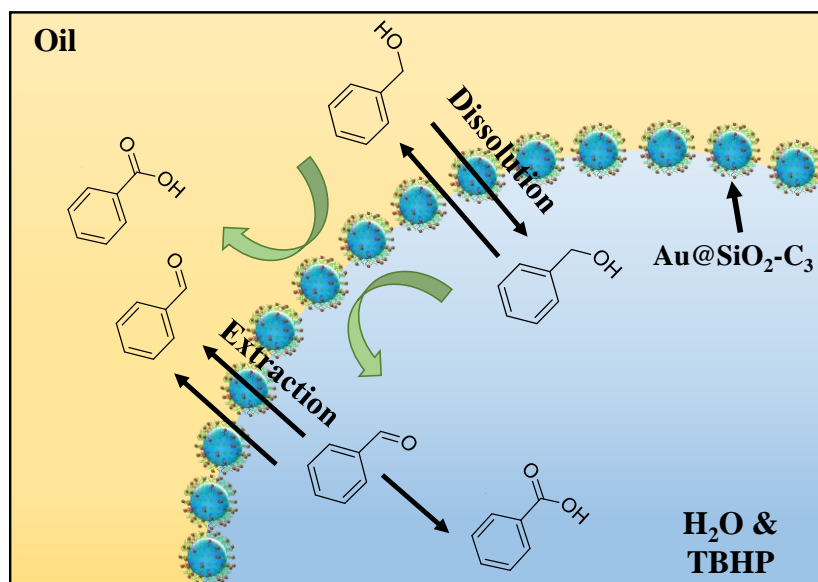


**Figure 13.** Comparison of benzyl alcohol conversion, benzaldehyde and benzoic acid selectivities under PIC system and in water and toluene single phases. Reaction conditions: 2.7 wt.% Au@SiO<sub>2</sub>-C<sub>3</sub> NPs, 1.5 mL benzyl alcohol in toluene (0.1 mol/L), 2.0 equiv. TBHP dissolved in 1.5 mL water, 11,500 rpm for 2 min, 80 °C, 3 h, 500 rpm. The test in toluene was conducted using 3 mL of toluene with benzyl alcohol (0.05 mol/L).

These results indicate that the catalytic activity of Au@SiO<sub>2</sub>-C<sub>3</sub> NPs is lower in toluene compared to the PIC system. At the same reaction volume and catalyst loading, the enhanced activity in PIC can be ascribed to the large interfacial contact area and the presence of catalyst at the water-oil interface (**Figure 14**). Moreover, benzaldehyde is more soluble in toluene than in benzyl alcohol, and its solubility is much lower in water than in benzyl alcohol [66, 67]. Benefiting from the solubility difference between benzyl alcohol and benzaldehyde in the biphasic system, benzaldehyde is promptly extracted by toluene avoiding further oxidation [68]. The combination of the large contact area, short diffusion distance and unique interfacial location of Au NPs provides high reaction efficiency of Au@SiO<sub>2</sub>-C<sub>3</sub> NPs in PIC system.

Overall, constructing a catalytic system with catalysts located at interface play an important role for developing base-free alcohol oxidation process. As a greener alternative, PIC system demonstrated: (1) improved catalytic activity; (2) ease of product and catalyst separation; (3) environmentally friendly. Since the grafting of such noble metallic particles on emulsifiers

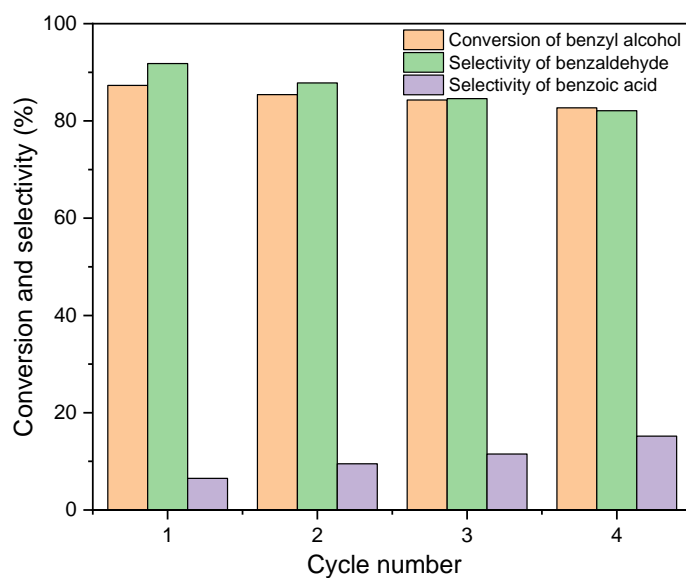
can be easily realized by diverse particles, we envisage this concept can be utilized as a versatile technique for the application in chemical engineering.



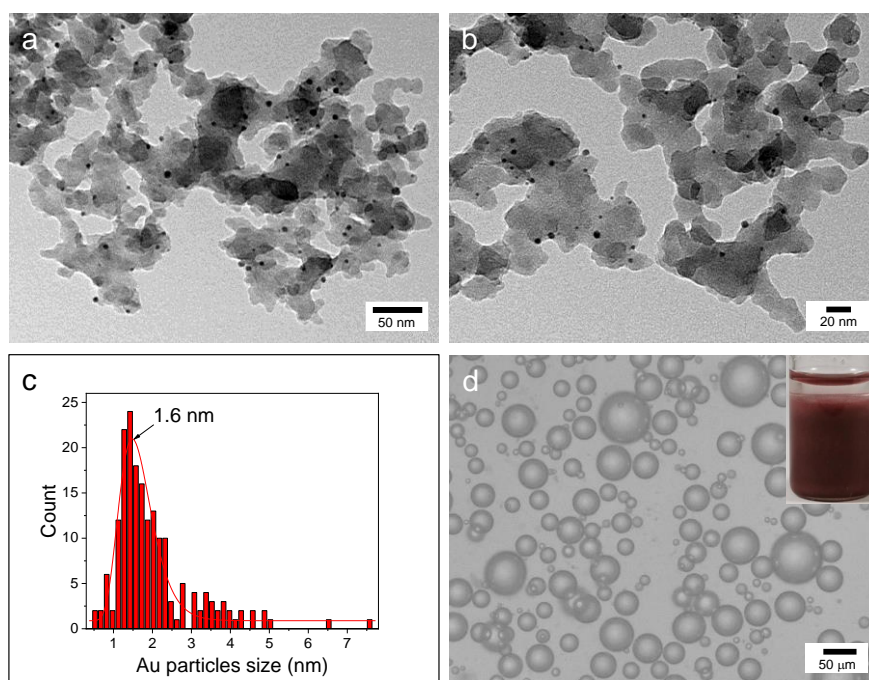
**Figure 14.** Schematic illustration of selective oxidation of benzyl alcohol to benzaldehyde and benzoic acid over  $\text{Au@SiO}_2\text{-C}_3$  catalytic NPs.  $\text{Au@SiO}_2\text{-C}_3$  NPs can catalyze the reaction at the water-oil interface and the substrate and product migrate to both the oil and water phases as the reaction proceeds.

### 3.4. Reusability

To assess the catalyst stability, we investigated the recyclability of  $\text{Au@SiO}_2\text{-C}_3$  NPs. After the reaction, centrifugation was carried out to achieve demulsification. The NPs were separated from the reaction mixture by washing with ethanol and drying in air before the subsequent run. As shown in **Figure 15**,  $\text{Au@SiO}_2\text{-C}_3$  NPs shows 83% conversion with 82% selectivity to benzaldehyde after the fourth run. The TEM image of recovered  $\text{Au@SiO}_2\text{-C}_3$  NPs shows that the Au NPs are well dispersed on the silica surface with an average size around 1.6 nm (**Figure 16a-c**), which is similar to that of freshly prepared  $\text{Au@SiO}_2\text{-C}_3$  NPs (1.1 nm). The optical micrograph image of well-defined Pickering emulsion after the fourth run confirms that the interfacial activity keeps unchanged (**Figure 16d and Table A-7**). Moreover, the average size of the emulsion droplets stabilized by the recovered  $\text{Au@SiO}_2\text{-C}_3$  is around 30  $\mu\text{m}$ , which is larger than that of the fresh emulsion (17  $\mu\text{m}$ ).



**Figure 15.** Catalytic performance of Au@SiO<sub>2</sub>-C<sub>3</sub> NPs in the oxidation of benzyl alcohol in four consecutive runs.



**Figure 16.** (a and b) TEM images of recovered Au@SiO<sub>2</sub>-C<sub>3</sub> NPs after the fourth run. (c) Particle size distribution of Au NPs in Au/SiO<sub>2</sub>-C<sub>3</sub> NPs after the fourth run. (d) Optical microscopy of Pickering emulsion droplets after the fourth run (the inset shows a photograph of the emulsion).



## 4. Conclusions

In conclusion, we designed and fabricated surface-active catalysts composed of modified silica NPs and ultra-small Au NPs for the oxidation of benzyl alcohol in a PIC system. To obtain surface-active properties with catalytic centers, C<sub>3</sub> chains and amine groups were introduced on the silica surface by silanization. The incorporation of amine groups allowed immobilization of Au NPs. Stable Pickering emulsion with large oil-water interface areas were generated using amphiphic Au@SiO<sub>2</sub>-C<sub>3</sub> NPs, these NPs outperformed hydrophilic Au@SiO<sub>2</sub> NPs in terms of emulsion volume and droplet size. Taking advantage of the emulsion properties and precise positioning of ultra-small Au NPs at the oil-water interface, Au@SiO<sub>2</sub>-C<sub>3</sub> NPs exhibited a remarkable catalytic performance in PIC system under base-free conditions, and the yield of benzaldehyde was 1.5 times higher than that obtained in toluene. Such a significant improvement is attributed to the pronounced increase of reaction interface to alleviate the diffusion barrier between oil-soluble and water-soluble reactants. This work broadens the scope of noble metal NPs loaded material as emulsifiers and provides new insights for constructing novel and efficient reaction system.

## 5. References

- [1] Z. Guo, B. Liu, Q. Zhang, W. Deng, Y. Wang, Y. Yang, Recent advances in heterogeneous selective oxidation catalysis for sustainable chemistry, *Chemical Society Reviews*, 43 (2014) 3480-3524.
- [2] R.A. Sheldon, I.W. Arends, A. Dijkman, New developments in catalytic alcohol oxidations for fine chemicals synthesis, *Catalysis Today*, 57 (2000) 157-166.
- [3] R.M. Williams, J.W. Medlin, Benzyl alcohol oxidation on Pd (111): aromatic binding effects on alcohol reactivity, *Langmuir*, 30 (2014) 4642-4653.
- [4] D. Ribeaucourt, B. Bissaro, F. Lambert, M. Lafond, J.-G. Berrin, Biocatalytic oxidation of fatty alcohols into aldehydes for the flavors and fragrances industry, *Biotechnology Advances*, (2021) 107787.
- [5] F. Menger, C. Lee, Oxidations with solid potassium permanganate, *The Journal of Organic Chemistry*, 44 (1979) 3446-3448.
- [6] D.G. Lee, U.A. Spitzer, Aqueous dichromate oxidation of primary alcohols, *The Journal of Organic Chemistry*, 35 (1970) 3589-3590.
- [7] A. De Mico, R. Margarita, L. Parlanti, A. Vescovi, G. Piancatelli, A versatile and highly selective hypervalent iodine (III)/2,2,6,6-tetramethyl-1-piperidinyloxy-mediated oxidation of alcohols to carbonyl compounds, *The Journal of Organic Chemistry*, 62 (1997) 6974-6977.
- [8] L. De Luca, G. Giacomelli, A. Porcheddu, A very mild and chemoselective oxidation of alcohols to carbonyl compounds, *Organic letters*, 3 (2001) 3041-3043.
- [9] C. Bolm, A.S. Magnus, J.P. Hildebrand, Catalytic synthesis of aldehydes and ketones under mild conditions using TEMPO/Oxone, *Organic Letters*, 2 (2000) 1173-1175.
- [10] S. Campisi, D. Ferri, A. Villa, W. Wang, D. Wang, O. Krocher, L. Prati, Selectivity control in palladium-catalyzed alcohol oxidation through selective blocking of active sites, *The Journal of Physical Chemistry C*, 120 (2016) 14027-14033.
- [11] J.M. Hoover, B.L. Ryland, S.S. Stahl, Copper/TEMPO-catalyzed aerobic alcohol oxidation: mechanistic assessment of different catalyst systems, *ACS catalysis*, 3 (2013) 2599-2605.
- [12] M. Li, S. Wu, X. Yang, J. Hu, L. Peng, L. Bai, Q. Huo, J. Guan, Highly efficient single atom cobalt catalyst for selective oxidation of alcohols, *Applied Catalysis A: General*, 543 (2017) 61-66.
- [13] G. Wu, E. Cao, P. Ellis, A. Constantinou, S. Kuhn, A. Gavriilidis, Continuous flow aerobic oxidation of benzyl alcohol on Ru/Al<sub>2</sub>O<sub>3</sub> catalyst in a flat membrane microchannel reactor: An experimental and modelling study, *Chemical Engineering Science*, 201 (2019) 386-396.
- [14] J.M. Campelo, T.D. Conesa, M.J. Gracia, M.J. Jurado, R. Luque, J.M. Marinas, A.A. Romero, Microwave facile preparation of highly active and dispersed SBA-12 supported metal nanoparticles, *Green Chemistry*, 10 (2008) 853-858.
- [15] Y. Pérez, R. Ballesteros, M. Fajardo, I. Sierra, I. del Hierro, Copper-containing catalysts for solvent-free selective oxidation of benzyl alcohol, *Journal of Molecular Catalysis A: Chemical*, 352 (2012) 45-56.
- [16] T. Mallat, A. Baiker, Oxidation of alcohols with molecular oxygen on solid catalysts, *Chemical reviews*, 104 (2004) 3037-3058.
- [17] C. Della Pina, E. Falletta, M. Rossi, Update on selective oxidation using gold, *Chemical Society Reviews*, 41 (2012) 350-369.

- [18] A.S.K. Hashmi, G.J. Hutchings, *Gold catalysis*, *Angewandte Chemie International Edition*, 45 (2006) 7896-7936.
- [19] L. Prati, M. Rossi, Gold on carbon as a new catalyst for selective liquid phase oxidation of diols, *Journal of Catalysis*, 176 (1998) 552-560.
- [20] F. Boccuzzi, A. Chiorino, M. Manzoli, D. Andreeva, T. Tabakova, FTIR study of the low-temperature water-gas shift reaction on Au/Fe<sub>2</sub>O<sub>3</sub> and Au/TiO<sub>2</sub> catalysts, *Journal of Catalysis*, 188 (1999) 176-185.
- [21] F. Zane, V. Trevisan, F. Pinna, M. Signoretto, F. Menegazzo, Investigation on gold dispersion of Au/ZrO<sub>2</sub> catalysts and activity in the low-temperature WGS reaction, *Applied Catalysis B: Environmental*, 89 (2009) 303-308.
- [22] M. Haruta, M. Dat é Advances in the catalysis of Au nanoparticles, *Applied Catalysis A: General*, 222 (2001) 427-437.
- [23] L.-X. Zheng, B. Peng, J.-F. Zhou, B.-Q. Shan, Q.-S. Xue, K. Zhang, High efficient and stable thiol-modified dendritic mesoporous silica nanospheres supported gold catalysts for gas-phase selective oxidation of benzyl alcohol with ultra-long lifetime, *Microporous and Mesoporous Materials*, (2022) 112140.
- [24] M.D. Hughes, Y.-J. Xu, P. Jenkins, P. McMorn, P. Landon, D.I. Enache, A.F. Carley, G.A. Attard, G.J. Hutchings, F. King, Tunable gold catalysts for selective hydrocarbon oxidation under mild conditions, *Nature*, 437 (2005) 1132-1135.
- [25] J. Ni, W.-J. Yu, L. He, H. Sun, Y. Cao, H.-Y. He, K.-N. Fan, A green and efficient oxidation of alcohols by supported gold catalysts using aqueous H<sub>2</sub>O<sub>2</sub> under organic solvent-free conditions, *Green Chemistry*, 11 (2009) 756-759.
- [26] Q. Gu, W.-H. Fang, R. Wischert, W. Zhou, C. Michel, M. Pera-Titus, AuCu/CeO<sub>2</sub> bimetallic catalysts for the selective oxidation of fatty alcohol ethoxylates to alkyl ether carboxylic acids, *Journal of Catalysis*, 380 (2019) 132-144.
- [27] G. Zhao, M. Ling, H. Hu, M. Deng, Q. Xue, Y. Lu, An excellent Au/meso- $\gamma$ -Al<sub>2</sub>O<sub>3</sub> catalyst for the aerobic selective oxidation of alcohols, *Green Chemistry*, 13 (2011) 3088-3092.
- [28] A. Abad, P. Concepci ón, A. Corma, H. Garc ía, A collaborative effect between gold and a support induces the selective oxidation of alcohols, *Angewandte Chemie International Edition*, 44 (2005) 4066-4069.
- [29] P. Wu, Y. Cao, L. Zhao, Y. Wang, Z. He, W. Xing, P. Bai, S. Mintova, Z. Yan, Formation of PdO on Au-Pd bimetallic catalysts and the effect on benzyl alcohol oxidation, *Journal of Catalysis*, 375 (2019) 32-43.
- [30] C.P. Ferraz, M.A.S. Garcia, É. Teixeira-Neto, L.M. Rossi, Oxidation of benzyl alcohol catalyzed by gold nanoparticles under alkaline conditions: weak vs. strong bases, *RSC advances*, 6 (2016) 25279-25285.
- [31] E.M. de Moura, M.A. Garcia, R.V. Gon çalves, P.K. Kiyohara, R.F. Jardim, L.M. Rossi, Gold nanoparticles supported on magnesium ferrite and magnesium oxide for the selective oxidation of benzyl alcohol, *RSC Advances*, 5 (2015) 15035-15041.
- [32] B. Das, M. Sharma, M.J. Baruah, B.P. Mounash, G.V. Karunakar, K.K. Bania, Gold nanoparticle supported on mesoporous vanadium oxide for photo-oxidation of 2-naphthol with hydrogen peroxide and aerobic oxidation of benzyl alcohols, *Journal of Environmental Chemical Engineering*, 8 (2020) 104268.

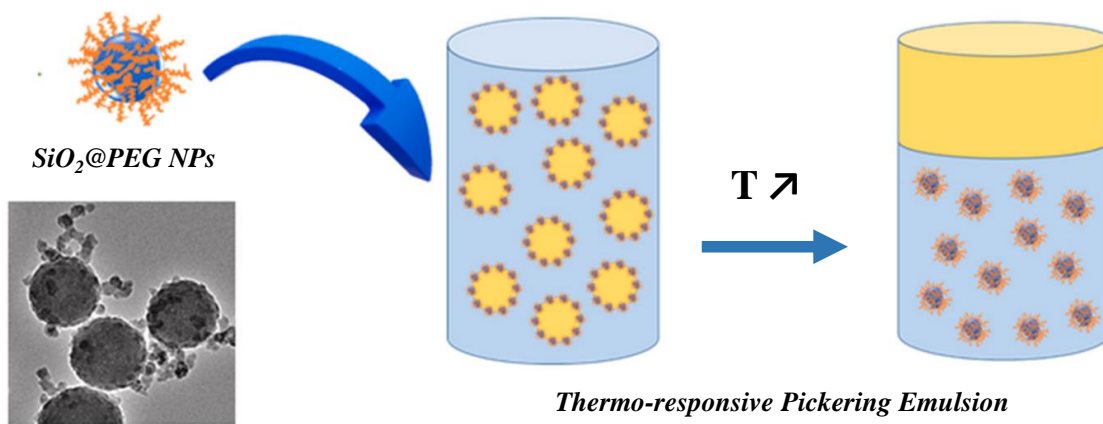
- [33] G.A. Ferreira, W. Loh, Planet–Satellite Nanostructures Based on Block Copolymer–Surfactant Nanoparticles Surface-Decorated with Gold and Silver: A New Strategy for Interfacial Catalysis, *Advanced Materials Interfaces*, 6 (2019) 1900348.
- [34] B. Ballarin, D. Barreca, E. Boanini, M.C. Cassani, P. Dambruoso, A. Massi, A. Mignani, D. Nanni, C. Parise, A. Zaghi, Supported gold nanoparticles for alcohols oxidation in continuous-flow heterogeneous systems, *ACS Sustainable Chemistry & Engineering*, 5 (2017) 4746-4756.
- [35] N. Al-Rifai, F. Galvanin, M. Morad, E. Cao, S. Cattaneo, M. Sankar, V. Dua, G. Hutchings, A. Gavriilidis, Hydrodynamic effects on three phase micro-packed bed reactor performance–Gold–palladium catalysed benzyl alcohol oxidation, *Chemical Engineering Science*, 149 (2016) 129-142.
- [36] P. Bujak, P. Bartczak, J. Polanski, Highly efficient room-temperature oxidation of cyclohexene and D-glucose over nanogold Au/SiO<sub>2</sub> in water, *Journal of Catalysis*, 295 (2012) 15-21.
- [37] D. Obermayer, A.M. Balu, A.A. Romero, W. Goessler, R. Luque, C.O. Kappe, Nanocatalysis in continuous flow: supported iron oxide nanoparticles for the heterogeneous aerobic oxidation of benzyl alcohol, *Green chemistry*, 15 (2013) 1530-1537.
- [38] B. Feng, Z. Hou, H. Yang, X. Wang, Y. Hu, H. Li, Y. Qiao, X. Zhao, Q. Huang, Functionalized poly (ethylene glycol)-stabilized water-soluble palladium nanoparticles: property/activity relationship for the aerobic alcohol oxidation in water, *Langmuir*, 26 (2010) 2505-2513.
- [39] M. Pera-Titus, L. Leclercq, J.M. Clacens, F. De Campo, V. Nardello-Rataj, Pickering interfacial catalysis for biphasic systems: from emulsion design to green reactions, *Angewandte Chemie International Edition*, 54 (2015) 2006-2021.
- [40] F. Chang, C.M. Vis, W. Ciptonugroho, P.C. Bruijninx, Recent developments in catalysis with Pickering Emulsions, *Green Chemistry*, 23 (2021) 2575-2594.
- [41] A.M.B. Rodriguez, B.P. Binks, Catalysis in Pickering emulsions, *Soft Matter*, 16 (2020) 10221-10243.
- [42] D.G. Ortiz, C. Pochat-Bohatier, J. Cambedouzou, M. Bechelany, P. Miele, Current trends in Pickering emulsions: Particle morphology and applications, *Engineering*, 6 (2020) 468-482.
- [43] J. Wu, G.H. Ma, Recent studies of Pickering emulsions: particles make the difference, *Small*, 12 (2016) 4633-4648.
- [44] H. Zhao, Y. Yang, Y. Chen, J. Li, L. Wang, C. Li, A review of multiple Pickering emulsions: Solid stabilization, preparation, particle effect, and application, *Chemical Engineering Science*, 248 (2022) 117085.
- [45] C. Li, Y. Pi, S. Liu, J. Feng, X. Zhang, S. Li, R. Tan, Phosphotungstate-Functionalized Mesoporous Janus Silica Nanosheets for Reaction-Controlled Pickering Interfacial Catalysis, *ACS Sustainable Chemistry & Engineering*, 9 (2021) 13501-13513.
- [46] W. Jing, H. Li, P. Xiao, B. Liu, J. Luo, R. Wang, S. Qiu, Z. Zhang, Ultrasmall amphiphilic zeolitic nanoreactors for the aerobic oxidation of alcohols in water, *Nanoscale*, 13 (2021) 9229-9235.
- [47] A. Corma, H. Garcia, Supported gold nanoparticles as catalysts for organic reactions, *Chemical Society Reviews*, 37 (2008) 2096-2126.
- [48] M. Stratakis, H. Garcia, Catalysis by supported gold nanoparticles: beyond aerobic oxidative processes, *Chemical Reviews*, 112 (2012) 4469-4506.
- [49] J. Ftouni, M. Penhoat, J.-S. Girardon, A. Addad, E. Payen, C. Rolando, Immobilization of gold nanoparticles on fused silica capillary surface for the development of catalytic microreactors, *Chemical Engineering Journal*, 227 (2013) 103-110.

- [50] A. Nozaki, T. Yasuoka, Y. Kuwahara, T. Ohmichi, K. Mori, T. Nagase, H.Y. Yasuda, H. Yamashita, Oxidation of Benzyl Alcohol over Nanoporous Au–CeO<sub>2</sub> Catalysts Prepared from Amorphous Alloys and Effect of Alloying Au with Amorphous Alloys, *Industrial & Engineering Chemistry Research*, 57 (2018) 5599-5605.
- [51] D.G. Duff, A. Baiker, P.P. Edwards, A new hydrosol of gold clusters. 1. Formation and particle size variation, *Langmuir*, 9 (1993) 2301-2309.
- [52] B. Yang, Pickering interfacial catalysis for oxidative cleavage by H<sub>2</sub>O<sub>2</sub> in biphasic systems, in, *Lille 1*, 2017.
- [53] S.L. Westcott, S.J. Oldenburg, T.R. Lee, N.J. Halas, Formation and adsorption of clusters of gold nanoparticles onto functionalized silica nanoparticle surfaces, *Langmuir*, 14 (1998) 5396-5401.
- [54] Y. Xi, B. Liu, S. Wang, X. Huang, H. Jiang, S. Yin, T. Ngai, X. Yang, Growth of Au nanoparticles on phosphorylated zein protein particles for use as biomimetic catalysts for cascade reactions at the oil–water interface, *Chemical Science*, 12 (2021) 3885-3889.
- [55] M.J. Garc á-Soto, O. González-Ortega, Synthesis of silica-core gold nanoshells and some modifications/variations, *Gold Bulletin*, 49 (2016) 111-131.
- [56] E. Skrzyńska, J. Ftouni, A.-S. Mamede, A. Addad, M. Trentesaux, J.-S. Girardon, M. Capron, F. Dumeignil, Glycerol oxidation over gold supported catalysts—“Two faces” of sulphur based anchoring agent, *Journal of Molecular Catalysis A: Chemical*, 382 (2014) 71-78.
- [57] R.G. Digigow, J.-F. Dechézelles, H. Dietsch, I. Geissbühler, D. Vanhecke, C. Geers, A.M. Hirt, B. Rothen-Rutishauser, A. Petri-Fink, Preparation and characterization of functional silica hybrid magnetic nanoparticles, *Journal of Magnetism and Magnetic Materials*, 362 (2014) 72-79.
- [58] E. Asenath Smith, W. Chen, How to prevent the loss of surface functionality derived from aminosilanes, *Langmuir*, 24 (2008) 12405-12409.
- [59] A. Zwijnenburg, A. Goossens, W.G. Sloof, M.W. Craje, A.M. van der Kraan, L. Jos de Jongh, M. Makkee, J.A. Moulijn, XPS and Mössbauer characterization of Au/TiO<sub>2</sub> propene epoxidation catalysts, *The Journal of Physical Chemistry B*, 106 (2002) 9853-9862.
- [60] M. Khawaji, D. Chadwick, Au–Pd NPs immobilised on nanostructured ceria and titania: impact of support morphology on the catalytic activity for selective oxidation, *Catalysis Science & Technology*, 8 (2018) 2529-2539.
- [61] P. Kumar, M.C. Mathpal, S. Ghosh, G.K. Inwati, J.R. Maze, M.-M. Duvenhage, W. Roos, H. Swart, Plasmonic Au nanoparticles embedded in glass: Study of TOF-SIMS, XPS and its enhanced antimicrobial activities, *Journal of Alloys and Compounds*, 909 (2022) 164789.
- [62] J.M. Kim, S.M. Chang, S.M. Kong, K.-S. Kim, J. Kim, W.-S. Kim, Control of hydroxyl group content in silica particle synthesized by the sol-precipitation process, *Ceramics International*, 35 (2009) 1015-1019.
- [63] M. Weng, C. Xia, S. Xu, Q. Liu, Y. Liu, H. Liu, C. Huo, R. Zhang, C. Zhang, Z. Miao, Lipase/chitosan nanoparticle-stabilized pickering emulsion for enzyme catalysis, *Colloid and Polymer Science*, 300 (2022) 41-50.
- [64] J. Su, Q. Guo, Y. Chen, W. Dong, L. Mao, Y. Gao, F. Yuan, Characterization and formation mechanism of lutein pickering emulsion gels stabilized by β-lactoglobulin-gum arabic composite colloidal nanoparticles, *Food Hydrocolloids*, 98 (2020) 105276.

- [65] L. Zheng, X. Cheng, L. Cao, Z. Chen, Q. Huang, B. Song, Enhancing pesticide droplet deposition through O/W Pickering Emulsion: Synergistic stabilization by Flower-like ZnO particles and polymer emulsifier, *Chemical Engineering Journal*, 434 (2022) 134761.
- [66] C. Yu, L. Fan, J. Yang, Y. Shan, J. Qiu, Phase-Reversal Emulsion Catalysis with CNT–TiO<sub>2</sub> Nanohybrids for the Selective Oxidation of Benzyl Alcohol, *Chemistry–A European Journal*, 19 (2013) 16192-16195.
- [67] L. Ni, C. Yu, Q. Wei, J. Chang, J. Qiu, Decoupling the role of carbon counterparts in Pickering emulsifier for an enhanced selective oxidation of benzyl alcohol, *Green Chemistry*, 22 (2020) 5711-5721.
- [68] S. Rautiainen, O. Simakova, H. Guo, A.-R. Leino, K. Kordás, D. Murzin, M. Leskelä, T. Repo, Solvent controlled catalysis: synthesis of aldehyde, acid or ester by selective oxidation of benzyl alcohol with gold nanoparticles on alumina, *Applied Catalysis A: General*, 485 (2014) 202-206.



# Chapter IV. Temperature-responsive Pickering emulsion stabilized by poly(ethylene glycol)-functionalized silica particles







## 1. Introduction

Emulsions are metastable mixtures of two immiscible liquid phases - a dispersed phase and a continuous phase, *e.g.* oil and water - that is stabilized either by surfactant or by solid particles [1,2]. Particle-stabilized emulsions, also called Pickering emulsions, are more stable than conventional emulsions. Pickering emulsions may be useful for reducing the surfactants amount and so, the risk for health and environment [3]. Although a long-term stability is generally the final aim of a formulation process for food, cosmetics, paints, *etc.*, a transitory stability (*i.e.* on demand destabilization) might be wanted for other applications such as emulsions polymerization [4], oil recovery [5] or catalyst recovery [6] in order to collect the product of interest. In these cases, additional disruption mechanisms need to be introduced to achieve the destabilization of the system, which may increase the costs and the energy consumption.

Bare hydrophilic silica nanoparticles (NPs) can stabilize water/polar oil emulsions without any surface functionalization even if they are partially wet by these oils [7,8]. Although the use of bare silica NPs is costless and timeless compared to surface functionalized NP, it may be appropriate to functionalize the silica NPs surface for preparing emulsions with other types of oils and giving them additional functionalities. The grafting of silanes with specific functional groups is well known and controlled [9,10] and permits to enhance the wetting properties. The grafting of other types of materials is also possible, *e.g.* inorganic species (alumina, metals...) [11,12] or polymers [13–15] which allows the preparation of different types of emulsions.

The surface functionalization can limit the desorption of particles from interface, for instance, but also allows to add stimuli-responsive properties to the emulsions. Developing amphiphilic particles and changing their surface properties, in other words their wettability, in response to a stimulus is very promising. As a result, stimuli-responsive Pickering emulsions have gained increased amounts of attention in recent years. Thus, various trigger-responsive materials have been prepared leading to Pickering emulsions being responsive itself to the trigger such as temperature, pH, light, magnetic field [2,16–18]. Using temperature change for

emulsion destabilization is one of the less invasive method to set up, compared to the addition of chemicals or change of the pH of the system. In addition, it can be reversible.

Polyethylene glycol (PEG), also called polyethylene oxide (PEO), and PEG methyl ether (mPEG) are water-soluble and temperature-responsive polymers [19]. The temperature increase induces a modification of the conformation of the polyoxoethylene chains (from polar to nonpolar due to dehydration of the ethylene oxide units) and emulsions stabilized with PEG-based surfactants can undergo a phase separation or a phase inversion (from oil-in-water to water-in-oil) [14,20–22]. Surface active particles are more attractive than surfactants since they form much more stable emulsions [23]. One approach to obtain a synergetic effect of a PEG-based surfactant and the highest stability provided by silica NPs has been studied by Yue Zhu *et al.* [24]. By combining silica NPs and polyoxyethylene monodecyl ethers ( $C_{10}E_n$ ), which adsorbs on the silica surface, they could obtain the formation of stable emulsions which are destabilized with temperature. However, the use of PEG adsorbed onto the silica surface may induce the release of some PEG molecules in one of the two phases when the emulsion is destabilized.

One way to overcome this issue is to covalently bind the PEG onto the silica NPs [21,25,26]. Although temperature-responsive Pickering emulsions prepared with PEG-functionalized silica particles has been reported in the literature [14], the preparation of the particles is a multi-step and time-consuming process - synthesis of NPs followed by the grafting of the different functional silanes.

Herein, we report on the elaboration and characterization of temperature-responsive Pickering emulsions stabilized with PEG-functionalized silica particles ( $SiO_2@PEG$ ). The particles were prepared through a one-step synthesis based on the hydrolysis and condensation of the silica precursor in the presence of PEG with various molecular weight (MW 200, 400, 550, 2000, 5000  $g.mol^{-1}$ ). The physicochemical properties of the NPs have been thoroughly characterized before the preparation of emulsions. We find that  $SiO_2@mPEG$  550 NPs form temperature-responsive Pickering emulsions with oils of different nature. These emulsions

undergo a clear temperature-triggered destabilization when heated from room temperature to 80 °C while no destabilization has been observed for emulsions stabilized with longer PEG chains (MW 2000 and 5000 g.mol<sup>-1</sup>). Polyoxometalates (POMs), which are used as catalysts, tend to spontaneously adsorb onto hydrophilic surface (such as PEG or polyethoxylated surfactant) through a self-assembly [27]. The use of SiO<sub>2</sub>@PEG NPs as support for POMs fulfill the concept of Pickering interfacial catalysis (PIC). Further investigations were conducted, including the grafting of POMs onto the SiO<sub>2</sub>@mPEG NPs and their use for the oxidative cleavage of cyclooctene.

## 2. Experimental section

### 2.1. Chemicals

All chemicals were used as purchased. Tetraethyl orthosilicate (TEOS) (98 wt.%, Sigma-Aldrich), ammonia (25 wt.%, Chem Lab), absolute ethanol (VWR), poly(ethylene glycol) 200 (Sigma-Aldrich), poly(ethylene glycol) 400 (Sigma-Aldrich), poly(ethylene glycol) 1500 (Acros organics), poly(ethylene glycol)mono methyl ether 550 (Sigma-Aldrich), poly(ethylene glycol)mono methyl ether 2000 (Sigma-Aldrich), poly(ethylene glycol)mono methyl ether 5000 (Sigma-Aldrich), cyclopentyl methyl ether (≥ 99.9 %, Sigma Aldrich), toluene (99.85 %, Acros Organics), heptane (Analytical reagent grade, Fischer Scientific), isopropyl myristate (Sigma Aldrich), paraffin oil (Cooper), squalane (99 %, Acros Organics). H<sub>3</sub>[P(W<sub>3</sub>O<sub>10</sub>)<sub>4</sub>] · xH<sub>2</sub>O (reagent grade, Sigma-Aldrich). Cyclooctene (98 %, TCI). D<sub>2</sub>O (99.9 %) was purchased from Euriso-top (France). All aqueous solutions were prepared with ultrapure water obtained from a Thermo Scientific system (12.2 MΩ.cm, Millipore AG).

### 2.2. Synthesis of bare silica nanoparticles

The silica particles were synthesized following procedure reported in the literature [28]. 13.5 mL of ultrapure water, 184 mL of absolute ethanol, and 41 mL of NH<sub>4</sub>OH were mixed in a 500 mL round-bottom flask and stirred at 300 rpm at 40 °C. 11 mL of TEOS was added at once to the mixture. It was left stirring for 1 hour with a reflux cooling. The particles suspension

was purified by several cycles of centrifugation and redispersion.

### 2.3. One-pot synthesis of polyethylene glycol silica nanoparticles (SiO<sub>2</sub>@PEG)

The SiO<sub>2</sub>@PEG NPs were synthesized according to a protocol adapted from [29]. 6 mL of TEOS and 72 mL of ethanol were mixed under vigorous stirring for 5 min at 65 °C. 17.1 mL of water and 3.8 mL of ammonia were added. 3 g of PEG (or mPEG) dissolved in ethanol are added dropwise within 5 min. The mixture was stirred for one hour with reflux cooling. The particles were washed by centrifugation and transferred into ultrapure water.

## 2.4. Physicochemical characterization of NPs

### 2.4.1. Dynamic Light Scattering (DLS)

Dynamic light scattering (DLS) experiments were carried out using a light scattering goniometer instrument from LS Instruments (3D LS Spectrometer, Switzerland) equipped with a 25 mW He-Ne laser light source (JDS Uniphase) operating at  $\lambda = 632.8$  nm. The scattering spectrum was measured using two single-mode fiber detections and two high-sensitivity APD detectors (SPCM-AQR-13-FC, PerkinElmer). The samples were filled into cylindrical tubes with a diameter of 7.5 mm and placed in the temperature-controlled index matching bath, where the temperature was fixed at 25 °C. Measurements were performed at scattering angles of 90°. The average hydrodynamic radius was obtained through a second order cumulant analysis.

### 2.4.2. $\zeta$ -Potential measurements

The  $\zeta$ -potential of the particles was measured on a Zetasizer Nano-ZS ZEN 3600 (Malvern Instruments, UK) at 25 °C. 20 mg of particles were dispersed in 1 mL of aqueous solutions.

### 2.4.3 <sup>1</sup>H NMR spectroscopy

The <sup>1</sup>H NMR spectra were recorded on a Bruker Avance 300 at 300 MHz (Bruker, USA). D<sub>2</sub>O was used as solvent for the analysis. Chemical shifts were given in ppm and were measured relative to the TMS.

### 2.4.4. Transmission Electron Microscopy

The transmission electron microscopy (TEM) micrographs were obtained on a TECNAI G2-20 Twin microscope (FEI, USA), equipped with a LaB6 filament operating at 200 kV. Two drops of nanoparticles suspension were deposited on a carbon–copper grid (CF200-Cu, Electron Microscopy Sciences, USA).

#### 2.4.5. Thermogravimetric analysis (TGA)

Thermogravimetric analyses (TGA) were performed using a Q500 instruments (TA Instruments, USA). In a typical analysis, 10-15 mg product was placed in a Pt crucible. The sample was at first equilibrated at 120 °C, and then heated at 10 °C/min to 900 °C, under nitrogen.

#### 2.4.6 Surface tension measurement

The surface tension measurements of sample were performed with a Krüss K100 tensiometer. In a typical experiment, the rod was immersed in the liquid studied at a rate of 10 mm.min<sup>-1</sup> and an immersion depth of 2 mm. Calibration with ultrapure water was carried out. For each measurement, the surface tension values were sampled every 3 s until the standard deviation was below 0.1 mN.m<sup>-1</sup>. Three measurements were taken in a row for each sample. No temperature correction was made to the previous measured values, since the observed deviations - between 0.1 and 0.7 mN.m<sup>-1</sup> - were larger than the temperature corrections, expected to be below 0.2 mN.m<sup>-1</sup>.

The measurements of the surface tension as a function of temperature were performed with 10 mL aqueous suspension of nanoparticles at 1 wt.% between 25 °C and 80 °C. An equilibrium time of 25 min was applied between the temperature increase and the measurement.

### 2.5. Preparation and characterization of emulsions

The emulsions were prepared using water phase containing the silica nanoparticles (1.5 mL) and different oils (1.5 mL). The emulsification was performed with an Ultraturrax T10 basic (IKA Works, Inc., Germany) for 60 s at 11500 rpm at room temperature.

Optical micrographs were acquired with a VHX-900 microscope from Keyence. The measurement of the droplets diameter size was performed with the Keyence software 1.6.1.0.

The distribution function (log-normal) of emulsion droplets diameters was obtained by treatment of at least 200 individual measurements using Origin 9.1® (OriginLab corporation, US) according to Eq. 1:

$$y = \frac{A}{\sqrt{2\pi}\omega\phi} \exp\left[-\frac{\left(\ln\frac{\phi}{\phi_m}\right)^2}{2\omega^2}\right] \quad (1)$$

where  $y$  is the probability for having droplets of diameter ( $\phi$ ),  $\omega$  is an asymmetric factor (*i.e.* measure of width), the peak will be approximately symmetric when  $\omega$  is small,  $\phi_m$  is the median droplets diameter ( $\phi_m$  corresponds to the peak center when the log-normal is approximately symmetric), and  $A$  is the amplitude and corresponds to the area under the curve. The  $\phi_m$ ,  $\omega$ , and  $A$  are parameters characterizing the size distribution of the droplets.

The emulsion stabilized with  $\text{H}_3\text{PW}_{12}\text{O}_{40}$ -decorated  $\text{SiO}_2$ @mPEG NPs were prepared as following. In a toluene/water biphasic system, 1.5 mL toluene and 1.5 mL  $\text{SiO}_2$ @mPEG aqueous dispersion were weight, followed by adding 3.0 wt.% solid  $\text{H}_3\text{PW}_{12}\text{O}_{40}$  directly. The emulsions were obtained after stirring at 11500 rpm for 2 min.

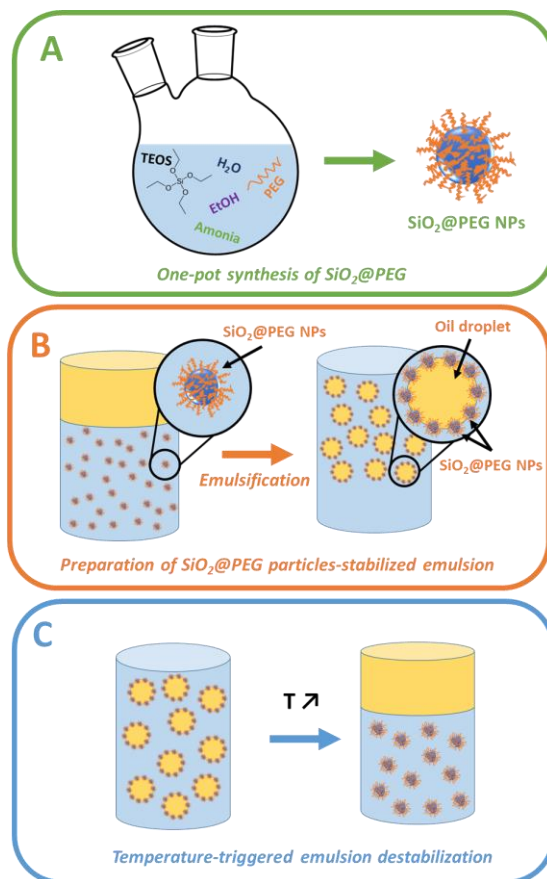
## 2.6. Temperature-responsive behavior of the emulsions

The temperature-responsive behavior of the emulsions was tested by heating the vials in a water bath a gentle stirring at 100 rpm up to 80 °C.

## 2.7. Catalytic tests

In a typical run, 1.5 mL toluene containing the given cyclootene (2 mol/L) and 1.5 mL water containing 3.5 equiv.  $\text{H}_2\text{O}_2$  (50 %) and 1.5 wt.%  $\text{SiO}_2$ @mPEG were added to a 5 mL vial, followed by adding 3.0 wt.%  $\text{H}_3\text{PW}_{12}\text{O}_{40}$ . The system was pre-emulsified using an Ultra-Turrax® (IKA T 25) at 11,500 rpm for 2 min. The reactor was sealed, heated at 65 °C for 6 h under stirring (500 rpm). After the reaction, the system was demulsified by centrifugation, the upper oil phase was separated by decantation, and it was dissolved in  $\text{CDCl}_3$ , whereas  $n$ -

dodecane was used as internal standard for analysis. The aqueous phase was diluted in deuterated DMSO using *n*-dodecanol as internal standard. The yield was measured by  $^1\text{H}$  NMR on an Advance 300 Bruker spectrometer at 300.12 MHz.



**Scheme 1.** Schematic illustration of the method of A) one pot synthesis of the SiO<sub>2</sub>@PEG NPs, B) Preparation of the emulsions stabilized by the SiO<sub>2</sub>@PEG NPs and C) Temperature-induced destabilization of the emulsion.

## 3. Results and Discussion

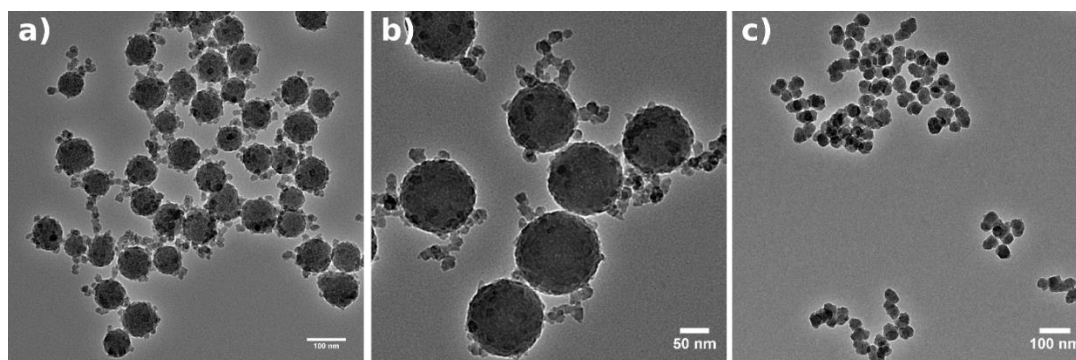
### 3.1. Synthesis and characterizations

#### 3.1.1. Transmission electron microscopy characterization

The morphology and the size of the SiO<sub>2</sub>@PEG NPs were studied by TEM (**Figure 1**). They present a spherical shape with rough surface. It is noteworthy the presence of small particles that are linked as a pearl necklace extending out the particles for SiO<sub>2</sub>@PEG 400 and



SiO<sub>2</sub>@mPEG 550 (**Figure 1a-b**). These small particles in such branch-like structure were not observed in previous studies [29]. The formation of such particles may be due to the condensation of silica onto the PEG chains extending out the main silica particles. The presence of small NPs (~ 20 nm) around and attached to the core make the particle rough and may help the stabilization of emulsions as it has been demonstrated by San Miguel *et al.* [30].



**Figure 1.** TEM images of a) SiO<sub>2</sub>@PEG 400, b) SiO<sub>2</sub>@mPEG 550 and c) SiO<sub>2</sub>@mPEG 5000 NPs synthesized by the one-step method.

### 3.1.2. Dynamic light scattering measurements

The size of the particles has also been measured by DLS (**Table 1**). As for TEM results, no clear trend has been observed as a function of PEG molecular weight. While for low molecular weight (200 to 550), PEG and mPEG gives the same range of size, *i.e.* 150-180 nm, for bigger PEG (or mPEG), a smaller size has been observed. It may be explained by the formation of much more silica nuclei on the PEG with longer chain (more ether groups) and thus, the final size of silica particles is low compared to other batches. However, the sizes measured by DLS are close to the sizes of the NPs (core + branches) measured on TEM pictures, particularly for SiO<sub>2</sub>@PEG 400 (125 nm measured on TEM), SiO<sub>2</sub>@mPEG 550 (200 nm measured on TEM) and SiO<sub>2</sub>@PEG 5000 (77 nm measured on TEM). It indicates that the chains of NPs are attached to the core.

In order to verify the presence of PEG onto the surface of silica particles, several characterizations have been performed. First, the  $\zeta$ -potential values of the NPs were measured as a function of the PEG (or mPEG) weight (**Table 1**). Short chain lengths have surface charges

comparable to bare silica. NPs functionalized with bigger PEG show a higher reduction of surface charge. Hence, short PEG chains extend less out of the surface of the NPs, which may explain values close to the  $\zeta$ -potential of silica. The increase of MW of PEG, which is a nonionic polymer, decreases the surface charge of the NPs [31].

**Table 1.** Size hydrodynamic diameter measured in DLS and  $\zeta$  potential of bare silica NPs and SiO<sub>2</sub>@PEG NPs dispersed in ultrapure water.

Particles	Hydrodynamic diameter	Zeta potential
	(nm)	(mV)
Bare silica	110	- 55
SiO <sub>2</sub> @PEG 200	180	- 59
SiO <sub>2</sub> @PEG 400	150	- 59.7
SiO <sub>2</sub> @mPEG 550	180	- 46
SiO <sub>2</sub> @mPEG 2000	320	- 29.1
SiO <sub>2</sub> @mPEG 5000	80	- 31.6

### 3.1.3. Nuclear magnetic resonance spectroscopy

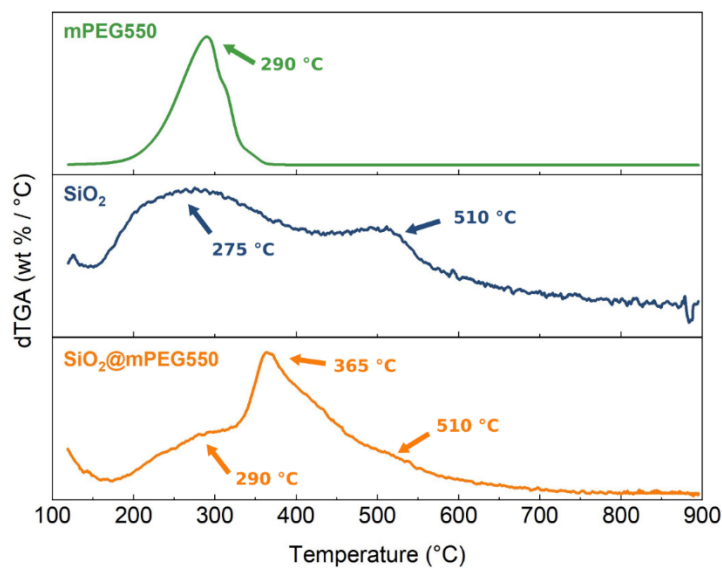
The presence of PEG on the surface of the NPs was investigated by <sup>1</sup>H NMR spectroscopy (**Figure A-6**). <sup>1</sup>H NMR spectrum of SiO<sub>2</sub>@mPEG 550 NPs was compared to the spectrum of silica NPs functionalized with mPEG 500 through the two-step protocol proposed by Björkegren *et al.* [14] were measured. Both spectra show peak that corresponds to the presence of PEG (3.6 ppm). This result suggests that the peak of SiO<sub>2</sub>@mPEG 5000 is less intense than the peak of the silica NPs functionalized through the two-step method[32]. The nature of interaction between silica and PEG is different for the two types of NPs. Particles grafted with a coupling agent have the PEG molecules covalently attached to their surface, which puts all these molecules in a similar environment resulting in a sharp peak. On the other hand, the broad peak of the SiO<sub>2</sub>@mPEG 550 particles prepared with one-pot method suggests that the molecules of PEG are in different environments, *i.e.* a part of the PEG is inside the SiO<sub>2</sub> core and the other part is outside of the core. The synthesis of SiO<sub>2</sub>@PEG consists in a modified

Stöber synthesis of silica in presence of PEG developed by Akbari et al [29]. According to Xu *et al.* [33], the hydrolysis step of the sol-gel process of the silica precursor competes with the transesterification between the PEG and silica precursor (TEOS) before the condensation. This method allows to entrap the PEG by a covalent binding, within the silica NPs but also onto the surface.

In order to check that the presence of PEG in the samples is not due to the residual PEG molecule – not attached on silica network – the NPs have been centrifuged and redispersed in water several times.  $^1\text{H}$  NMR spectra of two supernatants have been performed to control the absence of free PEG in the suspension (**Figure A-7**). The  $^1\text{H}$  NMR spectra of two supernatants have been performed after 3 and 5 washing cycles. While after three washing step, some free PEG molecules are still present, after five washing steps no more free PEG molecule are present (peak reduced to noise level). This result proves that the washing steps were effective to remove free PEG molecules.

#### 3.1.4. Thermostability

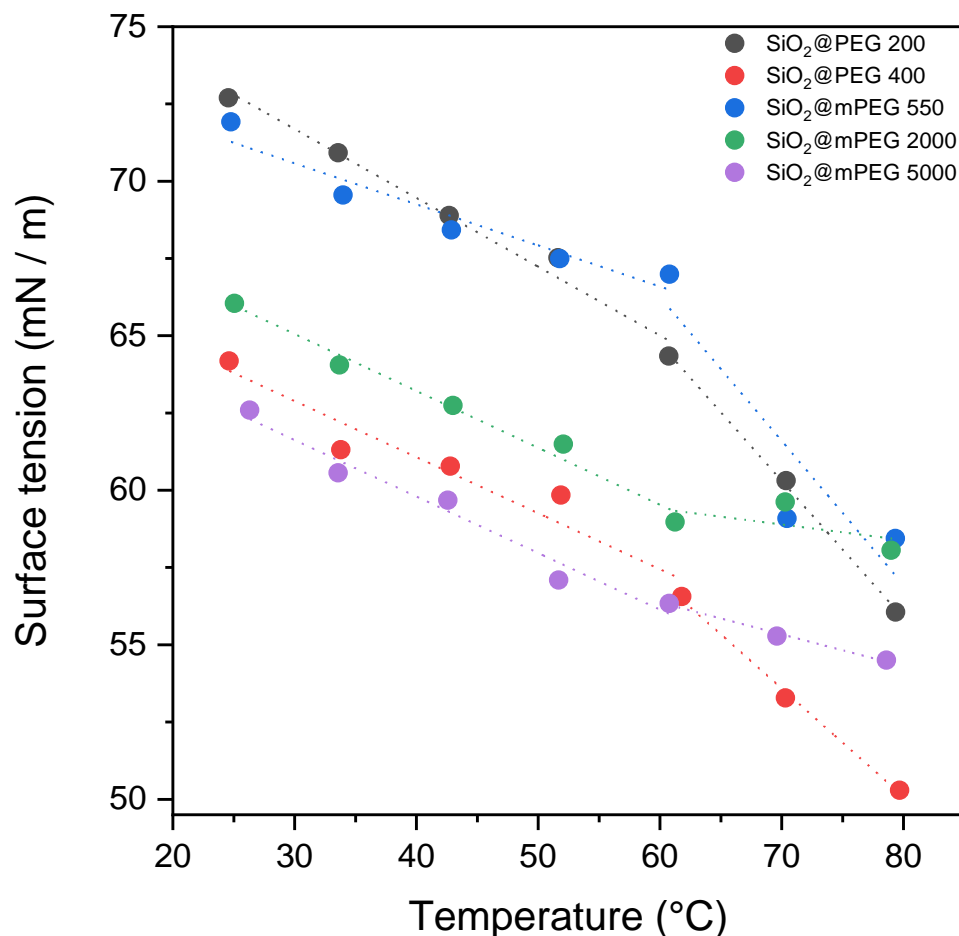
The  $\text{SiO}_2$ @PEG NPs were characterized with TGA measurements (**Figure 2**). First, the dTGA curve of the  $\text{SiO}_2$ @mPEG 550 shows a main peak at 365 °C and two shoulders at 290 °C and 510 °C. While the signal at 290 °C corresponds to the PEG degradation and silica dehydroxylation, the signal at 510 °C can be attributed to the dehydroxylation of isolated hydroxyl groups like it was measured for the bare silica NPs [34]. The main peak of the dTGA of  $\text{SiO}_2$ @mPEG 550 at 365 °C can be attributed to the degradation of grafted PEG species [35]. A peak at around 275 °C is also visible in the dTGA curve of the silica NPs that can be attributed to the dihydroxylation of some hydroxyl groups. The peak at 365 °C of dTGA curve of  $\text{SiO}_2$ @mPEG 550 is similar to the peak of  $\text{SiO}_2$ @GPTMS@PEG 2000. These results may suggest that the mPEG 550 is covalently attached to the NPs.



**Figure 2.** dTGA curves of mPEG 550, bare silica NPs and SiO<sub>2</sub>@mPEG 550 NPs. Experiments were conducted at 10 °C/min to 900 °C, under nitrogen.

### 3.1.5. Surface tension measurement

The surface tension of the NPs was measured in order to compare the surface activity of the SiO<sub>2</sub>@PEG with bare silica NPs. The surface tension of aqueous suspension of bare silica NPs is known to be around 72 mN.m<sup>-1</sup> whatever the concentration which indicates the negligible effect of their presence. [36,37]. Surprisingly, at room temperature, the surface tension of the aqueous suspension of SiO<sub>2</sub>@mPEG 550 NPs is at the same order, around 71 mN.m<sup>-1</sup> whatever the different concentrations measured (**Figure A-8**). Surface tensions of aqueous suspensions of SiO<sub>2</sub>@mPEG 5000 and SiO<sub>2</sub>@GPTMS@mPEG 2000 are 10 % lower at around 65 mN.m<sup>-1</sup>. These results would indicate that the short length of mPEG (MW 550) does not modify enough the surface tension of silica dispersion at room temperature. Hence, longer chain PEGs are more capable of reducing the surface tension with better steric stabilization on the surface once adsorbed. No significant change in surface tension has been observed by increasing the concentration of the NPs from 0.5 to 2.5 wt.%, whatever the nature of the NPs.



**Figure 3.** Surface tension as a function of temperature of aqueous suspensions of the different SiO<sub>2</sub>@PEG NPs with concentration (1 wt.%).

The surface tension of the aqueous suspensions of purified PEG-functionalized NPs has been also measured as a function of the temperature in order to determine the temperature-responsive behavior of the NPs (**Figure 3**). The measurements have been performed at a fixed NPs concentration (1 wt.%). Two groups of data can be observed. In one hand, the SiO<sub>2</sub>@PEG 200 and SiO<sub>2</sub>@mPEG 550 with a surface tension at around 72 mN.m<sup>-1</sup> that corresponds to the surface tension of water. The NPs have no or very small effects on the surface tension at room temperature. In the other hand, SiO<sub>2</sub>@PEG 400, SiO<sub>2</sub>@mPEG 2000 and SiO<sub>2</sub>@mPEG 5000 have a surface tension decreased at around 65 mN.m<sup>-1</sup> at room temperature, indicating they are surface active. Unlike the SiO<sub>2</sub>@PEG 200 and SiO<sub>2</sub>@mPEG 550, they should provide better stabilization for emulsions. These results may indicate that the NPs are surface active when the surface coverage of PEG is high enough [14]. The presence of PEG chains may be indeed more

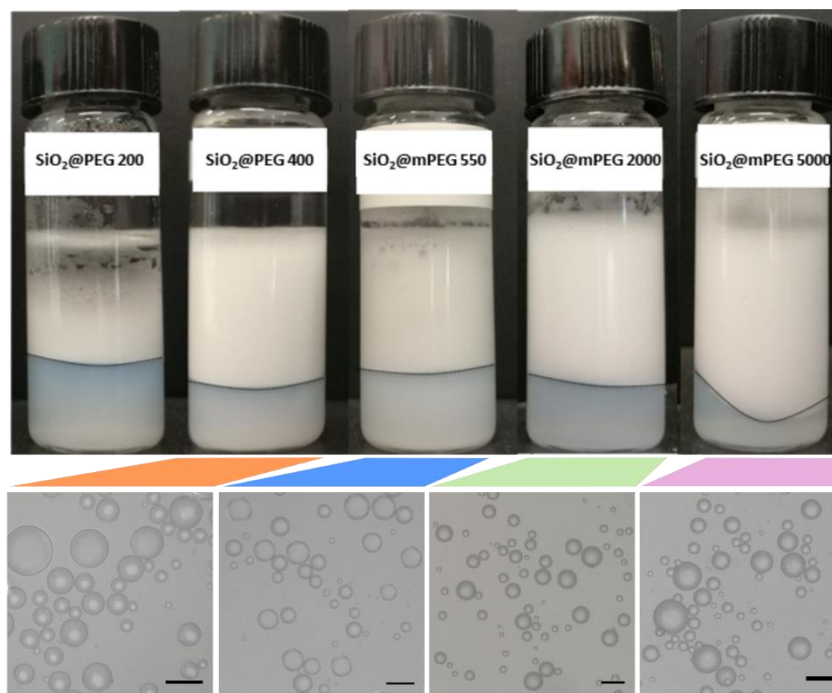
important onto the surface of the particles when using mPEG 2000 and mPEG 5000, with long chains.

When the temperature is increased up to 60 °C, the surface tensions of the dispersions decrease linearly and a break of the slope appears for higher temperatures. The surface tension of NPs functionalized with short chains of PEG (PEG 200, PEG 400 and mPEG 550) decreases faster for temperature higher than 60 °C while the surface tension of NPs functionalized with long chains of PEG is stabilized (mPEG 2000) or decreases slower (mPEG 5000). According to these results, the temperature-responsive behavior of Pickering emulsion were investigated at room temperature and at 80 °C, clearly above the temperature of change of behavior, *i.e.* T = 60 °C.

## 3.2. Physicochemical properties of the Pickering emulsions

### 3.2.1. Influence of the nanoparticles

Water / toluene emulsions (50/50) have been prepared with the SiO<sub>2</sub>@PEG NPs (**Figure 4**). As expected, particles grafted with small PEG, *i.e.* PEG 200, were poor stabilizers while O/W emulsion phase could be obtained with particles grafted with PEG of MW ≥ 400. [38]. The emulsions have been observed under optical microscope (**Figure 4**). The mean size of the droplets has been determined from the size distribution, obtained from the statistical analysis of the optical micrograph. It is around 35 μm for the emulsions stabilized with SiO<sub>2</sub>@PEG 400 and SiO<sub>2</sub>@mPEG 550 while smaller size of droplets for the emulsion stabilized with SiO<sub>2</sub>@mPEG 2000 and SiO<sub>2</sub>@mPEG 5000 has been measured.

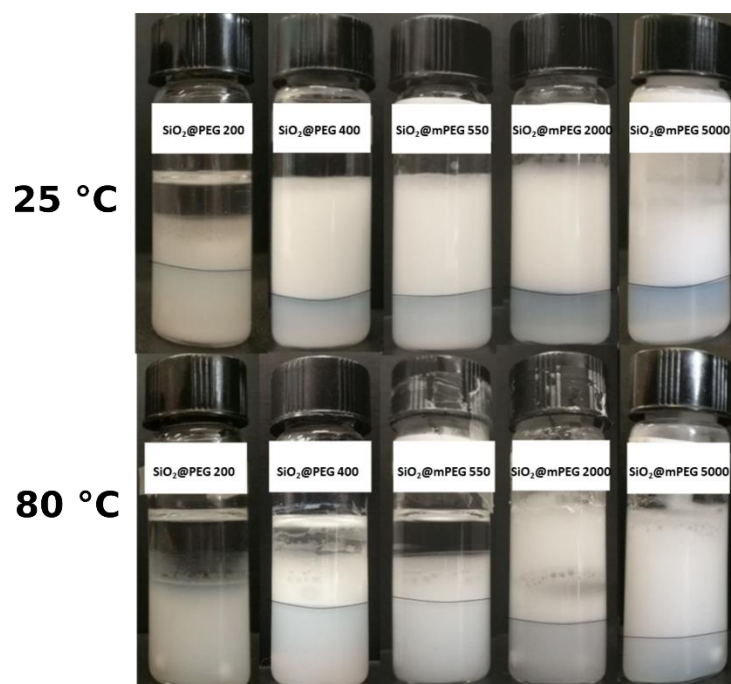


**Figure 4.** Appearance of the toluene/water (1:1 v/v) emulsions stabilized by silica NPs (1 wt.%) grafted with different types of PEG (top); Optical microscope pictures of the droplets for the corresponding emulsions (bottom). Scale bars: 50  $\mu\text{m}$ .

### 3.2.2. Temperature-responsive behavior of the Pickering emulsion

The temperature-responsive behavior of SiO<sub>2</sub>@PEG NPs-stabilized emulsions has been tested by applying an increase of temperature from 25 to 80 °C (**Figure 5**). Shorter chains of PEG are expected to have a better temperature-responsive behavior than long PEG chain according to the measurements of the surface tension (**Figure 3**). They require less energy to dehydrate compared to longer chains. SiO<sub>2</sub>@PEG 200 could not stabilize emulsion, hence it can be considered as unsuitable for the following. Both SiO<sub>2</sub>@PEG 400 and SiO<sub>2</sub>@mPEG 550 gave emulsions at room temperature and have presented a temperature-responsive behavior with temperature increase, *i.e.* a clear phase separation. Despite having stable emulsions, the particles with longer chains of PEG have almost no temperature-responsive behavior when heated (SiO<sub>2</sub>@mPEG 2000), as expected. Moreover, the emulsion stabilized by SiO<sub>2</sub>@mPEG 5000 maintains stable. The temperature responsive behavior of the PEG-functionalized silica particles can be attributed to the hydrophilic/hydrophobic balance of the PEG/mPEG chains. At low temperature, the balance between the ether oxygen of EO chain-water interaction and

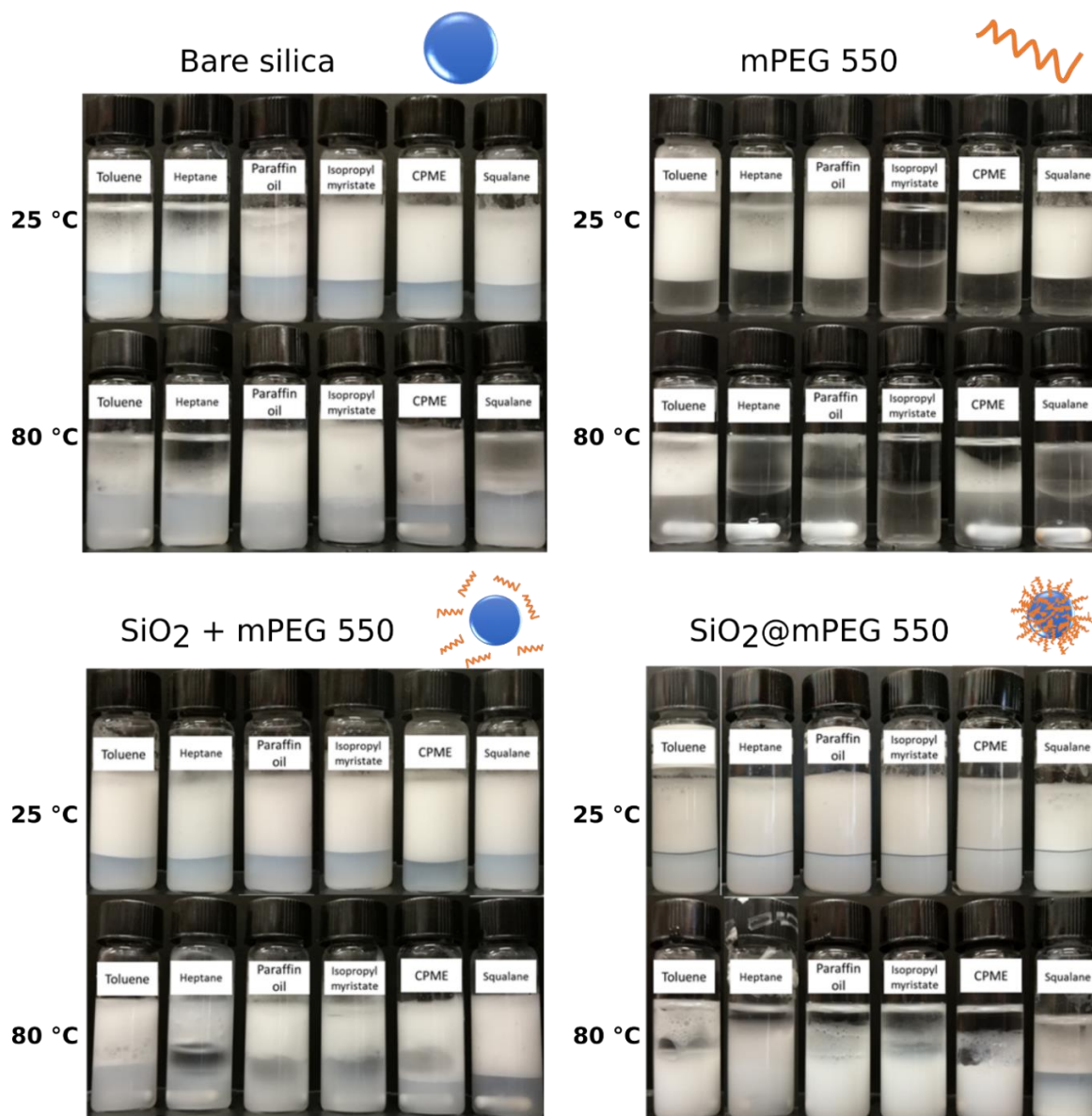
carbon-carbon backbones of PEG is enough to let the SiO<sub>2</sub>@PEG particles stabilizing emulsions [39]. With the increase of temperature, the hydrogen bonds between the EO chain and water become weaker [40]. At high temperature, the distribution of the PEG/mPEG chain at the oil-water interface is modified which results in the destabilization of the emulsion [41]. Especially, the SiO<sub>2</sub>@PEG particles become more hydrophilic with the increase of the chain length, improving the ability of EO units to form more hydrogen bonds with water. In this way, the increase in the chain length of the PEG also increases the energy required to break the hydrogen bonds between EO units and water molecules. According to these results and the previous characterizations, SiO<sub>2</sub>@mPEG550 NPs are the most suitable particles for stabilizing water / toluene emulsions and giving them a temperature-responsive behavior.



**Figure 5.** Pictures of the toluene/water (1:1 v/v) emulsions stabilized with silica particles (1 wt.%) grafted with different length of PEG, at 25 °C and 80 °C.

The influence of the nature and polarity of the oils on the final properties of the emulsions and their temperature-responsiveness have been investigated. The emulsions have been compared to emulsions prepared with bare silica NPs, pure mPEG 550 and a mixture of bare silica NPs and mPEG 550 (**Figure 6**).





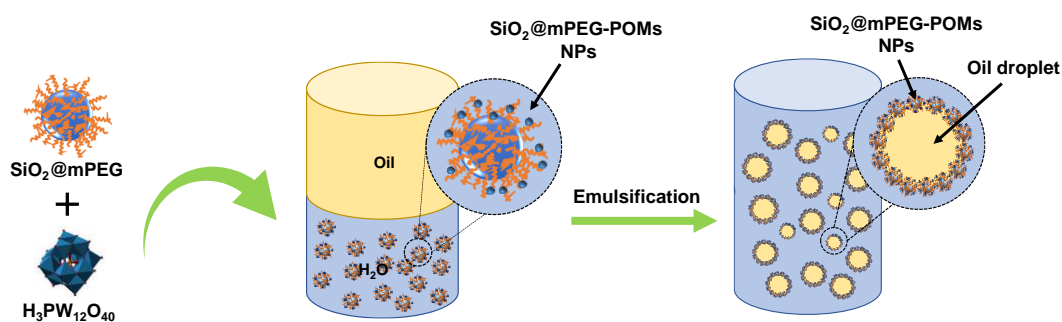
**Figure 6.** Appearance of the oil/water (1:1 v/v, different nature of oil) emulsions stabilized with bare silica (1 wt.%), mPEG 550 (0.07 wt.%), a mixture of bare silica and mPEG 550 (11:1 ratio, 1 wt.%) and silica particles (1 wt.%) grafted with type of PEG at 25 and 80 °C.

As expected, emulsions could be obtained with paraffin oil, isopropyl myristate, CPME and squalane [42]. A destabilization occurs when the temperature increases but it could be explained by the gentle stirring used to homogenize the temperature that may accelerate the natural destabilization of the emulsions. Pure mPEG 550 molecules stabilize emulsions with almost all oils (except isopropyl myristate, probably due to the poor solubility of mPEG in this oil). A temperature-triggered destabilization occurs except for toluene. Stable emulsions were obtained with the mixture silica NPs and mPEG 550 was used whatever the nature of the oil. A

weak temperature-triggered destabilization happens except for emulsion prepared with squalane. Hence, oils with higher polarity (*e.g.* heptane) are more favorable to obtain Pickering emulsions with bare silica and pure PEG [42,43]. When SiO<sub>2</sub>@mPEG 550 NPs were used, stable emulsions were obtained at room temperature and a clear destabilization occurs at 80 °C. Here, the results show that the SiO<sub>2</sub>@mPEG 550 NPs can form stable and temperature-responsive emulsions with oils of different nature.

### 3.3. Elaboration of Pickering interfacial catalysis (PIC) system

Stimuli-responsive materials present a great potential to design “smart” PIC process. Since Pickering emulsion is highly stable - with the densely packed NPs layers at the interface - the separation of the catalyst from the emulsion is performed by centrifugation or filtration. These two processes lead to the catalyst loss and energy consuming, which is unfavorable for the economic viability and sustainability of the chemical process. Therefore, the concept of “smart” Pickering emulsion responsive to an external trigger opens a new avenue for catalytic process. The use of stimuli-responsive nanomaterials allows to stabilize emulsion and also an external stimulus (such as pH, CO<sub>2</sub> or salt addition, light, magnetic or temperature) to trigger the adsorption/desorption process.

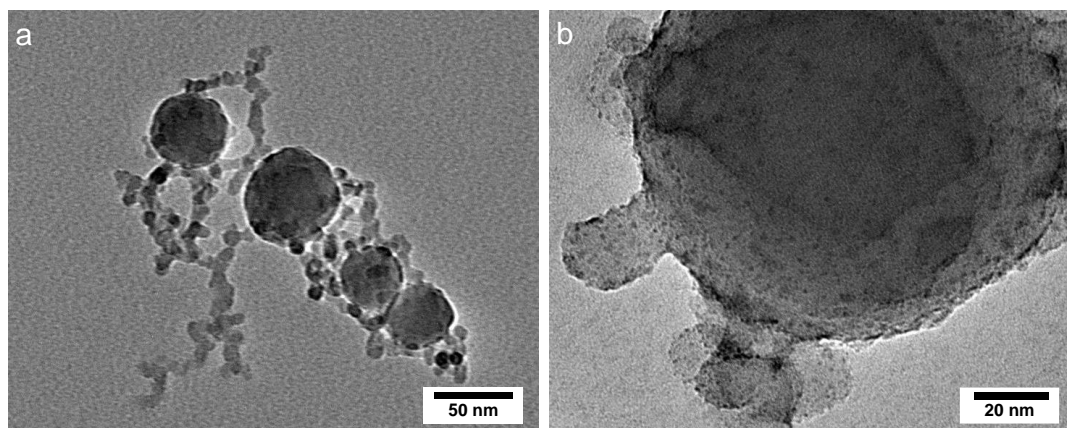


**Figure 7.** Schematic illustration of the self-assembly of SiO<sub>2</sub>@mPEG and H<sub>3</sub>PW<sub>12</sub>O<sub>40</sub> and the preparation of SiO<sub>2</sub>@mPEG-POMs particles-stabilized emulsion.

A PIC system is elaborated the oxidative cleavage of cyclooctene (**Figure 7**). To do so, POMs (H<sub>3</sub>PW<sub>12</sub>O<sub>40</sub>) have been grafted onto the SiO<sub>2</sub>@mPEG NPs [44]. The location of the catalytic sites at the water/oil interface provides a large interface area to overcome the diffusion barriers, and thus the improvement of the catalytic efficiency.

### 3.3.1. Transmission electron microscopy characterization

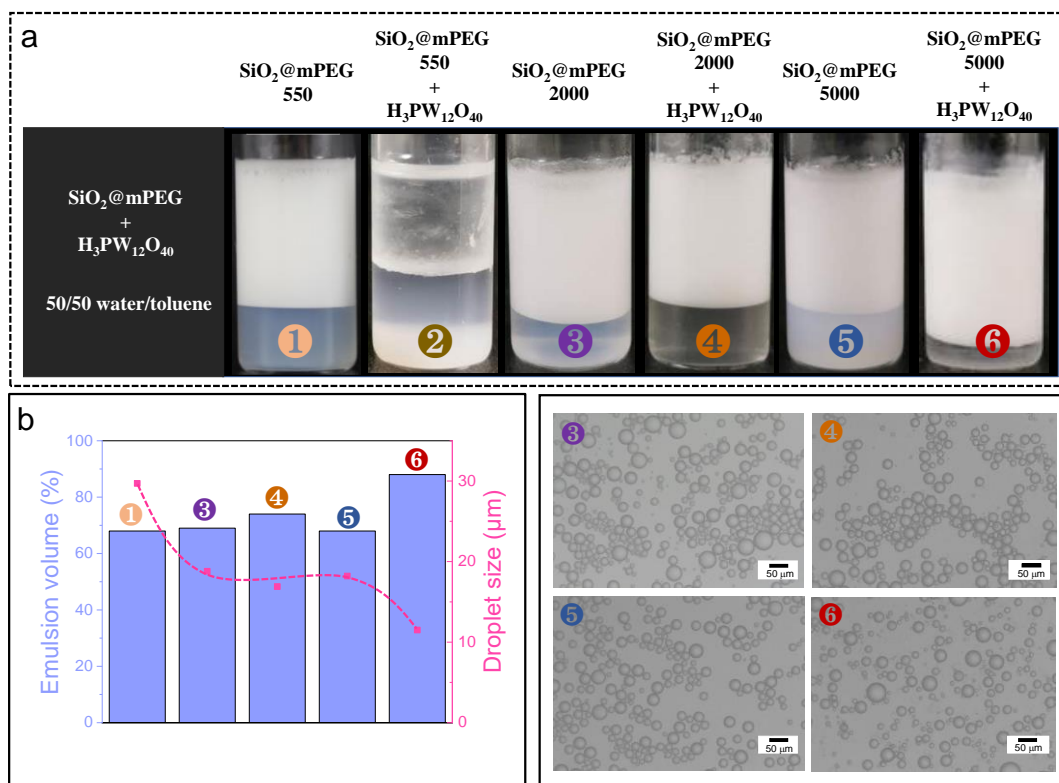
The surface structure and morphology of the  $\text{H}_3\text{PW}_{12}\text{O}_{40}$ -decorated  $\text{SiO}_2$ @mPEG 500 NPs were investigated by TEM. It can be observed that many tiny black dots are grafted onto the silica surface (**Figure 8b**), which are not present before the POM adsorption (**Figure 8a**). This demonstrates the completion of the self-assembly of  $\text{SiO}_2$ @mPEG500 and  $\text{H}_3\text{PW}_{12}\text{O}_{40}$ .



**Figure 8.** TEM micrograph of the  $\text{SiO}_2$ @PEG 550 NPs (a) and  $\text{SiO}_2$ @PEG 550-POM NPs (b).

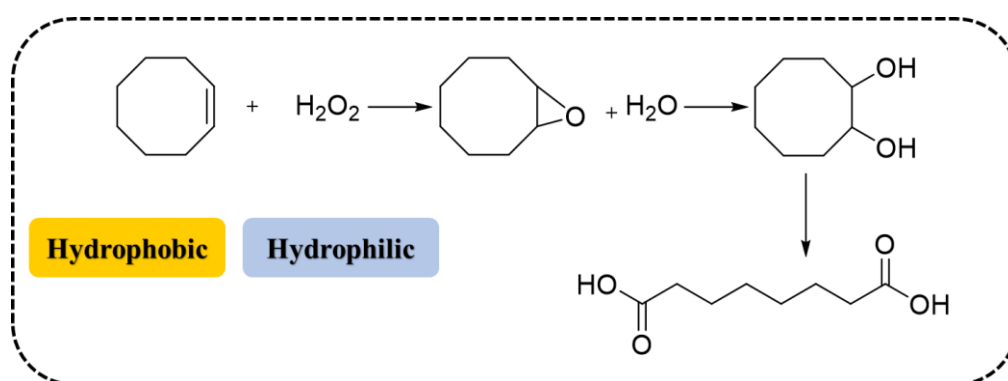
### 3.3.2. Preparation of Pickering emulsion

The emulsifying properties of the combination of  $\text{H}_3\text{PW}_{12}\text{O}_{40}$ -decorated  $\text{SiO}_2$ @mPEG 500 NPs for the biphasic system was studied (**Figure 9a**). As expected,  $\text{SiO}_2$ @mPEG 550,  $\text{SiO}_2$ @mPEG 2000 and  $\text{SiO}_2$ @mPEG 5000 NPs used as control experiments stabilized well-defined O/W emulsion. However, no emulsion can be obtained with  $\text{SiO}_2$ @mPEG 550 NPs after the addition of  $\text{H}_3\text{PW}_{12}\text{O}_{40}$  in the system.  $\text{SiO}_2$ @mPEG 2000 and  $\text{SiO}_2$ @mPEG 5000 NPs are more effective in emulsifying emulsion in the presence of  $\text{H}_3\text{PW}_{12}\text{O}_{40}$  (**Figure 9b and Table A-8**), with an increase of the emulsion volume from 69 % to 74 % and from 68 % to 88 %, respectively. The average droplet sizes depend on the different emulsifiers:  $\text{SiO}_2$ @mPEG 2000-POMs (17  $\mu\text{m}$ ) and  $\text{SiO}_2$ @mPEG 5000-POMs (12  $\mu\text{m}$ ). Such fine droplets could improve the catalytic activity of biphasic reaction with a short diffusion distance and high contact area [45].



**Figure 9.** (a) Photographs of emulsion stabilized by single 1.5 wt.% SiO<sub>2</sub>@mPEG NPs and a combination of 1.5 wt.% SiO<sub>2</sub>@mPEG and 3.0 wt.% H<sub>3</sub>PW<sub>12</sub>O<sub>40</sub> NPs; (b) The emulsion volume and average droplet size of the obtained emulsion (the guided line is added manually). The inset present the micrographs of the O/W emulsions. Conditions: 1.5 mL toluene, 1.5 mL water, 1.5 wt.% SiO<sub>2</sub>@mPEG, 3.0 wt.% H<sub>3</sub>PW<sub>12</sub>O<sub>40</sub>, emulsified at 11500 rpm for 2 min.

### 3.3.3. Catalytic results



**Figure 10.** Mechanism of oxidative cleavage of olefins by H<sub>2</sub>O<sub>2</sub> for epoxide, diol and acid formation.

The oxidative cleavage of cyclooctene in Pickering emulsion has been chosen as a reaction model in order to evaluate the catalytic performance of the POM-decorated SiO<sub>2</sub>@mPEG NPs

(**Table 2**). 2 mol/L cyclooctene dissolved in toluene as oil phase and H<sub>2</sub>O<sub>2</sub> were diluted in water as aqueous phase. With the addition of SiO<sub>2</sub>@mPEG and POMs, a stable emulsion was formed.

**Table 2** Catalytic results for the oxidative cleavage of cyclooctene in Pickering emulsion

<i>n</i>	SiO <sub>2</sub> @PEG	Catalyst	Emulsion	Conversion (%)	Yield of epoxide (%)	Yield of diol (%)	Yield of acid (%)
1	1.5 wt.% SiO <sub>2</sub> @mPEG 2000	/	yes	2	/	/	0.6
2	1.5 wt.% SiO <sub>2</sub> @mPEG 5000	/	yes	2	/	1	0.1
3	/	3.0 wt.% H <sub>3</sub> PW <sub>12</sub> O <sub>40</sub>	no	4	3	0.5	1
4	1.5 wt.% SiO <sub>2</sub> @mPEG 2000	3.0 wt.% H <sub>3</sub> PW <sub>12</sub> O <sub>40</sub>	yes	21	/	4	0.5
5	1.5 wt.% SiO <sub>2</sub> @mPEG 5000	3.0 wt.% H <sub>3</sub> PW <sub>12</sub> O <sub>40</sub>	yes	44	22	0.8	5
6 <sup>a</sup>	1.5 wt.% SiO <sub>2</sub> @mPEG 5000	3.0 wt.% H <sub>3</sub> PW <sub>12</sub> O <sub>40</sub>	yes	43	18	0.8	6

Reaction conditions: 1.5 mL toluene (2 mol/L cyclooctene), 3.5 equiv. H<sub>2</sub>O<sub>2</sub> were diluted in 1.5 mL water, emulsified with Ultra-Turrax at 11500 rpm for 2 min, reaction temperature 65 °C, 6 h, 500 rpm. <sup>a</sup> Without stirring.

To assess the influence of emulsion on the oxidation, the first series of experiments are carried out with SiO<sub>2</sub>@mPEG or with POMs. The experiments with SiO<sub>2</sub>@mPEG 2000 and SiO<sub>2</sub>@mPEG 5000 give a negligible conversion of cyclooctene (2%), confirming that the SiO<sub>2</sub>@mPEG NPs are not catalytically active for the oxidation. In the case of POMs alone, a low conversion (4%) is observed along with the negligible yield (1%) to suberic acid. For the combination of SiO<sub>2</sub>@mPEG 2000 and POMs, poor catalytic efficiency of cyclooctene (21% of conversion and yield of 4% to diol) could be due to the breaking of emulsion during the reaction. In contrast, significant yield of the main products is obtained with SiO<sub>2</sub>@mPEG 5000 and POMs under the same conditions. Around 44% of cyclooctene have been converted within 6 h at 65 °C (22% yield of epoxide and 5% yield of suberic acid). This is 11 times higher than the conversion obtained with a biphasic system (*i.e.* no emulsion). In order to demonstrate the

advantage of the PIC system, the oxidation of cyclooctene has been also evaluated under stirring-free conditions. Notably, almost no difference has been observed. The high catalytic performance of the system can be attributed to the synergistic effect of SiO<sub>2</sub>@mPEG 5000 NPs and POMs, which might provide a more efficient interface for the reactants and so, to enhance significantly the reactivity of the biphasic reaction.

## 4. Conclusion

A series of PEG-functionalized-SiO<sub>2</sub> NPs have been prepared *via* a one-step method and were used for the elaboration of temperature-responsive Pickering emulsions. The physicochemical properties of the NPs as well as the presence of PEG molecules anchored on the particles have been thoroughly studied. A drop of the surface tension has been observed near 60 °C for three length of PEG (MW 200, 400 and 550). Stable Pickering emulsions, obtained with several oils of different polarity, were stabilized with NPs functionalized different PEG length (except with the shortest, 200 g.mol<sup>-1</sup>). Emulsions stabilized with SiO<sub>2</sub>@mPEG 550 NPs underwent a clear destabilization with temperature (from room temperature to 80 °C) whatever the nature of the oil compared to the other PEG lengths studied and bare silica NPs, mPEG 550 and their mixture. By introducing POMs on the surface of SiO<sub>2</sub>@PEG NPs *via* self-assembly, a PIC system for oxidative cleavage of cyclooctene is conducted. Stable O/W Pickering emulsion can be obtained with the combination of SiO<sub>2</sub>@PEG and POMs. As a result, the use of SiO<sub>2</sub>@PEG 5000-POMs NPs as PIC platform enhanced the catalytic activity up to 11-fold for the biphasic oxidation of cyclooctene. However, further investigations should be performed to optimize the reaction conditions to improve the efficiency of the system and to get a faster stimulus-responsive demulsification.

## 5. References

- [1] B.P. Binks, W. Liu, J.A. Rodrigues, Novel Stabilization of Emulsions via the Heteroaggregation of Nanoparticles, *Langmuir*. 24 (2008) 4443–4446.
- [2] F. Gautier, M. Destribats, R. Perrier-Cornet, J.-F. Dechézelles, J. Giermanska, V. Héroguez, S. Ravaine, F. Leal-Calderon, V. Schmitt, Pickering emulsions with stimuable particles: from highly- to weakly-covered interfaces, *Physical Chemistry Chemical Physics* 9 (2007) 6455.
- [3] L. Leclercq, V. Nardello-Rataj, Pickering emulsions based on cyclodextrins: A smart solution for antifungal azole derivatives topical delivery, *European Journal of Pharmaceutical Sciences*. 82 (2016) 126–137.
- [4] Y. Liu, P.G. Jessop, M. Cunningham, C.A. Eckert, C.L. Liotta, Switchable Surfactants, *Science*. 313 (2006) 958.
- [5] J. Masliyah, Z. (Joe) Zhou, Z. Xu, J. Czarnecki, H. Hamza, Understanding Water-Based Bitumen Extraction from Athabasca Oil Sands, *The Canadian Journal of Chemical Engineering*. 82 (n.d.) 628.
- [6] S. Wiese, A.C. Spiess, W. Richtering, Microgel-Stabilized Smart Emulsions for Biocatalysis, *Angewandte Chemie Int. Ed.* 52 (2013) 576.
- [7] B.P. Binks, D. Yin, Pickering emulsions stabilized by hydrophilic nanoparticles: in situ surface modification by oil, *Soft Matter*. 12 (2016) 6858–6867.
- [8] Y. Chevalier, M.-A. Bolzinger, Emulsions stabilized with solid nanoparticles: Pickering emulsions, *Colloids and Surfaces A: Physicochemical and Engineering Aspects*. 439 (2013) 23–34.
- [9] S. Reculosa, S. Ravaine, Synthesis of Colloidal Crystals of Controllable Thickness through the Langmuir–Blodgett Technique, *Chemistry of Materials* 15 (2003) 598–605.
- [10] R.G. Digigow, J.-F. Dechézelles, H. Dietsch, I. Geissbühler, D. Vanhecke, C. Geers, A.M. Hirt, B. Rothen-Rutishauser, A. Petri-Fink, Preparation and characterization of functional silica hybrid magnetic nanoparticles, *Journal of Magnetism and Magnetic Materials*. 362 (2014) 72–79.
- [11] J.-F. Dechézelles, C. Ciotonea, C. Catrinescu, A. Ungureanu, S. Royer, V. Nardello-Rataj, Emulsions Stabilized with Alumina-Functionalized Mesoporous Silica Particles, *Langmuir*. 36 (2020) 3212–3220.
- [12] N. Griffete, J.-F. Dechézelles, F. Scheffold, Dense covalent attachment of magnetic iron oxide nanoparticles onto silica particles using a diazonium salt chemistry approach, *Chemical Communications* 48 (2012) 11364.
- [13] S. Reculosa, C. Poncet-Legrand, S. Ravaine, C. Mingotaud, E. Duguet, E. Bourgeat-Lami, Syntheses of Raspberry-like Silica/Polystyrene Materials, *Chemistry of Materials* 14 (2002) 2354–2359.
- [14] S.M.S. Björkegren, L. Nordstierna, A. Törnecrona, M.E. Persson, A.E.C. Palmqvist, Surface activity and flocculation behavior of polyethylene glycol-functionalized silica nanoparticles, *Journal of Colloid and Interface Science*. 452 (2015) 215–223.
- [15] V. Lapeyre, N. Renaudie, J.-F. Dechezelles, H. Saadaoui, S. Ravaine, V. Ravaine, Multiresponsive Hybrid Microgels and Hollow Capsules with a Layered Structure, *Langmuir*. 25 (2009) 4659–4667.
- [16] B. Brugger, B.A. Rosen, W. Richtering, Microgels as Stimuli-Responsive Stabilizers for Emulsions, *Langmuir*. 24 (2008) 12202–12208.

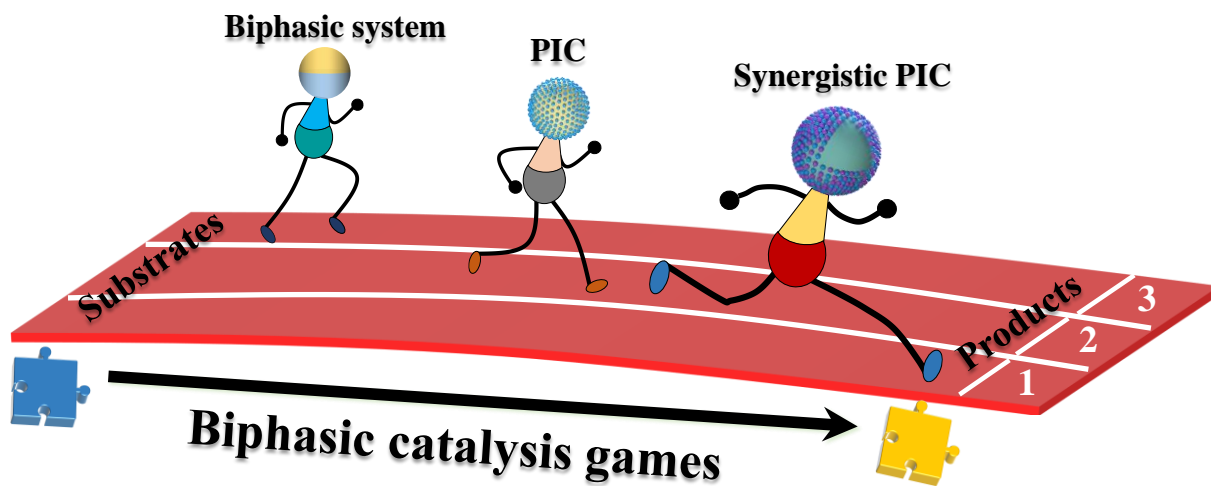
- [17] C.-Y. Xie, S.-X. Meng, L.-H. Xue, R.-X. Bai, X. Yang, Y. Wang, Z.-P. Qiu, B.P. Binks, T. Guo, T. Meng, Light and Magnetic Dual-Responsive Pickering Emulsion Micro-Reactors, *Langmuir*. 33 (2017) 14139–14148.
- [18] J. Zhou, X. Qiao, B.P. Binks, K. Sun, M. Bai, Y. Li, Y. Liu, Magnetic Pickering Emulsions Stabilized by Fe<sub>3</sub>O<sub>4</sub> Nanoparticles, *Langmuir*. 27 (2011) 3308–3316.
- [19] S. Saeki, N. Kuwahara, M. Nakata, M. Kaneko, Upper and lower critical solution temperatures in poly (ethylene glycol) solutions, *Polymer*. 17 (1976) 685–689.
- [20] B.R. Midmore, Synergy between silica and polyoxyethylene surfactants in the formation of O/W emulsions, *Colloids and Surfaces A: Physicochemical and Engineering Aspects*. 145 (1998) 133–143.
- [21] S. Björkegren, L. Nordstierna, A. Sundblom, A. Palmqvist, Clouding observed for surface active, mPEG-grafted silica nanoparticles, *RSC Advances* 9 (2019) 13297–13303.
- [22] S. Björkegren, M.C.A. Freixiela Dias, K. Lundahl, L. Nordstierna, A. Palmqvist, Phase Inversions Observed in Thermoresponsive Pickering Emulsions Stabilized by Surface Functionalized Colloidal Silica, *Langmuir*. 36 (2020) 2357–2367.
- [23] J. Jiang, Y. Zhu, Z. Cui, B.P. Binks, Switchable Pickering Emulsions Stabilized by Silica Nanoparticles Hydrophobized In Situ with a Switchable Surfactant, *Angewandte Chemie* 125 (2013) 12599–12602.
- [24] Y. Zhu, T. Fu, K. Liu, Q. Lin, X. Pei, J. Jiang, Z. Cui, B.P. Binks, Thermoresponsive Pickering Emulsions Stabilized by Silica Nanoparticles in Combination with Alkyl Polyoxyethylene Ether Nonionic Surfactant, *Langmuir*. 33 (2017) 5724–5733.
- [25] P. Lesot, S. Chapuis, J.P. Bayle, J. Rault, E. Lafontaine, A. Campero, P. Judeinstein, Structural–dynamical relationship in silica PEG hybrid gels, *Journal of Materials Chemistry*. 8 (1998) 147–151.
- [26] D.Y. Lee, S. Kang, Y. Lee, J.Y. Kim, D. Yoo, W. Jung, S. Lee, Y.Y. Jeong, K. Lee, S. Jon, PEGylated Bilirubin-coated Iron Oxide Nanoparticles as a Biosensor for Magnetic Relaxation Switching-based ROS Detection in Whole Blood, *Theranostics*. 10 (2020) 1997–2007.
- [27] B. Naskar, O. Diat, V. Nardello-Rataj, P. Bauduin, Nanometer-Size Polyoxometalate Anions Adsorb Strongly on Neutral Soft Surfaces, *The Journal of Physical Chemistry C*. 119 (2015) 20985–20992.
- [28] H. Giesche, Synthesis of monodispersed silica powders I. Particle properties and reaction kinetics, *Journal of the European Ceramic Society*. 14 (1994) 189–204.
- [29] A. Akbari, R. Yegani, B. Pourabbas, Synthesis of poly(ethylene glycol) (PEG) grafted silica nanoparticles with a minimum adhesion of proteins via one-pot one-step method, *Colloids and Surfaces A: Physicochemical and Engineering Aspects*. 484 (2015) 206–215.
- [30] A. San-Miguel, S.H. Behrens, Influence of Nanoscale Particle Roughness on the Stability of Pickering Emulsions, *Langmuir*. 28 (2012) 12038–12043.
- [31] B. Thierry, L. Zimmer, S. McNiven, K. Finnie, C. Barbé, H.J. Griesser, Electrostatic Self-Assembly of PEG Copolymers onto Porous Silica Nanoparticles, *Langmuir*. 24 (2008) 8143–8150.
- [32] J.M. Dust, Z.H. Fang, J.M. Harris, Proton NMR characterization of poly(ethylene glycols) and derivatives, *Macromolecules*. 23 (1990) 3742–3746.
- [33] H. Xu, F. Yan, E.E. Monson, R. Kopelman, Room-temperature preparation and characterization of poly (ethylene glycol)-coated silica nanoparticles for biomedical applications, *Journal of*



- Biomedical Materials Research. 66A (2003) 870–879.
- [34] J.M. Kim, S.M. Chang, S.M. Kong, K.-S. Kim, J. Kim, W.-S. Kim, Control of hydroxyl group content in silica particle synthesized by the sol-precipitation process, *Ceramics International*. 35 (2009) 1015–1019.
- [35] P. Maitra, J. Ding, H. Huang, S.L. Wunder, Poly(ethylene oxide) Silanated Nanosize Fumed Silica: DSC and TGA Characterization of the Surface, *Langmuir*. 19 (2003) 8994–9004.
- [36] T. Okubo, Surface tension of structured colloidal suspensions of polystyrene and silica spheres at the air-water interface, *Journal of Colloid and Interface Science*. 171 (1995) 55.
- [37] H. Ma, M. Luo, L.L. Dai, Influences of surfactant and nanoparticle assembly on effective interfacial tensions, *Physical Chemistry Chemical Physics* 10 (2008) 2207.
- [38] P. Finkle, H.D. Draper, J.H. Hildebrand, The theory of emulsification, *Journal of the American Chemical Society* 45 (1923) 2780.
- [39] H. Cai, W. Luo, Y. Zheng, Y. Zhang, L. Lai, S. Tang, Thermodynamic Parameters and Interfacial Properties of Poly(ethylene glycol)-octyl Sulfosuccinates, *Journal of Surfactants and Detergents*.
- [40] J. Israelachvili, The different faces of poly(ethylene glycol), (n.d.) 2.
- [41] F. Wang, J. Zhu, T. Yan, X. Pei, F. Zhang, R.J. Linhardt, Amphiphilic bromelain-synthesized oligo-phenylalanine grafted with methoxypolyethylene glycol possessing stabilizing thermo-responsive emulsion properties, *Journal of Colloid and Interface Science*. 538 (2019) 1–14.
- [42] J. Frelichowska, M.-A. Bolzinger, Y. Chevalier, Pickering emulsions with bare silica, *Colloids and Surfaces A: Physicochemical and Engineering Aspects*. 343 (2009) 70–74.
- [43] J. Jiang, Y. Zhu, Z. Cui, B.P. Binks, Switchable Pickering Emulsions Stabilized by Silica Nanoparticles Hydrophobized In Situ with a Switchable Surfactant, *Angewandte Chemie International Edition*. 52 (2013) 12373–12376.
- [44] T. Buchecker, X. Le Goff, B. Naskar, A. Pfitzner, O. Diat, P. Bauduin, Polyoxometalate/Polyethylene Glycol Interactions in Water: From Nanoassemblies in Water to Crystal Formation by Electrostatic Screening, *Chemistry – A European Journal* 23 (2017) 8434–8442.
- [45] A.M. Bago Rodriguez, L. Schober, A. Hinzmann, H. Gröger, B.P. Binks, Effect of Particle Wettability and Particle Concentration on the Enzymatic Dehydration of n-Octanaloxime in Pickering Emulsions, *Angewandte Chemie* 133(3) (2021) 1470-1477.

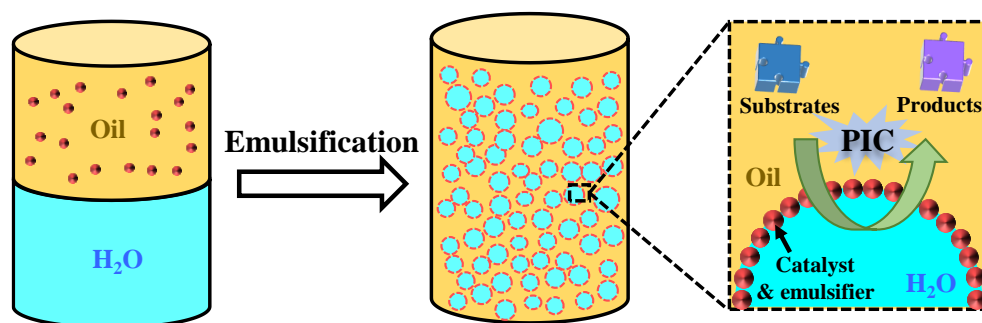
## Conclusion and outlooks

---





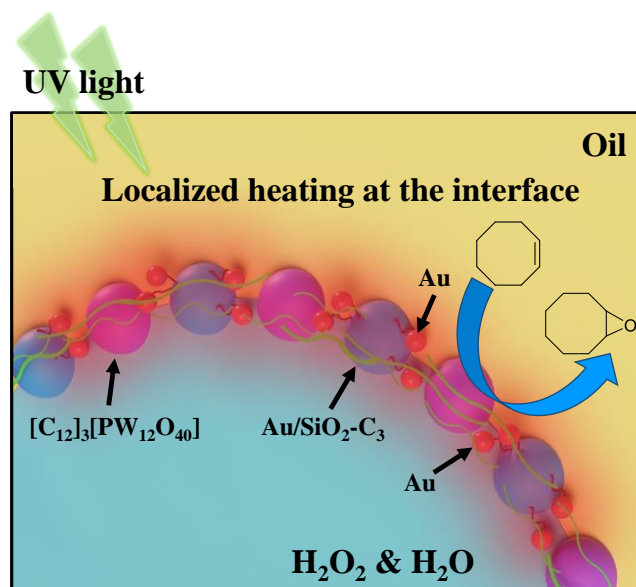
The present work focused on the development of **novel surface-active nanoparticles** for the fabrication of **Pickering emulsions** and their application to **catalytic oxidation**. In the Pickering interfacial catalysis (PIC) concept, water/oil (W/O) biphasic systems are emulsified by solid amphiphilic catalysts, creating a large interfacial surface that accelerates mass/heat transfer (**Figure 1**). This work places a particular emphasis on the preparation of multifunctional hybrid nanoparticles and their synergistic effect at W/O interface for PIC.



**Figure 1.** Schematic illustration of the solid particles at the oil-water interface in Pickering interfacial catalysis (PIC) system.

The current research highlights a promising way to integrate functional substances into multifunctional particles in order to tackle problems and challenges in the application of Pickering emulsions (**Chapter I**). Inspired by the synergistic effect between nanomaterials in Pickering emulsions, we designed an innovative PIC system for the **oxidation of cyclooctene** with  $\text{H}_2\text{O}_2$ , that benefits from the **photothermal effect of gold nanoparticles**  $\text{Au}/\text{SiO}_2\text{-C}_3$  and the catalytic properties of the **amphiphilic polyoxometalate nanoparticles**  $[\text{C}_{12}]_3[\text{PW}_{12}\text{O}_{40}]$  which have largely been studied and applied to PIC in previous theses in our group (**Chapter II**).  $\text{Au}/\text{SiO}_2\text{-C}_3$  combined with  $[\text{C}_{12}]_3[\text{PW}_{12}\text{O}_{40}]$  NPs **synergistically** improve not only the emulsion properties such as its stability but also allows **selective photo-activation** at the water/oil interface (**Figure 2**). As a result, the association of both these nanoparticles at the W/O interface exhibits an outstanding catalytic performance for the **oxidation of cyclooctene in emulsion under light irradiation ( $1 \text{ W}/\text{cm}^2$ ) at room temperature**, with a **catalytic efficiency of  $188 \text{ h}^{-1}$** . Compared to the process driven by conventional thermal-driven or at room temperature counterparts, light irradiation affords **1.6–4.5 times catalytic activity enhancement**. The enhanced catalytic efficiency can be attributed to the local

heating/activation effect of Au/SiO<sub>2</sub>-C<sub>3</sub> at the W/O interface in contact with [C<sub>12</sub>]<sub>3</sub>[PW<sub>12</sub>O<sub>40</sub>]. The oxidation of linear olefins is carried out to extend the scope of the system. The emulsify property and catalytic efficiency of the NPs are well maintained for **at least five consecutive runs**. In comparison to both traditional biphasic reaction and PIC system, the light-driven PIC system demonstrated: (1) enhanced catalytic performance; (2) mild and green reaction conditions; (3) easy of product separation and catalyst recovery.



**Figure 2.** Schematic illustration of the PIC system using self-assembled amphiphilic silica NPs loaded with Au NPs, acting as on-site heaters/plasmon activators, and [C<sub>12</sub>]<sub>3</sub>[PW<sub>12</sub>O<sub>40</sub>] NPs, acting as catalyst, under light irradiation.

The catalytic properties of the ultra-small gold nanoparticles for the oxidation of benzyl alcohol in PIC system have then been investigated (**Chapter III**). Surface-active catalysts composed of modified silica nanoparticles with **ultra-small gold nanoparticles (1.1 nm)** adsorbed onto their surface have been prepared and characterized. The **superior surface activity** Au@SiO<sub>2</sub>-C<sub>3</sub> NPs were able to stabilize Pickering emulsions, providing larger oil-water interface areas, favorable to a higher catalytic activity. Moreover, Au@SiO<sub>2</sub>-C<sub>3</sub> NPs outperform hydrophilic Au@SiO<sub>2</sub> NPs in terms of emulsion stability with smaller droplet sizes (17 and 38 μm for Au@SiO<sub>2</sub>-C<sub>3</sub> and Au@SiO<sub>2</sub>, respectively). Taking advantage of the emulsion properties and precise positioning of the ultra-small gold nanoparticles at oil/water interfaces, the Au@SiO<sub>2</sub>-C<sub>3</sub> NPs exhibit a remarkable catalytic performance under **base-free conditions**,

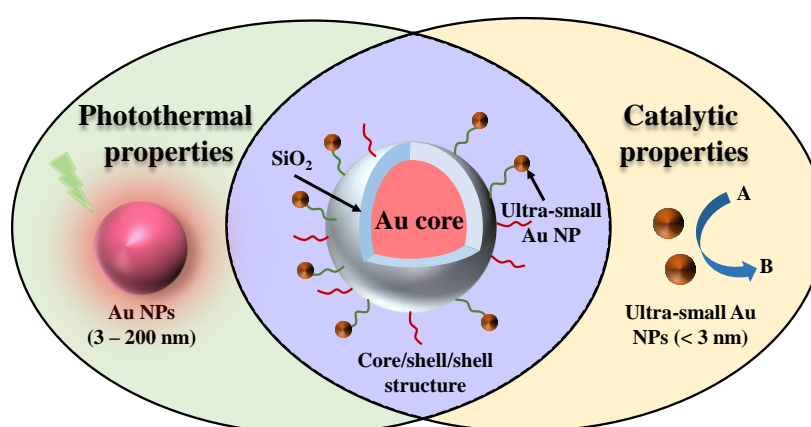
resulting in a benzyl alcohol conversion of 87% with the selectivity of 92% to benzaldehyde within 3 h at 80 °C. The yield of **benzaldehyde** is actually 1.5 times higher than the yield obtained in single oil phase catalysis system while the high selectivity of **benzoic acid** can be obtained with hydrophilic Au@SiO<sub>2</sub> catalysts in aqueous phase catalysis system with the addition of base. Moreover, the prepared Au@SiO<sub>2</sub>-C<sub>3</sub> NPs could be recycled and reused for at least four runs without apparent loss of activity. The enhanced catalytic performance is attributed to the increased interfacial area and the precise positioning of catalytic sites at the water/oil interface.

Finally, we have developed another types of Pickering nanoparticles based on **PEG-functionalized silica** which were obtained *via* a **one-step method** and which present an additional property for the elaboration of **temperature-responsive Pickering emulsions (Chapter IV)**. Thus, emulsions stabilized with **SiO<sub>2</sub>@mPEG 550 nanoparticles** undergo a clear destabilization with temperature (from room temperature to 80 °C) whatever the nature of the oil. The temperature responsive behavior can be attributed to the hydrophilic/hydrophobic balance of the PEG/mPEG chain at different temperature. This work has been published in *Colloids and Surfaces A: Physicochemical and Engineering Aspects*. By introducing tungstophosphoric acid H<sub>3</sub>PW<sub>12</sub>O<sub>40</sub> (POMs) onto the surface of the SiO<sub>2</sub>@PEG nanoparticles *via* self-assembly, the fabrication of PIC system for catalytic oxidation could be envisaged. Stable O/W Pickering emulsions can actually be stabilized by the combination of SiO<sub>2</sub>@PEG and POM with high emulsion volume (up to 88%) and uniform droplet size (12 μm). The catalytic performance of the prepared SiO<sub>2</sub>@PEG-POM NPs shows an **11-fold catalytic activity enhancement** in the emulsion system for the oxidation of cyclooctene compared to a simply stirred W/O and not stabilized biphasic system. The creation of a large contact area in the emulsion system is proposed to alleviate the diffusion barrier between oil-soluble and water-soluble reactants in favor of the catalytic activity enhancement.

Despite the great progress over the past few years regarding the fabrication and application of PIC systems, there is still considerable room to explore novel amphiphilic catalysts, especially using emulsifiers in combination with noble metallic nanoparticles, alloy

nanoparticles, or bio-substances. The precise design of the amphiphilic catalysts should greatly improve the catalytic performance with the construction of Pickering emulsion. Besides, the future opportunities and challenges of the PIC concept are specified as follows, in terms of material design and “**smart**” control PIC process.

The combination of Au/SiO<sub>2</sub>-C<sub>3</sub> and [C<sub>12</sub>]<sub>3</sub>[PW<sub>12</sub>O<sub>40</sub>] nanoparticles was found to efficiently catalyze the oxidation of olefins in emulsion under light irradiation, while ultra-small gold nanoparticles exhibited good catalytic activity in PIC system. As a perspective, two types of Au NPs can be merged into a multifunctional nanomaterial (**Figure 3**).

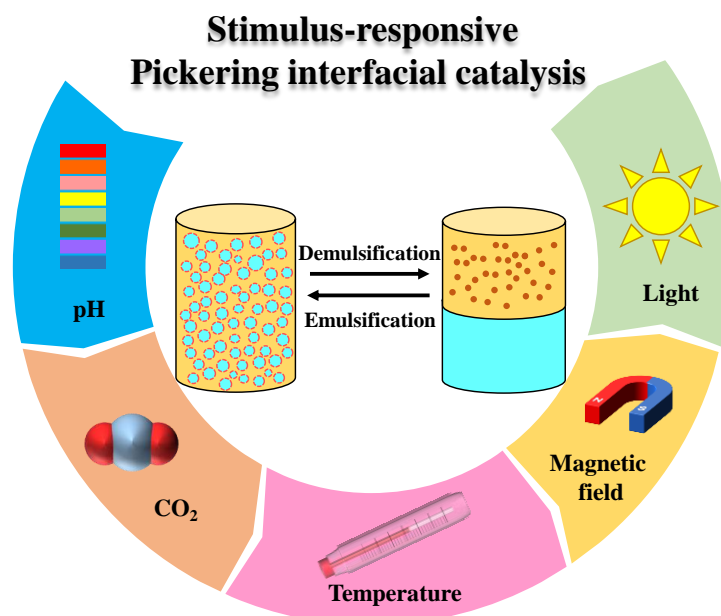


**Figure 3.** Schematic illustration of the multifunctional catalysts combining photothermal and catalytic properties.

Au NPs can be embedded in silica NPs to form a core/shell structure, followed by organosilane coating process that render the surface-active properties. Then, ultra-small Au NPs can be attached onto silica surface. By constructing plasmonic photothermal catalysts, **dual-functional roles (hot carrier excitation and photothermal conversion)** can synergistically contribute to the chemical reaction [1, 2]. The utilization of multifunctional catalysts under **plasmonic photothermal technology** could efficiently improve conversion efficiency under mild reaction conditions.

There has also been booming interest in the development of **switchable Pickering emulsions** (emulsification/demulsification or phase inversion), which are triggered by surface wettability change response to the external stimuli [3-5]. The smart control of the Pickering emulsions opens a new route for integrating the *in situ* catalyst recovery and product

**separation** during the catalytic reaction (**Figure 4**). Especially, external force (such as light, magnetic field and temperature) are attractive approach to control the stability of the emulsion because of the easy operation and no addition of extra components [6-8].



**Figure 4.** Schematic illustration of the stimulus-responsive Pickering interfacial catalysis system.

It is noteworthy that temperature has attracted considerable interest as a trigger for Pickering emulsions which provides a simple way to change reversibly the behavior of the system. Generally speaking, emulsions are often destabilized by increasing the temperature. However, catalytic reactions often require high temperatures to get good reaction activity. The balance point between rapid demulsification of emulsions and high stability is a front-burner issue to build “smart” PIC system. The construction of the more sophisticated emulsifiers endows with stimuli responsiveness or bifunctionality needs to be further systematically explored and requires the in-depth study in the application of the PIC system.



## References

- [1] S. Luo, X. Ren, H. Lin, H. Song, J. Ye, Plasmonic photothermal catalysis for solar-to-fuel conversion: current status and prospects, *Chemical Science* 12(16) (2021) 5701-5719.
- [2] J. Zhang, Y. Li, J. Sun, H. Chen, Y. Zhu, X. Zhao, L.-C. Zhang, S. Wang, H. Zhang, X. Duan, Regulation of energetic hot carriers on Pt/TiO<sub>2</sub> with thermal energy for photothermal catalysis, *Applied Catalysis B: Environmental* 309 (2022) 121263.
- [3] J. Tang, P.J. Quinlan, K.C. Tam, Stimuli-responsive Pickering emulsions: recent advances and potential applications, *Soft Matter* 11(18) (2015) 3512-3529.
- [4] F. Chang, C.M. Vis, W. Ciptonugroho, P.C. Bruijninx, Recent developments in catalysis with Pickering Emulsions, *Green Chemistry* 23(7) (2021) 2575-2594.
- [5] L. Ni, C. Yu, Q. Wei, D. Liu, J. Qiu, Pickering Emulsion Catalysis: Interfacial Chemistry, Catalyst Design, Challenges, and Perspectives, *Angewandte Chemie International Edition* (2022).
- [6] Z. Li, Y. Shi, A. Zhu, Y. Zhao, H. Wang, B.P. Binks, J. Wang, Light-responsive, reversible emulsification and demulsification of oil-in-water pickering emulsions for catalysis, *Angewandte Chemie* 133(8) (2021) 3974-3979.
- [7] T. Yang, Y. Zhang, J. Wang, F. Huang, M. Zheng, Magnetic switchable pickering interfacial biocatalysis: one-pot cascade synthesis of phytosterol esters from high-acid value oil, *ACS Sustainable Chemistry & Engineering* 9(36) (2021) 12070-12078.
- [8] C. Wang, H. Chi, F. Zhang, X. Wang, J. Wang, H. Zhang, Y. Liu, X. Huang, Y. Bai, K. Xu, Temperature-responsive Pickering high internal phase emulsions for recyclable efficient interfacial biocatalysis, *Chemical science* 13(30) (2022) 8766-8772.


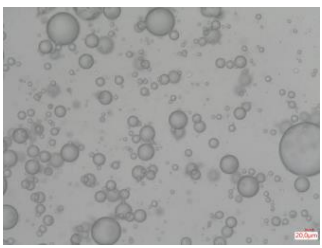
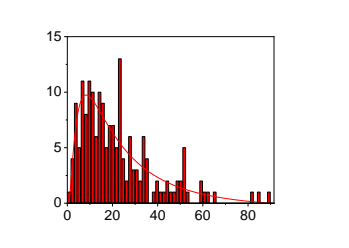

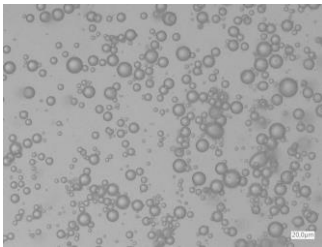
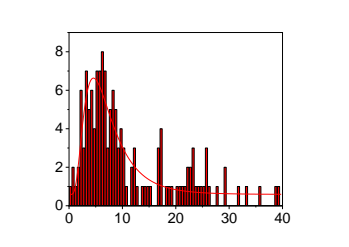
# Appendix

## Appendix 1 Detailed information of Pickering emulsion for chapter II

### A 1.1 Pickering emulsion stabilized by the combination of two NPs.

Reaction conditions: 80 mg NPs, 1.5 mL toluene, 1.5 mL H<sub>2</sub>O, emulsified with Ultra-Turrax at 11500 rpm for 2 min, the microscopic observations were monitored after 6 h.

**Table A-1 Emulsion stabilized by mixture of Au/SiO<sub>2</sub>-C<sub>3</sub> and [C<sub>12</sub>]<sub>3</sub>[PW<sub>12</sub>O<sub>40</sub>] with different mixing ratio.**

[C <sub>12</sub> ] <sub>3</sub> [PW <sub>12</sub> O <sub>40</sub> ]/ Au/SiO <sub>2</sub> -C <sub>3</sub> ratio (wt.%)	Photo	Emulsion volume ratio	Microscopic photograph (X400)	Distribution of the droplet size	Droplet size (μm)	PDI
0/100		0.85			21.9	0.9
20/80		0.97			6.4	0.5


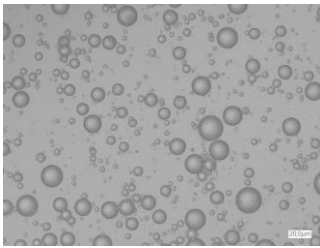
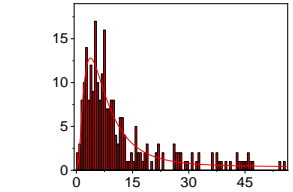

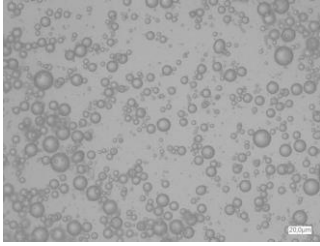
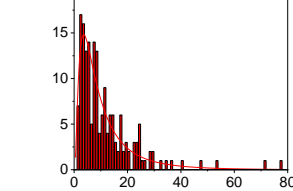

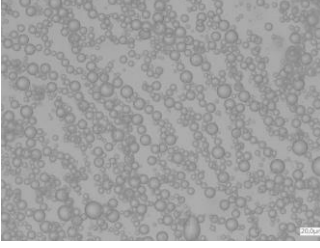
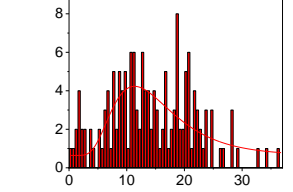

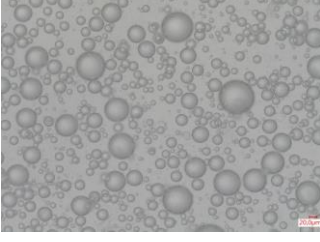
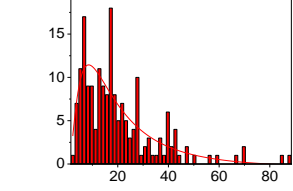

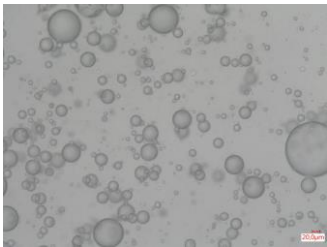
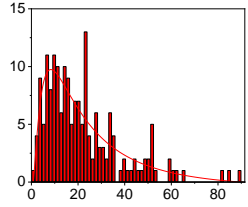

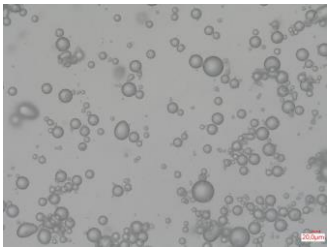
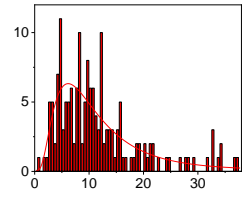

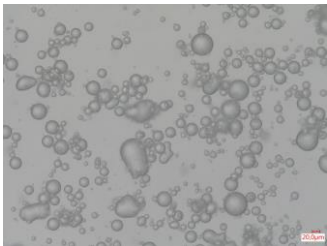
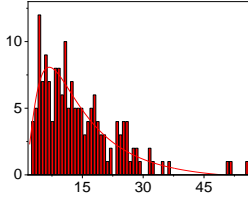

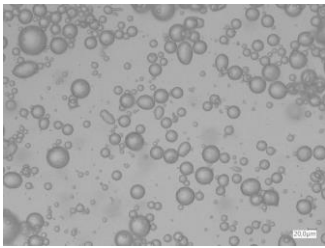
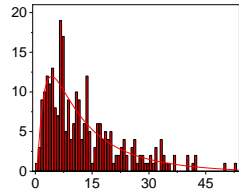

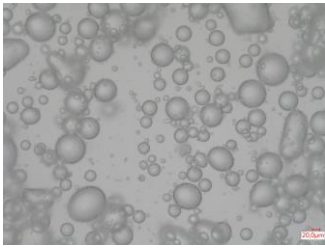
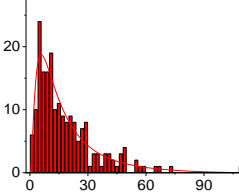

40/60		0.96			6.9	0.7
60/40		0.92			8.0	0.8
20/80		0.85			9.6	0.7
100/0		0.80			18.1	0.8

Table A-2 Emulsion stabilized by mixture of Au/SiO<sub>2</sub>-C<sub>3</sub> and H<sub>3</sub>PW<sub>12</sub>O<sub>40</sub> with different mixing ratio.

H <sub>3</sub> PW <sub>12</sub> O <sub>40</sub> / Au/SiO <sub>2</sub> -C <sub>3</sub> ratio (wt.%)	Photo	Emulsion volume ratio	Microscopic photograph (X400)	Distribution of the droplet size	Droplet size (μm)	PDI
0/100		0.85			21.9	0.9
20/80		0.86			9.6	0.6
40/60		0.92			13.1	0.8

60/40		0.91			11.6	0.9
20/80		0.72			14.8	0.9
100/0		/	/	/	/	/

### A 1.2 Pickering emulsion stabilized by the combination of two NPs with different parameters.

Reaction conditions: certain amount of NPs, 1.5 mL oil, 1.5 mL H<sub>2</sub>O, emulsified with Ultra-Turrax at 11500 rpm for 2 min, the microscopic observations were monitored after 6 h.

**Table A-3 Emulsion stabilized by a mixture of Au/SiO<sub>2</sub>-C<sub>3</sub> and [C<sub>12</sub>]<sub>3</sub>[PW<sub>12</sub>O<sub>40</sub>] with different oil and recycled NPs.**


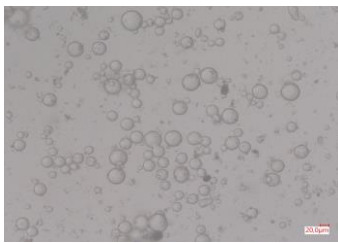
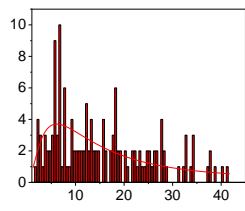

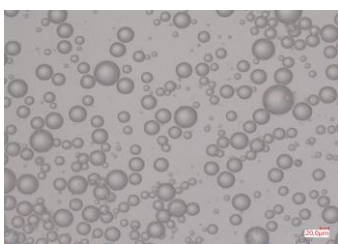
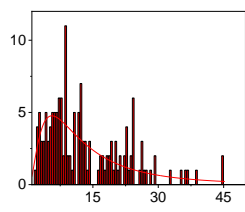

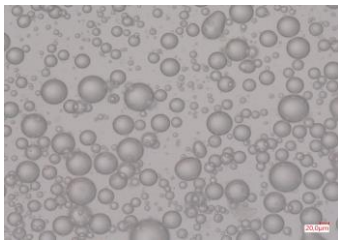
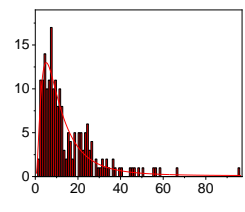

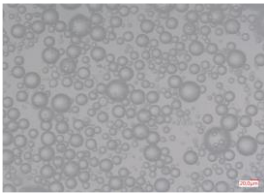
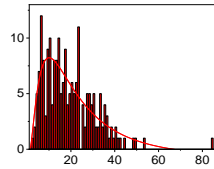

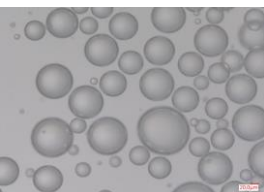
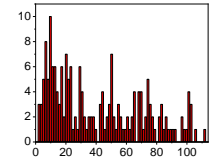

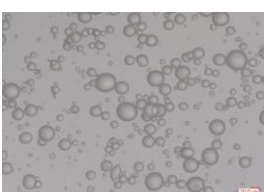
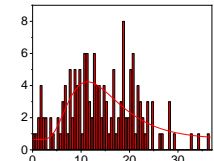


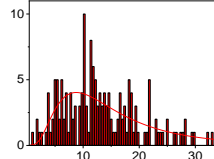
Emulsifiers	Photo	Oil type	Water/oil ratio	Emulsion volume ratio	Microscopic photograph (X400)	Distribution of the droplet size	Droplet size (μm)	PDI
1.0 wt.% Au/SiO <sub>2</sub> -C <sub>3</sub> + 1.8 wt.% [C <sub>12</sub> ] <sub>3</sub> [PW <sub>12</sub> O <sub>40</sub> ]		heptane	50/50	0.98			13.7	0.9
0.5 wt.% Au/SiO <sub>2</sub> -C <sub>3</sub> + 1.8 wt.% [C <sub>12</sub> ] <sub>3</sub> [PW <sub>12</sub> O <sub>40</sub> ]		Toluene	50/50	0.83			11.3	0.8
1.0 wt.% Au/SiO <sub>2</sub> -C <sub>3</sub> + 1.8 wt.% [C <sub>12</sub> ] <sub>3</sub> [PW <sub>12</sub> O <sub>40</sub> ]		Toluene	65/35	1.00			10.0	0.8


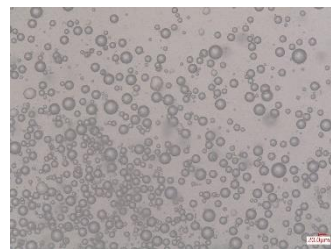
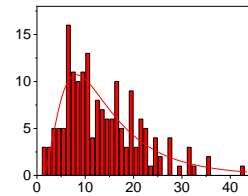
Table A-4 Emulsion stabilized by single SiO<sub>2</sub>-C<sub>3</sub>, single [C<sub>12</sub>]<sub>3</sub>[PW<sub>12</sub>O<sub>40</sub>], and the mixture of SiO<sub>2</sub>-C<sub>3</sub> and [C<sub>12</sub>]<sub>3</sub>[PW<sub>12</sub>O<sub>40</sub>] or H<sub>3</sub>PW<sub>12</sub>O<sub>40</sub>.

Emulsifiers	Photo	Emulsion volume ratio	Microscopic photograph (X400)	Distribution of the droplet size	Droplet size (μm)	PDI
1.8 wt.% [C <sub>12</sub> ] <sub>3</sub> [PW <sub>12</sub> O <sub>40</sub> ]		0.81			20.8	0.8
1.0 wt.% SiO <sub>2</sub> -C <sub>3</sub>		0.88			42.5	/
1.0 wt.% SiO <sub>2</sub> -C <sub>3</sub> + 1.8 wt.% H <sub>3</sub> PW <sub>12</sub> O <sub>40</sub>		0.88			14.1	0.4
1.0 wt.% SiO <sub>2</sub> -C <sub>3</sub> + 1.8 wt.% [C <sub>12</sub> ] <sub>3</sub> [PW <sub>12</sub> O <sub>40</sub> ]		0.85			13.0	0.6

### A 1.3 Pickering emulsion stabilized by the recycled NPs.

Reaction conditions: Recycled Au/SiO<sub>2</sub>-C<sub>3</sub> and [C<sub>12</sub>]<sub>3</sub>[PW<sub>12</sub>O<sub>40</sub>] NPs, 1.5 mL toluene, 1.5 mL H<sub>2</sub>O, emulsified with Ultra-Turrax at 11500 rpm for 2 min, the microscopic observations were monitored after 6 h.

**Table A-5 Emulsion stabilized by recycled Au/SiO<sub>2</sub>-C<sub>3</sub> and [C<sub>12</sub>]<sub>3</sub>[PW<sub>12</sub>O<sub>40</sub>].**


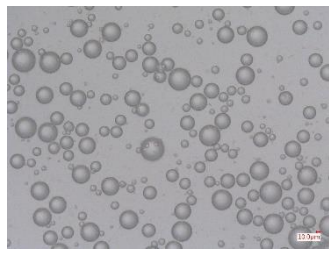
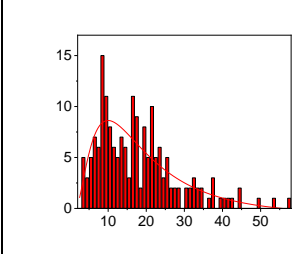

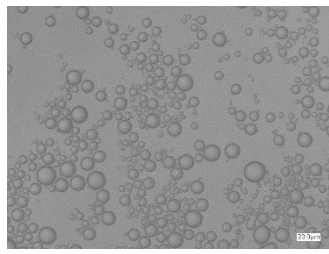
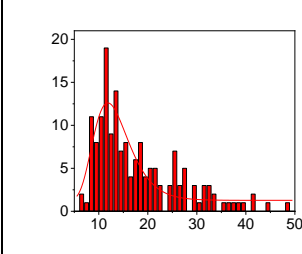
Emulsifiers	Photo	Oil type	Emulsion volume ratio	Microscopic photograph (X400)	Distribution of diameter	Droplet size (μm)	PDI
Recycled 1.0 wt.% Au/SiO <sub>2</sub> -C <sub>3</sub> + 1.8 wt.% [C <sub>12</sub> ] <sub>3</sub> [PW <sub>12</sub> O <sub>40</sub> ]		Toluene	0.86			12.6	0.6



## Appendix 2 Detailed information of Pickering emulsion for chapter III

Reaction conditions: 75 mg Au@SiO<sub>2</sub>-C<sub>3</sub> or Au@SiO<sub>2</sub> NPs, 1.5 mL toluene, 1.5 mL H<sub>2</sub>O, emulsified with Ultra-Turrax at 11500 rpm for 2 min, the microscopic observations were monitored after 12 h.

**Table A-6 Emulsion stabilized by ultra-small Au@SiO<sub>2</sub>-C<sub>3</sub>.**

Emulsifiers	Photo	Oil type	Emulsion type	Emulsion volume ratio	Microscopic photograph (X400)	Distribution of diameter	Droplet size (μm)	PDI
2.7 wt.% Au@SiO <sub>2</sub> -C <sub>3</sub>		Toluene	W/O	0.85			17.4	0.7
2.7 wt.% Au@SiO <sub>2</sub> -C <sub>3</sub>		Cyclohexane	W/O	0.81			14.0	0.3


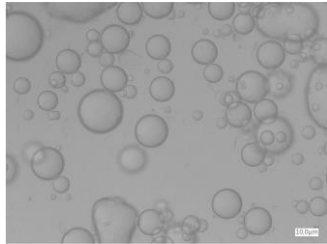
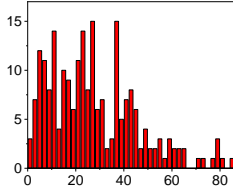

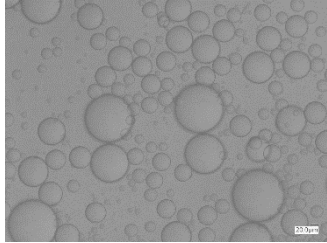
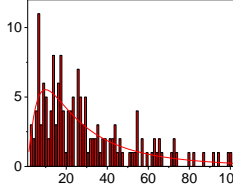

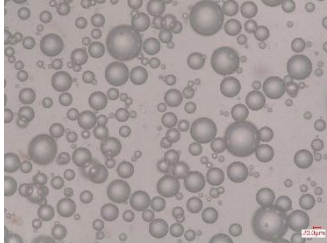
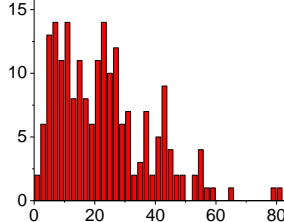
2.7 wt.% Au@SiO <sub>2</sub> -C <sub>3</sub>		Heptane	W/O	0.8			29.1	/
2.7 wt.% Au@SiO <sub>2</sub>		Heptane	O/W	0.65			38	0.9


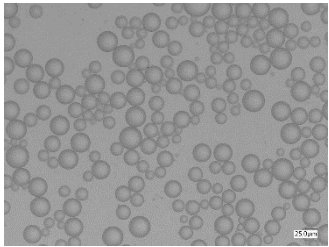
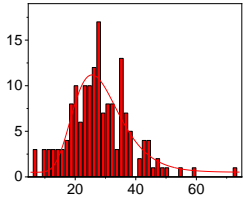

Table A-7 Emulsion stabilized by recycled Au@SiO<sub>2</sub>-C<sub>3</sub> NPs.


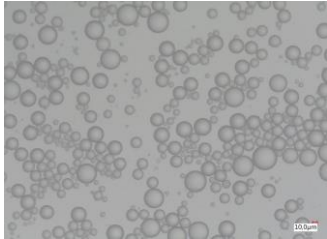
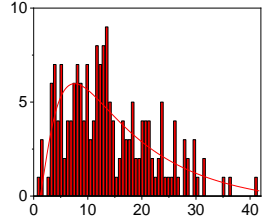

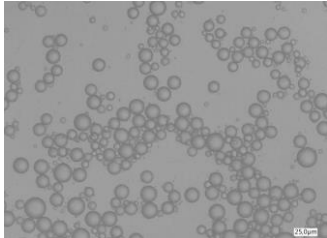
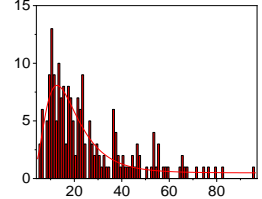

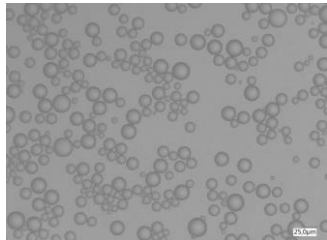
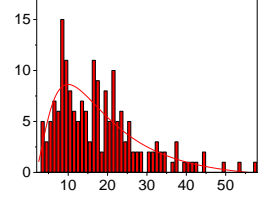

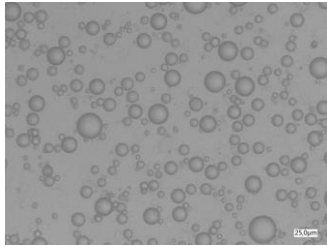
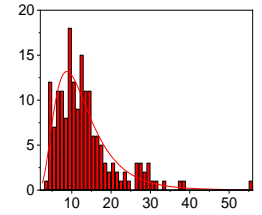
Emulsifiers	Photo	Oil type	Emulsion type	Emulsion volume ratio	Microscopic photograph (X400)	Distribution of diameter	Droplet size (μm)	PDI
Recycled Au@SiO <sub>2</sub> -C <sub>3</sub>		Toluene	W/O	0.82			29.6	/

### Appendix 3 Detailed information of Pickering emulsion for chapter IV

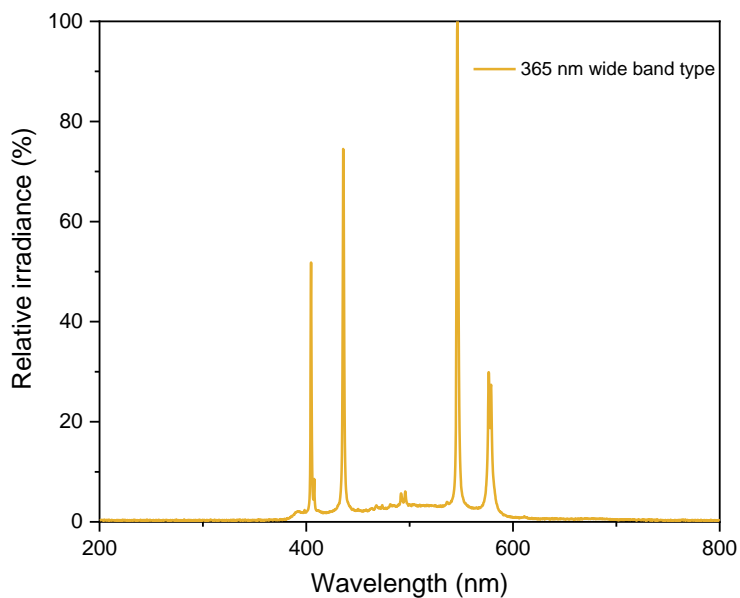
Reaction conditions: 42 mg  $\text{SiO}_2@m\text{PEG}$ , 88 mg  $\text{H}_3\text{PW}_{12}\text{O}_{40}$ , 1.5 mL toluene, 1.5 mL  $\text{H}_2\text{O}$ , emulsified with Ultra-Turrax at 11500 rpm for 2 min, the microscopic observations were monitored after one day.

**Table A-8 Emulsion stabilized by single  $\text{SiO}_2@m\text{PEG}$  and the mixture of  $\text{SiO}_2@m\text{PEG}$  and  $\text{H}_3\text{PW}_{12}\text{O}_{40}$ .**

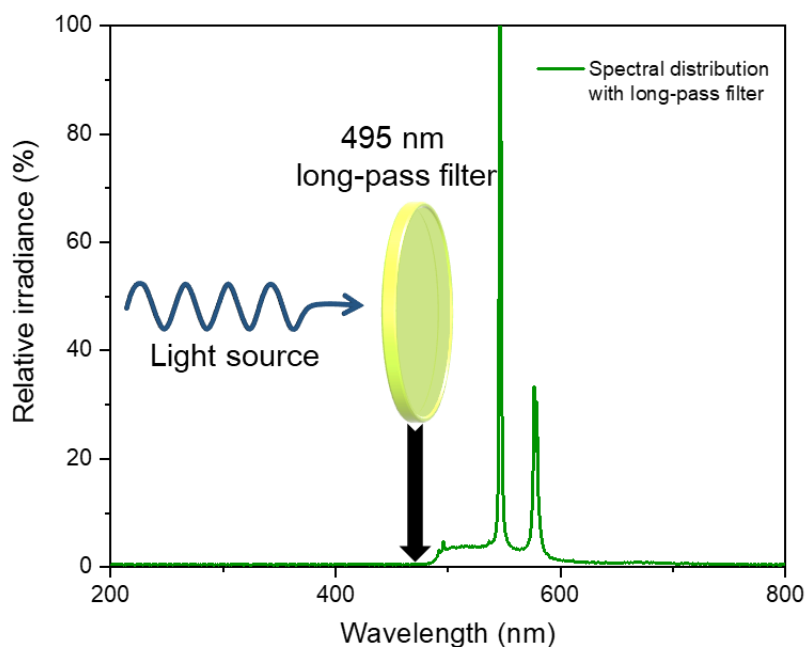
Emulsifiers	Photo	Emulsion type	Emulsion volume ratio	Microscopic photograph (X400)	Distribution of diameter	Droplet size ( $\mu\text{m}$ )	PDI
1.5 wt.% $\text{SiO}_2@m\text{PEG}$ 550		O/W	0.68			29.7	0.6
1.5 wt.% $\text{SiO}_2@m\text{PEG}$ 550 + 3.0 wt.% $\text{H}_3\text{PW}_{12}\text{O}_{40}$		/	/	/	/	/	/

1.5 wt.% SiO <sub>2</sub> @mPEG 2000		O/W	0.69			18.8	0.5
1.5 wt.% SiO <sub>2</sub> @mPEG 2000 + 3.0 wt.% H <sub>3</sub> PW <sub>12</sub> O <sub>40</sub>		O/W	0.74			16.9	0.5
1.5 wt.% SiO <sub>2</sub> @mPEG 5000		O/W	0.68			18.2	0.2
1.5 wt.% SiO <sub>2</sub> @mPEG 5000 + 3.0 wt.% H <sub>3</sub> PW <sub>12</sub> O <sub>40</sub>		O/W	0.88			11.5	0.5

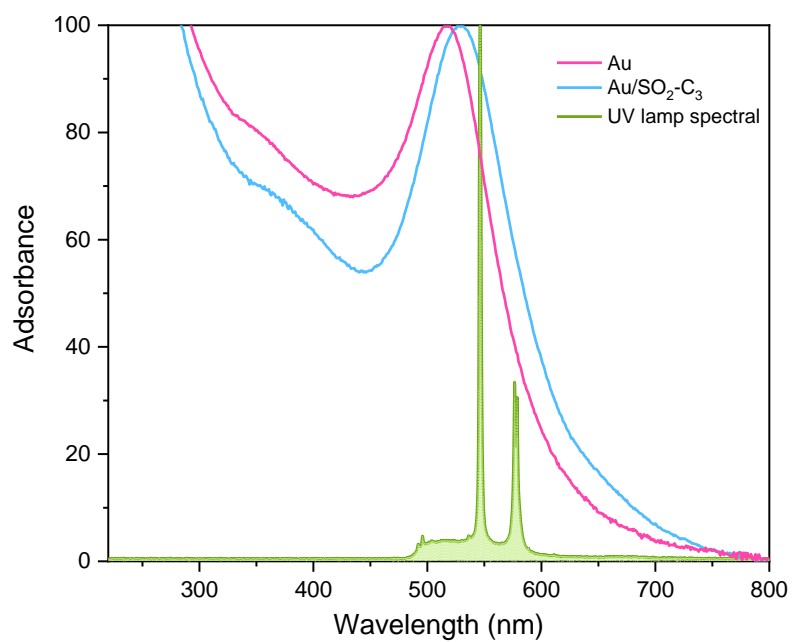
## Appendix 4 The UV spectral distribution of the lamp for chapter II



**Figure A-1.** The select wavelength range in the UV lamp and the measured power is 800 mW.



**Figure A-2.** The select wavelength range matched with 495 nm long-pass filter in the UV lamp. The measured power is 380 mW.



**Figure A-3.** The absorption spectra of Au dispersion, Au/SiO<sub>2</sub>-C<sub>3</sub> dispersion and the cutted spectral distribution of UV lamp. The overlapped area are the real absorption wavelength during the reaction.

## Appendix 5 Product identification for chapter II

### A 5.1. starting substrates

(1) Cyclooctene

$^1\text{H NMR}$  ( $\text{CDCl}_3$  as solvent):  $\delta$  (ppm) = 1.47 (m, 4H  $\text{CH}_2$ ), 2.14 (m, 4H,  $\text{CH}_2$ ), 5.78 (m, 2H,  $\text{CH}=\text{CH}$ ).

(2) Cyclohexene

$^1\text{H NMR}$  ( $\text{CDCl}_3$  as solvent):  $\delta$  (ppm) = 1.61 (m, 4H  $\text{CH}_2$ ), 1.98 (m, 4H,  $\text{CH}_2$ ), 5.67 (m, 2H,  $\text{CH}=\text{CH}$ ).

(3) Limonene

$^1\text{H NMR}$  ( $\text{CDCl}_3$  as solvent):  $\delta$  (ppm) = 1.65 (m, 3H  $\text{CH}_3$ ), 1.73 (m, 3H,  $\text{CH}_3$ ), 1.19 to 2.37 (m, 7H,  $\text{CH}_2$ ), 4.70 (m, 2H,  $\text{CH}=\text{CH}$ ), 5.40 (m, 1H, C-H)

(4) 1-octene

$^1\text{H NMR}$  ( $\text{CDCl}_3$  as solvent):  $\delta$  (ppm) = 0.87 (m, 3H,  $\text{CH}_3$ ), 1.04 to 1.53 (m, 8H,  $\text{CH}_2$ ), 2.02 (m, 2H,  $\text{CH}_2$ ), 4.91 (m, 1H, C-H), 4.97 (m, 1H, C-H), 5.77 (m, 1H, C-H)

### A 5.2. Epoxidation products

(1) Cyclooctene oxide

$^1\text{H NMR}$  ( $\text{CDCl}_3$  as solvent):  $\delta$  (ppm) = 1.21-2.02 (m, overlaid peaks,  $\text{CH}_2$ ), 3.10 (m, 2H,  $\text{CH}_2\text{-CO}$  epoxide).

(2) Cyclohexene oxide

$^1\text{H NMR}$  ( $\text{DMSO-d}_6$  as solvent):  $\delta$  (ppm) = 1.11 (m, 4H,  $\text{CH}_2$ ), 1.54-1.76 (2 peaks, 4H, axial and equatorial  $\text{CH}_2$ ), 3.10 (s, 2H,  $\text{CH-O}$ ), the peak of OH is often due to the presence of humidity.

(3) 1,2-Cyclohexanediol

$^1\text{H NMR}$  ( $\text{CDCl}_3$  as solvent):  $\delta$  (ppm) = 1.21-2.02 (m, overlaid peaks,  $\text{CH}_2$ ), 3.10 (m, 2H,  $\text{CH}_2\text{-CO}$  epoxide).

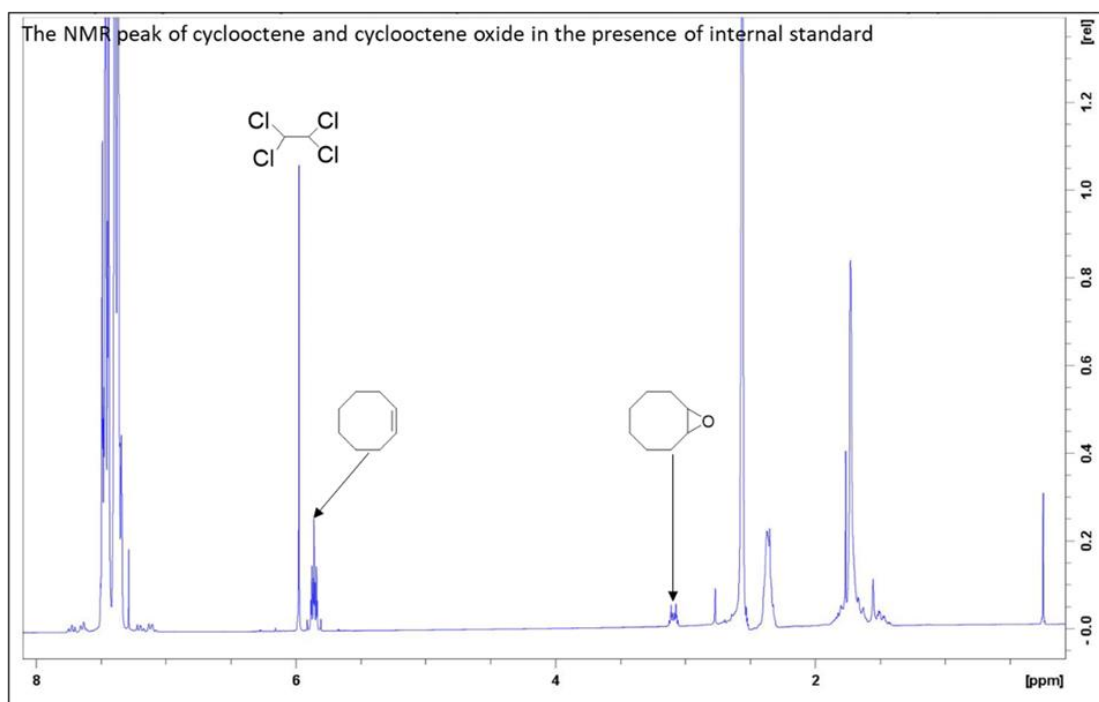
(4) Limonene oxide

$^1\text{H NMR}$  ( $\text{CDCl}_3$  as solvent):  $\delta$  (ppm) = 1.22 (m, 3H  $\text{CH}_3$ ), 1.60 (m, 3H,  $\text{CH}_3$ ), 1.72 to 2.17 (m, 7H,  $\text{CH}_2$ ), 3.05 (m, 1H,  $\text{CH-CO}$ ), 4.63 (m, 2H,  $\text{CH}=\text{CH}$ ).

(5) 1,2-epoxyoctane

$^1\text{H NMR}$  ( $\text{CDCl}_3$  as solvent):  $\delta$  (ppm) = 0.91 (m, 3H  $\text{CH}_3$ ), 1.31 (m, 8H,  $\text{CH}_2$ ), 1.46 (m, 1H, C-H), 1.53 (m, 1H, C-H), 2.47 (m, 1H,  $\text{CH-CO}$  epoxide), 2.91 (m, 1H,  $\text{CH-CO}$  epoxide)

## A 5.3. NMR spectra



**Figure A-4.**  $^1\text{H}$  NMR spectra of cyclooctene and cyclooctene oxide in the presence of  $\text{C}_2\text{H}_2\text{Cl}_4$  as internal standard and toluene used as solvent.



## Appendix 6 Product identification for chapter III

### A 5.1 substrate and product

(1) Benzyl alcohol

$^1\text{H}$  NMR ( $\text{CDCl}_3$  as solvent):  $\delta$  (ppm) = 2.3 (m, 1H O-H), 4.59 (m, 2H,  $\text{CH}_2$ ), 7.40 to 7.19 (m, 5H, C-H).

(2) Benzaldehyde

$^1\text{H}$  NMR ( $\text{CDCl}_3$  as solvent):  $\delta$  (ppm) = 7.51 (m, 2H C-H), 7.61 (m, 1H, C-H), 7.87 (m, 2H, C-H), 10.0 (m, 1H, C-H).

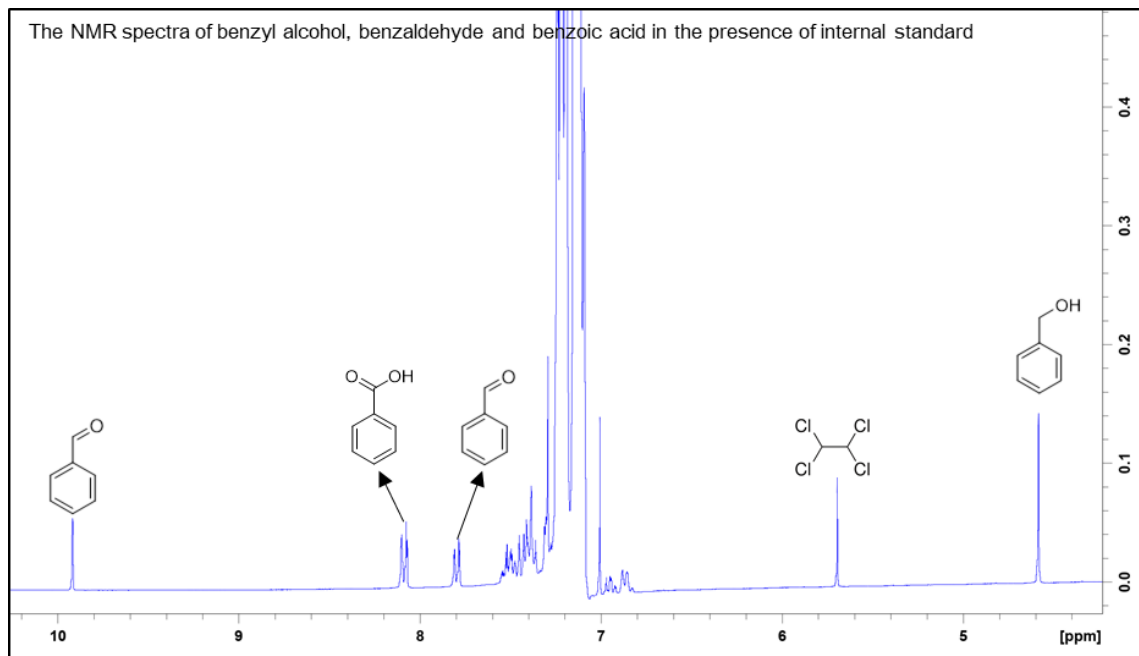
(3) Benzoic acid

$^1\text{H}$  NMR ( $\text{CDCl}_3$  as solvent):  $\delta$  (ppm) = 7.45 (m, 2H C-H), 7.62 (m, 1H, C-H), 8.12 (m, 2H, C-H), 12.09 (m, 1H, O-H).

(4) Benzyl benzoate

$^1\text{H}$  NMR ( $\text{CDCl}_3$  as solvent):  $\delta$  (ppm) = 5.354 (m, 2H,  $\text{CH}_2$ ), 7.46 to 7.26 (m, 5H, C-H), 7.41 (m, 2H, C-H), 7.55 (m, 1H, C-H), 8.07 (m, 2H, C-H).

### A 5.2. NMR spectra



**Figure A-5.**  $^1\text{H}$  NMR spectra of benzyl alcohol, benzaldehyde and benzoic acid in the presence of  $\text{C}_2\text{H}_2\text{Cl}_4$  as internal standard and toluene used as solvent.

## Appendix 7 Product identification for chapter IV

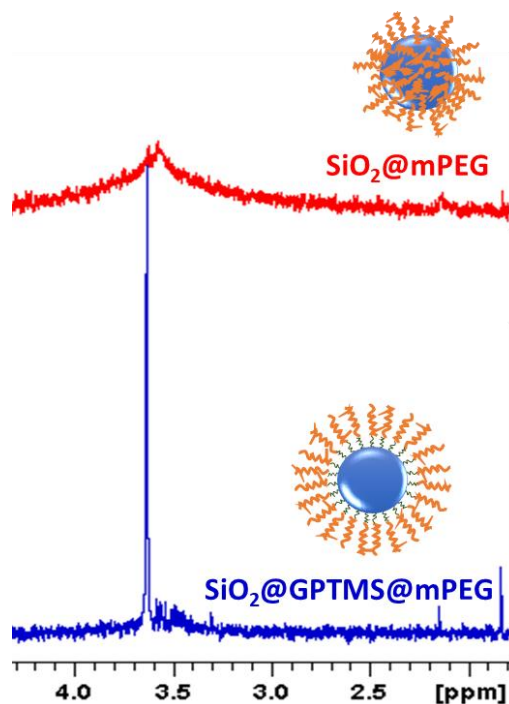


Figure A-6. <sup>1</sup>H NMR spectra of SiO<sub>2</sub>@mPEG 5000 and SiO<sub>2</sub>@GPTMS@mPEG 5000

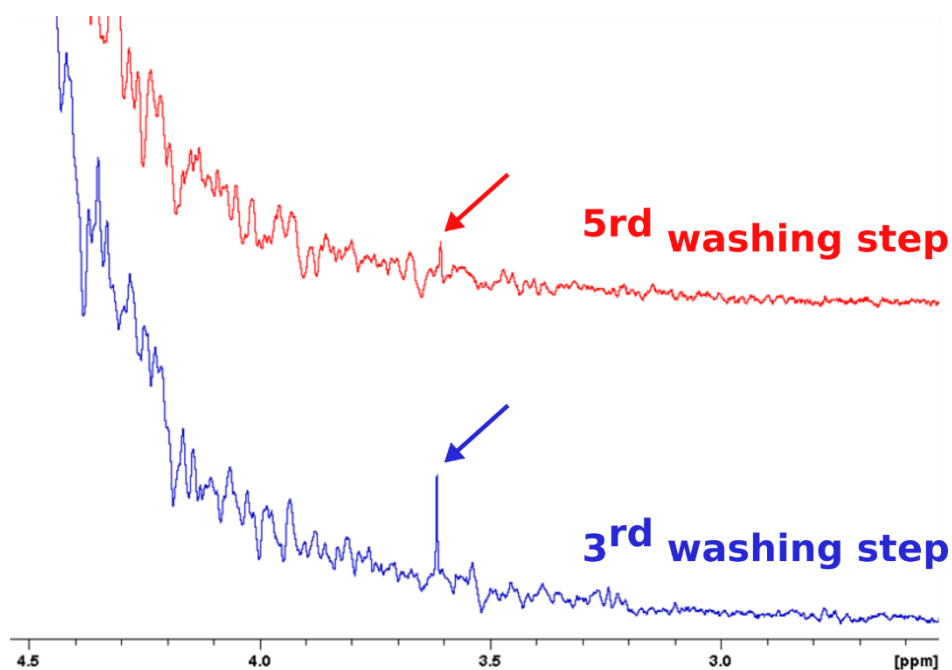
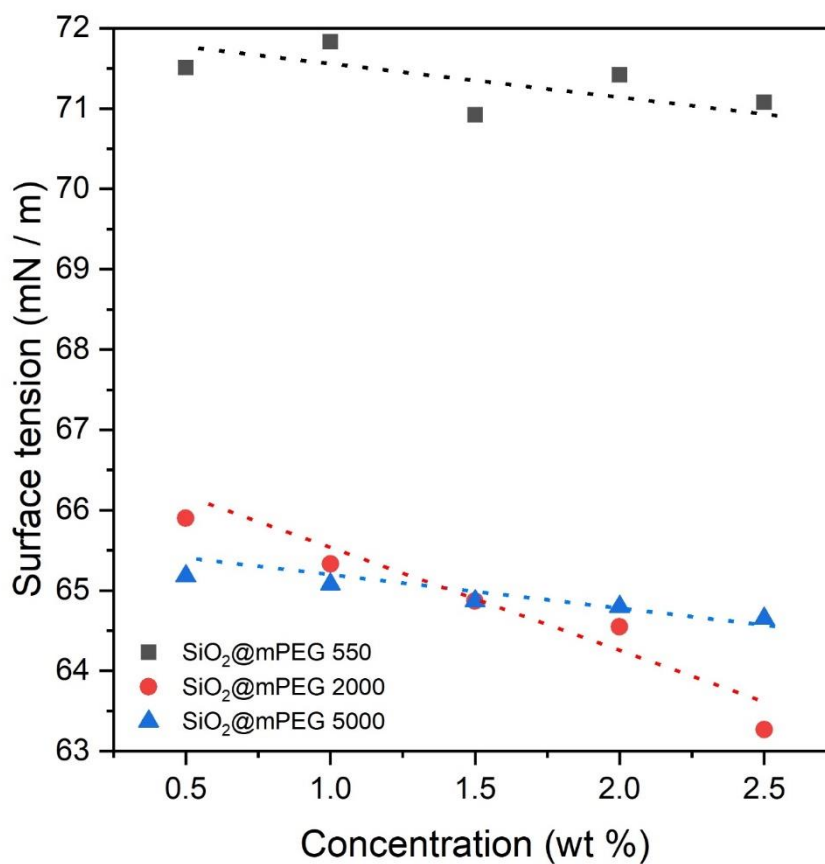


Figure A-7. <sup>1</sup>H NMR spectra of the aqueous supernatant after 3 (blue) and 5 (red) washing steps of SiO<sub>2</sub>@mPEG 5000 NPs.



**Figure A-8.** Surface tension of aqueous suspensions of SiO<sub>2</sub>@mPEG 550, SiO<sub>2</sub>@mPEG 2000 and SiO<sub>2</sub>@mPEG 5000 NPs as a function of concentration.

## Appendix 8 Published article

Colloids and Surfaces A: Physicochemical and Engineering Aspects 631 (2021) 127641



Contents lists available at ScienceDirect

## Colloids and Surfaces A: Physicochemical and Engineering Aspects

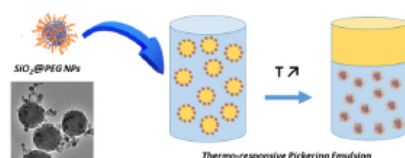
journal homepage: [www.elsevier.com/locate/colsurfa](http://www.elsevier.com/locate/colsurfa)

## Temperature-responsive Pickering emulsions stabilized by poly(ethylene glycol)-functionalized silica particles

Jean-François Dechezelles<sup>\*,1</sup>, Yaoyao Feng<sup>2</sup>, Fadi Fadil<sup>3</sup>, Véronique Nardello-Rataj<sup>\*,4</sup>

Université de Lille, CNRS, Centrale Lille, Université Artois, UMR 8181 - UCCS - Unité de Catalyse et Chimie du Solide, F-59000 Lille, France

## GRAPHICAL ABSTRACT



## ARTICLE INFO

**Keywords:**  
Pickering emulsion  
PEG  
Functionalized silica  
Temperature-responsive nanoparticles

## ABSTRACT

A series of PEG-functionalized silica nanoparticles with various molecular weight (MW 200, 400, 550, 2000, 5000 g.mol<sup>-1</sup>) have been prepared through a one-step synthesis and further used for the elaboration of temperature-responsive Pickering. The physicochemical properties of the nanoparticles were determined by TEM, TGA, DLS, surface tension and zeta potential measurements and the formed emulsions have been characterized by optical microscopy. The ability of SiO<sub>2</sub>@mPEG 550 to form temperature-responsive emulsions with oils of different nature has been explained by the hydrophilic/hydrophobic balance of the PEG/mPEG chains. The emulsions stabilized with PEG-functionalized SiO<sub>2</sub> NPs undergo a clear temperature-triggered destabilization from room temperature to 80 °C due to the modification of the distribution of the PEG/mPEG chain at the oil-water interface.

## 1. Introduction

Emulsions are metastable mixtures of two immiscible liquid phases - a dispersed phase and a continuous phase, e.g. oil and water - that is stabilized either by surfactant or by solid particles [1,2]. Particle-stabilized emulsions, also called Pickering emulsions, are more stable than conventional emulsions. Pickering emulsions may be useful

for reducing the surfactants amount and so, the risk for health and environment [3]. Although a long-term stability is generally the final aim of a formulation process for food, cosmetics, paints, etc., a transitory stability (i.e. on demand destabilization) might be wanted for other applications such as emulsions polymerization [4], oil recovery [5] or catalyst recovery [6] in order to collect the product of interest. In these cases, additional disruption mechanisms need to be introduced to

\* Corresponding authors.

E-mail addresses: [jean-francois.dechezelles@univ-lille.fr](mailto:jean-francois.dechezelles@univ-lille.fr) (J.-F. Dechezelles), [veronique.rataj-nardello@univ-lille.fr](mailto:veronique.rataj-nardello@univ-lille.fr) (V. Nardello-Rataj).

<sup>1</sup> ORCID: 0000-0002-4704-6404

<sup>2</sup> ORCID: 0000-0003-0551-9154

<sup>3</sup> ORCID: 0000-0002-9532-1901

<sup>4</sup> ORCID: 0000-0001-8065-997X

<https://doi.org/10.1016/j.colsurfa.2021.127641>

Received 5 May 2021; Received in revised form 13 September 2021; Accepted 26 September 2021

Available online 28 September 2021

0927-7757/© 2021 Elsevier B.V. All rights reserved.

achieve the destabilization of the system, which may increase the costs and the energy consumption.

Bare hydrophilic silica nanoparticles (NPs) can stabilize water/polar oil emulsions without any surface functionalization even if they are partially wet by these oils [7,8]. Although the use of bare silica NPs is costless and timeless compared to surface functionalized NP, it may be appropriate to functionalize the silica NPs surface for preparing emulsions with other types of oils and giving them additional functionalities. The grafting of silanes with specific functional groups is well known and controlled [9,10] and permits to enhance the wetting properties. The grafting of other types of materials is also possible, e.g. inorganic species (alumina, metals...) [11,12] or polymers [13–15] which allows the preparation of different types of emulsions.

The surface functionalization can limit the desorption of particles from interface, for instance, but also allows to add stimuli-responsive properties to the emulsions. Developing amphiphilic particles and changing their surface properties, in other words their wettability, in response to a stimulus is very promising. As a result, stimuli-responsive Pickering emulsions have gained increased amounts of attention in recent years. Thus, various trigger-responsive materials have been prepared leading to Pickering emulsions being responsive itself to the trigger such as temperature, pH, light, magnetic field [2,16–18]. Using temperature change for emulsion destabilization is one of the less invasive method to set up, compared to the addition of chemicals or change of the pH of the system. In addition, it can be reversible.

Polyethylene glycol (PEG), also called polyethylene oxide (PEO), and PEG methyl ether (mPEG) are water-soluble and temperature-responsive polymers [19]. The temperature increase induces a modification of the conformation of the polyoxoethylene chains (from polar to nonpolar due to dehydration of the ethylene oxide units) and emulsions stabilized with PEG-based surfactants can undergo a phase separation or a phase inversion (from oil-in-water to water-in-oil) [14,20–22]. Surface active particles are more attractive than surfactants since they form much more stable emulsions [23]. One approach to obtain a synergistic effect of a PEG-based surfactant and the highest stability provided by silica NPs has been studied by Yue Zhu et al. [24]. By combining silica NPs and polyoxyethylene monodecyl ethers ( $C_{10}E_n$ ), which adsorbs on the silica surface, they could obtain the formation of stable emulsions which are destabilized with temperature. However, the use of PEG adsorbed onto the silica surface may induce the release of some PEG molecules in one of the two phases when the emulsion is destabilized.

One way to overcome this issue is to covalently bind the PEG onto the silica NPs [21,25,26]. Although temperature-responsive Pickering emulsions prepared with PEG-functionalized silica particles has been reported in the literature [14,27], the preparation of the particles is a multi-step and time-consuming process - synthesis of NPs followed by the grafting of the different functional silanes.

Herein, we report on the elaboration and characterization of temperature-responsive Pickering emulsions stabilized with PEG-functionalized silica particles ( $SiO_2@PEG$ ). The particles were prepared through a one-step synthesis based on the hydrolysis and condensation of the silica precursor in the presence of PEG with various molecular weight (MW 200, 400, 550, 2000, 5000  $g\cdot mol^{-1}$ ). The physicochemical properties of the NPs have been thoroughly characterized before the preparation of emulsions. We find that  $SiO_2@mPEG$  550 NPs form temperature-responsive Pickering emulsions with oils of different nature. These emulsions undergo a clear temperature-triggered destabilization when heated from room temperature to 80 °C while no destabilization has been observed for emulsions stabilized with longer PEG chains (MW 2000 and 5000  $g\cdot mol^{-1}$ ). This work provides an interesting and easy approach to prepare temperature-responsive Pickering emulsions with PEG-modified silica particles that are synthesized via a one pot synthesis. Moreover, it demonstrates the possibility to stabilize emulsions without the presence of hydrophobic silanes on the silica surface.

## 2. Materials and methods

### 2.1. Chemicals

All chemicals were used as purchased. Tetraethyl orthosilicate (TEOS) (98 wt%, Sigma-Aldrich), ammonia (25 wt%, Chem Lab), absolute ethanol (VWR), poly(ethylene glycol) 200 (Sigma-Aldrich), poly(ethylene glycol) 400 (Sigma-Aldrich), poly(ethylene glycol)mono methyl ether 550 (Sigma-Aldrich), poly(ethylene glycol)mono methyl ether 2000 (Sigma-Aldrich), poly(ethylene glycol)mono methyl ether 5000 (Sigma-Aldrich), cyclopentyl methyl ether ( $\geq 99.9\%$ , Sigma Aldrich), toluene (99.85%, Acros Organics), heptane (Analytical reagent grade, Fischer Scientific), isopropyl myristate (Sigma Aldrich), paraffin oil (Cooper), squalane (99%, Acros Organics).  $D_2O$  (99.9%) was purchased from Euriso-top (France). All aqueous solutions were prepared with ultrapure water obtained from a Thermo Scientific system (12.2  $M\Omega\cdot cm$ , Millipore AG).

### 2.2. Synthesis of bare silica nanoparticles

The silica particles were synthesized following a procedure reported in the literature [28]. 13.5 mL of ultrapure water, 184 mL of absolute ethanol, and 41 mL of  $NH_4OH$  were mixed in a 500 mL round-bottom flask and stirred at 300 rpm at 40 °C. 11 mL of TEOS was added at once to the mixture. It was left stirring for 1 h with a reflux cooling. The particles suspension was purified by several cycles of centrifugation and redispersion.

### 2.3. One-pot synthesis of polyethylene glycol silica nanoparticles ( $SiO_2@PEG$ )

The  $SiO_2@PEG$  NPs were synthesized according to a protocol adapted from [29]. 6 mL of TEOS and 72 mL of ethanol were mixed under vigorous stirring for 5 min at 65 °C. 17.1 mL of water and 3.8 mL of ammonia were added. 3 g of PEG (or mPEG) dissolved in ethanol are added dropwise within 5 min. The mixture was stirred for one hour with reflux cooling. The particles were washed by centrifugation and transferred into ultrapure water.

### 2.4. Dynamic light scattering (DLS)

Dynamic light scattering (DLS) experiments were carried out using a light scattering goniometer instrument from LS Instruments (3D LS Spectrometer, Switzerland) equipped with a 25 mW He-Ne laser light source (JDS Uniphase) operating at  $\lambda = 632.8$  nm. The scattering spectrum was measured using two single-mode fiber detections and two high-sensitivity APD detectors (SPCM-AQR-13-FC, PerkinElmer). The samples were filled into cylindrical tubes with a diameter of 7.5 mm and placed in the temperature-controlled index matching bath, where the temperature was fixed at 25 °C. Measurements were performed at scattering angles of 90 °. The average hydrodynamic radius was obtained through a second order cumulant analysis.

### 2.5. $^1H$ NMR spectroscopy

The  $^1H$  NMR spectra were recorded on a Bruker Avance 300 at 300 MHz (Bruker, USA).  $D_2O$  was used as solvent for the analysis. Chemical shifts were given in ppm and were measured relative to the TMS.

### 2.6. Transmission electron microscopy

The transmission electron microscopy (TEM) micrographs were obtained on a TECNAI G2–20 Twin microscope (FEI, USA), equipped with a LaB6 filament operating at 200 kV. Two drops of nanoparticles suspension were deposited on a carbon–copper grid (CF200-Cu, Electron Microscopy Sciences, USA).

### 2.7. Thermogravimetric analysis (TGA)

Thermogravimetric analyses (TGA) were performed using a Q500 instruments (TA Instruments, USA). In a typical analysis, 10–15 mg product were placed in a Pt crucible. The sample was at first equilibrated at 120 °C, and then heated at 10 °C/min to 900 °C, under nitrogen.

### 2.8. Surface tension measurement

The surface tension measurements of sample were performed with a Krüss K100 tensiometer. In a typical experiment, the rod was immersed in the liquid studied at a rate of 10 mm.min<sup>-1</sup> and an immersion depth of 2 mm. Calibration with ultrapure water was carried out. For each measurement, the surface tension values were sampled every 3 s until the standard deviation was below 0.1 mN.m<sup>-1</sup>. Three measurements were taken in a row for each sample. No temperature correction was made to the previous measured values, since the observed deviations - between 0.1 and 0.7 mN.m<sup>-1</sup> - were larger than the temperature corrections, expected to be below 0.2 mN.m<sup>-1</sup>.

The measurements of the surface tension as a function of temperature were performed with 10 mL aqueous suspension of nanoparticles at 1 wt% between 25 °C and 80 °C. An equilibrium time of 25 min was applied between the temperature increase and the measurement.

### 2.9. Optical microscopy

Optical micrographs were acquired with a VHX-900 microscope from Keyence. The measurement of the droplets diameter size was performed with the Keyence software 1.6.1.0.

The distribution function (log-normal) of emulsion droplets diameters was obtained by treatment of at least 200 individual measurements using Origin 9.1® (OriginLab corporation, US) according to Eq. (1):

$$y = \frac{A}{\sqrt{2\pi}\omega\theta} \exp\left(-\frac{\left(\ln \frac{\theta}{\theta_m}\right)^2}{2\omega^2}\right) \quad (1)$$

where  $y$  is the probability of having droplets of diameter ( $\theta$ ),  $\omega$  is an asymmetric factor (i.e. measure of width), the peak will be approximately symmetric when  $\omega$  is small,  $\theta_m$  is the median droplets diameter ( $\theta_m$  corresponds to the peak center when the log-normal is approximately symmetric), and  $A$  is the amplitude and corresponds to the area under the curve. The  $\theta_m$ ,  $\omega$ , and  $A$  are parameters characterizing the size distribution of the droplets.

### 2.10. $\zeta$ -potential measurements

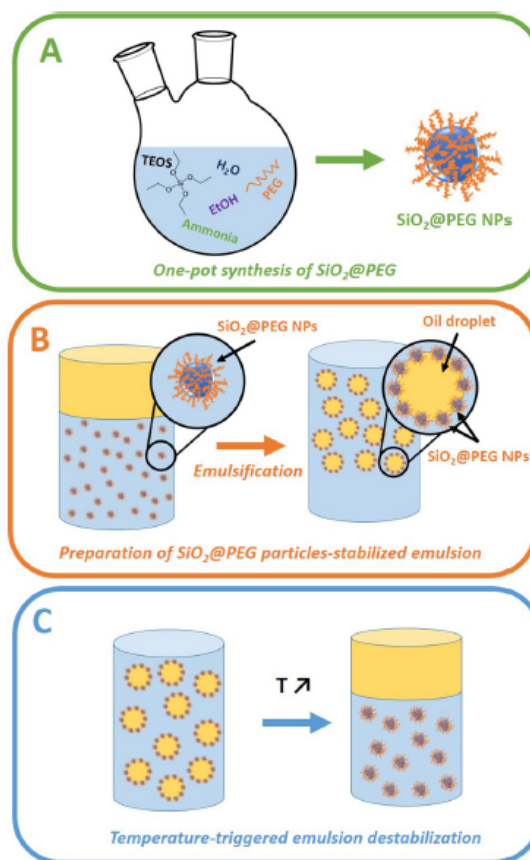
The  $\zeta$ -potential of the particles was measured on a Zetasizer Nano-ZS ZEN 3600 (Malvern Instruments, UK) at 25 °C. 20 mg of particles were dispersed in 1 mL of aqueous solutions.

### 2.11. Temperature-responsive behavior of the emulsions

The temperature-responsive behavior of the emulsions was tested by heating the vials in a water bath a gentle stirring at 100 rpm up to 80 °C. (Scheme 1).

### 2.12. Particle-stabilized emulsions preparation

The emulsions were prepared using water phase containing the silica nanoparticles (1.5 mL) and different oils (1.5 mL). The emulsification was performed with an Ultraturax T10 basic (IKA Works, Inc., Germany) for 60 s at 11,500 rpm at room temperature.



Scheme 1. Schematic illustration of the method of A) one pot synthesis of the SiO<sub>2</sub>@PEG NPs, B) Preparation of the emulsions stabilized by the SiO<sub>2</sub>@PEG NPs and C) Temperature-induced destabilization of the emulsion.

## 3. Results and discussion

The morphology and the size of the SiO<sub>2</sub>@PEG NPs were studied by TEM (Fig. 1). They present a rough surface unlike the bare silica NPs (Fig. S1-2). It is noteworthy the presence of small particles that are linked as a pearl necklace extending out the particles for SiO<sub>2</sub>@PEG 400 and SiO<sub>2</sub>@mPEG 550 (Fig. 1a–b). These small particles in such branch-like structure were not observed in previous studies [29]. The formation of such particles may be due to the condensation of silica onto the PEG chains extending out the main silica particles. The presence of small NPs (~20 nm) around and attached to the core make the particles rough and may help the stabilization of emulsions as it has been demonstrated by San Miguel et al. [30].

The size of the particles has also been measured by DLS (Table 1). As for TEM results, no clear trend has been observed as a function of PEG molecular weight. While for low molecular weight (200–550), PEG and mPEG gives the same range of size, i.e. 150–180 nm, for bigger PEG (or mPEG), a smaller size has been observed. It may be explained by the formation of much more silica nuclei on the PEG with longer chain (more ether groups) and thus, the final size of silica particles is low compared to other batches. However, the sizes measured by DLS are close to the sizes of the NPs (core + branches) measured on TEM pictures, particularly for SiO<sub>2</sub>@PEG 400 (125 nm measured on TEM), SiO<sub>2</sub>@mPEG 550 (200 nm measured on TEM) and SiO<sub>2</sub>@mPEG 5000

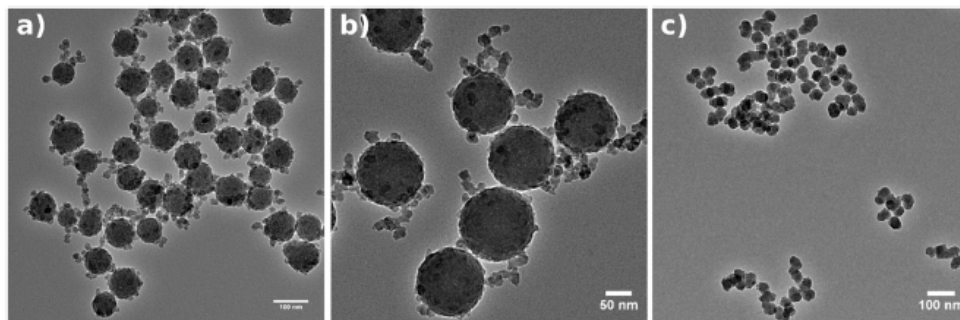


Fig. 1. TEM images of a)  $\text{SiO}_2$ @PEG 400, b)  $\text{SiO}_2$ @mPEG 550 and c)  $\text{SiO}_2$ @mPEG 5000 NPs synthesized by the one-step method.

Table 1

Size hydrodynamic diameter measured in DLS and  $\zeta$ -potential of bare silica NPs and  $\text{SiO}_2$ @PEG NPs dispersed in ultrapure water.

Particles	Hydrodynamic diameter (nm)	Zeta potential (mV)
Bare silica	110	-55
$\text{SiO}_2$ @PEG 200	180	-59
$\text{SiO}_2$ @PEG 400	150	-59.7
$\text{SiO}_2$ @mPEG 550	180	-46
$\text{SiO}_2$ @mPEG 2000	320	-29.1
$\text{SiO}_2$ @mPEG 5000	80	-31.6

(77 nm measured on TEM). It indicates that the chains of NPs are attached to the core.

In order to verify the presence of PEG onto the surface of silica particles, several characterizations have been performed. First, the  $\zeta$ -potential values of the NPs were measured as a function of the PEG (or mPEG) weight (Table 1). Short chain lengths have surface charges comparable to bare silica. NPs functionalized with bigger PEG show a higher reduction of surface charge. Hence, short PEG chains extend less out of the surface of the NPs, which may explain values close to the  $\zeta$ -potential of silica. The increase of MW of PEG, which is a nonionic polymer, decreases the surface charge of the NPs [31].

The presence of PEG on the surface of the NPs was investigated by  $^1\text{H}$  NMR spectroscopy. (Fig. SI-5)  $^1\text{H}$  NMR spectrum of  $\text{SiO}_2$ @mPEG 550 NPs was compared to the spectrum of silica NPs functionalized with mPEG 500 through the two-step protocol proposed by Björkegren et al. [14] were measured. Both spectra show peak that corresponds to the presence of PEG (3.6 ppm). This result suggests that the peak of  $\text{SiO}_2$ @mPEG 5000 is less intense than the peak of the silica NPs functionalized through the two-step method [32]. The nature of interaction between silica and PEG is different for the two types of NPs. Particles grafted with a coupling agent have the PEG molecules covalently attached to their surface, which puts all these molecules in a similar environment resulting in a sharp peak. On the other hand, the broad peak of the  $\text{SiO}_2$ @mPEG 550 particles prepared with one-pot method suggests that the molecules of PEG are in different environments, i.e. a part of the PEG is inside the  $\text{SiO}_2$  core and the other part is outside of the core. The synthesis of  $\text{SiO}_2$ @PEG consists in a modified Stober synthesis of silica in presence of PEG developed by Akbari et al. [29]. According to Xu et al. [33], the hydrolysis step of the sol-gel process of the silica precursor competes with the transesterification between the PEG and silica precursor (TEOS) before the condensation. This method allows to entrap the PEG by a covalent binding, within the silica NPs but also onto the surface.

The  $\text{SiO}_2$ @PEG NPs were characterized with TGA measurements (Fig. 2). First, the dTGA curve of the  $\text{SiO}_2$ @mPEG 550 shows a main peak at 365 °C and two shoulders at 290 °C and 510 °C. While the signal at 290 °C corresponds to the PEG degradation (as measured for pure

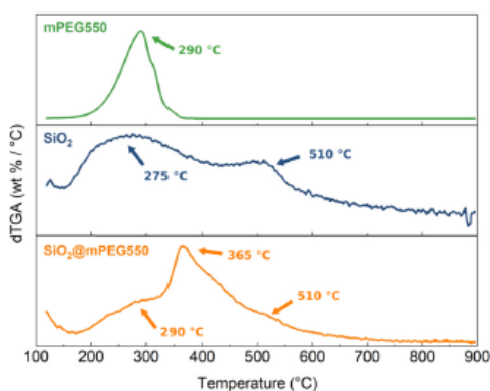


Fig. 2. dTGA curves of mPEG 550, bare silica NPs and  $\text{SiO}_2$ @mPEG 550 NPs. Experiments were conducted at 10 °C/min to 900 °C, under nitrogen.

mPEG 550, Fig. SI-4) and silica dehydroxylation, the signal at 510 °C can be attributed to the dehydroxylation of isolated hydroxyl groups like it was measured for the bare silica NPs [34]. The main peak of the dTGA of  $\text{SiO}_2$ @mPEG 550 at 365 °C can be attributed to the degradation of grafted PEG species [35]. A peak at around 275 °C is also visible in the dTGA curve of the silica NPs that can be attributed to the dihydroxylation of some hydroxyl groups. The peak at 365 °C of dTGA curve of  $\text{SiO}_2$ @mPEG 550 is similar to the peak of  $\text{SiO}_2$ @GPTMS@PEG 2000. These results may suggest that the mPEG 550 is covalently attached to the NPs.

In order to check that the presence of PEG in the samples is not due to the residual PEG molecule – not attached on silica network – the NPs have been centrifuged and redispersed in water several times.  $^1\text{H}$  NMR spectra of two supernatants have been performed to control the absence of free PEG in the suspension (Fig. SI-6). The  $^1\text{H}$  NMR spectra of two supernatants have been performed after 3 and 5 washing cycles. While after three washing steps, some free PEG molecules are still present, after five washing steps no more free PEG molecules are present (peak reduced to noise level). This result proves that the washing steps were effective to remove free PEG molecules.

The surface tension of the NPs was measured in order to compare the surface activity of the  $\text{SiO}_2$ @PEG with bare silica NPs. The surface tension of aqueous suspension of bare silica NPs is known to be around 72  $\text{mN}\cdot\text{m}^{-1}$  whatever the concentration which indicates the negligible effect of their presence [36,37]. Surprisingly, at room temperature, the surface tension of the aqueous suspension of  $\text{SiO}_2$ @mPEG 550 NPs is at the same order, around 71  $\text{mN}\cdot\text{m}^{-1}$  whatever the different concentrations measured (Fig. SI-7). Surface tensions of aqueous suspensions of

$\text{SiO}_2@m\text{PEG 5000}$  and  $\text{SiO}_2@m\text{GPTMS@mPEG 2000}$  are 10% lower at around  $65 \text{ mN}\cdot\text{m}^{-1}$ . These results would indicate that the short length of mPEG (MW 550) does not modify enough the surface tension of silica dispersion at room temperature. Hence, longer PEG chains are more capable of reducing the surface tension with better steric stabilization on the surface once adsorbed. No significant change in surface tension has been observed by increasing the concentration of the NPs from 0.5 to 2.5 wt%, whatever the nature of the NPs.

The surface tension of the aqueous suspensions of purified PEG-functionalized NPs has been also measured as a function of the temperature in order to determine the temperature-responsive behavior of the NPs. (Fig. 3) The measurements have been performed at a fixed NPs concentration (1 wt%). Two groups of data can be observed. In one hand, the  $\text{SiO}_2@m\text{PEG 200}$  and  $\text{SiO}_2@m\text{PEG 550}$  with a surface tension at around  $72 \text{ mN}\cdot\text{m}^{-1}$  that corresponds to the surface tension of water. The NPs have no or very small effects on the surface tension at room temperature. In the other hand,  $\text{SiO}_2@m\text{PEG 400}$ ,  $\text{SiO}_2@m\text{PEG 2000}$  and  $\text{SiO}_2@m\text{PEG 5000}$  have a surface tension decreased at around  $65 \text{ mN}\cdot\text{m}^{-1}$  at room temperature, indicating they are surface active. Unlike the  $\text{SiO}_2@m\text{PEG 200}$  and  $\text{SiO}_2@m\text{PEG 550}$ , they should provide better stabilization for emulsions. These results may indicate that the NPs are surface active when the surface coverage of PEG is high enough [14]. The presence of PEG chains may be indeed more important onto the surface of the particles when using mPEG 2000 and mPEG 5000, with long chains.

When the temperature is increased up to  $60^\circ\text{C}$ , the surface tensions of the dispersions decrease linearly and a break of the slope appears for higher temperatures. The surface tension of NPs functionalized with short chains of PEG (PEG 200, PEG 400 and mPEG 550) decreases faster for temperature higher than  $60^\circ\text{C}$  while the surface tension of NPs functionalized with long chains of PEG is stabilized (mPEG 2000) or decreases slower (mPEG 5000). According to these results, the temperature-responsive behavior of Pickering emulsions was investigated at room temperature and at  $80^\circ\text{C}$ , clearly above the temperature of change of behavior, i.e.  $T = 60^\circ\text{C}$ .

Water / toluene emulsions (50/50) have been prepared with the  $\text{SiO}_2@m\text{PEG NPs}$  (Fig. 4). As expected, particles grafted with small PEG, i.e. PEG 200, were poor stabilizers while O/W emulsion phase could be obtained with particles grafted with PEG of  $\text{MW} \geq 400$  [38]. The emulsions have been observed under optical microscope (Fig. 4). The mean size of the droplets has been determined from the size distribution,

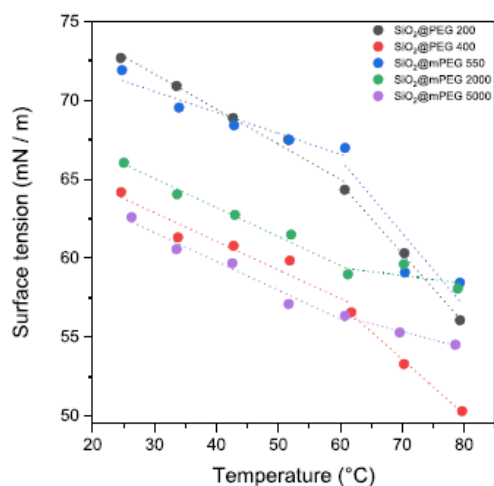


Fig. 3. Surface tension as a function of temperature of aqueous suspensions of the different  $\text{SiO}_2@m\text{PEG}$  NPs. Concentration (1 wt%).

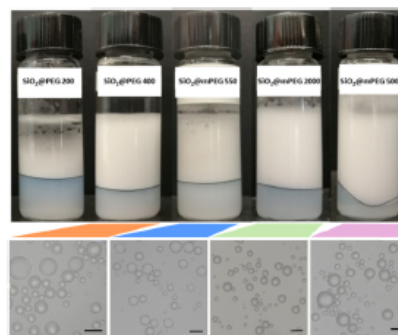


Fig. 4. Appearance of the toluene/water (1:1 v/v) emulsions stabilized by silica NPs (1 wt%) grafted with different types of PEG (top); Optical microscope pictures of the droplets for the corresponding emulsions (bottom). Scale bars:  $50 \mu\text{m}$ .

obtained from the statistical analysis of the optical micrographs. It is around  $35 \mu\text{m}$  for the emulsions stabilized with  $\text{SiO}_2@m\text{PEG 400}$  and  $\text{SiO}_2@m\text{PEG 550}$  while smaller size of droplets for the emulsion stabilized with  $\text{SiO}_2@m\text{PEG 2000}$  and  $\text{SiO}_2@m\text{PEG 5000}$  has been measured.

The temperature-responsive behavior of  $\text{SiO}_2@m\text{PEG}$  NPs-stabilized emulsions has been tested by applying an increase of temperature from  $25^\circ$  to  $80^\circ\text{C}$  (Fig. 5). Shorter chains of PEG are expected to have a better temperature-responsive behavior than long PEG chains according to the measurements of the surface tension (Fig. 3). They require less energy to dehydrate compared to longer chains.  $\text{SiO}_2@m\text{PEG 200}$  could not stabilize emulsion, hence it can be considered as unsuitable for the following. Both  $\text{SiO}_2@m\text{PEG 400}$  and  $\text{SiO}_2@m\text{PEG 550}$  gave emulsions at room temperature and have presented a temperature-responsive behavior with temperature increase, i.e. a clear phase separation. Despite having stable emulsions, the particles with longer chains of PEG have almost no temperature-responsive behavior when heated ( $\text{SiO}_2@m\text{PEG 2000}$ ), as expected. Moreover, the emulsion stabilized by  $\text{SiO}_2@m\text{PEG 5000}$  maintains stable. The temperature responsive behavior or the PEG-functionalized silica particles can be attributed to the hydrophilic/hydrophobic balance of the PEG/mPEG chains. At low temperature, the balance between the ether oxygen of EO chain-water interaction and carbon-carbon backbones of PEG is enough to let the  $\text{SiO}_2@m\text{PEG}$  particles stabilizing emulsions [39]. With the increase of temperature, the hydrogen bonds between the EO chain and water become weaker [40]. At high temperature, the distribution of the PEG/mPEG chains at the oil-water interface is modified which results in

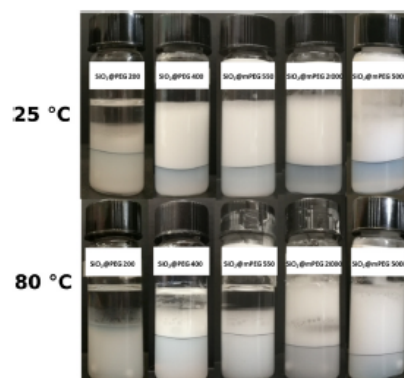


Fig. 5. Pictures of the toluene/water (1:1 v/v) emulsions stabilized with silica particles (1 wt%) grafted with different length of PEG, at  $25^\circ\text{C}$  and  $80^\circ\text{C}$ .



the destabilization of the emulsion [41]. Especially, the  $\text{SiO}_2$ @PEG particles become more hydrophilic with the increase of the chain length, improving the ability of EO units to form more hydrogen bonds with water. In this way, the increase in the chain length of the PEG also increases the energy required to break the hydrogen bonds between EO units and water molecules. According to these results and the previous characterizations,  $\text{SiO}_2$ @mPEG 550 NPs are the most suitable particles for stabilizing water / toluene emulsions and giving them a temperature-responsive behavior.

In order to verify the ability of  $\text{SiO}_2$ @mPEG 550 NPs to stabilize emulsion with other oils, several emulsions have been prepared with different oils: toluene, heptane, paraffin oil, isopropyl myristate, CPME and squalane. (Fig. SI-9–13) The influence of the nature and polarity of the oils on the final properties of the emulsions and their temperature-responsiveness have been investigated. The emulsions have been compared to emulsions prepared with bare silica NPs, pure mPEG 550 and a mixture of bare silica NPs and mPEG 550 (Fig. 6). As expected, emulsions could be obtained with paraffin oil, isopropyl myristate, CPME and squalane [42]. A destabilization occurs when the temperature increases but it could be explained by the gentle stirring used to homogenize the temperature that may accelerate the natural destabilization of the emulsions. Pure mPEG 550 molecules stabilize emulsions with almost all oils (except isopropyl myristate, probably due to the poor solubility of mPEG in this oil). A temperature-triggered destabilization occurs except for toluene. Stable emulsions were obtained with the mixture silica NPs and mPEG 550 was used whatever the nature of the oil. A weak temperature-triggered destabilization happens except for emulsion prepared with squalane. Hence, oils with higher polarity (e.g. heptane) are more favorable to obtain Pickering emulsions with bare silica and pure PEG [42,43]. When  $\text{SiO}_2$ @mPEG 550 NPs were used, stable emulsions were obtained at room temperature and a clear

destabilization occurs at 80 °C. Here, the results show that the  $\text{SiO}_2$ @mPEG 550 NPs can form stable and temperature-responsive emulsions with oils of different nature.

#### 4. Conclusion

A series of PEG-functionalized- $\text{SiO}_2$  NPs have been prepared via a one-step method and were used for the elaboration of temperature-responsive Pickering emulsions. The physicochemical properties of the NPs as well as the presence of PEG molecules anchored on the particles have been thoroughly studied. A drop of the surface tension has been observed near 60 °C for three length of PEG (MW 200, 400 and 550). Stable Pickering emulsions, obtained with several oils of different polarity, were stabilized with NPs functionalized different PEG length (except with the shortest, 200  $\text{g}\cdot\text{mol}^{-1}$ ). Emulsions stabilized with  $\text{SiO}_2$ @mPEG 550 NPs underwent a clear destabilization with temperature (from room temperature to 80 °C) whatever the nature of the oil compared to the other PEG lengths studied and bare silica NPs, mPEG 550 and their mixture.

Further investigations are currently conducted, including the grafting of polyoxometalates onto the poly(ethylene glycol)-functionalized silica particles for catalytic applications. Polyoxometalates, which are used as catalysts, tend to spontaneously adsorb onto hydrophilic surface (such as PEG or polyethoxylated surfactant) through a self-assembly [44, 45]. After a completed reaction, the catalyst is usually collected by filtration or centrifugation which are time and energy consuming techniques and not suitable for industrial process. The use of  $\text{SiO}_2$ @PEG NPs as support for polyoxometalates would help to recover the catalysts and the products after a temperature-trigger destabilization.

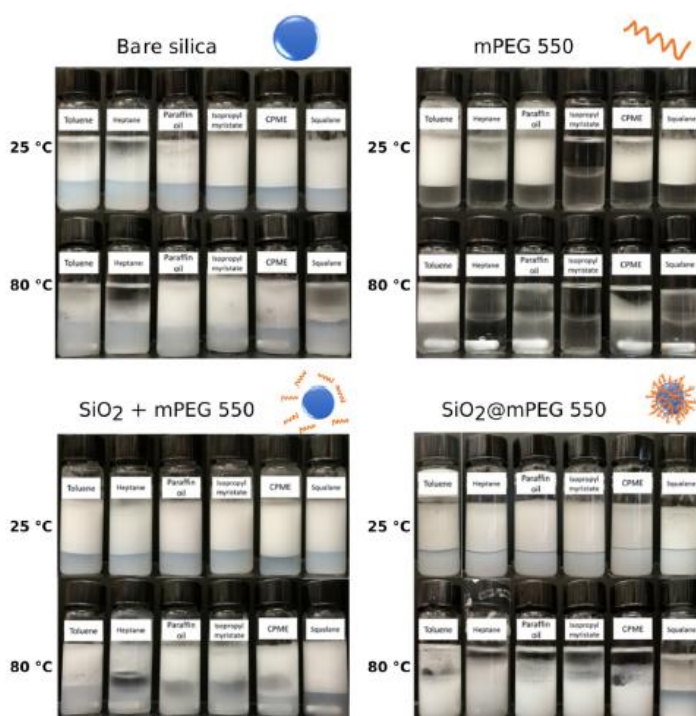


Fig. 6. Appearance of the oil/water (1:1 v/v, different nature of oil) emulsions stabilized with bare silica (1 wt%), mPEG 550 (0.07 wt%), a mixture of bare silica and mPEG 550 (11:1 ratio, 1 wt%) and silica particles (1 wt%) grafted with mPEG 550 at 25 and 80 °C.

J.-F. Dechézelles et al.

#### CRediT authorship contribution statement

Jean-François Dechézelles: Conceptualization, Performing the experiments and research work, Data analysis, Writing – original draft, Writing revised. Yaoyao Feng: Investigation, Data analysis. Fadi Fadil: Investigation, Data analysis. Véronique Nardello-Rataj: Conceptualization, Funding acquisition, Project administration, Revising manuscript.

#### Declaration of Competing Interest

The authors declare that they have no known competing financial interests or personal relationships that could have appeared to influence the work reported in this paper.

#### Acknowledgements

The Chevreul Institute is thanked for its help in the development of this work through the ARCHI-CM project supported by the “Ministère de l’Enseignement Supérieur de la Recherche et de l’Innovation”, the Region “Hauts-de-France”, the ERDF program of the European Union and the “Métropole Européenne de Lille”. Financial supports from Erasmus + (Fadi Fadil) and from China Scholarship Council (Yaoyao Feng) are gratefully acknowledged.

#### Appendix A. Supporting information

Supplementary data associated with this article can be found in the online version at doi:10.1016/j.colsurfa.2021.127641.

#### References

[1] B.P. Binks, W. Liu, J.A. Rodrigues, Novel stabilization of emulsions via the heteroaggregation of nanoparticles, *Langmuir* 24 (2008) 4443–4446, <https://doi.org/10.1021/la800084d>.

[2] F. Gautier, M. Destribats, R. Perrier-Cornet, J.-F. Dechézelles, J. Giemanska, V. Héroguez, S. Ravaine, F. Leal-Calderon, V. Schmitt, Pickering emulsions with stimulative particles: from highly- to weakly-covered interfaces, *Phys. Chem. Chem. Phys.* 9 (2007) 6455–6462, <https://doi.org/10.1039/b710226g>.

[3] L. Leclercq, V. Nardello-Rataj, Pickering emulsions based on cyclodextrins: a smart solution for antifungal azole derivatives topical delivery, *Eur. J. Pharm. Sci.* 82 (2016) 126–137, <https://doi.org/10.1016/j.ejps.2015.11.017>.

[4] Y. Liu, P.G. Jessop, M. Cunningham, C.A. Eckert, C.L. Liotta, Switchable surfactants, *Science* 313 (2006) 958–960.

[5] J. Masliyah, Z. (Joe) Zhou, Z. Xu, J. Czamecki, H. Hamza, Understanding water-based bitumen extraction from athabasca oil sands, *Can. J. Chem. Eng.* 82 (2004) 628–654.

[6] S. Wiese, A.C. Spiess, W. Richtering, Microgel-stabilized smart emulsions for biocatalysis, *Angew. Chem. Int. Ed. Engl.* 52 (2013) 576–579.

[7] B.P. Binks, D. Yin, Pickering emulsions stabilized by hydrophilic nanoparticles: in situ surface modification by oil, *Soft Matter* 12 (2016) 6858–6867, <https://doi.org/10.1039/C6SM01214K>.

[8] Y. Chevalier, M.-A. Bolzinger, Emulsions stabilized with solid nanoparticles: pickering emulsions, *Colloids Surf. A Physicochem. Eng. Asp.* 439 (2013) 23–34, <https://doi.org/10.1016/j.colsurfa.2013.02.054>.

[9] S. Reculosa, S. Ravaine, Synthesis of colloidal crystals of controllable thickness through the langmuir–blodgett technique, *Chem. Mater.* 15 (2003) 598–605, <https://doi.org/10.1021/cm021242w>.

[10] R.G. Digigow, J.-F. Dechézelles, H. Dietsch, I. Geissbühler, D. Vanhecke, C. Geers, A.M. Hirt, B. Rothen-Rutishauser, A. Petri-Fink, Preparation and characterization of functional silica hybrid magnetic nanoparticles, *J. Magn. Mater.* 362 (2014) 72–79, <https://doi.org/10.1016/j.jmmm.2014.03.026>.

[11] J.-F. Dechézelles, C. Ciotonea, C. Catrinescu, A. Ungureanu, S. Royer, V. Nardello-Rataj, Emulsions stabilized with alumina-functionalized mesoporous silica particles, *Langmuir* 36 (2020) 3212–3220, <https://doi.org/10.1021/acs.langmuir.9b03900>.

[12] N. Griffete, J.-F. Dechézelles, F. Scheffold, Dense covalent attachment of magnetic iron oxide nanoparticles onto silica particles using a diazonium salt chemistry approach, *Chem. Commun.* 48 (2012) 11364–11366, <https://doi.org/10.1039/c2cc35462d>.

[13] S. Reculosa, C. Poncet-Legrand, S. Ravaine, C. Mingotaud, E. Duguet, E. Bourgeat-Lami, Syntheses of raspberry-like silica/polystyrene materials, *Chem. Mater.* 14 (2002) 2354–2359, <https://doi.org/10.1021/cm011652s>.

[14] S.M.S. Björkregren, L. Nordstierna, A. Törncrena, M.E. Persson, A.E.C. Palmqvist, Surface activity and flocculation behavior of polyethylene glycol-functionalized

*Colloids and Surfaces A: Physicochemical and Engineering Aspects* 631 (2021) 127641

silica nanoparticles, *J. Colloid Interface Sci.* 452 (2015) 215–223, <https://doi.org/10.1016/j.jcis.2015.04.043>.

[15] V. Lapeyre, N. Renaudie, J.-F. Dechézelles, H. Saadaoui, S. Ravaine, V. Ravaine, Multiresponsive hybrid microgels and hollow capsules with a layered structure, *Langmuir* 25 (2009) 4659–4667, <https://doi.org/10.1021/la9003438>.

[16] B. Brugger, B.A. Rosen, W. Richtering, Microgels as stimuli-responsive stabilizers for emulsions, *Langmuir* 24 (2008) 12202–12208, <https://doi.org/10.1021/la8015854>.

[17] C.-Y. Xie, S.-X. Meng, L.-H. Xue, R.-X. Bai, X. Yang, Y. Wang, Z.-P. Qiu, B.P. Binks, T. Guo, T. Meng, Light and magnetic dual-responsive pickering emulsion microreactors, *Langmuir* 33 (2017) 14139–14148, <https://doi.org/10.1021/acs.langmuir.7b03642>.

[18] J. Zhou, X. Qiao, B.P. Binks, K. Sun, M. Bai, Y. Li, Y. Liu, Magnetic pickering emulsions stabilized by Fe<sub>3</sub>O<sub>4</sub> nanoparticles, *Langmuir* 27 (2011) 3308–3316, <https://doi.org/10.1021/la1036844>.

[19] S. Saeki, N. Kuwahara, M. Nakata, M. Kaneko, Upper and lower critical solution temperatures in poly (ethylene glycol) solutions, *Polymer* 17 (1976) 655–659, [https://doi.org/10.1016/0032-3861\(76\)90208-1](https://doi.org/10.1016/0032-3861(76)90208-1).

[20] B.R. Midmore, Synergy between silica and polyoxyethylene surfactants in the formation of O/W emulsions, *Colloids Surf. A Physicochem. Eng. Asp.* 145 (1998) 133–143, [https://doi.org/10.1016/S0927-7757\(98\)00577-9](https://doi.org/10.1016/S0927-7757(98)00577-9).

[21] S. Björkregren, L. Nordstierna, A. Sundblom, A. Palmqvist, Clouding observed for surface active, mPEG-grafted silica nanoparticles, *RSC Adv.* 9 (2019) 13297–13303, <https://doi.org/10.1039/C9RA00361D>.

[22] S. Björkregren, M.C.A. Freixiela Dias, K. Lundahl, L. Nordstierna, A. Palmqvist, Phase inversions observed in thermoresponsive pickering emulsions stabilized by surface functionalized colloidal silica, *Langmuir* 36 (2020) 2357–2367, <https://doi.org/10.1021/acs.langmuir.9b03648>.

[23] J. Jiang, Y. Zhu, Z. Cui, B.P. Binks, Switchable pickering emulsions stabilized by silica nanoparticles hydrophobized in situ with a switchable surfactant, *Angew. Chem.* 125 (2013) 12599–12602, <https://doi.org/10.1002/ange.201305947>.

[24] Y. Zhu, T. Fu, K. Liu, Q. Lin, X. Pei, J. Jiang, Z. Cui, B.P. Binks, Thermoresponsive pickering emulsions stabilized by silica nanoparticles in combination with alkyl polyoxyethylene ether nonionic surfactant, *Langmuir* 33 (2017) 5724–5733, <https://doi.org/10.1021/acs.langmuir.7b00273>.

[25] P. Lesot, S. Chapuis, J.P. Bayle, J. Rault, E. Lafontaine, A. Campero, P. Judeinstein, Structural–dynamical relationship in silica PEG hybrid gels, *J. Mater. Chem.* 8 (1998) 147–151, <https://doi.org/10.1039/a704963h>.

[26] D.Y. Lee, S. Kang, Y. Lee, J.Y. Kim, D. Yoo, W. Jung, S. Lee, Y.Y. Jeong, K. Lee, S. Jon, PEGylated bilirubin-coated iron oxide nanoparticles as a biosensor for magnetic relaxation switching-based ros detection in whole blood, *Theranostics* 10 (2020) 1997–2007, <https://doi.org/10.7150/tno.39662>.

[27] S. Björkregren, L. Nordstierna, A. Törncrena, A. Palmqvist, Hydrophilic and hydrophobic modifications of colloidal silica particles for pickering emulsions, *J. Colloid Interface Sci.* 497 (2017) 250–257, <https://doi.org/10.1016/j.jcis.2016.10.031>.

[28] H. Giesche, Synthesis of monodispersed silica powders I. Particle properties and reaction kinetics, *J. Eur. Ceram. Soc.* 14 (1994) 189–204, [https://doi.org/10.1016/0955-2219\(94\)90007-6](https://doi.org/10.1016/0955-2219(94)90007-6).

[29] A. Akbari, R. Yegani, B. Pourabbas, Synthesis of poly(ethylene glycol) (PEG) grafted silica nanoparticles with a minimum adhesion of proteins via one-pot one-step method, *Colloids Surf. A Physicochem. Eng. Asp.* 484 (2015) 206–215, <https://doi.org/10.1016/j.colsurfa.2015.07.042>.

[30] A. San-Miguel, S.H. Behrens, Influence of nanoscale particle roughness on the stability of pickering emulsions, *Langmuir* 28 (2012) 12038–12043, <https://doi.org/10.1021/la30224v>.

[31] B. Thierry, L. Zimmer, S. McNiven, K. Finnie, C. Barbé, H.J. Griesser, Electrostatic self-assembly of PEG copolymers onto porous silica nanoparticles, *Langmuir* 24 (2008) 8143–8150, <https://doi.org/10.1021/la8007206>.

[32] J.M. Dust, Z.H. Fang, J.M. Harris, Proton NMR characterization of poly(ethylene glycol) and derivatives, *Macromolecules* 23 (1990) 3742–3746, <https://doi.org/10.1021/ma00218a005>.

[33] H. Xu, F. Yan, E.E. Monson, R. Kopelman, Room-temperature preparation and characterization of poly (ethylene glycol)-coated silica nanoparticles for biomedical applications, *J. Biomed. Mater. Res.* 66A (2003) 870–879, <https://doi.org/10.1002/jbm.a.10057>.

[34] J.M. Kim, S.M. Chang, S.M. Kong, K.-S. Kim, J. Kim, W.-S. Kim, Control of hydroxyl group content in silica particle synthesized by the sol-precipitation process, *Ceram. Int.* 35 (2009) 1015–1019, <https://doi.org/10.1016/j.ceramint.2008.04.011>.

[35] P. Maitra, J. Ding, H. Huang, S.L. Wunder, Poly(ethylene oxide) silanated nanosize fumed silica: DSC and TGA characterization of the surface, *Langmuir* 19 (2003) 8994–9004, <https://doi.org/10.1021/la034048c>.

[36] T. Okubo, Surface tension of structured colloidal suspensions of polystyrene and silica spheres at the air-water interface, *J. Colloid Interface Sci.* 171 (1995) 55–62.

[37] H. Ma, M. Luo, L.L. Dai, Influences of surfactant and nanoparticle assembly on effective interfacial tensions, *Phys. Chem. Chem. Phys.* 10 (2008) 2207–2213, <https://doi.org/10.1039/b718427c>.

[38] P. Finkle, H.D. Draper, J.H. Hildebrand, The theory of emulsification, *J. Am. Chem. Soc.* 45 (1923) 2780–2788.

[39] H. Cai, W. Luo, Y. Zheng, Y. Zhang, L. Lai, S. Tang, Thermodynamic parameters and interfacial properties of poly(ethylene glycol)-octyl sulfosuccinates, *J. Surfactants Deterg.* (2021), <https://doi.org/10.1002/jsde.12497>.

[40] J. Israelachvili, The different faces of poly(ethylene glycol), (n.d.) 2.

[41] F. Wang, J. Zhu, T. Yan, X. Pei, F. Zhang, R.J. Linhardt, Amphiphilic bromelain-synthesized oligo-phenylalanine grafted with methoxypolyethylene glycol

J.-F. Dechézelles et al.

- possessing stabilizing thermo-responsive emulsion properties, *J. Colloid Interface Sci.* 538 (2019) 1–14, <https://doi.org/10.1016/j.jcis.2018.11.082>.
- [42] J. Frelichowska, M.-A. Bolzinger, Y. Chevalier, Pickering emulsions with bare silica, *Colloids Surf. A Physicochem. Eng. Asp.* 343 (2009) 70–74, <https://doi.org/10.1016/j.colsurfa.2009.01.031>.
- [43] J. Jiang, Y. Zhu, Z. Cui, B.P. Binks, Switchable pickering emulsions stabilized by silica nanoparticles hydrophobized in situ with a switchable surfactant, *Angew. Chem. Int. Ed.* 52 (2013) 12373–12376, <https://doi.org/10.1002/anie.201305947>.
- [44] T. Buchecker, X. LeGoff, B. Naskar, A. Pfitzner, O. Diat, P. Bauduin, Polyoxometalate/polyethylene glycol interactions in water: from nanoassemblies in water to crystal formation by electrostatic screening, *Chem. Eur. J.* 23 (2017) 8434–8442, <https://doi.org/10.1002/chem.201700044>.
- [45] B. Naskar, O. Diat, V. Nardello-Rataj, P. Bauduin, Nanometer-size polyoxometalate anions adsorb strongly on neutral soft surfaces, *J. Phys. Chem. C* 119 (2015) 20905–20992, <https://doi.org/10.1021/acs.jpcc.5b06273>.

*Colloids and Surfaces A: Physicochemical and Engineering Aspects* 631 (2021) 127641